A Method for Implementation of Damage Detection Algorithms for Civil Structural Health Monitoring Systems

by

MARTIN EDWARD TUREK

B.E.Sc., The University of Western Ontario, 2000
M.A.Sc., The University of British Columbia, 2002

A THESIS SUBMITTED IN PARTIAL FULFILMENT

OF THE REQUIREMENTS FOR THE DEGREE OF

DOCTOR OF PHILOSOPHY

in

THE FACULTY OF GRADUATE STUDIES

(Civil Engineering)

THE UNIVERSITY OF BRITISH COLUMBIA

June, 2007

Abstract

The field of structural health monitoring for civil structures is of great interest to the academic community, and increasingly to industry as well. Many SHM systems have begun to appear on real structures around the world. These systems provide remote access to many types of measurements, using many types of sensors. A typical result obtained for these systems may be to obtain stress and strain values, direct load measurements, corrosion levels or to validate an analytical model. However, of the systems that make vibration measurements, few are using that data for condition assessment. An important tool to aid in the interpretation of vibration data for condition assessment is a damage detection algorithm. These algorithms are not being used in those systems; there are many reasons for this, particularly related to the complexity of civil structures and the nature of real data. This thesis presents a method for implementation of those algorithms into a SHM system, considering the performance of the algorithms and some of the effects of real data.

The implementation method has two main parts: development of a damage detection methodology (DDM) to be used in the system, and development of a way to evaluate the performance of the DDM if it were applied to a real structure. The DDM is created as a framework from within which available damage detection algorithms can be implemented into the SHM system. The structure of the DDM is that it uses multiple damage detection algorithms simultaneously. This is done acknowledging the limitations of available algorithms and attempts to improve accuracy and robustness by combining them to exploit their individual advantages. The evaluation of the DDM is accomplished by creating a set of calibrated damage simulations (CDS). Ambient vibration signals are simulated using a FEM, and various aspects of the simulation are calibrated using real vibration signals obtained from an ambient vibration test. The goals of the implementation method are to obtain an evaluated and modified DDM, and the optimal layout of the sensors for the best performance of the DDM.

The CDS method was developed and illustrated using a 3D frame example. It was shown that the method could produce simulations that were good representations of real data. The DDM was developed using two simple examples, a 2D truss and a 3D frame. The DDM incorporated three damage detection techniques to create its final predictions. It was shown that the combined DDM provided better predictions than any of the techniques individually. The

developed CDS and DDM were then applied to two real building case studies. Through the application of the implementation method, it was found that the DDM as developed with the 3D frame example was not directly applicable to the real building cases. It was found that the DDM might work only under certain conditions, such as modifying the finite element model used for damage detection and increasing the number of measured points in the SHM system. In addition an optimization scheme for the location of the sensors was proposed. These results demonstrated the benefit of applying the implementation method.

Table of Contents

List of Tables

List of Figures

Acknowledgments

I would first like to acknowledge my research advisor, Dr. Carlos Ventura, for his contributions both to this thesis, and in providing me with opportunities to grow both professionally and personally. With him I have been able to perform tests of many structures, attend many conferences, and not only become to exposed to, but become a part of the international community of my research.

I would like to acknowledge my research committee and the contributions they have made to this research project. First Dr. Reza Vaziri and Dr. Terje Haukaas from the University of British Columbia, and Dr. Steven Kuan from the Government of British Columbia, who provided expertise in development and completion of this project. Second, Dr. Dennis Bernal of Northeastern University, Boston; his technical expertise and advice were important in the development of this research.

I would like to acknowledge Felix Yao, the manager of the EERF. His assistance with technical issues throughout the process was invaluable.

Next I would like to a few of my friends and colleagues that made significant contributions to my life during the last several years. The first is Dr. Houman Ghalibafian, who recently finished his PhD in November 2006. The two of us went through the entire process together for both our Master's and PhD, and he is the one person who truly understood what it was all about. Also Dr. Kristopher Chandroo, a great friend of the last fifteen years, who finished his Doctor of Veterinary Medicine Degree in June 2005. He provided me with the motivation in the dark times. And last, Charles-Philippe Lamarche, from Ecole Polytechnique in Montreal. He came to UBC in 2003, and became an important friend, who promised to start a company when I finished, but instead decided to start his own PhD. If you read this Charles, good luck.

I would need to acknowledge my family, for sticking with me for not just one, but two graduate degrees. They put up with two years of a Master's degree, and then to add almost five more years says a lot about their love and patience. Much of this work is dedicated to all of you.

And lastly I would like to acknowledge Amba, who has amazingly enough kept me sane throughout these last two years. And amazingly enough I didn't drive her insane. Especially

since I came and worked at home for most of the really stressful parts. I love you, and now we can plan the wedding..

Funding for this research was provided by the Natural Science and Engineering Research Council Canada.

Chapter 1. Introduction

The use of structural health monitoring (SHM) technology for civil structures is a topic of great interest to both academia and industry. This is evidenced by the vast amount of literature available on the subject. Many examples of SHM systems are beginning to appear on real structures; a good reference compiling descriptions of SHM systems currently in place around the world can be found on the website of the International Society for Structural Health Monitoring of Intelligent Infrastructure (ISHMII). These systems tend to be designed for a specific need, usually aimed at determining certain properties of the structure (loads, stresses), validating an analytical model or monitoring for changes in a certain measured parameter. For example, the Putlitz bridge in Germany has a monitoring system to determine the actual loads being applied to the bridge, since the present traffic has exceeded the original design loads [ISHMII, 2003]. Another example is the Confederation Bridge in eastern Canada, which is subjected to severe environmental conditions [ISHMII, 2004]. A comprehensive system featuring many types of sensors is installed to monitor certain properties and to note changes in those properties; in particular to look for material deterioration. A majority of the systems are of this fashion containing multiple types of sensors, including vibration sensors, strain gauges, load cells, temperature and wind sensors, among others.

This research focuses on vibration-based SHM technology and damage detection. The desire to combine multiple types of sensors as above is best described in an overview paper on vibration-based health monitoring [Hsieh et al., 2006]. From several representative case studies they state that *'vibrational data have been shown to be most useful when used in conjunction with other monitoring systems if a remote and robust damage detection scheme is desired'*. This statement is important establishing the fact that while vibration-based SHM is studied independently, ultimately the final systems will feature a multi-disciplinary array of technology.

From that perspective, it is worth noting that of the ISHMII case studies, not many have vibration sensors, measuring either velocity or acceleration, and fewer still discuss online processing of the vibration data for condition assessment. An example of a structure that is heavily instrumented for vibrations is the Esplanade Riel Pedestrian Bridge, in Manitoba, Canada [Bogdanovic, 2005]. This bridge has 30 accelerometers installed; however this is a case where they are installed mostly for research use. The best example of a SHM system

incorporating damage detection is on the major bridges in Hong Kong, including the Ting Kau [ISHMII, 2004b] and the Tsing Ma [Zukewich, 2006] bridges. These bridges are a part of the Wind and Structural Health Monitoring System (WASHMS) and have several hundred sensors each. There is a proposed damage detection scheme in place for the Ting Kau bridge; but it is not yet part of the regular operation. Based on these and other examples in the literature, it is apparent that there is a gap between the use of vibration-based SHM technology and the interpretation of the measurements. This is a key aspect to add the necessary value to vibration monitoring technology and to make it widely accepted and feasible.

An important tool to aid in the interpretation of vibration measurements for condition assessment is a damage detection algorithm (DDA). A DDA is a technique or a process that utilizes vibration data and attempts to identify damage or changes in the structural system. In the literature, the goals of damage detection are usually divided into four levels [Rytter, 1993]:

- Damage identification – to detect the presence of damage
- Damage localization – to find the location of the damage
- Damage quantification – to identify the amount of damage
- Damage prognosis – to determine the remaining life of the structure

DDA's will address all or some of these in different ways; a list of some of the methods that have been developed for civil applications is presented in Section 2.5. All of the methods have advantages and disadvantages; but a key issue is that it is not clear from the literature is how they will perform in a real structure with real data. A paper which discusses the performance of vibration-based techniques for damage detection was presented by Humar et al. [2006]. The paper identifies nine types of typical damage identification algorithms, and tests them using simulated cases. The paper acknowledges that while the algorithms work in theory, *'a number of difficulties persist in vibration-based damage identification .. as a result most .. fail when applied to practical civil engineering structures'*. Four problems were identified, including:

1) Low sensitivity of modal parameters to damage
2) Incomplete nature of measured vibration characteristics
3) Complexity of DDA's
4) Effects other than damage

A recent relevant example regarding the use of DDA's in a real system is from a 13-story steel moment frame building in California [Rodgers and Celebi, 2006]. The building was monitored

and data was available from several earthquakes including 1994 Northridge. The study outlined in the paper applied several simple damage assessment schemes, but very notably stated that *'the combination of a large real structure and low instrumentation density precluded the application of many recently proposed advanced damage detection methods..'*. This emphasizes Points 2 and 3 above, and is a recurring theme in the literature. A question can then be posed: is there a way to use these advanced methods?

The goal of this research project is to examine the gap between the application of DDA's into the system and real structures, and make an attempt at responding to this question. Ultimately this is done by proposing a concept for a method for implementation of damage detection algorithms for civil structural health monitoring systems. The implementation method is comprised of two main ideas:

- A framework for a damage detection methodology must be developed;
- The damage detection methodology must be sufficiently evaluated.

In this thesis, the damage detection methodology (DDM) is based on combining several damage detection techniques together and its evaluation is based on creating a series of calibrated damage simulations (CDS) using measured information from the real structure. Consequently the implementation method is for existing structures. The DDA's that are of interest in this thesis are those that compare the condition of the structure before and after a potentially damaging event.

The proposed implementation method includes elements that address the first three points listed above; in general tese are issues that can be dealt with using a single set of measurements from the real structure. The issues arising from effects other than damage (Point 4) are very significant, and represent a major reason why the technology has not been implemented to date. The effects include environmental and operating conditions, which have a tendency to change the measured properties in ways that are not due to damage, and cause the algorithms to fail. These problems will typically be dealt with by long-term monitoring and compiling information on those conditions and how they affect the structure. A discussion of these issues,

including definitions of the problems and a review of proposed solutions in the research is presented in Section 2.6.

1.1. Research Concept

The implementation method is divided into two main components: the development of simulations to be used for the evaluation of the system, and the development of the damage detection methodology to be implemented. It is described as in Figure 1.1.

The implementation method can be generally summarized in three steps; details are provided in Chapter 4. The first step of the implementation method involves developing the calibrated damage simulations for the structure of interest; this is done using the results of an ambient vibration test. A finite element model of the structure is created, and it can be designed and updated using available tools and information from the AVT. Next a vibration simulation is performed using results of the ambient vibration test to improve the simulation quality. The two main results that can be utilized are the measured input and damping; the measured ground vibrations can be used as an input excitation for the simulation and the measured damping estimates are used as the damping values for the simulation. The last part of the calibrated simulation process is to add noise to the datasets.

The second step of the implementation method as shown in Figure 1.1 is to choose the layout of the sensors. This is simply deciding from which locations on the finite element model to extract vibration time history records. The initial selection would be based on a typical sensor layout for a monitoring system; there are ways of doing this depending on the type of structure, such as three horizontal sensors per floor in a building.

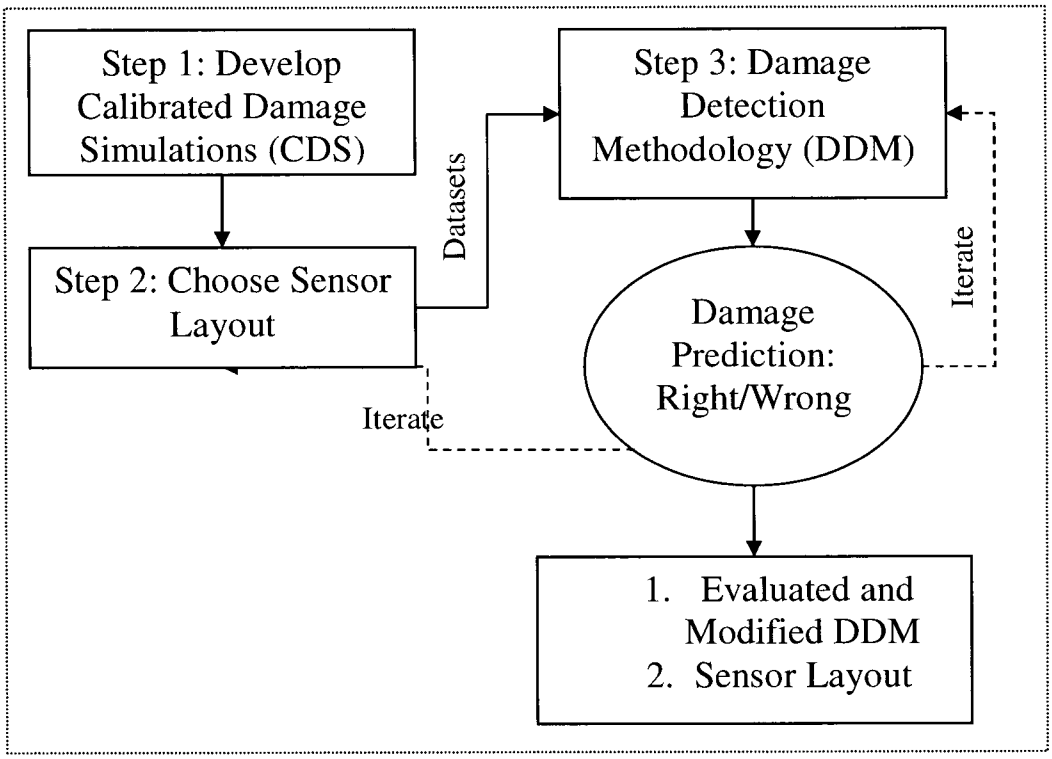

Figure 1.1: The Implementation Method

Once the sensor layout has been chosen, and the simulated datasets have been created, the third step is to create the DDM to be used in the system. The DDM as a part of the implementation method is defined as a *framework from which the damage detection algorithms can be implemented into the SHM system.* To develop the DDM, first the type of damage detection algorithms to be used must be chosen. This choice will depend on many factors, such as the type of input and the desired output. The main concept of the DDM in this research project is that a combination of at least two damage detection algorithms must be incorporated into the methodology. This is done for two reasons: to improve the accuracy, and to improve the robustness of the damage prediction. It is seen in the literature that each damage detection algorithm has advantages and disadvantages; those disadvantages may prevent successful detection of damage in some cases. By having multiple independent predictions in the methodology, the predictions can be validated and the likelihood of missing or making incorrect predictions can be reduced. In the development of the DDM, simple examples are used at first to define all of the necessary parameters. Then more complex examples, and if possible data from a real structure that is available, can be used to further refine the DDM and address any issues with its performance.

The DDM is evaluated by processing the set of calibrated simulations and making a prediction. If the prediction using the chosen sensor layout and DDM is incorrect, then the overall process is iterated. An iteration can involve going back to the DDM and performing a major change (such as adding or removing damage detection algorithms), or a minor change (such as a small modification to certain parameters within the methodology); or an iteration can involve modifying the layout of the sensors. Successful iterations will result in the final DDM including the damage detection algorithms and the optimal layout of the sensors for the DDM.

It is noted that this method does not focus on details such as instrumentation and electronics; items such as choice of instrumentation, connections and computing systems are considered to be a separate issue.

1.2. Objectives, Scope and Organization of Thesis

The objectives of the thesis are:

- To develop a method for implementation of damage detection algorithms for structural health monitoring systems for civil structures;
- This method should:
  - Provide a framework from within which available damage detection algorithms can be implemented;
  - Provide a means to evaluate the performance of those algorithms;
  - Provide a method to find the optimal layout of sensors as required by the damage detection algorithms.

The scope of the thesis is as follows:

- The SHM systems described by this work are based on the measurement of ambient vibration signals; it does not cover other types of measurement such as strain gauges;
- The method is intended for existing structures;
- The implementation method described by this thesis is based on two main ideas:
  - A damage detection methodology (DDM) must be created;
  - The DDM is to be evaluated by a simulation.
- The creation of the DDM is to be done by:

  - The combination of multiple damage detection algorithms to improve accuracy and robustness;
  - The DDM that is presented using existing damage detection algorithms and as such is intended to demonstrate this concept; it is not intended to be presented as a new damage detection algorithm;
  - The DDM is developed using a simple 2D truss and a 3D frame.
- The simulations used to evaluate the DDM are created based the results of an ambient vibration test of the structure; input, damping and noise are controlled based on the results; this is done to create more realistic simulations and referred to as the Calibrated Damage Simulations (CDS).
- The CDS concept is demonstrated using the 3D frame.
- The implementation method is applied to real building case studies; through this application the DDM is evaluated and the sensor layout is found.
- The CDS method considers only effects that can be measured by a single test; other effects such as those due to temperature changes cannot be dealt with in this way and are not considered here.

The organization of the thesis is as follows:

- Chapter 2 – Covers an overview of the field of structural health monitoring including:
  - A detailed description of various areas of SHM.
  - Identification of the important industry and research groups in each area.
  - A literature review covering the important and relevant papers in SHM.
- Chapter 3 – Covers the theoretical background for the software and techniques that are used in this thesis.
- Chapter 4 – Provides an overview of the implementation method.
- Chapter 5 – Presents the development of the Calibrated Damage Simulations using the 3D Frame example; this is presented in a detailed way.
- Chapter 6 – Presents the development of the Damage Detection Methodology using a 2D truss and the 3D Frame; this is presented in a detailed way.
- Chapter 7 –Application of the implementation method to the real building case studies; this is presented as a summary.
- Chapter 8 – Conclusions and final recommendations.

- Appendix – Details of the application in Chapter 7.

Chapter 2. Background on Structural Health Monitoring

The field of structural health monitoring (SHM) is very multi-disciplinary and relies on many aspects of dynamic testing and analysis. In this chapter a brief background on the fundamental concepts, including some history and current research on these topics, is presented. Detailed theory on the key topics of this research will be presented in Chapter 3. The information presented in this section is not exhaustive; there is a substantial amount of literature available. Instead a few representative references are provided for each topic. The format of this chapter is to describe SHM in a layered way; the focus is on vibration-based SHM so the material covered will focus on vibration testing and analysis tools.

2.1. Structural Health Monitoring in General

Structural health monitoring is defined in this thesis as a technique in which the condition of a structure can be assessed by means of some sort of quantity measurement on that structure. The condition can be anything relating to the structure, such as loads, cracks, corrosion, etc. The measured quantities can be anything which will ultimately provide information on that condition, such as strains, loads, accelerations, etc. The key aspect of this definition is that for a complete SHM system, there must be two parts: a measurement part (hardware) and an analysis part (software). The hardware will contain all aspects of the measurement or monitoring system. The software being referred to here is intended to post-process the information obtained by the hardware; that information must be translated into a form that is relevant for the final users. An example of the hardware would be a remote vibration monitoring system; and example of a software component would be a damage detection algorithm. These are all described in more detail in subsequent sections.

The full-scale testing of civil structures, both in forced-vibration and ambient vibration formats began to occur readily in the 1970's. SHM is a field that utilizes the results of those tests, and began to develop in the 1990's. Much of the evolution of SHM for civil engineering comes from applications in mechanical and aerospace engineering. A comprehensive review of structural control (which is the major field relating issues such as vibration testing and structural health monitoring) was presented by Housner et al. [1997]. This paper was written by several of the top researchers in the field and contains an exhaustive literature review, including

a section on health monitoring of civil structures. Although this paper was written many years ago, it contains some relevant comments and recommendations for future directions that have both been observed in the literature since its publication, and/or have not yet been solved by the research community. One of the key points is the recognition that this is a very complex field, and that *'there is a need for a 'toolkit' of methods to deal with the variety of approaches required to cope with all the potential applications'*. This paper also acknowledges that although there already had been many applications for health monitoring that were successful, *'the damage assessment of complex structures such as buildings and bridges remains a challenging task for civil engineers'*. This remains true almost 10 years later. A more recent paper [Aktan et al., 2005] discusses the issues with modal analysis as a method for health monitoring. One question addressed was whether dynamic testing could be relied upon for health monitoring. The authors believe that the possibility for success of the method exists, but more effort is needed to evaluate the technology with real data. In terms of recommended developments of the field to push forward the used of modal analysis in SHM, the authors have paid particular attention on the improvement of the reliability of the experimental results.

2.1.1. Research Groups

This section describes some of the research groups that are involved in SHM. It does not necessarily include all of the groups in the field, but attempts to cover the major ones. In each case the group is identified, a description of their specialization and one or two key references are given. For simplicity they are listed in alphabetical order. This list focuses on groups who are working on the entire process of SHM; not just sensing or monitoring alone.

BAM, Federal Institute for Materials Research and Testing, Germany

Division VII.2 – Buildings and Structures, Structural Health Monitoring and Condition Analysis

This group is working on a wide range of tasks from all aspects of SHM. An example is a sensor design for a system on the Putlitz Bridge, Germany [Rohrmann, 2003]. This bridge is being subjected to loads which are much higher than the original design loads; the SHM system is intended to find the actual bearing capacity of the bridge. The system uses both strain and velocity measurements.

Bridge Engineering Center, IOWA State University, Ames, Iowa

The BEC has been instrumenting bridges since the early 1990's. An important project that this group recently accomplished was to compile a report for the Wisconsin Department of Transportation that identifies companies dealing with various aspects of SHM [Phares et al., 2005]. The report was published in two volumes, which examined over 100 synthesized technologies. This report is indicative of the widespread involvement in SHM, and shows how most of the resources available address parts of SHM only and not the entire problem.

Cornell University, Ithica, NY

School of Civil and Environmental Engineering, Computational SHM and Prognosis Group

This is a relatively new group that is working on details of SHM such as corrosion and service life. One publication involves examination of damage detection using minimal physical testing [Kouchmeshky et al., 2006]. The work uses a co-evolutionary algorithm that searches for damage scenarios and the optimal physical tests. The idea is to find the maximum information about the location of damage while minimizing the measurement locations.

Drexel University, Philadelphia, PA

Intelligent Infrastructure and Transportation Safety Institute

This group is a university-government-industry partnership, established in 1997. Its primary objective is exploring and understanding the issues involved in objectively evaluating, integrating and managing all the components of a transportation system from one single platform. They have done significant work in addressing the practical issues of SHM, including a paper on issues for management [Aktan et al., 1998]. More recently, the senior researchers of this group published a conference paper regarding an overview of the field of SHM [Aktan et al., 2005]. Another key contribution is the Development of a *Model Health Monitoring Guide for Major Bridges* [Aktan et al., 2003]. The guide outlines various aspects of monitoring and modelling, including recommendations for instrumentation and data acquisition.

EMPA, Switzerland

Department of Civil Engineering, Structural Dynamics and Adaptive Structures

This research group is working on developing systems and methods for large structures. They have a cable-stayed bridge research platform set up in the lab, working on all types of SHM

issues [Gsell et al., 2004]. They have done damage detection studies on a highway bridge [Huth et al., 2003]. They are also working on various types of wireless sensors and their issues for SHM.

Hong Kong Polytechnic University, Kowloon, Hong Kong

Department of Civil and Structural Engineering, Research Centre for Urban Hazards Mitigation

This is a large research group mostly doing work on SHM of bridges, but also on tall buildings. They have done work on instrumentation and damage assessment of several bridges, including the Kap Shui Mun Bridge [Ko, 2002]. The bridge is being monitored as part of the Wind and Structural Health Monitoring System (WASHMS). The system contains intensive instrumentation on several of Hong Kong's major bridges, including strain, acceleration, wind speed, etc. The entire system is run by a central command centre.

Institut de recherche en informatique et systèmes aléatoires (IRISA), France

Sisthem (Statistical Inference for Structural Health Monitoring) Team

This group is working on various aspects of SHM including modal analysis, identification and damage detection. In particular they have done work with sub-space methods [Basseville et al., 2004; Mevel et al., 2003] and looking at the effect of temperature on monitoring of civil structures [Balmès et al., 2006].

Korean Advanced Institute of Science and Technology, Korea

Smart Infra-Structure Techology Center (SISTec)

This group was established in July 2002. They are working in all aspects of SHM, including an integrated system of smart monitoring, assessment, control and maintenance. Although their mandate is to advance the technology of SHM, it is not clear what progress they have made in recent years.

Los Alamos National Laboratory, Los Alamos, NM

UCSD/LANL Engineering Institute

The approach to SHM at Los Alamos National Laboratory is to focus on the integration of various technologies to develop a robust and cost effective system. They are accomplishing

this through what they term as a 'statistical pattern recognition paradigm'. The paradigm contains several aspects, from testing to processing to modelling. A summary of the SHM work done at LANL is presented by [Farrar et al., 2000]. They have also authored several overview papers on damage identification methods, in particular one that is referenced often in papers on the subject [Farrar and Doebling, 1997]. More recently discussion has moved to damage prognosis [Farrar and Lieven, 2007] which is the ability to predict the remaining life of a structure.

Massachusetts Institute of Technology, Boston, MA

Infrastructure Science & Technology Group

This group is working on the general application of technology to civil infrastructures, including assessment technologies. An example of their work directly applicable to SHM is found in [Buyukozturk and Yu, 2003]. This is a very detailed paper discussing the development of a SHM concept for seismic loading. Several model identification and damage detection algorithms are described, with detailed examples. A laboratory flagpole structure is described as a benchmark for instrumentation, but application of the SHM concepts to the structure is not presented.

Stanford University, Stanford, CA

Department of Civil and Environmental Engineering

This group has been doing a significant amount of research on all areas of SHM, in conjunction with the California Strong Motion Instrumentation Program [Naeim et al., 2005]. This group is attempting to address the issue of practical application of the technology to real structures. The project is attempting to develop a comprehensive SHM methodology using several aspects of damage identification and earthquake engineering, particularly focusing on integration of FEMA guidelines.

Stanford University, Stanford, CA

John A. Blume Earthquake Engineering Center

A research group based also at Stanford University has done some substantial work towards implementation of SHM systems, including the development of a framework for health monitoring of structures [Straser et al., 2000]. This work addressed wireless vibration sensing,

development of damage assessment procedures and the environmental effects of the experimental results.

University of British Columbia, Vancouver, BC

Earthquake Engineering Research Facility

A recent research project [Mirza, 2006] at the University of British Columbia focused on the implementation of damage detection techniques to bridges. A combination of a damage detection technique and a non-linear analysis approach was used to assess the condition of the bridge after an earthquake. The focus also involved the performance of the method with minimal instrumentation. The group at UBC was also responsible for providing the experimental testing on the IASC/ASCE Benchmark study [Dyke, et. al., 2003] that is used in this thesis (See Chapter 5).

University of Central Florida, Orlando, FLA

Civil Infrastructure Systems

This is a relatively new group; however the group leader was previously a member of the Drexel Intelligent Infrastructure and Transportation Safety Institute and has published many works in SHM of civil structures. A recent paper [Catbas et al., 2006] outlines the application of modal-flexibility based damage detection to two real bridge case studies: The Seymour Bridge in Cincinnati, USA and the Z-24 Bridge in Switzerland. Both bridges were decommissioned and used for damage studies. The paper mostly deals with forced vibration testing and discusses issues due to repeatability of testing and environmental variations. One important result is that from an investigation of minimum damage that can be attributed to damage (in terms of deflections) with confidence was found to be about a 10% change.

University of Tokyo, Tokyo, Japan

Bridge & Structure Laboratory, Dept. of Civil Engineering

This laboratory has a SHM group, working on application of technologies. They are primarily focused on train bridges. Many graduate theses on various aspects of SHM have been completed in this group; one example deals with identification of damage quantity using piezoelectric actuator-sensors [Ritdumrongkul, 2005].

Washington University in St. Louis, St. Louis, MO

Structural Control and Earthquake Engineering Laboratory

This group does research in various areas of SHM, including damage detection and testing of structures including application of new sensor technologies. Recently a PhD thesis was completed covering a framework for SHM of civil structures [Giraldo, 2006]. The project focussed on the SHM of a highway bridge and was applied to simulated datasets. Additional focuses of the project include the ability to detect damage regardless of the environmental effects (ie. temperature) and the automation of the process. The proposed framework was found to be successful but required a high number of mode shapes.

2.1.2. Organizations

ASCE SHM Task Group

The International Association of Structural Control (IASC) – ASCE Structural Health Monitoring Task Group was established to provide direction and consistency to the research activities among its member groups. One of the major projects this group has initiated was a SHM benchmark study involving damage detection of a laboratory steel frame building [Dyke et al., 2003]. Many papers have been published in conferences and journals regarding the work done by the group, and a summary of these papers and the project in general is presented by Turek and Ventura [2005].

ISHMII

The International Society for Structural Health Monitoring and Intelligent Infrastructure (ISHMII) is a web-based organization intended to create a centralized information resource for SHM. It was founded by several groups in 2003. They have spearheaded several workshops and recently an international conference. The website contains a database of publications, including a newsletter for a society, as well as a series of case studies, describing over 50 installed SHM systems.

ISIS

The Intelligent Sensing for Innovative Structures (ISIS) Canada Research Network, headquartered at the University of Manitoba, represents a network of 14 Canadian Universities working towards implementation of advanced structural materials and sensing technologies. They are focused on the use of fibre-reinforced polymers and fibre optic sensors and are

currently monitoring several structures across Canada, including the Taylor Bridge in Headlingley, Manitoba and the Portage Creek Bridge in Victoria, BC. The group has many publications, but one of the most significant contributions is a set of guidelines for structural health monitoring [Mufti, 2001]. These guidelines include an overview of their recommended process, case histories, and descriptions of different test methods including ambient vibration.

2.1.3. Conferences, Work Shops and Courses

The field of SHM has grown substantially and consequently several conferences and work shops have been established. These include:

- The International Work Shop on SHM
- The Asia-Pacific Work Shop on SHM
- The European Work Shop on SHM
- The International Conference on SHM of Intelligent Infrastructure

2.1.4. Journals and Texts

Several journals which are dedicated to the field of SHM are available. These include:

- Structural Health Monitoring: An International Journal (Sage Publishing)
- Structural Control and Health Monitoring (Wiley Publishing)
- Structural Durability and Health Monitoring (Tech Science Press)

There are also a few texts which are focused on SHM. One is a book entitled 'Sensing Issues in Civil Structural Health Monitoring' [Ansari, 2005]. This book offers a unique introduction covering several practical aspects of SHM. Another is entitled 'Structural Health Monitoring' [Balageas et al., 2006], which is a compilation of English translations of French Journal articles.

2.1.5. Companies

Several companies have emerged which specialize in SHM, some of which have been around for several years. This list only includes those groups that feature monitoring systems that report some information regarding the condition of the structure. Companies specializing in monitoring or sensors only are listed in the next section.

Bridge Diagnostics, Inc. (Boulder, CO)

Company specializing in bridges including: load testing, long-term monitoring including strains, fatigue monitoring. Since 1989 they have tested over 250 bridges.

Physical Acoustics Corporation, (Princton Jct, NJ).

They specialize in acoustic emission testing of bridge cables, and have been in operation since 1972.

Smartec SA (Switzerland)

Works in monitoring of structures and has been working in SHM since about 1995. They have working on many bridges around Europe and the world; they also have instrumented a few buildings.

Smart Structures LLC (Rantoul, IL)

This company is working on the supply, installation and management of systems for high-tech bridge monitoring. Currently they are working on three bridges, one in the USA and two in China.

Vienna Consulting Engineers (Austria)

Company specializing in a bridge monitoring system (BRIMOS). The complete system will provide a condition assessment including damage detection and life-cycle costs.

2.2. Remote Monitoring and Sensors

The first sub-topic of SHM to discuss is the hardware. The two components of hardware to be considered are the sensors and the monitoring system. The sensors represent the component of the system that transduces a physical quantity into an electrical form. Two typical examples of this are the accelerometer and strain gauge. Sensors can come in many other forms including temperature gauges, wind speed gauges and humidity sensors. For the accelerometer, there are several forms, including piezoelectric and force-balance types. The force-balance type features a mass on a spring that moves relative to the sensor case transducing voltage proportional to the acceleration. The piezoelectric-type require some sort of charge and they contain a material that responds to external forces in such a way that will output voltage proportional to the acceleration.

Most of the current sensors are analog, meaning there is a continuous analog voltage being output to the data acquisition system. The next steps in the technology of sensors include three major feature upgrades:

1) Digital Output
2) On-board Processing
3) Wireless

For digital output, the sensor features an onboard digital to analog converter (rather than in the data acquisition system), which results in a digital output. This is important because one of the limitations of analog sensors is in the accuracy of the voltage output. Longer cables tend to deteriorate the voltage level thereby jeopardizing the quality of the signal. With a digital output the signal cannot deteriorate, and standard ribbon or Ethernet cables can be used, rather than the typical heavy-shielded cables that are required, which are relatively expensive.

Sensors with onboard processing process the data from its raw acceleration format, which is the most common form, into whatever form that the user requires. Part of the drive to do this is because of wireless sensors. Since one of the issues that have slowed the development of wireless sensing technology is the lack of sufficient battery life, the ability to transmit less information can be very useful.

Many of the research groups that are carrying out research in structural health monitoring sensing at the current time are working on some form of wireless network. This is very significant for many structures in which cables are not practical, either because of difficult access or that the structure is simply too large. There are several ways being explored to eliminate the need for cables. One of the requirements of a measurement system is that the sensors be synchronized in time. Traditionally with wired systems the sensors are connected to the same data acquisition system simultaneously during data recording. With a true wireless system, the sensors would still be connected to the same system but transmit wirelessly simultaneously. Another way of eliminating cables is by using GPS. The sensors would not necessarily be connected to the data acquisition system, but instead record data onboard, and have the time and space of the sensor set synchronized via GPS. A third method to eliminate cables is to have sensors which are time synchronized through internal clocks and record data onboard. This method may be the best solution for many vibration tests in real structures

because of the limitations of both wireless networks and GPS. In the case of a tall concrete building there is no GPS access throughout the structure and wireless signals tend to not travel very well. The wireless network application would be best applied to an open structure such as a bridge.

There is à significant amount of work ongoing in this field, such as work on MEMS (Micro Electro Mechanical Systems) sensors [Chung, et al., 2004]. A review paper was presented by Lynch [2004] that summarizes this extensive work, and describes some of the unique advantages and disadvantages of this technology. One of the most common techniques is using standard PC wireless networks and creating a wireless IP cloud on the structure [Celebi et al., 2004], to form communication links for the sensors back to the base acquisition system.

The technology of an individual sensor has progressed greatly and there are many different variations for each possible sensor. However the means of tying the data together over an entire structure and transporting that information to the required users is of critical importance. The standard vibration monitoring system that has been used to date involves a standard strong motion type accelerometer, connected with cables to a data acquisition system mounted on or near the structure. The system then would be accessible over the internet offering access to the engineer or owner.

2.2.1. Research Groups

Many research groups currently working in SHM are working on the development of sensors, particularly wireless, for use in SHM systems. This section provides a few reference examples of some of these.

University of Southern California, Los Angeles, CA

Embedded Networks Laboratory

This group is focusing on sensors, and in particular is working on a system called 'Wisden' which is intended for use in SHM. An example of a design for SHM systems features a software system called TENET that is intended to allow for programming of the sensors [Paek et al., 2006].

University of Michigan, Ann Arbor, MI

Laboratory for Intelligent Structural Technology

This is a group specializing in design of wireless sensors and other technologies for SHM systems. A few examples of their work includes a study verifying sensors using MR-dampers [Chang et al., 2006] and a study of sensor network implementation [Lynch et al., 2006].

Stanford University, Stanford, CA

Engineering Informatics Group

This is a group specializing in a wireless sensing network. An example of their work is on the development of a sensor with on-board processing [Lu et al., 2006].

2.2.2. Companies

This section provides a few reference examples of companies that specialize in either monitoring or sensors.

Acellent Technologies Inc. (Sunnyvale, CA) – software and hardware systems

Advanced Structure Monitoring, Inc. (Cupertino, CA) - existing since 2003, and utilizes the 'Diagnostic Network Patch' system.

Campbell Scientific, Inc. (International; In Canada: Edmonton, AB) – sensors and data acquisiton

Crossbow Technology, Inc. (San Jose, CA) - wireless Sensors, Accelerometers

Digitexx Data Systems, Inc. (Pasadena, CA) – sensors and structural monitoring software. Digitexx has worked with the USGS [Çelebi et al., 2004] and has extensive experience in California.

EENTEC (St. Louis, MO) Strong motion instruments including force-balance accelerometers.

Kinemetrics, Inc. (Pasadena, CA) Specializing in sensors, including accelerometers. Also offering software systems including the Oasis – online SHM system.

Microstrain, Inc. (Vermont, USA) – bridge SHM, sensors

Structural Health Monitoring Systems (Manitoba, Canada) – bridge monitoring.
Summit Instruments (Akron, OH) – accelerometers and other instruments

Texas Measurements (College Station, TX) – instruments including strain gauges and data acquisition

Vibra-Metrics (Princeton Jct, NJ) – accelerometers

2.3. Vibration Testing

Since the remote monitoring system provides vibration data from the structure, it is useful to discuss the concept of vibration testing and how vibration data is processed. A vibration test is performed to obtain either the vibration levels of the structure for a particular loading or operating condition, or to obtain its dynamic characteristics. The dynamic characteristics, or modal parameters, can be defined as the natural frequencies, the associated mode shapes and damping values. These are properties of the structure that depend on its stiffness, mass and various energy dissipating mechanisms. These characteristics will affect how the structure vibrates under different dynamic loads, such as those due to traffic, wind or earthquakes.

The actual testing process involves measuring vibrations over various locations on the structure, and analyzing the data. Vibrations are typically measured as accelerations, and digitally recorded as time history signals. These signals can then be processed and analyzed in a variety of ways, either in the time domain or frequency domain. The source of the vibrations can be from a known input, such as a shaker or a hammer, or unknown inputs, such as ambient conditions. Hammer and shaker tests are referred to as forced-vibration tested. Vibration testing can also be used to obtain response information of a structure, such as absolute accelerations, relative displacements etc. A comprehensive guide to vibration testing of structures is presented in the Handbook for Dynamic Data Acquisition and Analysis [IES, 1995].

In a forced-vibration test, a spectrum of the output is computed from the measured output signals (typically a response such as acceleration), and likewise a spectrum of the input is computed from the measured input signals (typically a force). The output is then divided by the

input to create a frequency-response-function (FRF). This FRF contains information about the resonant modes, and a series of FRF's at various measured degrees of freedom will allow for the derivation of the mode shapes. Since the FRF's were created from both inputs and outputs, the amplitude of the 7mode shapes are scaled and calibrated accordingly to preserve the inertial and elastic properties of the structure. A single-input single-output (SISO) test is one where each point on the structure is measured and excited individually; a matrix of the FRF's is created later. A good practical example can be found in [Brinkman and Maciaoce, 1982].

Typically forced-vibration tests are done with multiple-inputs multiple-outputs (MIMO). This way the entire structure can be measured simultaneously and the mode shapes are available immediately. However, the key issues remains the same: the input must be measured and then not only can the modal parameters be obtained but scaled structural details such as mass and stiffness can also be obtained. However, forced-vibration tests are often not practical in the field on large civil structures. The alternative is known as *ambient vibration testing*. Unlike forced vibration testing, the forces applied to a structure in ambient vibration testing are not controlled. The structure is assumed to be excited by wind, traffic and human activity. The measurements, typically accelerations, are taken for a long duration to ensure that all the modes of interest are sufficiently excited. Ambient vibration testing is known more generally (particularly to mechanical engineers) as 'operational modal analysis', to civil engineers as 'output-only modal analysis', and more recently as 'natural input modal analysis' (NIMA). Several review papers have been written about ambient testing, including one by Ivanovic, Trifunac and Todorovska [2000], Ventura and Turek [2005] and Cunha and Caetano [2005]. The first paper reviews testing done primarily in California, the second testing performed in Western Canada and the last is a more general overview of the transition from Input-Output to Output-Only testing in Civil Engineering.

Currently there is research ongoing to obtain additional structural performance information from vibration measurements besides only the dynamic characteristics. A paper by Hjelm et al. [2005] describes a method to determine the structural stress histories from NIMA. Another paper by Aenlle et al. [2005] describes a method to estimate structural load from NIMA. Although in the early development stages, these techniques could have a significant impact on the overall development of the vibration testing/structural control field.

2.3.1. Analysis of Ambient Vibration Data

There are many ways to analyse a set of ambient vibration data for a structure, both in time-domain and frequency domain. A paper by Zhang, Brincker and Andersen [2005] presents a review of the major techniques used for the analysis of ambient or operational modal data. The paper describes four time-domain approaches, NExT-type, ARMAV model-based, stochastic realization-based and stochastic subspace-based methods. It also describes two frequency domain approaches, including the FDD-type and the output-only LSCF-type methods.

The methods used in this research are Frequency Domain Decomposition (FDD) and Stochastic Subspace Identification (SSI). These are a frequency domain and time domain approach, respectively. These two methods are implemented with the ARTeMIS Extractor software developed by Structural Vibration Solutions [SVS, 2005]. Both of these methods will be described in detail in Chapter 3.

2.4. Finite Element Model Updating

One of the purposes of conducting ambient vibration tests on large civil structures is to use the modal information obtained to validate and/or improve a finite element model of the structure being investigated. Currently the nature of the output-only modal analysis methods only permit the determination of the natural frequencies, associated mode shapes, estimates of the modal damping values. Information on modal participation factors and modal mass participation cannot be obtained. Nevertheless, it is possible to update a finite element model using results from ambient vibration tests by making use of natural frequencies and mode shapes only.

An attempt to correlate experimental and analytical modal properties of a high-rise building using a manual updating process is described by Ventura and Horyna [2000]. Although an acceptable match was obtained between the analytical and experimental dynamic response of the building, this technique showed limitations, mainly the number of parameters that one can vary concurrently in order to obtain such a match. Recent developments in automated FEM updating software, such as FEMtools [DDS, 2004], offers the ability to perform updates on complex structures using multiple target responses and parameters. A paper describing the use of the automated technique on that same high-rise building is described by Ventura et al. [2005]. The study showed the advantage of an automated tool for using more information

simultaneously; however it is still up to the judgement of the analyst to determine how to perform the updating and the realism of the results. The best use of a tool such as FEMTools is to use it first for the design of the FEM; correlation between the model and test data can be made at every step of the design. Then, once the design has been completed, the model can be refined by an automated process.

2.4.1. Vibration Based Model Updating

Vibration-based model updating compares modal parameters obtained from the developed finite element model and those obtained from the real structure. In many cases complete details of an existing structure are not known and therefore the validity of any developed finite element models is undefined. By obtaining real structural information and performing a correlation and updating procedure, a better finite element model can be created.

The process of vibration-based model updating is illustrated in Figure 2.1. It follows these general steps:

i) generate a base finite element model from the information available
ii) compute the modal parameters of the finite element model
iii) perform a vibration test of the real structure
iv) calculate the modal parameters from the data obtained
v) perform a correlation analysis between the FEM and real structure modal parameters
vi) decide which structural parameters are uncertain and can be changed and choose which modal parameters to match
vii) update the model, changing the structural parameters to match the modal parameters (also referred to as *responses*)
viii) perform correlation analysis to check status of the updating; iterate if necessary

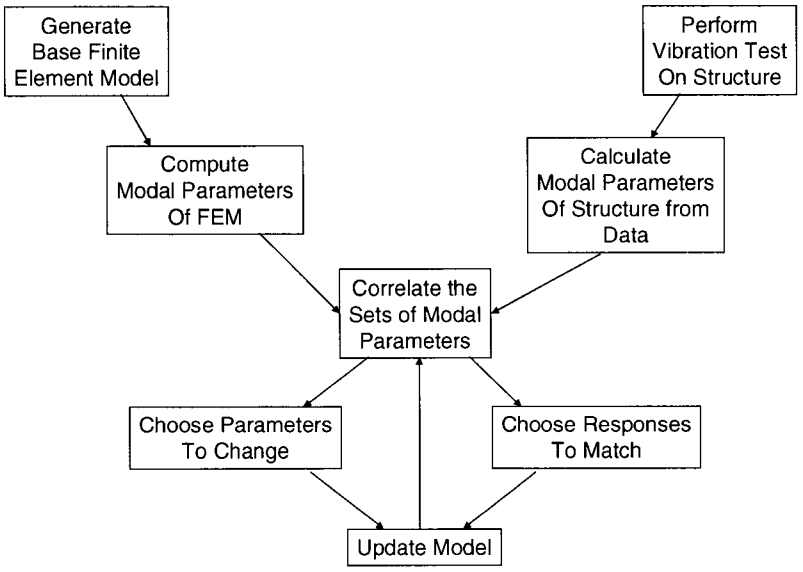

Figure 2.1: Concept of Vibration-Based Finite Element Model Updating

2.5. Damage Detection

Damage detection is the process of identifying damage in a structure by some means other than visual inspection. In most cases this is accomplished by fitting the structure with a series of transducers, collecting data and analyzing this data for the detection process. Many damage detection algorithms have been developed, many of them coming from a mechanical engineering origin, and evolving into civil engineering applications. There are several review papers in the literature, such as those by Los Alamos National Laboratory [Farrar and Sohn, 2001, Farrar and Doebling, 1997, Humar et al., 2006]. None of the review papers cover all of the methods that are either available or under development. Due to the number of the methods currently in the literature, this section gives only a representative example of the some of the methods available.

Damage detection may also be referred to as Non-Destructive Evaluation (NDE) or Non-Destructive Testing (NDT). Those tend however to be focussed towards localized damage or deterioration, such as corrosion in a reinforced concrete beam. The term non-destructive therefore implies that the corrosion in the reinforcing could be identified without cutting the beam. Damage detection, although essentially referring to the same general idea, usually refers to global damage identification, such as that done with vibration properties. In Section 2.5.1 several of the vibration-based damage detection techniques for civil engineering applications are introduced.

In this thesis *damage detection* refers to the overall concept; it can then be divided into four sub-groups or levels as typically represented in the literature. These are as follows:

1. Damage identification – determines if the structure is damaged
2. Damage localization – determines where the structure is damaged
3. Damage quantification – determines how much the structure is damaged
4. Damage prognosis – determines the remaining life of the structure

DDA's will address all or some of these in different ways; in general they can be divided into two groups: model-based and response-based. Model-based DDA's are those that require a FEM or some other sort of model to determine structural parameters such as stress and stiffness; typically the models are validated by the vibration data. Response-based DDA's are those that only deal with the data itself; examples include wavelet methods, statistical methods and parametric modeling techniques. The idea is that they examine the data directly and look for changes without the need for an analytical model.

2.5.1. Damage Detection Techniques for Civil Structures

This section provides a list of some of the damage detection algorithms/techniques that can be found in the literature. For each brief description of the technique is provided. This is not intended to be a critical review or a comparison of techniques; it simply identifies techniques that are available. Note that the names identifying each are not necessarily the proper technique names; in some cases they are simply a descriptive title.

Two-stage Bayesian model-updating approach [Yuen et al., 2004]
This method first identifies the modal parameters from the structure. Next a probability density function for the stiffness parameter of the structure is then constructed, and based on multiple datasets, probabilities of changes in that stiffness parameter are computed.

Statistical model-updating approach [Lam et al., 2004]
This method first identifies the modal parameters from the structure using a probability density function of the spectral density matrix; then a finite element structural model is updated and changes in prescribed stiffness parameters are identified.

Matrix Updating Technique [Caicedo et al., 2004]

Two-stage approach that first identifies the modal parameters, and from those parameters the individual floor stiffnesses are obtained. Damage is then identified as changes in floor stiffness. This method requires some knowledge of the floor mass; either absolutely or relatively.

Damage Locating Vector Technique [Bernal and Gunes, 2004]

This process first creates a state-space realization from all available signals. Then the flexibility matrices are extracted from that realization and changes in the matrices are computed. Next a singular value decomposition of the change in flexibility matrix is taken and the damage locating vectors are found in the null space of the SVD. The DLV's are applied as static loads to a structural model; damage is identified as being in the members possessing zero stress.

Stochastic Damage Locating Vector Technique [Bernal, 2006]

The DLV technique is derived for cases where the vibration input is known; therefore the scaled flexibility matrices can be obtained. The SDLV technique is a special derivation to account for a lack of input data. The derivation forms an 'equivalent' change in flexibility and proves that the SVD of that matrix gives essentially the same result as that from the scaled change in flexibility from the DLV technique.

Proportional Flexibility Matrix Technique [Duan et al., 2005; Bernal and Gunes, 2004]

The PFM technique is another technique to find the equivalent flexibilities for use in the DLV technique when the input is not known. The idea is that when a matrix proportional (by a scalar value) to the actual flexibility matrix of the structure is found, it can be shown that a SVD of that proportional matrix gives identical results.

First-order/Second-order technique [Luş et al., 2004]

This technique first finds a first-order minimal state-space realization using only input-output measurements then extract the physical parameters (mass, damping, stiffness) of the underlying second-order system.

Hilbert-Huang based approach [Yang et al., 2004]

Two methods are proposed for extracting damage information from measured data: an empirical mode decomposition-based method, that will extract damage spikes due to sudden changes in structural stiffness; the second incorporates the EMD with a Hilbert transform, allowing for determination of the damage time instants and to determine the natural frequencies and damping ratios before and after damage.

Wavelet approach [Hera and Hou, 2004]

Spikes in the wavelet details are interpreted as damage; damaged region is determined by the spatial distribution of the observed spikes.

Intelligent Parameter Varying Technique [Saadat et al., 2003]

This technique is developed for detecting damage in base-excited structures. This method combines the benefits of parametric methods, which seek to determine the 'optimal parameters' of an assumed structural model, and those of non-parametric methods, which don't require any prior knowledge of a model's structure.

Partial observer model [Bernal and Hernandez, 2005]

The partial observer model is created from prior small events, with the response measured at all available channels during a consequent event. Damage is indicated by differences in the model and the measured response.

Sensitivity-Based Model Updating [Kharrazi et al., 2002; Wu and Li, 2005]

This technique uses sensitivity-based model updating for damage detection. The idea is that a model of the structure is created for the undamaged state; then the modal characteristics are computed. Then, a future set of modal characteristics from the real structure (possibly in a damaged state) are obtained. The model is then updated using a sensitivity-based approach to match those real modal parameters. If damage is present in the structure, ideally the updated members will represent those that are damaged. The difficulty with the technique is that the number of variables in the updating tend to be large (ie. all members in the structure); therefore this technique works best when combined with another technique.

Statistical Pattern Recognition Techniques [Sohn et al., 2001]

These techniques essentially process the raw time history data and examine various statistical parameters. Variations in the parameters are considered to be the damage features.

Damage Index Method [Park et al., 1998]

This method employs pattern recognition techniques, and requires that the structure be defined in 'pattern space'. Then the pattern spaces are compared and using a set of computed damage indicators, the damage severity is computed as a ratio from 0 to 1.

2.6. Issues for Vibration-Based SHM

There are many issues that arise when using vibration-based SHM and in particular damage detection algorithms. One paper that is a very comprehensive discussion on these issues is by Moon and Aktan [2006]. The paper defines the many issues around *epistemic* uncertainty in constructed systems, or 'what is unknown' about the structure and the test procedure, and separates that from the uncertainties caused by natural randomness associated with vibration testing and data. Three issues can be defined with respect to external factors, all of which may have an effect on the measured parameters in a way that interferes with the interpretation of damage:

1) Environmental conditions –such as humidity and temperature
2) Boundary conditions – such as soil properties and soil stiffness, affected by ground shaking and moisture
3) Excitation – excitation levels and frequency content

Another paper [Catbas and Aktan, 2002], emphasizes these points with an example based on real bridges, using a strain influence coefficient-based damage index. The paper offers an interesting disscusion on selecting a damage index in the context of these issues.

The effects of environmental variation on modal parameters, and in particular temperature, are the most widely discussed in the literature. The issue is that temperature may arouse changes in the measured parameters that are more significant than changes due to damage. Two highly publicized examples are from the Z24 bridge in Switzerland and the I40 bridge in New Mexico, USA. The Z24 bridge was monitored for several years, measuring temperature and vibrations, under varying environmental conditions and several cases of imposed damage. A study was undertaken that examined the contribution to the measurements from the excitation source and

temperature effects [Peeters et al., 2001]. It was found that the results from processing ambient data were comparable to that from a shaker; it was also found that the modal parameters were affected by temperature in an approximately bilinear way, and that if the temperature effect was taken out by a statistical process the damage could successfully be identified. Temperature was only recorded in one location on the bridge and this was found to be satisfactory. For the I40 bridge [Zukewich, 2006b], similar studies were performed, however the most significant result was that one of the bridge girder sections was cut to simulate damage; it was found that even with a severe cut through most of the cross-section, the changes in modal parameters due to the temperature effects tended to be greater than that of the damage.

Another example of temperature affecting the modal parameters was on the Pedestrian Bridge at the University of British Columbia, Vancouver, Canada [Ventura et al., 2002]. This is a unique situation with a glass enclosed structure, in which the temperature was noted to increase by 20° Celsius, with a resulting change in the first mode of 7%. Another bridge that reported the changes was one in Saskatchewan, Canada [Siddique et al., 2005]. Changes in the first modes of 8, 12 and 12% were observed for a temperature range of -8° C to 35° C. Significant shifts in frequency were noted near freezing, which is likely due to the soil-structure-interaction effect of the ground water freezing.

A recent paper presented an overview of environmental and operating variability and its effect on SHM [Sohn, 2007]. This paper stressed the need for data normalization, and categorized the various issues as described above, including several case studies, and outlined much of the ongoing research to deal with these issues. One method attempts to use a mathematical transformation of the identified modal parameters [Giraldo et al., 2006]. The advantage of this method is that an explicit measurement of the temperature is not necessary. Anther technique takes an existing subspace identification method [Balmes et al., 2006] and modifies it using a thermal model [Nasser et al., 2005]. The thermal model is based on predicting the effect of temperature for a simple beam. The effect is then removed in the damage detection process. Another paper presents a way to better obtain the modal parameters in light of the temperature problem with an algorithm using *Complex Mode Indicator Functions* and *Enhanced Frequency Response Functions* [Catbas et al., 2004].

In addition to effects of external conditions, another major issue is regarding unknowns with the structure itself. Since in a constructed system there are many variables that can not be controlled, it is important to address whether an SHM approach is using physics-based models or others, such as response-based algorithms. Similar to all aspects of analytical modeling, using physics-based models is ideal but has many limitations. An example of how these conditions can affect the modal parameters is shown on a prestressed concrete bridge example [Huth et al., 2005]. The study stated that early stage damage identification was impossible due to closing of cracks, which effectively regains the structural stiffness. In the paper by Moon and Aktan [2006], nine attributes of constructed systems that affect the unknowns are defined. Most of their experience deals with aged bridge systems, and issues such as material uncertainty, geometry changes due to expansion joints, load variability, among others.

Another paper examines the modal parameters that are used for damage detection, and showed that the modal flexibilities were most sensitive to damage (rather than frequencies and mode shapes) and could be best utilized towards identification [Zhao and DeWolf, 1999]. However, depending on the process, it is not easy to find those flexibilities. A similar study was done examining SHM of bridges, and concluded that statistical pattern recognition was more robust, and that the extraction of modal parameters was not the best use of vibration data [Owen and Pearson, 2004]. Ultimately it is desired to find the best balance between robustness, ease and cost of implementation, and the usefulness of the results.

It is noted that in general all of these issues tend toward the use of monitoring for a solution (in combination with ideas described above). A database of all of the measurable parameters should be created; and then issues of variation and repeatability could be dealt by comparing similar conditions. In addition, an effort is needed to automate all of these processes, such as the work done by Giraldo [2006].

Chapter 3. Theoretical Background

This chapter will present the technical theory behind this research project. Several commercial software packages are used, as well as several programs coded in MATLAB. The chapter is written in a way to cover specifically the theory that applies to the project, but also covers important background for any of the methods described.

Section 3.1 introduces the concept of the linear dynamic system, and presents it from the perspective of the electrical engineer, and from the civil engineer, and tries to show that they are essentially the same. Section 3.2 expands on the linear model of Section 3.1, and discusses various forms of parametric models and their estimation. Section 3.3 discusses a special form of parametric model, the state-space formulation. This form is derived from the classical structural dynamic system. Section 3.4 and 3.5 introduce two of the system identification methods used by the ARTeMIS Extractor software. These are the Frequency Domain Decomposition method, and the Stochastic Subspace Identification method. Section 3.6 discuss the finite element model updating techniques applied using the FEMTools software, with focus on the modules used for typical civil engineering applications. Section 3.7 discusses the theory behind the Damage Locating Vector technique, which is the deterministic version of the main damage detection technique used in this research. The remaining two sections, 3.8 and 3.9 describe the two stochastic versions of the DLV technique, which are the Stochastic Damage Locating Vector (SDLV) and Proportional Flexibility Matrix (PFM) techniques.

3.1. Linear Dynamic Systems

The topic of linear dynamic systems is available in many texts and references, and will not be discussed in a large amount of detail here. Instead this section will discuss the fundamental concepts of linear dynamic systems, and starting with the concepts as taught to electrical engineers, show how the way that structural dynamics as taught to civil engineers is just a special case of the former. The two main books that will be used for reference are *Linear Dynamic Systems and Signals*, by Gajić [2003] and *Dynamics of Structures: Theory and Application to Earthquake Engineering*, by Chopra [1995]. The former is intended for 2nd and 3rd year electrical engineering students; the latter is intended for civil engineering students and is typically used in 4th year and graduate courses.

The most general form of a *linear, time-invariant, single-input, single-output* system is given by:

$$\frac{d^n y(t)}{dt^n} + a_{n-1}\frac{d^{n-1} y(t)}{dt^{n-1}} + \cdots + a_1 \frac{dy(t)}{dt} + a_0 y(t) = f(t) \qquad \textbf{Eq. 3.1}$$

This *n*-order differential equation describes the system in terms of parameters, a_n. Once the linear parameters have been identified, and the input is known, the equation can be solved with various methods to find the output, *y(t)*. The input is also known as the *system excitation*, and the output is also known as the *system response*. A typical solution to the differential equation has two parts, the homogeneous solution and the particular solution.

$$y(t) = y_h(t) + y_p(t) \qquad \textbf{Eq. 3.2}$$

The homogeneous solution is a result of the initial conditions, and the particular solution is a result of the forcing function. In engineering terms this is known to be the *system natural response* and the *system forced response* respectively. We also know these in structural dynamics as *free-vibration* or *transient response*, and *steady-state response*. The fundamental concept behind a linear dynamic system is that once the system parameters are defined, they do not change with time. Therefore if the input is changed by some mathematical way, for example doubled in amplitude, the output would also double in amplitude.

Any of the texts on this topic will describe the various types of excitation, and the corresponding solutions to determine the response. Except where specifically necessary, those will not be repeated here. However, an interesting fact that can be noted in terms of excitation, is the difference between the electrical and civil engineering approaches to explaining this topic. The electrical engineering text describes the input as signals, and the fundamental forms (such as the dirac delta impulse, the step, ramp, etc.) as being the smallest building blocks of digital signals. The civil engineering texts describe these as forcing functions, and as being applied loads to the structure.

The dynamic model as described by Chopra is the classical single-degree-of-freedom equation of motion:

$$m\ddot{y}(t) + c\dot{y}(t) + ky(t) = f(t) \qquad \textbf{Eq. 3.3}$$

This is simply the 2nd order ($n=2$) form of Eq. 3.1. The parameters in the model are the mass, m, the damping coefficient, c, and the stiffness, k. This equation can be derived by using D'Alembert's principle, which simply imposes static equilibrium at any time t. The equilibrium forces are the inertial force, $m\ddot{y}(t)$, the damping force, $c\dot{y}(t)$, and the stiffness, or restoring force, $ky(t)$. So it can be said that the inertia of the structure is proportional to its mass and acceleration, damping force is proportional to velocity and restoring force is proportional to displacement. While these are described as real physical phenomena, the model form is still simply a parametric linear dynamic model.

The next topic important for structural engineers is the move from SDOF models to the multi-DOF form. This is shown as follows:

$$M\ddot{Z}(t) + C\dot{Z}(t) + KZ(t) = F(t) = Bu(t) \qquad \textbf{Eq. 3.4}$$

Now the parameters are given in matrix form. The size of the matrices (n) will be determined by the number of DOFs in the system. The form in Eq. 3.4 is known as the coupled form, because each of the DOF's is dependent on each other in the solution. The solution of a coupled MDOF system can get challenging, so the simplest method is to solve the eigenvalue problem to determine the modal parameters of the system, and decouple the equation into n SDOF systems. Each of the SDOF systems is solved in the usual way, and their solutions are then added to form the complete response. This is referred to as Modal Analysis. The eigenvalue problem is stated as:

$$\left[K - \omega_n^2 M\right]\phi_n = 0 \qquad \textbf{Eq. 3.5}$$

It is well known that to solve the problem posed by Eq. 3.5, the determinate of the matrix in parenthesis is first set equal to zero (since the modes φ cannot be zero) to obtain the frequencies ω. These values can then be substituted back into the equation to obtain the unscaled mode shapes.

The equation of motion can then be uncoupled by creating the modal mass, modal damping and modal stiffness as shown in Eq. 3.6. These are called the generalized mass, generalized damping and generalized stiffness. These terms will be substituted into Eq. 3.3, and one equation is created for each mode, and solved as a SDOF system.

$$m_n = \phi_n^T M \phi_n ; c = \phi_n^T C \phi_n ; k = \phi_n^T K \phi_n \quad \text{Eq. 3.6}$$

3.2. Parametric Models and Identification

The parametric form of the linear dynamic model was introduced in Eq. 3.1. In this section, variations of the model are discussed, as well as the methods to solve for the parameters. In Eq. 3.1, only the output is parameterized. In a more general form, the input can be parameterized, and an error or *disturbance* term is added.

$$A(q)y(t) = \sum_{i=1}^{nu} \frac{B_i(q)}{F_i(q)} u_i(t - nk_i) + \frac{C(q)}{D(q)} e(t) \quad \text{Eq. 3.7}$$

The variable q is called the shift operator, and each of the functions, A, B, C, D, F, are difference equation polynomials in q. This general form can be specialized into four typically used forms:

ARX

$$A(q)y(t) = B(q)u(t - nk) + e(t) \quad \text{Eq. 3.8}$$

ARMAX

$$A(q)y(t) = B(q)u(t - nk) + C(q)e(t) \quad \text{Eq. 3.9}$$

OE

$$y(t) = \frac{B(q)}{F(q)} u(t - nk) + e(t) \quad \text{Eq. 3.10}$$

BJ

$$y(t) = \frac{B(q)}{F(q)} u(t - nk) + \frac{C(q)}{D(q)} e(t) \quad \text{Eq. 3.11}$$

The above four models are the *auto-regressive with disturbance* (ARX), the *auto-regressive moving-average with disturbance* (ARMAX), the *output-error* (OE) and the *Box-Jenkins* (BJ). What is described above as the 'shift operator polynomials' (ie. *A(q)*) are compact ways of writing difference equations. For example, the expanded ARMAX model is:

$$y(t) + a_1 y(t-1) + \ldots + a_{na} y(t - na) = b_1 u(t - nk) + \ldots + b_{nb} u(t - nk - nb + 1) + e(t) + c_1 e(t-1) + \ldots + c_{nc} e(t - nc) \quad \text{Eq. 3.12}$$

To understand what each of the shift order polynomials represent, it is useful to start with a simple linear relationship:

$$y(t) = G(q)u(t) + v(t) = G(q)u(t) + H(q)e(t)$$
$$= \sum_{k=1}^{\infty} g(k)u(t-k) + H(q)e(t) \qquad \textbf{Eq. 3.13}$$

The function *G(q)* is the transfer function of the system; two additional relationships can be written as:

$$G(q) = \sum_{k=1}^{\infty} g(k)q^{-k}; q^{-1}u(t) = u(t-1) \qquad \textbf{Eq. 3.14}$$

The term *g(k)* is the impulse response of the system; *G(q)* and *g(k)* form a Fourier transform pair. The polynomial *H(q)* is based on describing the noise as a filtered white noise, where *e(t)* is white noise with variance λ, and

$$\Phi_v(\omega) = \lambda\left|H(e^{i\omega})\right|^2 \qquad \textbf{Eq. 3.15}$$

The middle form of Eq. 3.13 presents a time-domain representation of the system. The functions *G(q)* and *H(q)* can then be represented in polynomial form, which will lead to the parametric models described above. In the ARX model this corresponds to:

$$G(q) = q^{-nk}\frac{B(q)}{A(q)}; H(q) = \frac{1}{A(q)} \qquad \textbf{Eq. 3.16}$$

For the ARMAX form in Eq. 3.9, the polynomials can be written in terms of the delay operator q^{-1}:

$$A(q) = 1 + a_1 q^{-1} + \ldots\ldots + a_{na} q^{-na}$$
$$B(q) = b_1 + b_2 q^{-1} + \ldots\ldots + b_{nb} q^{-nb+1} \qquad \textbf{Eq. 3.17}$$
$$C(q) = 1 + c_1 q^{-1} + \ldots + c_{nc} q^{-nc}$$

In Eq. 3.17, the indices *na*, *nb*, and *nc* represent the orders of the respective polynomials. From the second equation in Eq. 3.14, it can be seen how the delay operators in Eq. 3.17, when multiplied by the input (*u(t)*), act to transform the input to a shifted form (*u(t-nk)*).

3.2.1. Model Estimation

The most common way of estimating the parameters in the models above is through a least-squares or prediction error method. The prediction errors are computed as:

$$e(t) = H^{-1}(q)[y(t) - G(q)u(t)] \qquad \text{Eq. 3.18}$$

And it must be solved to minimize the sum of squared errors:

$$V_N(G,H) = \sum_{t=1}^{N} e^2(t) = \sum_{t=1}^{N} \left(H^{-1}(q)[y(t) - G(q)u(t)\right)^2 \qquad \text{Eq. 3.19}$$

Partial derivatives are then taken of Eq. 3.19 with respect to each of the parameters to set up a system of equations to solve.

3.3. State-Space Formulation of Linear Systems

The discussion of the state-space formulation starts with a typical 2nd order multi-degree of freedom system, shown in Eq. 3.4. This form describes the system by accelerations, velocities and displacements simultaneously. The matrix *B* allocates the inputs to the correct DOF's. For a lumped parameter, proportionately-damped system, classical modal analysis can be applied to extract the modal parameters. In this case the three matrices *M*, *C*, *K* are symmetric and typically diagonal. If the 2nd order system can no longer be modeled using proportional damping, the general viscous case must be used. In that case, the modes are no longer classical, or real-valued, and become complex-valued. Now a different approach to the solution is required. Start with the resulting characteristic matrix equation:

$$\left[\lambda^2[M] + \lambda[C] + [K]\right]\{\psi\}e^{\lambda t} = \{0\} \qquad \text{Eq. 3.20}$$

The following substitutions are made to solve Eq. 3.20:

$$x^d(t) = \begin{bmatrix} Z(t) \\ \dot{Z}(t) \end{bmatrix}; P_c = \begin{bmatrix} C & M \\ M & 0 \end{bmatrix}; Q = \begin{bmatrix} K & 0 \\ 0 & -M \end{bmatrix} \qquad \text{Eq. 3.21}$$

So Eq. 3.20 becomes:

$$[P_c]\{\dot{x}^d(t)\} + [Q]\{x^d(t)\} = \begin{bmatrix} B \\ 0 \end{bmatrix}\{u(t)\} \qquad \text{Eq. 3.22}$$

In this formulation, x^d is known as the continuous-time deterministic state vector, which describes the displacement and velocities for each DOF at time *t*. With a solution form of $\{Z(t)\} = \psi e^{\lambda t}$, the solution to Eq. 3.22 becomes:

$$\{x^d(t)\} = \begin{Bmatrix} \psi \\ \lambda\psi \end{Bmatrix} e^{\lambda t} = \{\tilde{\psi}\}e^{\lambda t} \qquad \text{Eq. 3.23}$$

Substituting Eq. 3.23 into Eq. 3.22 gives the generalized eigenvalue problem:

$$[\lambda[P_c]+[Q]]\{\tilde{\psi}\}=\{0\} \qquad \textbf{Eq. 3.24}$$

The eigenvalues and eigenvectors that results from Eq. 3.24 come in conjugate pairs. The above described technique can be referred to as $2m$ space analysis, since it features a state vector that contains the displacements and velocities, or 2x the number of DOF's. In a more general case, n can be infinite and the state vector can be infinite in length. This leads to the traditional discussion of state-space representations.

By left-multiplying Eq. 3.22 by $-[P_c]^{-1}$, A_c and B_c can be defined:

$$x(t)=\begin{pmatrix}Z(t)\\ \dot{Z}(t)\end{pmatrix};A_c=\begin{bmatrix}0 & I\\ -M^{-1}K & -M^{-1}C\end{bmatrix};B_c=\begin{bmatrix}0\\ -M^{-1}B\end{bmatrix} \qquad \textbf{Eq. 3.25}$$

and then substituted into Eq. 3.22 to get the *first-order state equation*:

$$\dot{x}(t)=A_c x(t)+B_c u(t) \qquad \textbf{Eq. 3.26}$$

This describes the internal states of the system. To relate this to observed states (or measurements), a second equation is required to complete the state-space formulation:

$$y(t)=Cx(t)+Du(t) \qquad \textbf{Eq. 3.27}$$

This is known as the *observation equation*. The elements from Eq. 3.26 and Eq. 3.27 are described as follows:

$\dot{x}(t)$ -the continuous time state vector (n x 1; n being the model order)

A_c -the system matrix (as described in Eq. 3.25)

B_c -the input gain matrix (as described in Eq. 3.25)

$y(t)$ -the measured output

C -the observation matrix, which segregates the measured outputs from the rest of the states (m x n; so that no matter how high of a model order is chosen, the information can be related back to the n dof's that were measured)

D -the direct feed-through matrix (which is zero unless accelerations are measured)

The matrices C and D are of the following form:

$$C=\left[L_{Z(t)}-L_{\ddot{Z}(t)}M^{-1}K \quad L_{\dot{Z}(t)}-L_{\ddot{Z}(t)}M^{-1}C\right]$$

$$D=\left[L_{\ddot{Z}(t)}M^{-1}B\right] \qquad \textbf{Eq. 3.28}$$

The model order chosen, n, is essentially the number of DOFs for this representation. For most typical modeling situations, the number of measured DOFs is less. The discrete time stochastic state space representation is formed as:

$$x_{k+1} = Ax_k + w_k;\ y_k = Cx_k + v_k \qquad \textbf{Eq. 3.29}$$

Where w_k and v_k are the *process noise* and *measurement oise* respectively. The process noise accounts for modeling uncertainty. Part of the reason for using the state-space formulation as opposed to the classical one in Eq. 3.4 is in the ease of transition to the discrete time formulation, which is needed for use in measured data, which are always discretized.

It is also noted that the A matrix in the discrete form is not the same as A_c, the continuous form. The relationship is shown in Eq. 3.30. The matrix C however, does not change. It also can be shown that the modal parameters of the system can be taken directly from the eigendecompositon of A_c.

$$A = e^{A_c \Delta t} \qquad \textbf{Eq. 3.30}$$

There are several forms for the stochastic state space model [see Pridham, 2004], some of which include the innovations representation, containing the Kalman states, etc. These deal primarily with load modeling concepts, and are not strictly necessary for the extraction of the A and C matrices as described in Section 3.7.

3.4. Frequency Domain Decomposition (FDD)

There are two system identification methods available in the ARTeMIS Extractor software. The first is the Frequency-domain decomposition method, which is essentially a two-step method. The first step involves signal processing of the data sets, and the second step is a geometric operation on the processed data. To explain this, first start with a set of M time-history records, each described by $a_n(t), 0 \le t < N$. Next perform all of the auto- and cross-spectral densities for each pair of signals in the dataset (there will be MxM pairs). Then assemble these spectral density functions into a 3-dimensional matrix, with an MxM matrix of spectral density pairs for each frequency interval (i). The number of frequency intervals depends on the number of points in the CSD estimates. For an example with 3 measured channels (x, y and z), this would look like the following:

$$SD_{\omega_i} = \begin{bmatrix} SD_{\omega_i}^{xx} & SD_{\omega_i}^{xy} & SD_{\omega_i}^{xz} \\ SD_{\omega_i}^{yx} & SD_{\omega_i}^{yy} & SD_{\omega_i}^{yz} \\ SD_{\omega_i}^{zx} & SD_{\omega_i}^{zy} & SD_{\omega_i}^{zz} \end{bmatrix} \quad \text{Eq. 3.31}$$

The next step is to perform a singular-value decomposition on the matrix $SD_{\omega i}$. This is shown as follows:

$$svd(SD(\omega_i)) = U_i S_i V_i^T \quad \text{Eq. 3.32}$$

Where U_i contains the column singular-vectors, and S_i is a diagonal matrix containing the singular values. The reason that this is a geometric technique is that in the matrix shown in Eq. 3.31, the spectral density values, which give a measure of the energy at that particular frequency step, are only related to pairs of signals. The act of performing a SVD on the matrix, connects all of the points together and now relates an energy amplitude coefficient (the singular value) to a geometric shape which connects all of the points. These geometric shapes essentially represent a set of SDOF systems. For frequencies near a structural mode, the highest singular values will be those associated with that shape. When modes are close, there will be several singular values with significant amplitudes. When a shape is not related to a structural mode, and is possibly related to noise, it will be associated with a low singular value. Completed unrelated shapes would be associated with a zero singular value.

The theoretical derivation of the technique is presented in a paper by Brincker et al., [2000]. The key result is that the spectral density can be written as a sum of the modes that contribute at a given frequency. Typically only one or two modes contribute at any one frequency. This is expressed by:

$$G_{yy}(j\omega) = \sum_{k \in Sub(\omega)} \frac{d_k \phi_k \phi_k^T}{j\omega - \lambda_k} + \frac{\bar{d}_k \bar{\phi}_k \bar{\phi}_k^T}{j\omega - \bar{\lambda}_k} \quad \text{Eq. 3.33}$$

In Eq. 3.33, the over-bar denotes complex conjugate. *Sub(ω)* represents the set of modes that contribute at the frequency ω. This equation shows that the spectral density can be decomposed into its mode shapes, and that is what occurs with the singular value decomposition.

3.5. Stochastic Subspace Identification (SSI)

This method was initially described by Van Overschee and De Moor [1996] and has been reworked and modified by several groups since then. One in particular was Pridham [2004] and

the some of the issues regarding the practical implementation of the technique were discussed in Pridham [2003]. The following discussion comes primarily from the latter paper, and from a recent conference paper by Brincker [2006] that attempts to explain some of the more difficult concepts of the technique.

The first step for the SSI technique is to form the dataset into a Hankel[1] matrix. This is done by transposing the data into row vectors, and creating a subsequent data matrix of size m x n, where m is the number of sensors (channels of data) and n is the total number of datapoints. The data is then put into the Hankel matrix as a 'block-row', with total rows in each block being m. Then the first parameter to be selected by the user is a value i, which is the number of block-rows, also called the *projection horizon*. This will be explained in more detail later.

The total number of rows of the formed Hankel matrix will be $2 \cdot i \cdot m$. The total number of columns (usually denoted by j) is calculated by:

$$j = n - 2 \cdot i + 1 \qquad \textbf{Eq. 3.34}$$

(it is also possible for the user to also select j; the formulation shown would be considered the default). The reason for Eq. 3.34 is as follows: the first block row of the matrix will be truncated to datapoints 1 to n-2i+1. The next block row would contain datapoints 2 to n-2i+2. The next row 3 to n-2i +3, etc. This is essentially shifting the data for each block row. This formulation then requires a minimum amount of data, n, for a specific value of i chosen. The total number of block rows in the matrix is 2i and not i, and that is because the matrix is split in to a past and future horizon. This is common in many identification methods where part of the data is used for the input, and the remainder of the data is the output (ie. part of the data is used to create the model, and the rest is used to validate it). Based on all of this, the form of the matrix, Y, is shown in Eq. 3.35. (with indices starting at zero).

[1] From Mathworld.com: a Hankel matrix is one with constant skew diagonals; ie. if you took the values of the first row and shifted them one to the left, this would be the next row, etc.

Eg: $H = \begin{bmatrix} 1 & 2 & 3 \\ 2 & 3 & 0 \\ 3 & 0 & 0 \end{bmatrix}$

The factor $1/\sqrt{j}$ is to account for scaling during the data projections. The matrix is shown as partitioned into the past horizon (top) and future horizon (bottom).

$$Y_{0|2i-1} = \frac{1}{\sqrt{j}} \left[\begin{array}{cccc} y_0 & y_1 & \cdots & y_{j-1} \\ \cdots & \cdots & \cdots & \cdots \\ y_{i-2} & y_{i-1} & \cdots & y_{i+j-3} \\ y_{i-1} & y_i & \cdots & y_{i+j-2} \\ \hline y_i & y_{i+1} & \cdots & y_{i+j-1} \\ y_{i+1} & y_{i+2} & \cdots & y_{i+j} \\ \cdots & \cdots & \cdots & \cdots \\ y_{2i-1} & y_{2i} & \cdots & y_{2i+j-1} \end{array}\right] \qquad \textbf{Eq. 3.35}$$

A description of the reason for the Hankel matrix formation is given by Brincker [2006]. It relates the formulation to the unbiased estimate of the correlation matrix at time lag *k*, which is shown as the following:

$$\hat{R}_k = \frac{1}{N-k} Y_{1:N-k} Y_{k:N}^T \qquad \textbf{Eq. 3.36}$$

This correlation, *R*, can be created from a single dataset, or even one channel of data, by splitting it into two *Y* matrices, one from datapoints *1:N-k*, and one from *k:N*. This is analogous to *past* and *future*. The resulting correlation gives the free decay of the system, containing all of the required dynamic characteristics. To obtain these correlations, or free decays, the next step of the SSI is to perform the projection on the Hankel matrix.

There are many descriptions and formulations of the orthogonal or oblique projection in the literature, but here we can start with the simplest formulation and then later attempt to describe it in different ways.

The projection, Π, is obtained as follows:

$$\Pi_i = Y_f Y_p^T (Y_p^T Y_p^T)^{-1} Y_p \qquad \textbf{Eq. 3.37}$$

Here Y_f and Y_p refer to the above mentioned future and past partitions of the Hankel matrix. The process shown in Eq. 3.37 projects the row space of Y_f onto the row space of Y_p. The subscript *i* indicates that the projection contains information regarding the states (or state sequence), $\tilde{X}_i = [x_i, x_{i+1}, \ldots, x_{i+j-1}]$.

The projection is mathematically composed of:

$$\Pi_i = \Gamma_i X_f \qquad \textbf{Eq. 3.38}$$

Where Γ is denoted as the observability matrix of the system and X_f is the future state of the system. The form in Eq. 3.38 is actually a column of Π, and can be described as a *stacked free decay*, to unknown initial conditions x. The observability matrix has the following form:

$$\Gamma_i = \begin{bmatrix} C \\ CA_d \\ CA_d^2 \\ \cdots \\ CA_d^{i-1} \end{bmatrix} \qquad \textbf{Eq. 3.39}$$

In this form, the subscript i denotes that the matrix contains all i blocks (or that the state sequence is unshifted).

This matrix, Γ, can be obtained from a singular value decomposition of Π, which is shown to be (typically):

$$\Pi = U \cdot S \cdot V^T \qquad \textbf{Eq. 3.40}$$

$$\Gamma = U \cdot S^{1/2} \qquad \textbf{Eq. 3.41}$$

also

$$X_0 = S^{1/2} \cdot V^T \qquad \textbf{Eq. 3.42}$$

The above three equations are performed on a weighted version of Π, and this is done differently for various forms of the SSI, as described by Pridham [2004]. The weighting matrices are a form of filter applied to the data, and are applied such as:

$$\Pi_{weighted} = W_1 \Pi W_2 \qquad \textbf{Eq. 3.43}$$

W_1 is chosen to be of full rank and W_2 is chosen to obey $rank(Y_p) = rank(Y_p W_2)$.

The Canonical Variate Analysis (CVA) weighting is as follows:

$$W_1 = T_0^{-1/2}; W_2 = I \qquad \textbf{Eq. 3.44}$$

Where T is the Toeplitz covariance matrix of the following form:

$$T_k = \begin{bmatrix} R_k & R_{k-1} & \cdots & R_{k+1-i} \\ R_{k+1} & R_i & \cdots & R_{k+2-i} \\ \cdots & \cdots & \cdots & \cdots \\ R_{k+i+1} & R_{k+1-2} & \cdots & R_k \end{bmatrix} \qquad \textbf{Eq. 3.45}$$

And $T_0 = Y_f Y_f^T$.

From the paper by Brincker [2006], it is shown that by removing one block from the top of Γ and one block from the bottom (shifting the states) to get:

$$\Gamma_{2:i} A_d = \Gamma_{1:i-1} \qquad \textbf{Eq. 4.46}$$

A_d can be found by regression. In the paper by Pridham [2003], this is illustrated by a least squares solution from the state estimates, X. This is essentially the same thing, and is shown in the next section. From Eq. 3.39, it can be seen that the matrix C is extracted from the first block of Γ. For the purposes of obtaining the modes, A_d and C are all that is required. This is done with the following equations:

$$A_d = \Psi[\mu_i]\Psi^{-1} \qquad \textbf{Eq. 3.47}$$

$$\mu_i = \exp(\lambda_i) \qquad \textbf{Eq. 3.48}$$

$$\lambda_i = \frac{\ln(\mu_i)}{\Delta T} \qquad \textbf{Eq. 3.49}$$

$$\omega_i = |\lambda_i| \qquad \textbf{Eq. 3.50}$$

In Eq. 3.47 and Eq. 3.48, μ is the discrete-time poles, or eigenvalues, which are then converted to continuous time in Eq. 3.39. Mode shapes are found from:

$$\Phi = C \cdot \Psi \qquad \textbf{Eq. 3.51}$$

3.5.1. Additional Perspectives on SSI

The complexity of understanding the SSI method comes from an attempt to relate the process to the data and the real physics of the system. The main component is the projection, and an alternative explanation is given by Brincker [2006]. The paper by Pridham [2003] goes through a detailed derivation, and for now this will not be dealt with. Brincker says the following:

When dealing with stochastic responses, projection is defined as a conditional mean: (keeping the notation from Pridham)

$$\Pi = E(Y_f | Y_p) \qquad \textbf{Eq. 3.52}$$

The conditional mean is described completely by its covariances, assuming a Gaussian process. The covariances are given by the first four matrices of Eq. 3.37, while the last matrix represents the conditions.

The least squares solution shown by Pridham [2003] is as follows:

$$\begin{pmatrix} \hat{A} \\ \hat{C} \end{pmatrix} = \begin{pmatrix} \hat{X}_{i+1} \\ Y_{i|i} \end{pmatrix} X_i^* \qquad \textbf{Eq. 3.53}$$

In Eq. 3.42, Xi+1 is the shifted state, which is obtained from:

$$X_{i+1} = \hat{\Gamma}_{i-1}^* \hat{\Pi}_{i-1} \qquad \textbf{Eq. 3.54}$$

Where Γi-1 is obtained by deleting the last l rows of Γi, and the shifted projection is given by $\Pi_{i-1} = Y_f^- / Y_p^+$ and $Y_f^- = Y_{i+1:2i-1}; Y_p^+ = Y_{0:i}$. The asterisk (*) refers to the *pseudo-inverse*.

3.6. Sensitivity-Based Finite Element Model Updating

In Chapter 2, the concept of finite element model updating was introduced. In this research, the specific technique applied is sensitivity-based updating. The actual procedure is automated through the use of sensitivity coefficients [Dascotte et al., 1995]. This works in the following general way. The sensitivity matrix is computed for all of the responses and all of the parameters.

$$\boldsymbol{S = \Delta R / \Delta P} \qquad \textbf{Eq. 3.55}$$

The matrix S contains all of the sensitivity coefficients, ΔR represents the changes in the response values and ΔP represents the changes in the parameters. In generating the sensitivity matrix for a given state of the model, a change in the parameters is prescribed and the resulting changes in responses are observed. The sensitivity coefficients can be computed in a variety of ways, but in general are stated as a ratio as in Eq. 3.55.

Once the sensitivity matrix is computed, parameter changes for a specified response change (ie. differences between the base theoretical model and the real structure) can be determined as follows.

$$\Delta P = S^{-1} \Delta R \qquad \textbf{Eq. 3.56}$$

These obtained parameter changes are applied to the original model, and this becomes the updated model.

The method above is implemented using the FEMTools software. This software has many modules, but the four of interest for this work are the finite element solver, the correlation analysis, the sensitivity analysis and updating module. Discussion of the correlation analysis will be deferred to the next section, and the last two modules are discussed here. Details of the FEMTools formulations are from the FEMTools Theoretical Manual [DDS, 2006].

There are two different ways to compute sensitivities in FEMTools: by differential analysis, and by finite-difference analysis. The formula shown in Eq. 3.55 is representative of the finite-difference method. In differential analysis, the element matrices must be derived. As a result, the differential method is more of a closed-form analysis, and the finite-difference is more of a numerical type.

In addition to these two main types of analysis, the sensitivity coefficients can be evaluated as absolute, relative or normalized. There are also several types of sensitivities. In this current discussion, only the types used for this research will be discussed. First, the general form of differential sensitivity analysis is introduced:

$$[S] = S_{ij} = \left[\frac{\delta R_i}{\delta P_j}\right] \qquad \textbf{Eq. 3.57}$$

In this form, i represents the responses, and j the parameters. Responses always refer to results from the experimental analysis to be used as targets; parameters always refer to those parameters in the FEM to be updated. Three sensitivity coefficients will be discussed here. The first is Resonance Frequency differential sensitivities.

First, the objective function must be derived. This is done by starting with the governing equation for the eigenvalue analysis of an undamped system. Then this equation is diffentiated with respect to the parameter P_j, and pre-multiplied by $\{\psi_i\}^T$. This gives:

$$\{\psi_i\}^T [K] \frac{\delta\{\psi_k\}}{\delta P_j} = \frac{\{\psi_i\}^T}{\delta P_j} [K] \{\psi_k\}$$
$$\{\psi_i\}^T [M] \frac{\delta\{\psi_k\}}{\delta P_j} = \frac{\{\psi_i\}^T}{\delta P_j} [M] \{\psi_k\} \qquad \textbf{Eq. 3.58}$$

For $i = k$ the following expression is obtained:

$$\frac{\delta f_i}{\delta P_j} = \frac{\{\psi_i\}^T \left(\frac{\delta[K]}{\delta P_j} - 4\pi^2 f_i^2 \frac{\delta[M]}{\delta P_j} \right) \{\psi_i\}}{8\pi^2 f_i \left(\{\psi_i\}^T [M] \{\psi_i\} \right)} \qquad \textbf{Eq. 3.59}$$

Eq. 3.59 results in the differential sensitivity of the resonance frequency. It contains two terms, one for the changes in the stiffness, and one for changes in the mass.

The second of the three is the mode shape differential sensitivities. This sensitivity vector is considered to be a combination of the N lowest mode shapes:

$$\frac{\delta\{\psi_i\}}{\delta P_j} = \sum_{k=1}^{N} a_k^i \{\psi_k\} \qquad \textbf{Eq. 3.60}$$

To find the expression a, a similar derivation to the previous can be used. It will not be presented here, instead the final expression is:

$$a_k^i = -\frac{1}{2} \{\psi_i\}^T \frac{\delta[M]}{\delta P} \{\psi_i\} if k = i \qquad \textbf{Eq. 3.61}$$

The last of the three is the MAC-Value differential sensitivities. The concept of MAC will be introduced in the next section, but for completeness the sensitivity is stated here:

$$\frac{\delta MAC}{\delta P} = 2 \left[\frac{\{\psi_e\}^T \{\psi_a\} \frac{\delta\{\psi_a\}}{\delta P}}{\{\psi_e\}^T \{\psi_e\} \{\psi_a\}^T \{\psi_a\}} - \frac{\left(\{\psi_e\}^T \{\psi_a\} \right)^2 \{\psi_a\}^T \frac{\delta\{\psi_a\}}{\delta P}}{\{\psi_e\}^T \{\psi_e\} \left(\{\psi_a\}^T \{\psi_a\} \right)^2} \right] \qquad \textbf{Eq. 3.62}$$

For the finite difference sensitivities, the more formal presentation is:

$$\frac{\Delta R_i}{\Delta P_j} = \frac{R_i(P_j + \Delta P_j) - R_i(P_j)}{\Delta P_j} \qquad \textbf{Eq. 3.63}$$

The form of the three cases above is the same, except that in each case the partial derivative, δ, is replaced by the change, Δ. For this type of analysis, two things must be considered. Since the sensitivity is based on the step ΔP_j, and this is not known a priori, it must be estimated. The second consideration is that the sensitivity matrix is formed column after column, one at a time. For resonance frequency sensitivities, this requires two eigenvalue solutions for each column.

3.6.1. Correlation of Experimental Model to Finite Element Model

The correlation analysis module is used to compare the experimental results with the finite element module. This module contains many features, such as mode shape expansion and truncation, and mode shape scaling, but for this section we will focus only on the correlations. The main feature is global mode shape correlation, and the formula used is the modal assurance criterion (MAC). This is a measure of the squared cosine of the angle between two mode shapes. Its equation is:

$$MAC(\psi_a,\psi_e)=\frac{\left|\{\psi_a\}^T\{\psi_e\}\right|^2}{\left(\{\psi_a\}^T\{\psi_a\}\right)\left(\{\psi_e\}^T\{\psi_e\}\right)} \qquad \textbf{Eq. 3.64}$$

MAC values are normalized to a value of 1 of the modes are identical; 0 if they are orthogonal. Several other correlation methods are available, but the next most important aspect of the module to discuss is the concept of the correlation coefficients. These coefficients are based on errors of responses, and are used in the updating procedure as convergence criterion. One example would be the average MAC values (MACMEAN):

$$CC=1-\frac{1}{M}\sum_{i=1}^{M}C_{R_i}MAC_i \qquad \textbf{Eq. 3.65}$$

The term C_R is the relative error on the response value.

3.6.2. Model Updating Procedure

The general updating procedure that is given in Eq. 3.56 can be rewritten in terms of the response change, and then expressed in terms of a Taylor series expansion truncated to the linear term:

$$\{R_e\}=\{R_a\}+[S](\{P_u\}-\{P_o\}) \qquad \textbf{Eq. 3.66}$$

For the above expression, the subscripts refer to experimental, analytical, updated, and original. Three parameter estimation techniques can be used. The first is the pseudo-inverse method. The idea is to solve for the parameters by inversion of the sensitivity matrix, as in Eq. 3.56.

However, if the number of parameters is lower than the number of equations, which is usually the case, the sensitivity matrix is not invertible. It can be done using the pseudo-inverse concept. In the following expression, the + sign denotes pseudo-inverse.

$$\{\Delta P\} = [S]^{+}\{\Delta R\} = \left([S]^{T}[S]\right)^{-1}[S]^{T}\{\Delta R\} \qquad \textbf{Eq. 3.67}$$

This expression can be solved using a least-squares method. The next technique for updating is by the use of Bayesian parameter estimation. It is a similar form except that it includes weighting coefficients on the parameters and responses. The updating is done by minimizing a weighted error as follows:

$$E = \{\Delta R\}^{T}[C_R]\{\Delta R\} + \{\Delta P\}^{T}[C_P]\{\Delta P\} \qquad \textbf{Eq. 3.68}$$

The error is minimized through the following algorithm:

$$\{P_u\} = \{P_o\} + [G]\{-\Delta R\} \qquad \textbf{Eq. 3.69}$$

where the gain matrix, G, is

$$[G] = [C_P]^{-1}[S]^{T}\left([C_R]^{-1} + [S][C_P]^{-1}[S]^{T}\right)^{-1} \qquad \textbf{Eq. 3.70}$$

This form of the gain matrix only applies is there are more parameters than equations, which is generally the case. In Eq. 3.68 and Eq. 3.70, the C matrices represent diagonal matrices containing confidence values, either for the parameters or the responses (depending on the subscript shown). These values are designated by the analyst, using their judgment. The final updating method is a Weighted Least Squares parameter estimation. This is achieved if [CP]=0, then the gain matrix becomes:

$$[G] = \left([S]^{T}[C_R][S]\right)^{-1}[S]^{-1}[C_R] \qquad \textbf{Eq. 3.71}$$

3.7. Damage Locating Vector (DLV) Technique

The DLV method is a 2-stage method for damage detection. First, the flexibility matrices are extracted from various cases of measured structural states. Then, a set of DLV's are extracted from the change in the flexibility matrices, and are applied as loads to the structure. These DLV's are arranged in a way so that the resulting stresses in the structure are zero (or close to) over the damaged members. In other words, those are the members that do not participate in the resistance to those loads.

First it is useful to understand the deterministic version of the method, that is to say when input data is available and the scaled flexibility matrices can be determined. The simplest explanation of the concept is offered by Zonta and Bernal [2006]. In this paper, the flexibility matrix of a system is described as:

$$\alpha = \Phi\Omega^{-1}\Phi^{T} \qquad \textbf{Eq. 3.72}$$

Eq. 3.72 contains both the system eigenvalues, ω^2, on the diagonal of Ω, and the scaled mode shapes Φ. These can be obtained from a real structural system using some form of forced-vibration testing.

The next step in the DLV method is to compute a change in flexibility, ie. $\Delta\alpha$. This requires the computation of flexibility for a known 'linear', or baseline, undamaged state of the structure, and then some future, unknown state (potentially damaged). The next step is to perform a singular value decomposition (SVD) on the $\Delta\alpha$ matrix, and find the 'null' singular values. These null values are either identically zero or within a user specified tolerance. Those null values then relate to singular vectors (from the same SVD), and these are the DLV's. These DLV's are taken to be loads applied to the structure as mentioned previously. While computationally simple, the theory is more complex, and is introduced by Bernal [2002].

Start with the idea that flexibility (F) multiplied by a force (p) gives a displacement:

$$F \cdot p = x \qquad \textbf{Eq. 3.73}$$

Next take the structure as above (Eq. 1), and consider a vector of loads L applied:

$$\alpha \cdot L = X \qquad \textbf{Eq. 3.74}$$

Where X is a matrix of displacements, given at the measured dof's of the structure (The flexibility matrix α is also given in terms of the measured dof's).

Next consider 2 states, call them α_U, the undamaged flexibility, and α_D, the (potentially) damaged flexibility. Consider the case where the vector of loads, L, applied to each state, produces the same displacements.

$$\alpha_U \cdot L = \alpha_D \cdot L; \qquad \textbf{Eq. 3.75}$$

or

$$(\alpha_U \cdot L) - (\alpha_D \cdot L) = 0 \qquad \textbf{Eq. 4.76}$$

Which leads to:

$$(\alpha_U - \alpha_D)\, L = 0; \qquad \text{or} \qquad \Delta\alpha \cdot L = 0 \qquad \textbf{Eq. 3.77}$$

What this means is that the damaged members, or at least those that exhibit some change, do not participate in the static behaviour of the structure due to the applied loads. Otherwise the displacements would not be equal. So from Eq. 3.77, one can infer that either $\Delta\alpha = 0$, which would imply there is no change and hence no damage, or that $\Delta\alpha$ is rank deficient[2] and that L is a basis for the null space[3] (L being zero is meaningless). The general form $A \cdot x = 0$ is used to find the null space (solving for x), but the most efficient way is through a singular value decomposition of that matrix. In this case, that becomes:

$$\Delta\alpha = [U] \cdot \begin{bmatrix} S_r & 0 \\ 0 & 0 \end{bmatrix} \cdot \begin{bmatrix} \tilde{V}^T \\ L^T \end{bmatrix} \qquad \textbf{Eq. 3.78}$$

The matrix containing the singular values is shown in partitioned form, with the zero values representing the null space in the lower right corner. These are then associated with the lower set of row vectors in the right matrix, designated by L^T. These are the DLV's.

These loads L are then applied to a FEM of the structure, and a static analysis can be performed. Over several different DLV's, the stresses in the undamaged elements may vary, but the ones that are damaged will always be zero or close to it. The paper by Zonta and Bernal (2006) gives a good simple example of a determinate and an indeterminate case. Another issue covered in that paper is with regards to the situation where you have less modes than measured dof's. (ie. the mode matrix is tall). When Eq. 3.72 is formed, the flexibility will only be an approximation. From their example, the truncated matrix was not much different from the exact one, and the main difference was that there were no exact zero values that resulted from the singular value decomposition. In those cases a threshold value was used to determine the approximate null space.

---

[2] Rank deficiency occurs when the rank of a matrix is less than its order; rank being the number of linearly independent rows and order being the number of variables, or columns. In this case that is the number of sensors.

[3] The null space of A is the vector x satisfying the following relation: $A \cdot x = 0$. It forms one of the fundamental subspaces of a matrix. The vectors spanning the null space can be found from $\text{svd}(A) = U \cdot S \cdot T^T$, where the singular vectors in T corresponding to the null singular values in S span the null space. These vectors form the basis for the null space.

There are a few practical issues with the DLV method, one in particular is how to find ΔF when the input is not known. Two methods are available to finding the equivalent unscaled ΔF, and they are presented next. Several points can be made about the DLV technique in genearl:

i) Since the available datasets are not perfect, finding the exact null space and hence exact zero singular values is usually not possible. As a result, a threshold to determine the null space must be used; for example normalizing the singular values to maximum 1 and then taking all values less than 0.1 as the null space.

ii) Flexibility matrices that are formed from a set of modes that is less than the number of sensors or DOF's used creates a rank deficient matrix. This will result in a matrix with a null space equal to the order of rank deficiency. Any vectors that are associated with this pre-existing null space will not be DLV's. Therefore it is important to carefully consider the number of sensors to use in the analysis when a limited number of modes are available.

iii) The DLV technique actually works by excluding members that are not damaged; for each DLV that is applied, any member that is not damaged has a normalized stress about the threshold value. Any members that remains after the application of all DLV's define the potentially damaged set.

3.8. Stochastic Damage Locating Vector (SDLV) Technique

In the DLV technique as it was explained in Section 3.7, scaled mode shapes are required to form the flexibility matrices. In output-only or ambient vibration applications, the scaled mode shapes are not available. Therefore, an 'equivalent' flexibility matrix must be found; two ways of determining this from unscaled modes are used in this thesis. The first is the Stochastic Damage Locating Vector technique [Bernal, 2006]. Once the equivalent flexibility is found, the remainder of the DLV techniques applies as before. The accuracy of these methods is dependent only on the approximation of the flexibility; if the flexibility is exact than the DLV technique will provide exact results.

The method can be best described by the following steps:

1. Obtain the discrete time state-space matrices, A_d and C.
2. Truncate the identified model order to be $\leq 2m$. (m being the number of measurements.)
3. Form the matrices H_p and L according to:

$$H_p = \begin{bmatrix} C_c \cdot A_c^{1-p} \\ C_c \cdot A_c^{-p} \end{bmatrix}; L = \begin{bmatrix} I \\ 0 \end{bmatrix}$$ **Eq. 3.79**

4. Compute Q:

$$Q = -C_c \cdot A_c^{-(p+1)} \cdot H_p^* \cdot L$$ **Eq. 3.80**

(indicates pseudo-inverse)*

5. Q is computed for both the undamaged case, Q_u, and the potentially damaged case, Q_d
6. Compute:

$$\Delta Q = Q_d - Q_u$$ **Eq. 3.81**

7. Compute the svd of ΔQ^T
8. The DLV's are taken to be the right-side singular vectors associated to the null-singular values (or within tolerance).
9. Apply the DLV's to the appropriate dof's to a linear model and evaluate the stresses.

The steps 6 to 9 are similar to that of the deterministic DLV method, so this discussion will focus on the development of the first 5 steps.

The essential problem with the DLV method in the stochastic case, is that the modes identified can not be scaled, and as a result the flexibility matrices can not be obtained. More specifically, for the state-space formulation, the matrix B_c can not obtained. This can be circumvented by applying a number of constraints to the problem.

The derivation is based on looking explicitly at various cases dependent on the measurement type, be it displacement, velocity or acceleration. Each of these has a different effect on the observation equation Eq. 3.27. Starting with the case where the measurements are displacements, and there will be no direct transmission (ie. $D = 0$):

$$y = C_c^{dis} x$$ **Eq. 3.82**

Then differentiating and substituting Eq. 3.26, and then repeating gives the following two equations:

$$\dot{y} = C_c^{dis} A_c x + C_c^{dis} B_c u$$ **Eq. 3.83**

$$\ddot{y} = C_c^{dis} A_c^2 x + C_c^{dis} A_c B_c u + C_c^{dis} B_c \dot{u} \quad \textbf{Eq. 3.84}$$

Since there also is no direct transmission for velocity, from Eq. 3.83, it is apparent that:

$$C_c^{dis} B_c = 0 \quad \textbf{Eq. 3.85}$$

And by definition:

$$D_c = C_c^{dis} A_c B_c \quad \textbf{Eq. 3.86}$$

Eq. 3.85 shows that B_c is in the null space of C and Eq. 3.86 provides a relationship between B_c and D_c. To complete the derivation of Eq. 3.79 the following process is valid:

$$C_c^{vel} = C_c^{dis} A_c \quad \textbf{Eq. 3.87}$$

$$C_c^{acc} = C_c^{vel} A_c \quad \textbf{Eq. 3.88}$$

$$C_c^{dis} B_c = C_c^{vel} A_c^{-1} B_c = C_c^{acc} A_c^{-2} B_c = 0 \quad \textbf{Eq. 3.89}$$

$$C_c^{dis} A_c B_c = C_c^{vel} B_c = C_c^{acc} A_c^{-1} B_c = D_c \quad \textbf{Eq. 3.90}$$

Eq. 3.89 and Eq. 3.90 can be rewritten in compact form, with $p=0$ for measured displacements, $p=1$ for velocities, and $p=2$ for accelerations.

$$C_c A_c^{-p} B_c = 0; C_c A_c^{1-p} B_c = D_c \quad \textbf{Eq. 3.91}$$

The two equations of Eq. 3.91 can be combined to write:

$$H_p B_c = L D_c \quad \textbf{Eq. 3.92}$$

And H_p and L are given above by Eq. 3.79. The general solution of Eq. 3.92 is:

$$B_c = H_p^* L D_c + V \cdot g \quad \textbf{Eq. 3.93}$$

If the model is truncated so that the model order n is no larger than twice the number of sensors, m, V will vanish from Eq. 3.93. The truncation will be explained later. Therefore, Eq. 3.93 presents a way to find B_c without knowledge of the inputs. It is apparent however, that the matrix D_c is unknown; but due to several conditions and the fact that:

$$F = -C_c A_c^{-(p+1)} B_c \quad \textbf{Eq. 3.94}$$

Where F is the flexibility. Subsitituting Eq. 3.93 (with Vg = 0) into Eq. 3.94 gives:

$$F = Q D_c \quad \textbf{Eq. 3.95}$$

Where Q is given by Eq. 3.80. The trick is that D_c need not be explicity know since what is important is ΔF, and through a few more computations it can be shown that all that is important is ΔQ^T. For the complete derivation see Bernal [2006].

3.8.1. Truncation of A and C

It is noted that to have V vanish from Eq. 3.93 the model order n must be no larger than twice the number of measurements, m. One way to truncate the model is as follows:

From the standard eigendecompostition:

$$A_{n,n} = \Phi\Lambda\Phi^{-1} \qquad \textbf{Eq. 3.96}$$

Say truncate to $2m$:

$$A_{2m,2m} = \Lambda_{2m} \qquad \textbf{Eq. 3.97}$$

Eq. 3.97 states that the new matrix, $A_{m,m}$ is simply the diagonal matrix Λ taking those eignevalues of interest (totaling $2m$).

The new matrix C is the old C multiplied by the columns of Φ associated with the $2m$ eigenvalues:

$$C = C\Phi_{2m} \qquad \textbf{Eq. 3.98}$$

The reason that Eq. 3.97 is described as 'the eigenvalues of interest' is that the results of the eigendecomposition are not always in the exact order necessary, so they may not be the first $2m$ eigenvalues, rather an arbitrary $2m$ eigenvalues of the original set of n.

3.9. Proportional Flexibility Matrix Technique

The second method of obtaining the equivalent flexibility from output-only data is the the Proportional Flexibility Matrix (PFM) technique. The PFM technique is based on the idea that although the scaled flexibilities can not be determined from output only data, a proportional matrix that differs only by a scalar can be found. The complete derivation shown here is presented by [Duan et al., 2005]. The idea of a proportional matrix was also presented in [Bernal, 2004]. The fundamental concept of the PFM technique is that the mode shapes obtained in the output only analysis, although unscaled for the measured structure, can be

considered scaled to some other, 'dummy', structure. The mass matrix, M_r, from the dummy structure can then be obtained from the typical mass scaling relationship:

$$\Phi^T M_r \Phi = I \qquad \textbf{Eq. 3.99}$$

Then setting up the eigenvalue problem for both the dummy and real structure, and then adding the two equations, one gets:

$$\left(M_r - \frac{1}{r_i^2} M_0 \right) \phi_i = 0 \qquad \textbf{Eq. 3.100}$$

Assuming that the real mass matrix, M_0 is diagonal, the equation in this form contains one more unknown than available equations. The modal scaling factor r cannot be identified at all with the output only analysis. To deal with this, M_0 is scaled by a factor r_m so that the elements are normalized to a maximum of 1. Then a new term $\eta = r_i^2 r_m$ is created, and Eq. 3.100 becomes, with the normalized real mass matrix:

$$\left(M_r - \frac{1}{\eta_i} \overline{M}_0 \right) \phi_i = 0 \qquad \textbf{Eq. 3.101}$$

Now that there are enough equations for the variables, the η term can be found for each mode. The flexibility matrix can now be formed as:

$$F = \frac{1}{r_1^2} \sum_{i=1}^{N} \frac{1}{\gamma_i^2 \omega_i^2} \phi_i \phi_i^T \qquad \textbf{Eq. 3.102}$$

where $\gamma_i = \frac{\eta_i}{\eta_1}$. The form in Eq. 3.102 is the scaled flexibility with the first modal mass, r_1. The summation term can be referred to as the *proportional flexibility matrix*. The change in flexibilities can then be written as:

$$\Delta F = \frac{1}{r_1^2} \left(F_{pu} - \frac{r_{1u}^2}{r_{1d}^2} F_{pd} \right) \qquad \textbf{Eq. 3.103}$$

The term in brackets can be referred to as the proportional change in flexibility, ΔF_p. Two considerations are made to finalize the PFM technique:

i) since ΔF_p and ΔF differ only by a scalar, they will contain the same null space. Therefore the DLV's can be obtained from a singular value decomposition of ΔF_p.

ii) Eq. 14 contains the first modal masses (r_{1u}, r_{1d}) for the undamaged and damaged cases; these can be replaced by $\frac{\eta_{1u}}{\eta_{1d}}$, but only if the factor r_m is the same for both cases. This means that the element chosen for normalization must remain unchanged from the undamaged to the damaged states.

Chapter 4. Overview of the Implementation Method

This chapter introduces the implementation method in more detail. Section 4.1 will first describe the concept; Section 4.2 will describe the Calibrated Damage Simulations; Section 4.3 will describe the Damage Detection Methodology and Section 4.4 presents details of the overall process of the implementation method.

4.1. Concept of the Implementation Method

To describe the implementation method, it is first useful to establish the goals for the final SHM system. The system that is desired would operate schematically as shown in Figure 4.1.

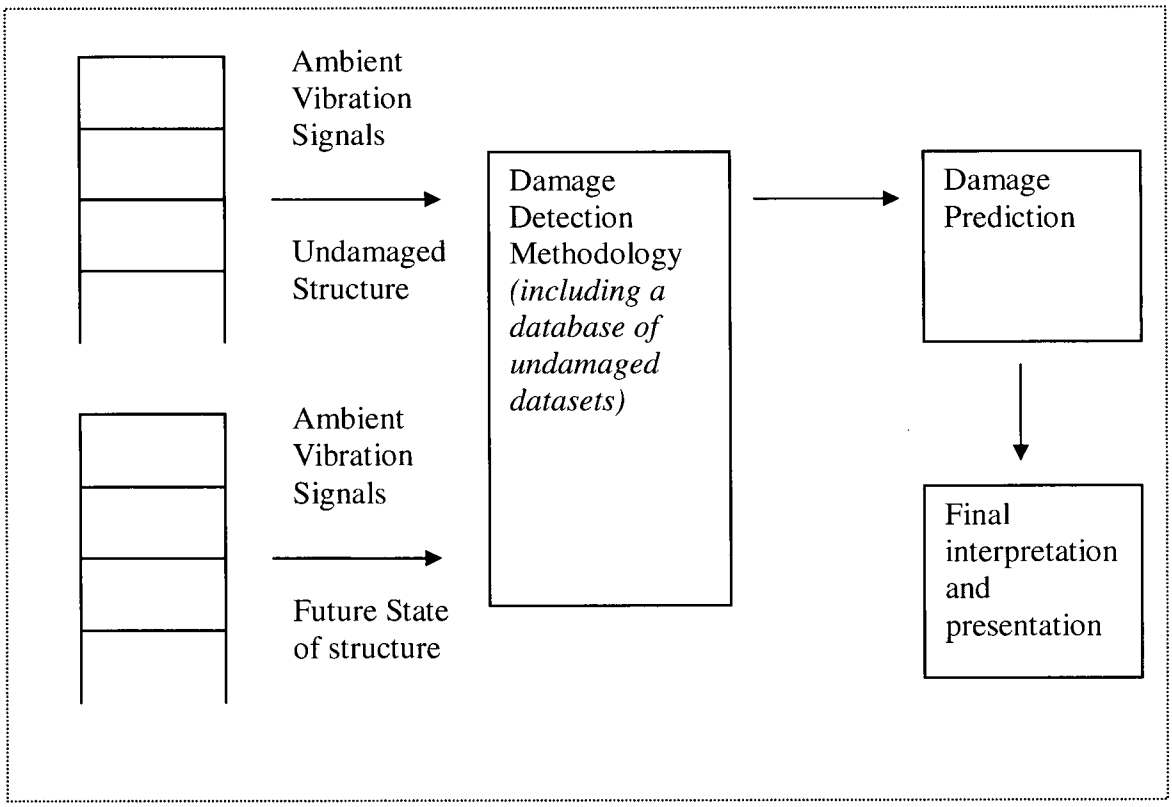

Figure 4.1: SHM System Concept

The system is based on the measurement of ambient vibration signals, and a database of vibration data is required for the undamaged state of the structure. Then ambient vibration signals from a future state of the structure are obtained. The signals from the future state are processed with the DDM comparing the structure to its known undamaged state. A damage prediction is made, and then the results are interpreted and presented to the user of the system.

One of the difficulties with the implementation of a these systems is with the performance of the damage detection methodology. There are many different vibration-based damage detection algorithms, but as it has been discussed in this thesis, it is difficult to determine whether these algorithms will work with real structures. The primary goal of this research therefore is to explore the idea of developing a method to implement those algorithms in a real system. Since the primary obstacle for implementation is evaluating these algorithms and determining if they will work, then consequently the method focuses on evaluating the damage detection algorithms.

The development of the implementation method began originally with the idea of developing a framework for a health monitoring system; this framework attempted to look at the application of the technology, offering all of the information that an owner or engineer might need. The fundamental idea was that this system would require a fusion of technologies, including software and sensor types.

The second evolution of the project dealt with the evaluation of the damage detection methodology. When working with various damage-detection techniques, it is relevant to examine the simulations that were used to develop them. As a result an improvement in the simulation techniques was explored, particularly regarding the noise and errors in the signals. This was done by using parametric models in the time domain, and also in the frequency domain. In the end it was determined that the benefit gained from the proposed technique was too minor (see Chapter 5); particularly that the noise did not have a major effect on the analysis, and that it was not possible to deal properly with the errors with the technique. A simpler way of improving the simulations was then developed, which focused more on the application of ambient vibration results on the simulations.

The third and current evolution of the project came about with an assessment of the main question trying to be addressed, which is essentially how to apply this technology into practice. By examination of the two main ideas (ie. the damage detection and the simulations), it became evident that they could be combined to create a method for implementation. The two main components of the implementation method then are the design of the damage detection methodology (DDM) and the development of the set of calibrated damage simulations (CDS).

These are each described in more detail in the next few sections, and then lastly a description of how the implementation method is intended to work as a whole. Details of the CDS method are presented in Chapter 5 and the DDM is presented in Chapter 6.

4.2. Calibrated Damage Simulations

The development of the calibrated damage simulations (CDS) is the first key concept of the implementation method. One of the main ideas behind this project is that the DDM must be properly evaluated; the best way to do this would be to damage the building of interest and obtain real datasets. Since this is not feasible for a real structure, a simulation must be performed. The idea of the calibrated simulations is that they will reproduce as closely as possible the actual measured vibrations of the structure. They are calibrated using the results of an ambient vibration test on the undamaged operating state of the structure. Then a FEM of the structure is constructed, and ambient vibration simulations are performed with the model using various aspects of the AVT to calibrate the results.

The CDS method is divided into several steps, described as follows:

1. An ambient vibration test of the building is performed; the sensor set up should be close to that of the final SHM system that is to be created.
2. An FEM is designed and updated by correlation with the frequencies and modes from the AVT.
3. The FEM is used for the simulations. In the simulations, several things can be used from the AVT:
   i. the modal damping estimates
   ii. the simulation input; created by using the actual measured ground level vibrations in combination with a random white noise signal.
4. Damage cases must be chosen as to best represent the likely damage scenarios expected; it is useful to consult with the design engineer for this phase.
5. Once the datasets have been created, noise is added to the signals. The noise is created from a random white noise that has been 'coloured' by fitting with a trendline obtained from the measured signal spectrum. This is done to ensure that the noise affects the entire signal bandwidth in a similar way.
6. The sensor locations must be chosen, typically based on the AVT layout.

7. The final datasets are created by extracting time history records from the chosen sensor set locations.

Details of the development of the CDS are presented in Chapter 5. It is illustrated using the IASC/ASCE Benchmark Frame, since there are real damaged datasets available.

4.3. Damage Detection Methodology

The development of the DDM is the second key concept of the implementation method. The main philosophy behind the damage detection methodology for this thesis is that it combines multiple damage detection algorithms. This is done in acknowledgment of the fact that the available damaged detection techniques each have advantages and disadvantages; the disadvantages typically prevent them from being used in a practical application. The concept of combining these techniques together is an attempt to exploit the advantages of each algorithm. The goal is to achieve a DDM that is both robust and accurate, and able to be implemented on a real structure. The methodology that is presented in this thesis uses two damage detection algorithms as the primary 'core' of the methodology, then the predictions are processed statistically, and last filtered through a third damage detection technique in an attempt to eliminate false predictions.

It is typical practice to begin the development of a DDA using simple examples; in this project, the DDM is developed in the same way. Then the methodology is 'evolved' to adapt to more complex examples; this will be illustrated in Chapter 6.

4.4. Implementation Method

Once the two main components have been developed, iterations of the implementation method can be performed. The method is described in detail as in Figure 4.2. The first step is to choose the initial sensor layout for the building. Then the simulated datasets from those points in the FEM are extracted, and processed with the DDM. If the results are not satisfactory, the process is iterated in one of two ways. If the results are incorrect but reasonable, then the sensor layout can be iterated. This is considered the optimization process of the method; the optimal layout of the sensors (ie. minimal number to find the damage) can be determined. If the results are incorrect and not satisfactory, iterations of the DDM can be made. A minor iteration is

considered to be modification of the settings within the DDM, such as DLV threshold. A major iteration is one that may require addition or removal of a damage detection algorithm.

Once the damage predictions are correct, the outputs of the method can be presented. The implementation method provides information regarding the evaluated DDM and all of its settings, and the optimal layout of the sensors for the DDM. It is noted that the optimization of the sensor layout discussed here is based on the requirements of the DDM, and is unrelated to other methods of optimization of sensor layout, such as for modal identification.

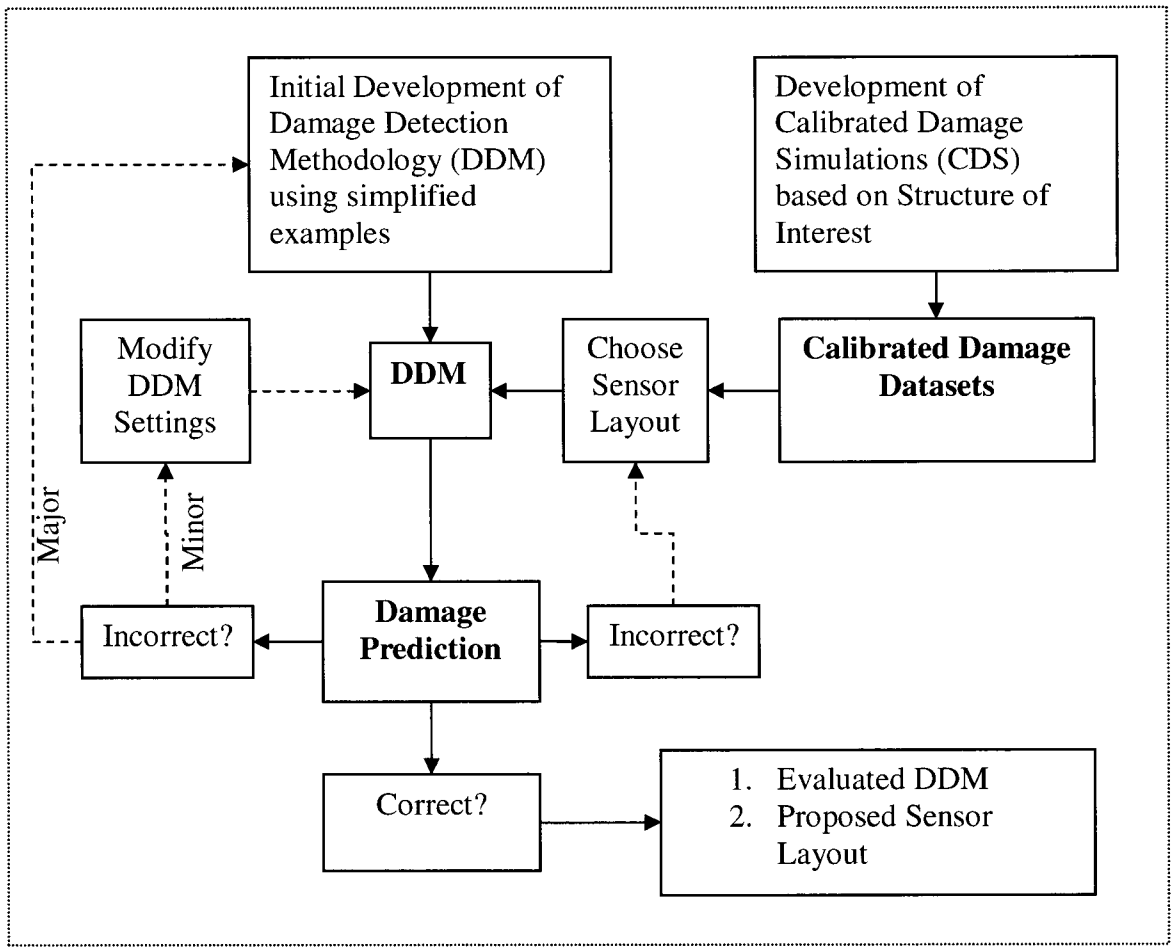

Figure 4.2: Implementation method

Chapter 5. Development of the Calibrated Damage Simulations

One of the important aspects of the development of SHM technology is to address the means of evaluating its essential component, the damage detection techniques. There are two ways to accomplish this: either by performing a physical test or by a simulation. The physical test can be performed on either a laboratory structure [Ventura et al., 2003] or on a real structure that can be damaged [Maeck and De Roeck, 2003]; or from actual data from a real damaging event [Bernal and Hernandez, 2005]. Physical tests tend to be rare and expensive, and can provide limited knowledge for a small number of cases. Simulations are much easier to implement, and can offer almost infinite possibilities for damage cases and sensor setups. However, the primary difficulty with simulations is determining their level of realism.

This chapter describes a method to create a calibrated simulation based on utilizing the results of an ambient vibration test. Various results from the ambient test can be used, such as the modes and frequencies for updating of the FEM, the measured ground vibrations for use as input, the real damping values obtained, and a better characterization of the measured noise. The method will be described using as an example the frame from the IASC/ASCE SHM Benchmark study.

5.1. Illustrative Example: IASC/ASCE Benchmark Frame

In order to evaluate various damage detection methods, a benchmark problem based on a scale-model steel-framed building at the University of British Columbia was established in 1999. The concept of the study was to provide various groups with vibration data from damaged and undamaged cases of the frame and allow the groups to perform analysis based on their methodologies and report the results. The benchmark problem was created by the International Association of Structural Control (IASC) and the American Society of Civil Engineers (ASCE) SHM Task Force. The frame is referred to in this thesis as the 3D frame.

The 3D frame is a four-storey, two-by-two bay, one-third-scale model that has been used for various structural engineering research studies. A photo of the frame is shown in Figure 5.1. It is 3.6m high with total width of 2.5m. Each floor is 0.9m high, and each bay is 1.25m wide. The frame is composed of hot rolled 300W steel members. The columns are B100x9 sections

and the beams are S75x11 sections. For in-plane floor stability, 50mm square tubes are used. For in-plane lateral stability of the entire frame, pairs of 12mm threaded diagonal steel rods are used. Floor mass is simulated using sets of four steel plates, the first three floors having a mass of 454kg each, and the top floor having a mass of 340kg. A schematic of the frame in plan is shown in Figure 5.2. The schematic defines the directions that are referred to as the 'weak' (W) and 'strong' (S) axes, which makes reference to the orientation of the columns.

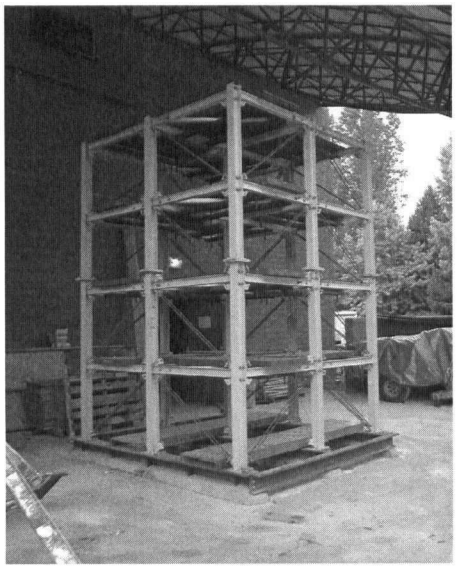

Figure 5.1: Photo of Frame – SE corner

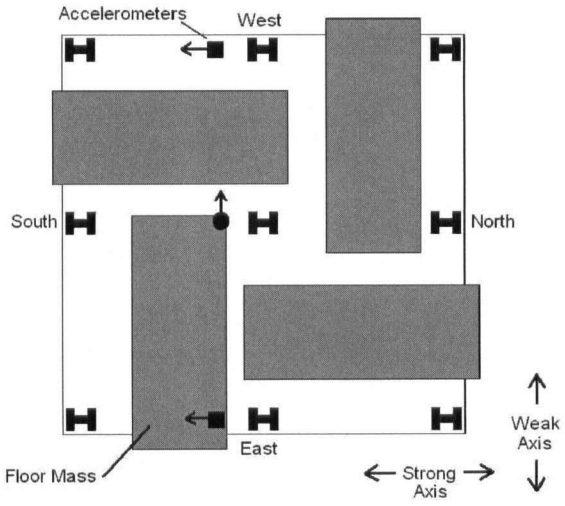

Figure 5.2: Floor Schematic

In August 2002, the steel frame was set up outside of the Structures Lab at the University of British Columbia, and a series of tests were performed. The structure was tested using forced and ambient testing techniques to capture the dynamic characteristics of the frame in the undamaged state and various damaged configurations. A series of damage cases were implemented based on removing the cross-bracing and loosening the beam-to-column connections. Full details of these tests are presented in the next section. These tests were referred to as the second experimental phase; a previous test was performed in 2000.

5.2. Ambient Vibration Test of 3D frame

The second experimental phase included shaker, hammer and ambient vibration tests on undamaged and damaged configurations of the frame. A total of 10 configurations of the frame were tested, each by all three methods. The configurations are described by Table 5.1 and Figure 5.3. Table 5.1 defines the configuration number, and the braces that were removed to

simulate damage. Case 1 was the undamaged state of the frame. It is noted that a second set of damage cases, based on the frame with all of the braces removed, were created to examine the damage to connections. These are not presented here, however, the datasets from the unbraced-undamaged configuration was used in the design of the FEM of the frame. That will be described in Section 5.3. Full detail of the tests can be found in [Turek and Ventura, 2005].

To measure the structural response, fifteen force-balance accelerometers were placed on the structure. A line of sensors was placed along a floor of the frame as shown in Figure 5.2. Two sensors were placed at the outside edges measuring the strong direction response, and one sensor was placed in the centre measuring the weak direction response. The torsional modes would be captured by the out-of-phase motions of the two sensors in the strong-direction. This is a typical measurement layout for a building. For the ambient vibration tests the shaker was turned off and the ambient vibration of the structure was recorded for several minutes. The ambient vibration data was analyzed using the ARTeMIS Extractor software. The dynamic characteristics were obtained using the FDD technique.

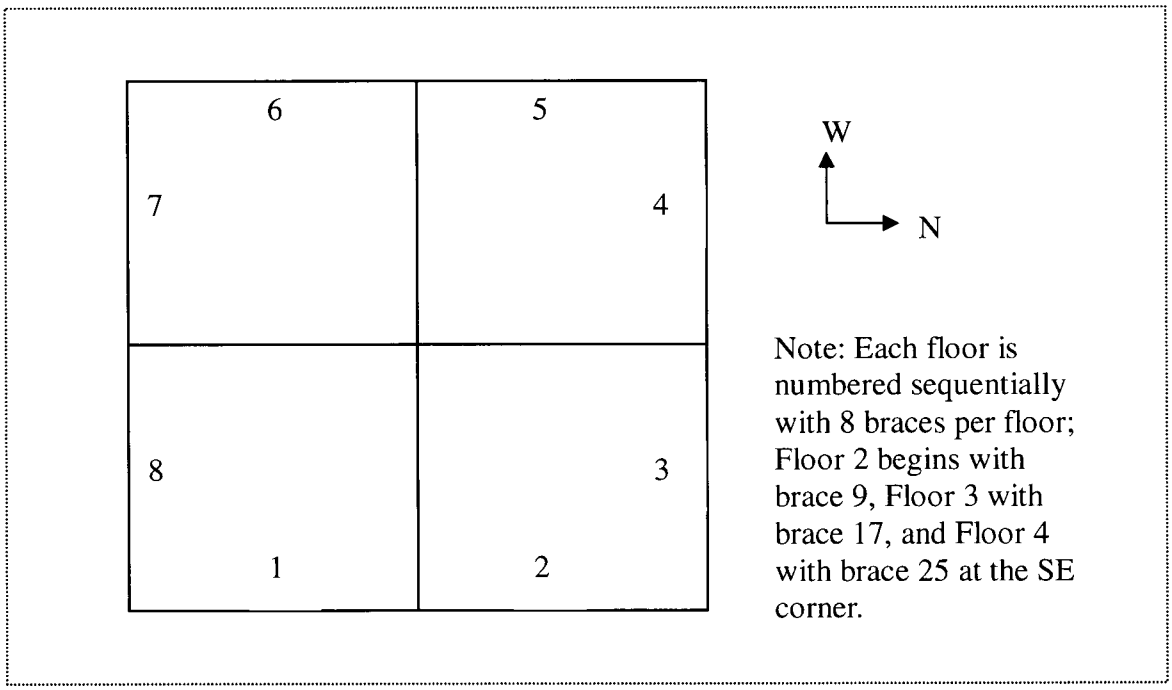

Figure 5.3: Brace Numbering – Plan View of Typical Floor

Table 5.1: Damage Configuration Details

Configuration	Brace(s) removed
1	None
2	1, 2, 9, 10, 17, 18, 25, 26 (Entire East face)
3	1, 9, 17, 25 (Entire south bay, East face)
4	1, 25
5	1
6	11, 12 (North face second storey)

Table 5.2 summarizes the modal frequencies for the first 6 cases. A plot of the first three singular value lines is shown in Figure 5.4. There are six peaks that can be associated with structural modes of the frame, the first five are listed in the table and the mode shapes from Case 1 are shown in Figure 5.5 and Figure 5.6. There is a strong peak at 19.9 Hz that is associated with an operating frequency, and is not related to a structural mode. Only the figures from Case 1 are shown for brevity; the plots for all 6 cases are similar in appearance.

Table 5.2: Ambient Vibration Results – Benchmark Structure

		Frequency [Hz]									
Mode		*1*		*2*		*3*		*4*		*5*	
		Freq	*Dir*	*Freq*	*Dir*	*Freq*	*Dir*	*Freq*	*Dir*	*Freq*	*Dir*
Configuration	1	7.493	1W	7.772	1S	14.47	1T	18.85	2W	21.01	2S
	2	5.184	1S	7.736	1W	12.75	1T	15.02	2S	20.13	2W
	3	6.652	1S	7.630	1W	13.48	1T	18.90	2S	20.03	2W
	4	7.351	1S	7.617	1W	13.97	1T	16.02	2S	20.12	2W
	5	7.458	1S	7.604	1W	14.04	1T	20.61	*	20.61	*
	6	5.958	1W	7.786	1S	13.19	1T	18.85	2W	21.00	2S

**note: modes 4 and 5 (2W and 2S) in Case 5 are coupled*

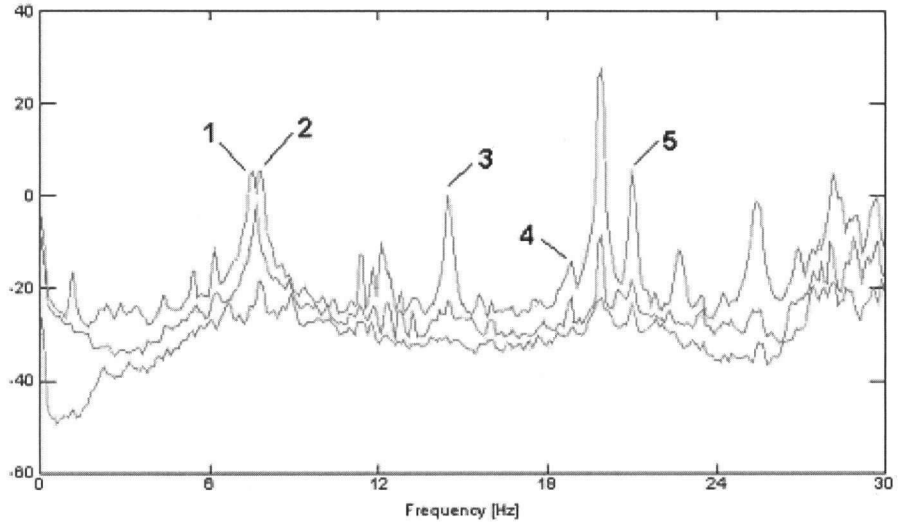

Figure 5.4: Singular Value Decomposition Plot from Case 1

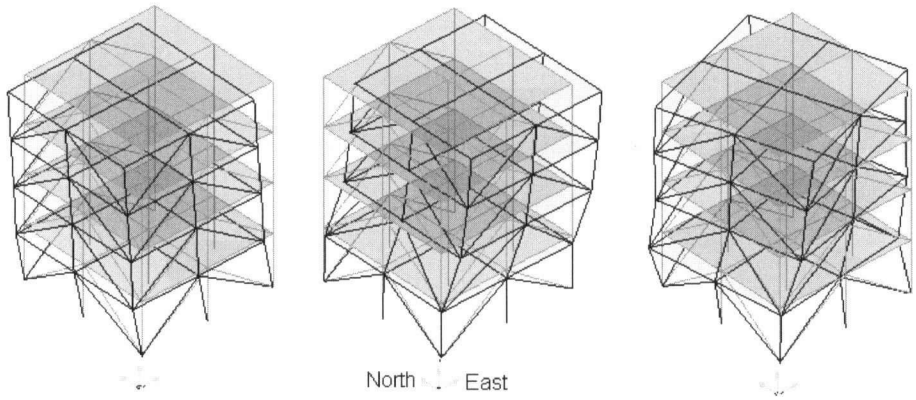

Figure 5.5: 3D frame Mode 1 (1st E/W), Mode 2 (1st N/S) and Mode 3 (1st Tor)

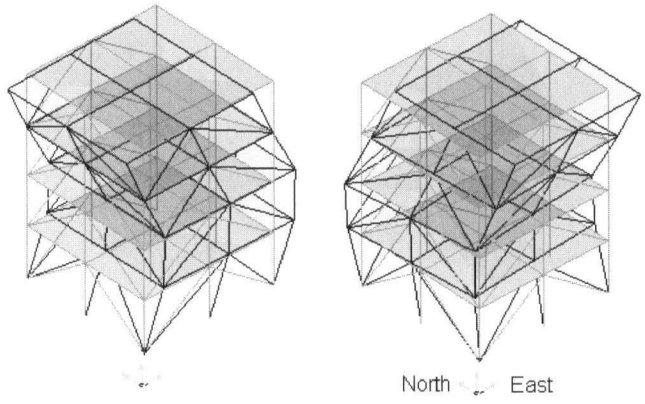

Figure 5.6: 3D frame Mode 4 (2nd E/W) and Mode 5 (2nd N/S)

5.3. Design and Updating of FEM

For the application of the various damage detection methods used in this work, a FEM of the 3D frame was developed. Several previous models were created, both in FEMTools and SAP2000 [Kharrazi et al., 2002, Turek et al., 2005]. For this work, a revised model using a better representation of the frame joints was developed.

For the frame as described, the members were divided into two categories: those with properties with a reasonable degree of certainty in their values, and those that do not. With respect to those with certainty, it is understood that these members are not necessarily perfect; there may be small imperfections on material properties and cross sections. However, these small errors should have negligible effect on the overall behaviour of the structure. Table 5.3 and Table 5.4 outline the various members and these properties.

Table 5.3: 3D frame members with certain parameters

Member type	Cross-section	Material Properties
Column	A, Ix, Iy, Iz	Rho, E, nu
Beam	A, Ix, Iy, Iz	Rho, E, nu
Floor brace	A, Ix, Iy, Iz	Rho, E, nu

Table 5.4: 3D frame members with uncertain parameters

Member type	Cross-section	Material Properties
Braces	A, Ix, Iy, Iz	E
Joint connections:		
-spring elements	Rotational stiffness	
Mass distribution	t of plates, point mass values	N/A

The FEM of the 3D frame was created using frame elements for the braces, beams, floor beams and columns. The steel plates were modeled as shell elements. This was done in an attempt to properly model the mass distribution. Previous models used point masses at the floor nodes, but it was difficult to exactly model the distribution in this way.

5.3.1. Joint connections

The joint connections are the most important part of the model to design. The default finite element connection is rigid, creating a frame that is too stiff and does not allow for any modifications of the connection stiffness. It is important then to model the connections using an element that allows for modification of joint stiffness. In the previous models [Kharrazi 2002, Turek 2005] an attempt was made to model the joints using small 50mm beam sections at the interface between the columns and beams. These small sections had the same initial properties as the beams themselves, but then were used as variables for the updating of the model. In order to achieve a good match between the model and the test results, the beam properties (both sectional properties and modulus of elasticity) were changed substantially. There were many attempts to justify this, the main being the use of the beams as a 'black box' element whose properties now were essentially a 'joint stiffness parameter' and did not necessarily represent actual physical properties of a beam. Several problems were inherent in this method however:

1. The length of the small beam connectors to use is uncertain: is 50mm too small/too large to properly model this type of connection?
2. Once the connection was updated to match the test results, local modes near the connections began to appear, and also a large amount of in-plane flexibility of the connectors at those locations. The solution to this problem was either manual modification of the parameters and/or using node constraints to fix the floors back to a rigid state.

While a decent model could be achieved through this method, a more rational approach was desired. For this, it was decided to use spring elements between the columns and the beams.

Previously, a test was done on a joint of the 3D frame by a group of researchers at UBC [Ventura et al., 1997]. The test featured a point load application to the tip of a beam which was connected to a column as shown in Figure 5.7. The results of the test would allow for a better determination of the actual joint stiffness.

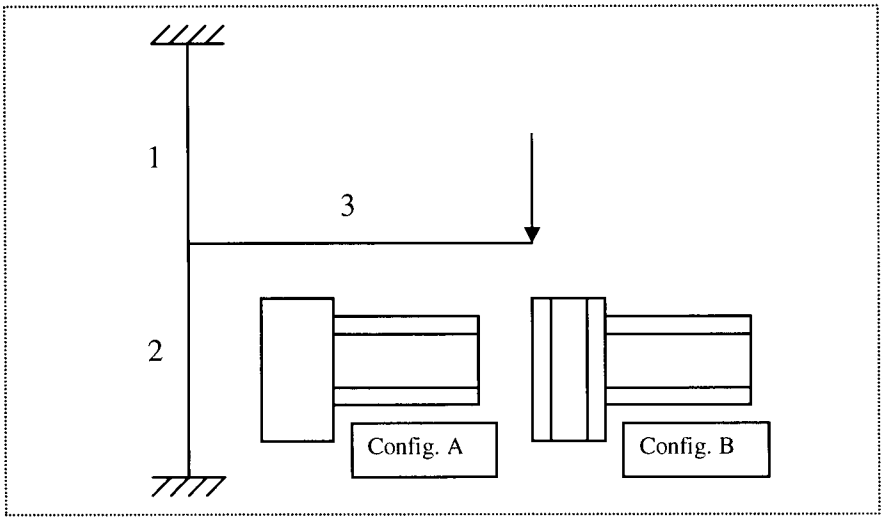

Figure 5.7: UBC Joint test configuration

The beam in Figure 5.7 is always oriented with the strong axis horizontal; the test was repeated both for the case where the beam was connected to the web (Config. A), and connected the flange (Config. B), of the column. The resulting flexibilities/stiffness of the overall joint assembly was determined and is shown in Table 5.5.

Table 5.5: Joint properties from test

Configuration	Flexibility [mm/kN]	Stiffness [kN/m]
A	9	111
B	4	250

In order to determine an appropriate rotational stiffness for the spring elements at the joints, SAP2000 was used with 'link' elements (links and springs are similar element types). A FEM was created to simulate the UBC joint test using the appropriate beam/column properties, using a layout as shown in the figure. The two columns (elements 1 and 2) were rigidly connected at their ends but their common node was allowed to rotate. This would create a more rigid connection that the one used in the lab tests, but it was considered acceptable for this approximation. Next a 1.25m element was created (element 3), but instead of being rigidly connected to the columns, an infinitesimal link element was added between them. All of the DOF's of the link were fixed except for the rotation that affected the tip displacement of the beam. To determine the deflection caused by the bending of the beam only, one end of the beam was fixed with the 1 kN load applied to the free end. This resulted in a deflection of 2.7mm.

The joint rotation then would need to account for an additional 6.3mm of displacement when the beam was oriented in the weak direction, and 1.3mm when in the strong direction.

To develop the rotational stiffness required of the link, the above displacements were approximated in radians by division of the length, ie. 2.7/1250 or 6.3/1250, depending on the direction. Both of these rotations would be caused by a 1000N*1.25m moment, or 1250N*m. Dividing the moment by the rotation in radians gives the estimates of the link stiffness. The resulting rotational stiffnesses (as starting values in the model) are:

K_θ; weak dir: 250,000 N*m/rad

K_θ; strong dir: 1,200,000 N*m/rad

When these two values were placed in the model, it resulted in displacements of 10mm for the weak direction, and 3mm for the strong direction. The errors are considered to be due to the flexibility of the columns. Since these are 'approximate values' for the model, this is an acceptable difference.

These initial stiffness parameters were placed in the FEM, and the modal parameters were computed. Throughout the updating process, the FEM modal parameters are correlated with the real modal parameters obtained as in Section 4.2.2. The two properties to correlate are frequency, correlated as a relative difference (%), and mode shape, correlated using the MAC value (%). Good correlations are achieved by observing low frequency differences and high MAC values. Table 5.6 presents the correlation from the initial FEM of the unbraced model. The MAC values are all high (>90%) but some of the modes have a poor frequency correlation. Ideally the frequency error is less than 1%, but to match all of the modes is difficult. Therefore in general a frequency error of less than 5% is desired, particularly in the lower modes. Throughout this chapter frequency and MAC correlations will be used to compare various models.

Table 5.6: Unbraced Model: Original Correlations

Mode	Description	FEA [Hz]	EMA [Hz]	Diff. [%]	MAC [%]
1	1st E/W	2.61	2.64	-1.10	99.4
2	1st N/S	4.46	3.63	22.98	95.8
3	1st Tor	4.57	4.33	5.48	95.0
4	2nd E/W	8.84	8.49	4.14	99.0
5	2nd N/S	14.92	12.00	24.31	96.1
6	2nd Tor	15.28	13.97	9.36	90.3
7	3rd E/W	17.20	16.20	6.16	95.3

5.3.2. Joint Updating: Unbraced Configuration

When the initial stiffness values were input to the unbraced model and correlation was made between the model and test modes, it was found that the weak direction modes were in good agreement, but the strong direction was too stiff (as seen by the large frequency difference). An automated updating was performed, using all of the modes as responses, and the spring stiffness values as parameters. The updated correlations are shown in Table 5.7. It can be observed that the translational modes improved significantly, particularly modes 2 and 5. The frequency difference from the torsional mode however is seen to increase.

Table 5.7: Unbraced Model, Updated Spring Stiffness

Mode	Description	FEA [Hz]	EMA [Hz]	Diff. [%]	MAC [%]
1	1st E/W	2.63	2.64	-0.43	99.5
2	1st N/S	3.57	3.63	-1.54	96.8
3	1st Tor	3.93	4.33	-9.36	95.1
4	2nd E/W	8.89	8.49	4.67	99.1
5	2nd N/S	12.83	12.00	6.87	94.0
6	2nd Tor	13.78	13.97	-1.34	90.1
7	3rd E/W	17.24	16.20	6.42	95.5
8	3rd N/S	26.04	21.75	19.64	54.9

The stiffness parameters were updated to:

K_θ: weak dir, updated: 257,280 N*m/rad (+28.6%)

K_θ: strong dir, updated: 405,765 N*m/rad (-66.2%)

This appears to be a drastic change, in particular for the strong direction. To check the validity of the change, the new stiffness value was placed into the SAP2000 joint model. The resulting

deflection was 7.9mm versus the original 5.7mm. This difference (28%) was considered to be acceptable. For one, the resulting change in deflection (as a percentage) is less than the change in stiffness; and also it is reasonable that the stiffness of the joints change when placed in a system rather than alone as in the test.

It is noted that the number of modes in the various table may vary; in Table 5.6 there is 7 modes and in Table 5.7 there is 8 modes. This is simply because the software does not display modes with MAC values less that 50%.

5.3.3. Mass distribution

An excellent correlation between the translational mode frequencies has been achieved, but not for the third mode, which is the first torsion. The FEM torsional frequency was lower than that of the EMA by about 10%. This would be due to a rotational mass distribution which was too far from the center of stiffness of the structure. Bringing the mass distribution closer to the centre would then lower the frequency. This is accomplished by first adding a point mass element to the inside corner of each of the plates. The distribution would then be changed by reducing the thickness of the plates, and adding mass to the point elements equal to the amount lost by the plates. This method does not change the total mass of the frame nor the translational mass distribution, thereby resulting in the same translational frequencies while changing the torsional ones. A manual updating was performed, reducing the thickness of the plates while added the appropriate amount of mass. It was found that a reduction of 25% of the plate thicknesses produced the best results. The updated correlations are shown in Table 5.8.

Table 5.8: Final Updated Unbraced Frame Correlations

Mode	Description	FEA [Hz]	EMA [Hz]	Diff. [%]	MAC [%]
1	1st E/W	2.62	2.64	-0.70	99.4
2	1st N/S	3.56	3.63	-1.96	96.8
3	1st Tor	4.35	4.33	0.33	94.7
4	2nd E/W	8.86	8.49	4.39	99.0
5	2nd N/S	12.77	12.00	6.38	93.7
6	2nd Tor	15.23	13.97	9.05	89.5
7	3rd E/W	17.19	16.20	6.11	95.2
8	3rd N/S	25.81	21.76	18.59	62.0

To examine the possibility of additional refinement to the model, an updating was performed on other parameters of the frame. In particular, the modulus of elasticity and density of steel were considered as uncertain, and a potential fluctuation of +/- 10% was permitted. It was found that this had a tendency to reduce the average error (5.94% for those of Table 5.8; 4.54% for E; 4.73% for ρ) but this had the effect of improving the higher mode correlations while lessening the lower mode correlations. In both of the later cases the 4th mode was matched almost exactly. It was decided that it was best to stay with the results from Table 5.8, where the first 3 modes had the best correlation.

5.3.4. Braced Model

Next braces were added to the model. For the braces, the parameters with the most uncertainty are the nominal area and the modulus of elasticity of the threaded rods. There is also variability in the behaviour of each rod due to the end connection detail. The rods are tightened by hand at each end, which means that there is variability in the tension, and thus the frequency and the effective length of each brace. Modeling this phenomenon is rather difficult, so it is simpler to modify the modulus of elasticity to account for these effects. For the updating process, a starting value of E for steel of 200,000 MPa was used.

The nominal area to use for the cross-sectional properties is an important detail, since these are threaded rods, and the actual area which takes load is debatable. As a starting point, from the Canadian Steel Design Code, the nominal area, A_n, is taken to be 0.75*A.

The above starting values for the braces were input to the model. A spreadsheet computing the A, I_x, I_y, and I_z for the braces was developed to allow for a manual updating. It was found that these default values were too high, creating braces that were too stiff. Consequently this results in frequencies that are too high. The initial correlation for the braced model before updating are shown in Table 5.9.

Table 5.9: Initial Braced Model Correlations

Mode	Description	FEA [Hz]	EMA [Hz]	Diff. [%]	MAC [%]
1	1st E/W	8.26	7.49	10.32	99.8
2	1st N/S	8.81	7.78	13.22	99.2
3	1st Tor	14.22	14.49	-1.84	94.3
4	2nd E/W	22.38	19.89	12.54	97.2
5	2nd N/S	24.07	21.03	14.44	86.7

Upon a few iterations of the manual update, it was found that a value of $A_n = 0.5*A$, and E=140,000 MPa provided good estimations of the frequencies. These values were considered acceptable due to the uncertainties at the end connections. The resulting correlations of the first update are given in Table 5.10.

Table 5.10: Brace Update: Global E and Nominal Area

Mode	Description	FEA [Hz]	EMA [Hz]	Diff. [%]	MAC [%]
1	1st E/W	7.17	7.49	-4.22	99.8
2	1st N/S	7.76	7.78	-0.25	99.1
3	1st Tor	12.27	14.49	-15.31	94.3
4	2nd E/W	19.96	19.89	0.35	97.8
5	2nd N/S	21.97	21.03	4.47	86.7

The next observation of the results was that there is a discrepancy between the lateral stiffness of the E/W and N/S directions of the frame. In particular, while there was a good match between the first N/S mode, there remained an almost 5% error between the first E/W mode. This was addressed by separating the braces into two groups, and then updating the E/W group to match the first frequency. The updated correlation are shown in Table 5.11. The updated E for the new group of braces was 155,660 MPa (+11.2%). This illustrates the point made above which stated that the actual stiffness of each brace varies, and that in reality the two values for E used in the model represent the mean values for a distribution of stiffness values for the braces.

Table 5.11: Brace Update: E/W E Only

Mode	Description	FEA [Hz]	EMA [Hz]	Diff. [%]	MAC [%]
1	1st E/W	7.47	7.49	-0.20	99.8
2	1st N/S	7.77	7.78	-0.11	99.1
3	1st Tor	12.54	14.49	-13.41	94.3
4	2nd E/W	20.64	19.89	3.79	97.7
5	2nd N/S	22.00	21.03	4.61	86.6

As with the unbraced model, it can be seen in Table 5.11 that there is a discrepancy between the torsional modes even though the translational modes match well. As before this is dealt with by adjusting the plate thickness and the point masses. The results in Table 5.11 already include the 25% reduction used for the unbraced model. It was found that an additional 25%, for a total of 50% reduction, was required for a match in the braced model. The final correlations are shown in Table 5.12. Examples of mode shape pairs for modes 1 and 4 are shown in Figure 5.8 and Figure 5.7. The red lines represent the EMA modes and the blue represent the FEM.

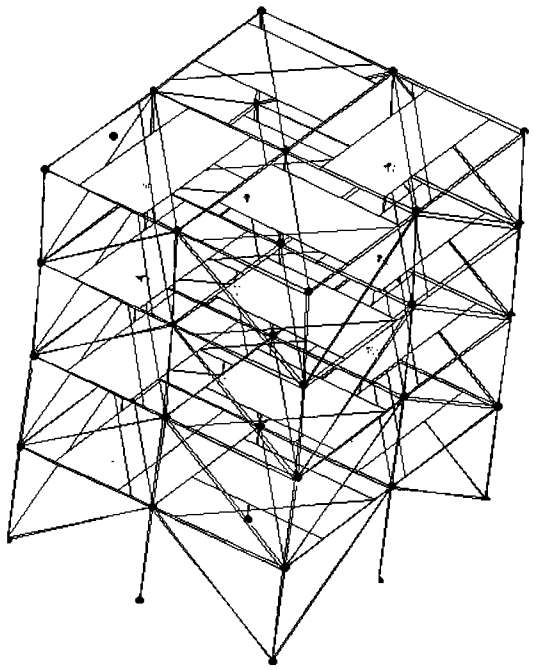

Figure 5.8: Mode Shape Pair - 1st E/W

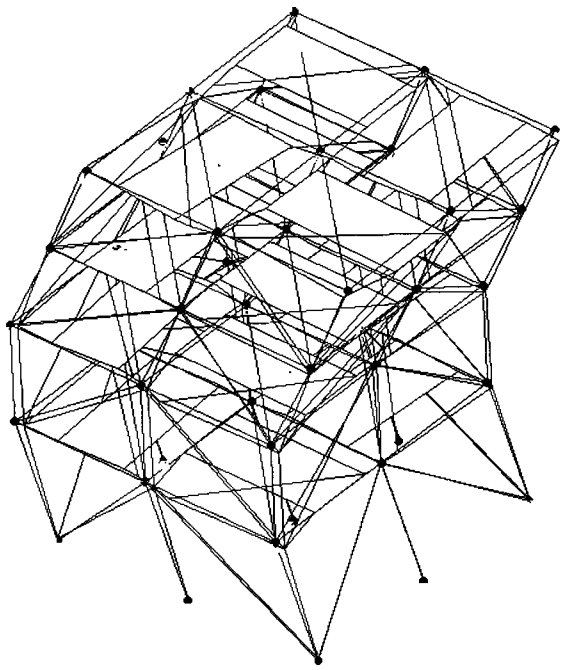

Figure 5.9: Mode Shape Pair – 2nd N/S

Table 5.12: Final Braced Model Correlations

Modes	Description	FEA [Hz]	EMA [Hz]	Diff. [%]	MAC [%]
1	1st E/W	7.46	7.49	-0.38	99.8
2	1st N/S	7.75	7.78	-0.34	99.0
3	1st Tor	14.24	14.49	-1.72	94.0
4	2nd E/W	20.39	19.89	2.51	97.3
5	2nd N/S	21.70	21.03	3.19	85.9

5.3.5. Development of SAP 2000 model for analysis

The program FEMTools does not offer sufficient capabilities for the simulation of vibrations. Therefore, an identical model was created in SAP2000. Since there are some differences in the way the two software represent and formulate elements, and in the computation of modes, a correlation with the SAP model and the test modes was performed. The results are shown in Table 5.13. It can be seen that there are only very small differences in frequencies and MAC values from the FEMTools model. The model is shown in Figure 5.10. The final results of the frame model were very good, with all of the frequencies having less than 5% error and high MAC values.

Table 5.13: SAP 2000 Model Correlations

Modes	FEA [Hz]	EMA [Hz]	Diff. [%]	MAC [%]
1	7.45	7.49	-0.49	99.8
2	7.75	7.78	-0.39	99.1
3	14.27	14.49	-1.49	94.0
4	20.47	19.89	2.90	97.5
5	21.87	21.03	3.99	86.0

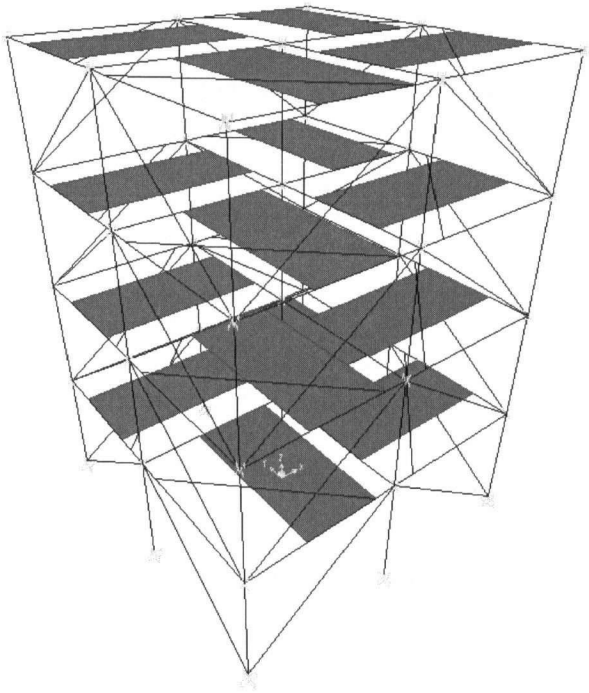

Figure 5.10: SAP 2000 Model of 3D frame

5.4. Vibration Simulations Using the SAP2000 Model

The main component of developing the CDS is the actual simulation using SAP2000. To do the calibrated simulation, information from the results of the ambient vibration test is used, and to determine the effect of how the improvement can be made, it is first useful to compare the results of a basic simulation with the real datasets.

The two spectra shown in Figure 5.11 and Figure 5.12 are from the real structure and the simulated structure respectively. When looking at the two spectra, differences that are important and could affect the quality of the damage detection results can be seen. Obviously the main aspect to consider is the quality of the modes themselves. In the simulated spectrum, only the modes appear, well formed and free of any noise and or other possible irregularities. The primary differences between the modes that appear in these two spectra are the amplitude, frequency and damping. It is not easily possible to deal with amplitude, because these are from ambient vibration results, and the analysis methods used cannot properly scale modes.

The difference in frequency between any given mode and the corresponding real mode that has been measured can be referred to as the frequency error. The error mainly arises from modeling errors in the FEM, but can also come from identification errors in the real data. These identification errors however are typically small.

The damping is observed to vary between the spectra primarily by the width of the modal peaks and also by changes in the amplitude. For example in the simulated case if the chosen damping is too low the peaks tend to be sharper and have higher amplitude. If the chosen damping is too high the peaks in a simulated spectrum might not appear at all.

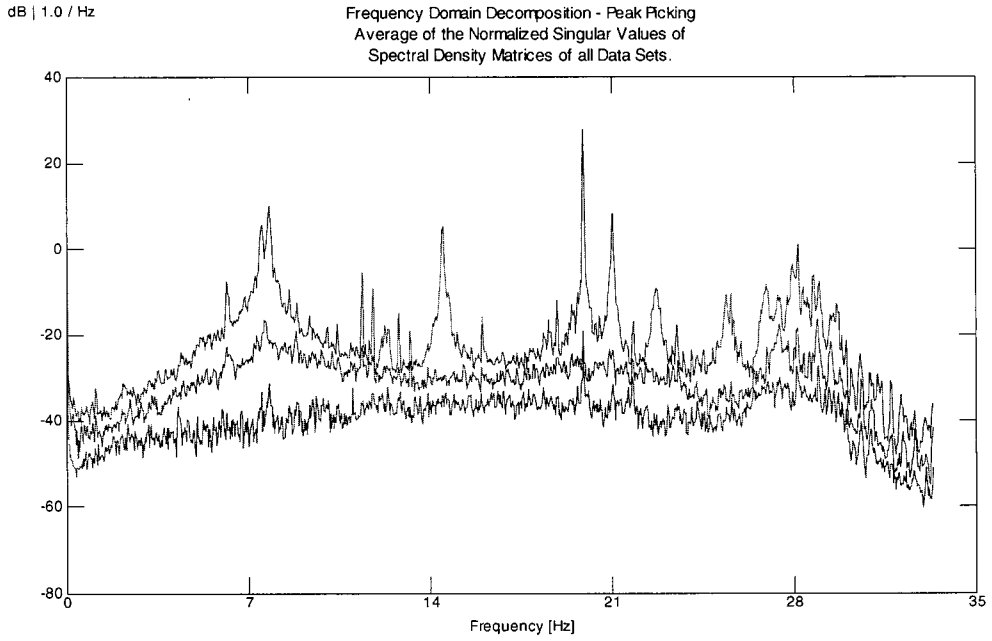

Figure 5.11: Spectrum from Real Structure

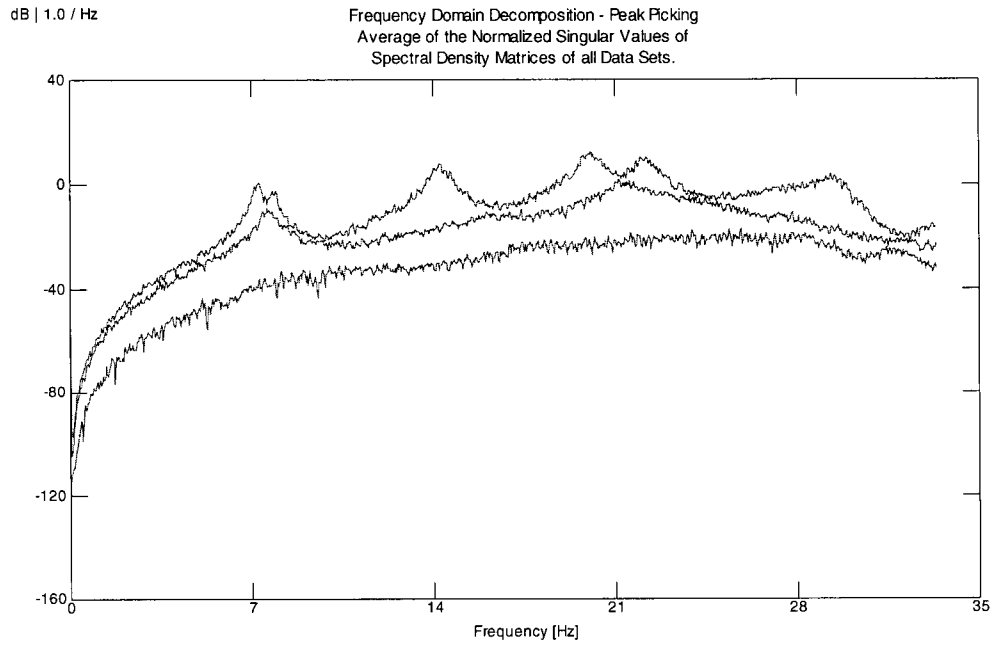

Figure 5.12: Spectrum from Plain Simulation –2% Damping – GWN input

The noise is the next issue to consider, and is difficult to deal with due to its random nature. Having a random white noise signal added to the simulated signals is typically an efficient way to deal with noise. However in doing this, some aspects may be neglected and the effect of noise on the signal may not be exactly as desired. For example, if a random white noise signal is added across the bandwidth of interest it may have a large effect on certain frequencies with lower amplitudes yet the dominant modes with higher amplitudes may not be affected at all. Also there are additional noise effects that appear in the results that are not simply measurement noise. These can be called 'environmental noise' effects that appear in the spectra as large peaks at certain frequencies in the data, rather than random noise that affects the entire bandwidth.

It is useful to consider each of the above described aspects individually and how they can be dealt with by using information obtained from the ambient vibration test. They can be described in four separate parts: the simulation input, the damping values chosen for the simulation, the errors between real and simulated spectrum and the noise and how it is added to the simulated signals. The next four subsections will discuss these issues and show examples using the 3D frame.

5.4.1. Simulation Input Using Measured Ground Motion

The input chosen for the simulation is very important and will have a critical affect on the resulting signals. The simplest input to use is white noise, and it can be applied in two different ways. The first way is to excite the supports in either the horizontal directions or in both horizontal and vertical directions. The second way is to apply a horizontal excitation to the faces of the structure, simulating wind. Since the base excitation should be sufficient to excite most of the modes, the wind application is not considered here.

Using only a white noise input may not consider important real loading effects. If there are peaks in the actual ground input due to the soil modes or due to vibrations traveling through the ground that appear in the spectrum of the response, those peaks will not appear if only white noise inputs are used. This concept is illustrated in the next few figures. Figure 5.13 shows a spectrum from a realization of a Gaussian white noise signal. It was created in the bandwidth of 0.1 to 50 Hz and from a signal of 60000 points.

Figure 5.14 shows the spectrum of the actual measured ground motion. Both sets of signals were scaled to have an RMS of 0.01. It is obvious from these plots that the energy distribution in the spectrum is not the same; the white noise signal energy being evenly distributed, while the real spectrum is concentrated around certain frequencies. It is also noted that the amplitude of the white noise spectrum only varies by 2dB, while the real spectrum varies by almost 50dB.

Another option for the input is to combine a white noise realization with the measured ground motion. A spectrum for this option is shown in Figure 5.15. This would allow for the concentrated peaks to excite the structure appropriately, while adding a more uniform excitation to the entire bandwidth.

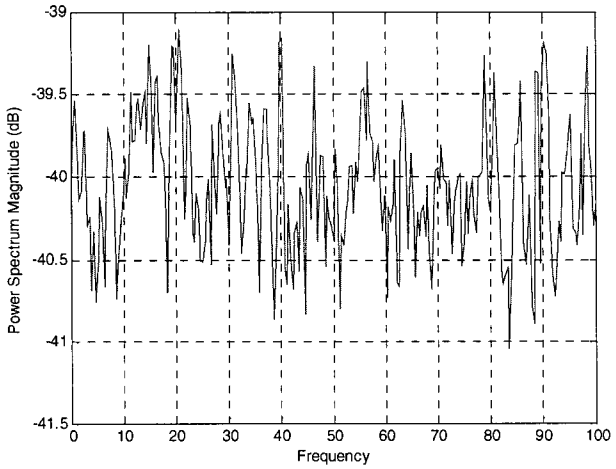

Figure 5.13: Power Spectrum of a Realization of Gaussian White Noise

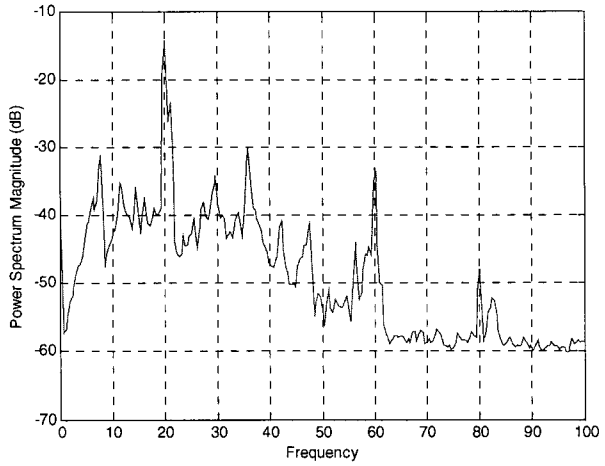

Figure 5.14: Power Spectrum of Real Ground Motion

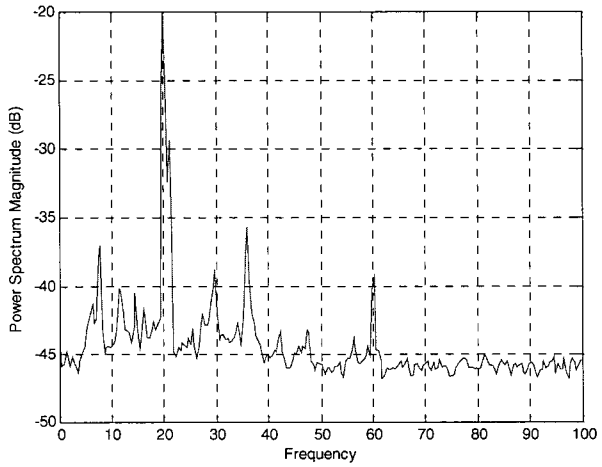

Figure 5.15: Power Spectrum of Combined Real and Gaussian Input

The results of using the ground motion input and combined input are shown in Figure 5.16 and Figure 5.17. Immediately in Figure 5.16 it can be seen that the real input causes the spectrum to look more like that of Figure 5.11, however, not all of the modes are properly excited. Therefore, by using the combined input, the excitation is more evenly spread and a better response is achieved, as in Figure 5.17.

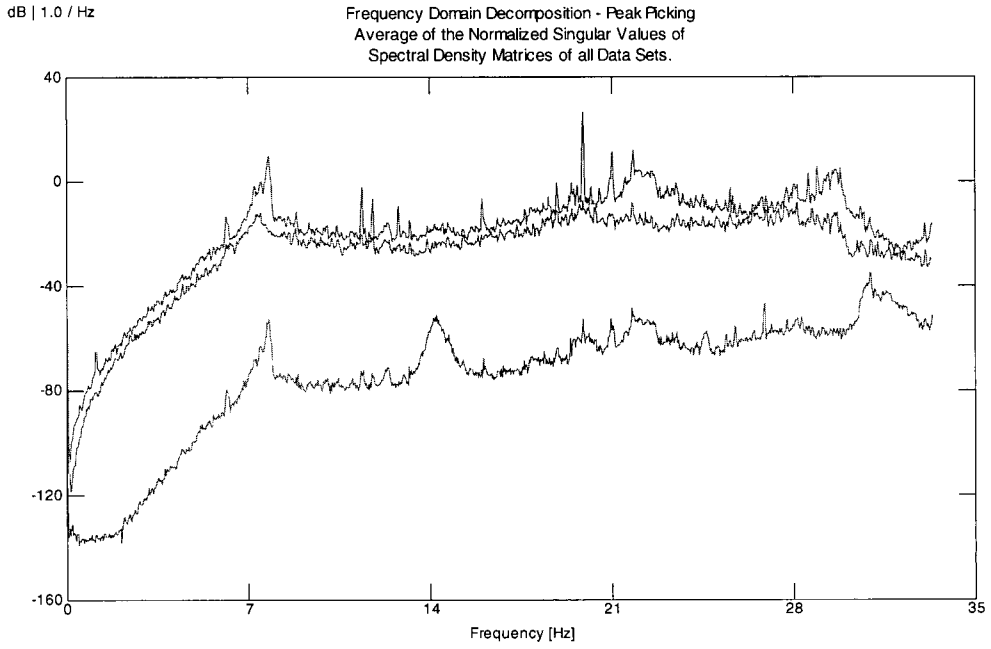

Figure 5.16: Spectrum of Plain Simulation –2% Damping, real ground motion input

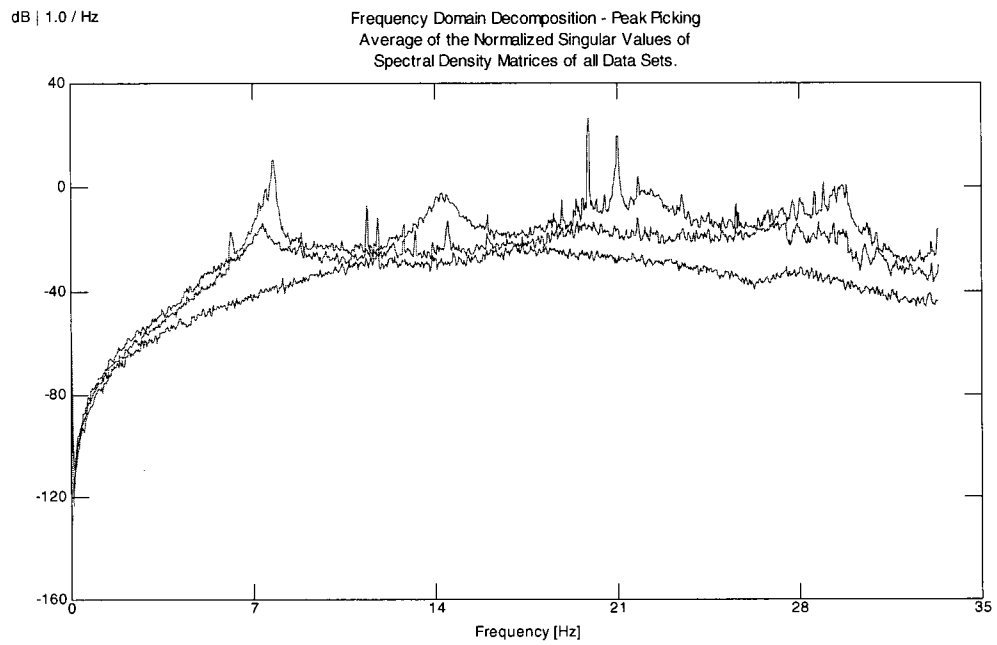

Figure 5.17: Spectrum of Plain Simulation –2% Damping, Combination Input

5.4.2. Simulation using measured viscous damping estimates

By comparing the real and simulated spectra (Figure 5.11 and Figure 5.12) it is evident that in the simulated case the chosen damping value of 2% is too high due to the poor definition of the modal peaks. During the analysis of the ambient vibration data, estimates of the real damping values for the structure can be obtained. In an analysis software such as ARTeMIS Extractor, there are several methods available to process the data and to estimate damping. From experience, the Stochastic Subspace Identification (SSI) method provides the best damping estimates. The modal damping estimates obtained from the analysis of the 3D frame data are: 0.438%, 0.458%, 0.126%, 0.0035% and 0.055%. The remainder of the modes in the simulation were given damping values of 0.5%. By these numbers, a chosen value of 2% results gives damping values of four times higher on average.

The spectrum in Figure 5.18 is from a simulation using the real damping values. It can be seen that the definition of the modes is clearer and is a better representation of the real spectrum. When the measured ground motion is used as input (shown in Figure 5.19), and then the ground motion combined with the white noise input is used with the real damping values, (as shown in Figure 5.20) it can be seen that the simulated spectrum is becoming a good representation of the real spectrum (Figure 5.11).

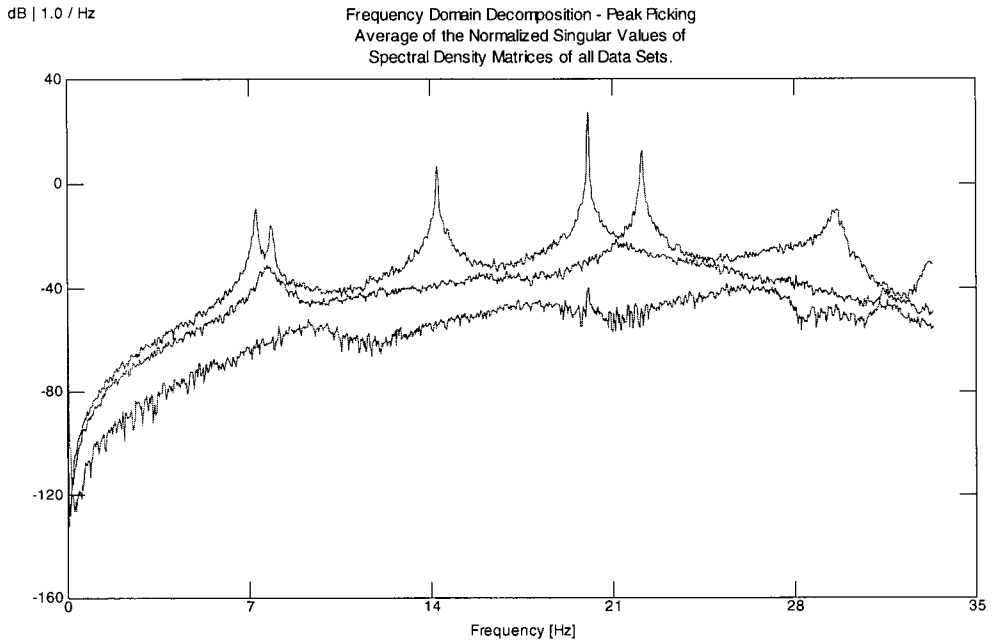

Figure 5.18: Spectrum of Plain Simulation –Real Damping, GWN Input

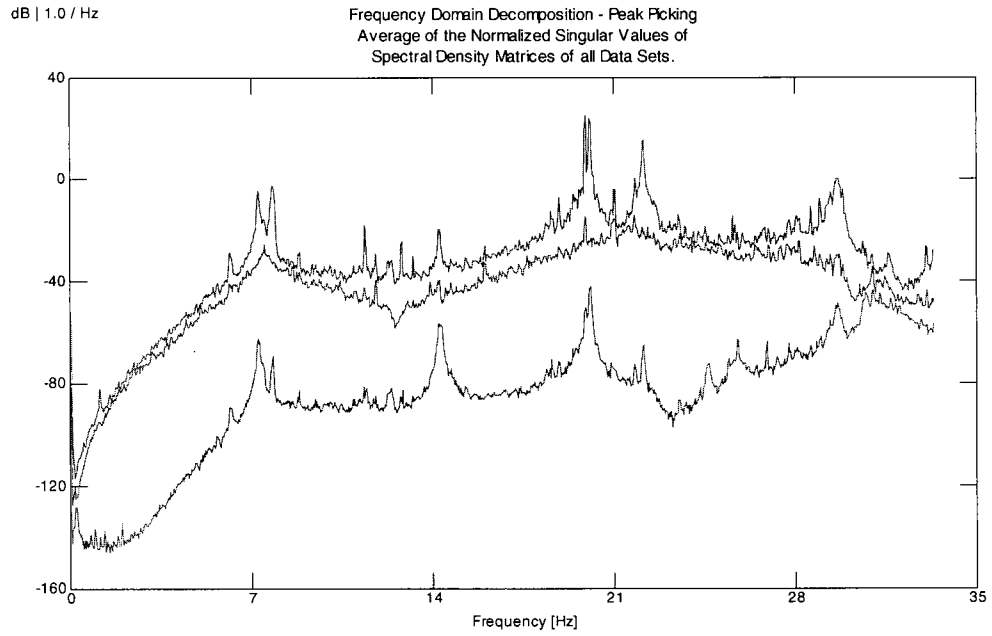

Figure 5.19: Spectrum of Plain Simulation –Real Damping, Real Ground Motion Input

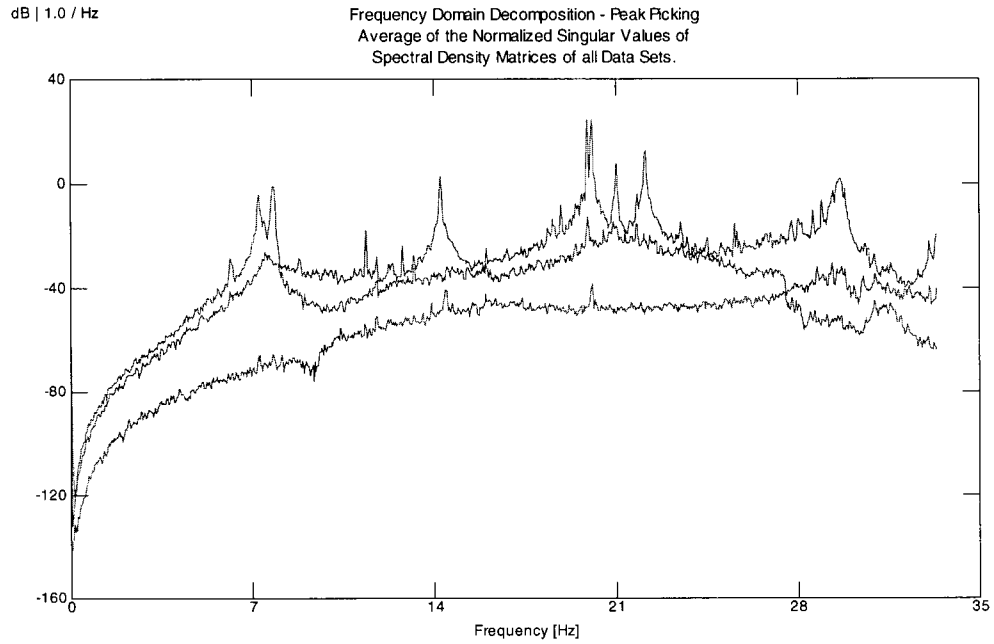

Figure 5.20: Spectrum of Plain Simulation –Real Damping, Combined Input

5.4.3. Dealing with Simulation Errors

The next issue to deal with is the errors between the real spectrum and the simulated spectrum. The errors discussed here are divided into two types: amplitude and frequency. By considering the amplitude of a mode obtained using an output only type analysis, it can be quickly rationalized that since the amplitude is arbitrarily determined, it is not strictly necessary to deal with amplitude errors unless they are extreme.

The issue of frequency error is much more significant in terms of the possible analyses that are required (ie. damage detection). It can be seen when comparing the spectra of Figure 5.11 and Figure 5.12 that the errors between the various mode pairs (ie FEM and EMA) are not the same. This makes it impossible to use a simple correction such as shifting the entire spectrum.

In order to learn more about the distribution of errors between modes, the 3D frame is very valuable, since the real modes are available for the five damage cases from Table 5.1. The model used for simulation can then be damaged in the same way to examine the comparison of the frequency errors.

Table 5.14 shows the frequency errors (between the real modes and the model modes) as a percentage for the six cases, which includes the undamaged case. It can be seen that the error between any given mode varies among the cases. As a result, taking the errors from the undamaged case and then applying them to a future damage simulation will not necessarily be correct.

Table 5.14: Relative Frequency Errors Between Real and Simulation for the 6 Benchmark Cases

Mode	Case 1 [%]	Case 2 [%]	Case 3 [%]	Case 4 [%]	Case 5 [%]	Case 6 [%]
1	-3.23	6.41	3.28	-4.95	-5.01	0.36
2	0.81	-7.45	-5.55	2.63	2.35	0.31
3	-1.85	0.89	-0.12	-0.60	-0.69	1.49
4	0.23	12.98	-0.67	-1.12	0.04	0.00
5	4.17	-1.76	5.76	15.57	14.37	14.08

One way of dealing with this variation of error, is to examine a single mode taking the error percentages and use them as a sample set (ie. a row of the table). Then a distribution is created based on these samples and considered to be random variables of frequency error for that mode. Then, for a future damage case, a random realization of error percentage can be taken from that distribution, and applied as a correction. However, since the simulation of an arbitrary damage state automatically sets up a series of random errors between the simulation and the actual structure if it were damaged, adding an additional realization of random error does not change the results in a meaningful way. Based on this argument, it is then suggested that when a damage scenario is simulated, it already contains a random realization of the error between frequencies and it is not necessary to deal with the error any further in this manner.

Therefore, the only real way of dealing with the error between frequencies is in the initial stages when the finite element model is designed and updated. Therefore an idea of the acceptable error between the real and simulated modes is necessary, and must be controlled.

5.4.4. Adding Noise to the Simulation

The final issue for the simulations is noise. The most common way seen in the literature is to add a Gaussian white noise signal that is representative of the measurement noise. This noise signal is added as a certain percentage of the RMS of the real signal, typically a value of 1% to 5% RMS is used. When a method such as Frequency Domain Decomposition that deals with noise very well is used, the added white noise signal typically has minimal affect on the overall results. Particularly when a white noise signal that has an even affect on the entire bandwidth, it can be seen that in areas where the energy in the spectrum is higher the noise will have minimal effect, while in areas where the energy is lower, the noise may distort the signal significantly. It can be seen that adding a white noise to the signal has a tendency only to raise the noise floor. Figure 5.21 shows 10% RMS Gaussian white noise added to the original simulation and Figure 5.22 shows 10% RMS Gaussian white noise added to the combined input and real damping simulation.

It is therefore suggested that a way of improving this is to use a coloured noise. The coloured noise can be obtained by finding a trendline through the real spectrum, ie. by using a moving average. Then the white noise signal is created, and in the frequency domain the noise spectrum can be multiplied by the trendline. The coloured noise spectrum is then taken back to the time domain and added to the signals. The noise signal then will affect all parts of the bandwidth according to the actual energy at that frequency. Figure 5.23 shows the coloured noise added to the combined input and real damping simulation. The spectrum in the figure was computed with a smoothing factor of 10 on the trendline.

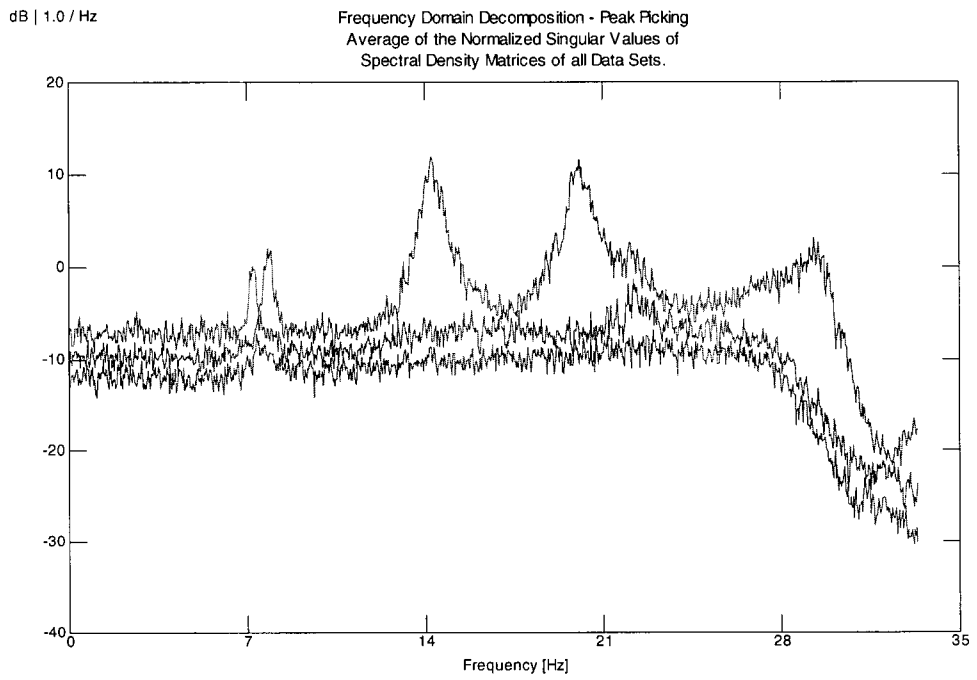

Figure 5.21: Spectrum of simulation with 10% RMS GWN, GWN Input, 2% Damping

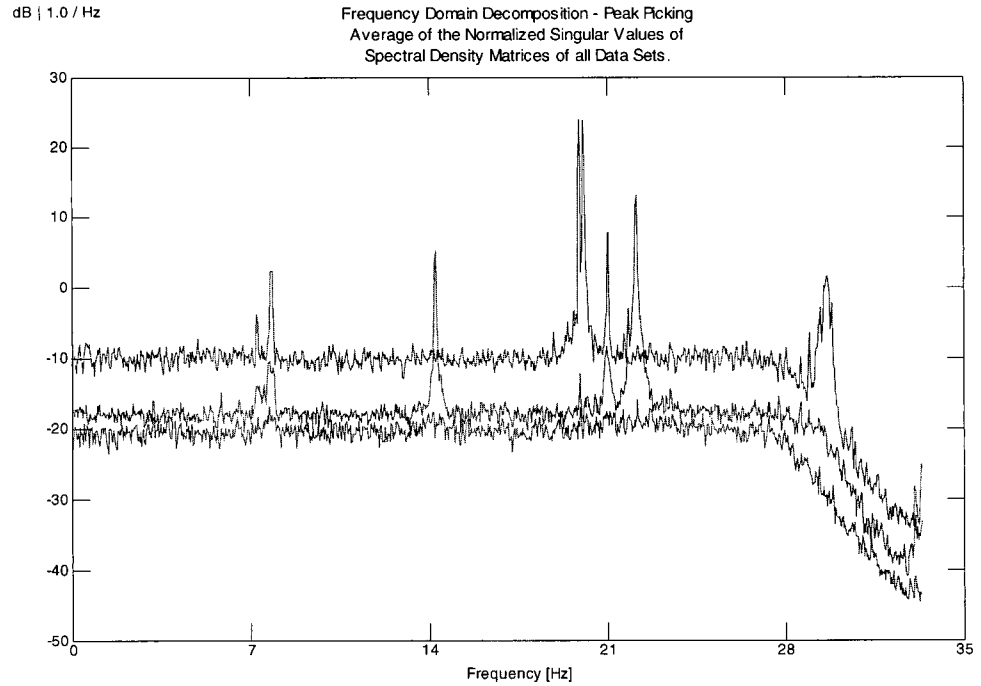

Figure 5.22: Spectrum of simulation with 10% RMS GWN, Combination Input with Real Damping

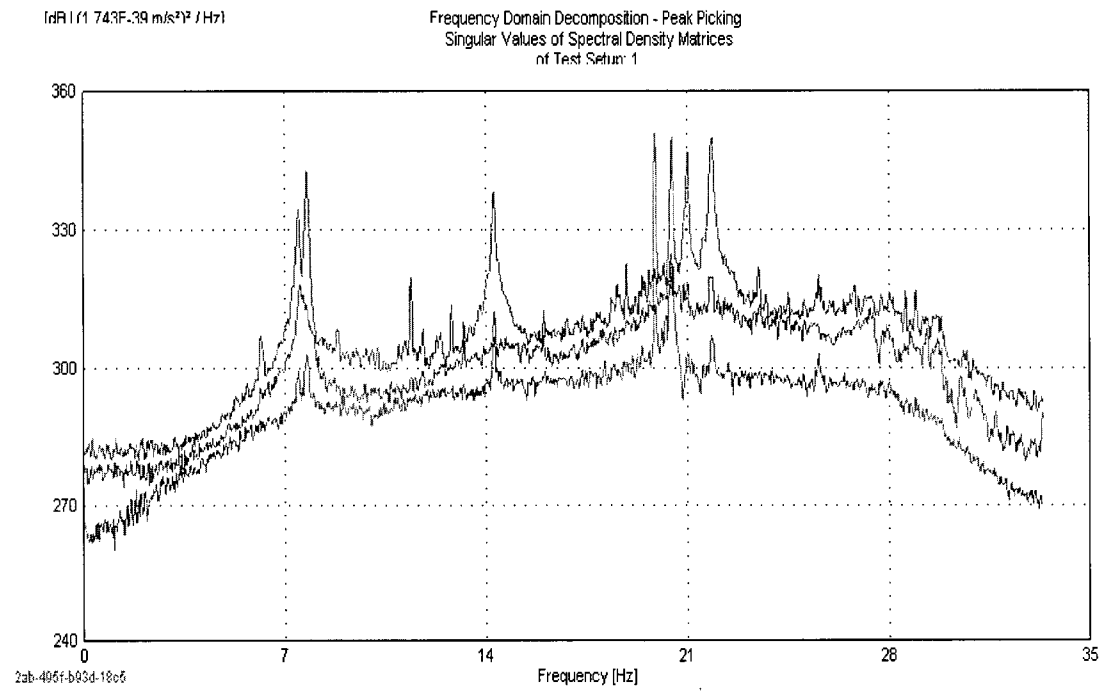

Figure 5.23: Spectrum of Simulated Case 1 With Coloured Noise Added (20% RMS)

It is noted that with the sophisticated techniques that are being applied to the signals the noise generally has a relatively small affect. Also with the continued development of new sensors that have very large signal to noise ratios and low noise floors it is reasonable to conclude that the noise is not the most significant restriction on the performance of the required analysis.

5.5. Summary of Method for Calibrated Simulations

Based on the discussion from Section 4.2.4, a method for performing calibrated simulations can be established. The steps can be generalized as follows:

i) Perform an ambient vibration test on the structure of interest
ii) Design and update a FEM of the structure
iii) Simulation: choose damage cases
iv) Simulation: use measured ground motion plus Gaussian white noise as input
v) Simulation: use real damping obtained from AVT
vi) Add noise to simulation with a coloured noise signal

5.6. Calibrated Simulations of 3D frame

The method summarized in Section 5.5 was applied to the 3D frame model for the undamaged case plus 15 damaged cases. Damage cases 2 to 6 are those from Figure 5.3 and Table 5.1. To validate the realism of the calibrated simulations, they can be correlated to the real damage cases of the 3D frame. To do this, the simulated datasets are processed with the ARTeMIS extractor program, and then correlated to the real datasets that were processed with ARTeMIS. These are presented in Table 5.15 to Table 5.20. In each table, the exact SAP value, the SSI-CVA value from ARTeMIS and damping estimate are shown. The EMA frequency and damping values are from the ARTeMIS EFDD method. Last the difference in frequency, damping and MAC between the SSI and EMA values is presented.

Table 5.15: Case 1 Correlations

Modes	SAP [Hz]	SSI-CVA [Hz] (2048)	Damping [%]	EMA [Hz]	Damping [%]	Freq. Diff. [%]	Damp. Diff. [%]	MAC [%]
1	7.450	7.451	0.300	7.49	0.438	-0.52	-46.00	99.68
2	7.750	7.752	0.578	7.78	0.458	-0.36	20.76	96.41
3	14.269	14.27	0.134	14.49	0.126	-1.54	5.97	94.47
4	20.466	20.47	0.012	19.89	0.004	2.83	66.67	98.94
5	21.869	21.86	0.072	21.03	0.055	3.80	23.61	88.18

Table 5.16: Case 2 Correlations

Modes	SAP	SSI-CVA [Hz]	Damping [%]	EMA [Hz]	Damping [%]	Freq. Diff. [%]	Damp. Diff. [%]	MAC [%]
1	5.532	5.54	0.465	5.184	0.537	6.43	-15.48	97.78
2	7.393	7.425	0.255	7.756	0.771	-4.46	-202.35	99.42
3	12.936	12.93	0.146	12.72	0.400	1.62	-173.97	92.35
4	17.040	17.04	0.007	15.03	0.382	11.80	-5357.14	88.14
5	20.261	20.27	0.260	20.08	0.497	0.94	-91.15	98.59

Table 5.17: Case 3 Correlations

Modes	SAP	SSI-CVA [Hz]	Damping [%]	EMA [Hz]	Damping [%]	Freq. Diff. [%]	Damp. Diff. [%]	MAC [%]
1	6.841	6.834	0.661	6.651	0.376	2.68	43.12	90.73
2	7.431	7.451	0.196	7.641	0.820	-2.55	-318.37	96.64
3	13.525	13.52	0.148	13.44	0.376	0.59	-154.05	94.01
4	20.01	20.01	0.026	18.92	0.263	5.45	-911.54	85.05
5	20.41	20.42	0.144	20.01	0.394	2.01	-173.61	98.63

Table 5.18: Case 4 Correlations

Modes	SAP	SSI-CVA [Hz]	Damping [%]	EMA [Hz]	Damping [%]	Freq. Diff. [%]	Damp. Diff. [%]	MAC [%]
1	7.428	7.417	0.712	7.593	0.687	-2.37	3.51	98.32
2	7.477	7.479	0.394	7.351	0.614	1.71	-55.84	84.21
3	13.972	13.96	0.239	13.98	0.207	-0.14	13.39	93.08
4	20.427	20.43	0.003	19.73	0.339	3.43	---	93.95
5	20.593	20.59	0.051	20.13	0.399	2.23	-682.35	27.24

Table 5.19: Case 5 Correlations

Modes	SAP [Hz]	SSI-CVA [Hz]	Damping [%]	EMA [Hz]	Damping [%]	Freq. Diff. [%]	Damp. Diff. [%]	MAC [%]
1	7.429	7.435	0.367	7.597	0.584	-2.18	-59.13	98.23
2	7.558	7.553	0.603	7.455	0.433	1.30	28.19	97.00
3	14.01	14.01	0.098	14.04	0.208	-0.21	-112.24	94.07
4	20.429	20.43	0.003	19.89	0.002	2.64	33.33	94.63
5	21.536	21.53	0.035	20.67	0.503	3.99	-1337.14	47.31

Table 5.20: Case 6 Correlations

Modes	SAP [Hz]	SSI-CVA [Hz]	Damping [%]	EMA [Hz]	Damping [%]	Freq. Diff. [%]	Damp. Diff. [%]	MAC [%]
1	6.087	6.122	0.146	5.956	0.261	2.71	-78.77	99.38
2	7.750	7.75	0.610	7.803	0.847	-0.68	-38.85	98.71
3	13.352	13.35	0.152	13.15	0.264	1.50	-73.68	91.19
4	20.421	20.42	0.024	19.89	0.007	2.60	70.83	98.47
5	21.748	21.76	0.043	20.99	0.087	3.54	-102.33	63.12

The tables show that the simulated mode shapes have a very high MAC value in almost all of the cases. The average MAC value is 87.56, with only four values that are lower than 80%.

Cases 16 to 25 were created randomly, and instead of having members removed to represent damage, only a reduction in cross-sectional properties was imposed (66% of all properties). This was in an effort to created more realistic damage scenarios. The members damaged in Cases 16 to 25 are presented in Table 5.21. These damage cases will be used in the next section for the development of the damage detection methodology. The identified modes and damping values using ARTeMIS are presented in Table 5.22 to Table 5.31. Each table gives the exact SAP frequency, the FDD and SSI-CVA results from ARTeMIS. The MAC values shown in these tables compare the two ARTeMIS modes identified with ARTeMIS. When the MAC value is low (<90%) it indicates that the mode was not very clearly identified. The reason that the case numbering skips to 16 here is that Cases 7 to 10 were for the unbraced damage cases as mentioned in Section 4.2.2.; and Case 11 to 15 are from another set of plain simulations of the 3D frame, which will be discussed in Section 4.3.3. These tables are referred to as 'self-correlations' because there is no real data to compare too. Instead, the FDD and SSI methods in ARTeMIS are compared.

Table 5.21: Random Damage Cases

Case	Damaged Members
16	6
17	1, 12, 11
18	14,16,23
19	22
20	27,28
21	16,29
22	10,18,27
23	25,31
24	6,28
25	8,9,24,28

Table 5.22: Case 16 Self-Correlations

Mode	SAP [Hz]	FDD [Hz]	SSI-CVA [Hz]	Damping [%]	MAC [%]
1	7.43	7.454	7.427	0.305	96.29
2	7.66	7.682	7.687	0.121	99.99
3	14.14	14.13	14.14	0.210	99.98
4	20.44	20.44	20.44	0.006	99.99
5	21.72	21.71	21.73	0.080	99.94

Table 5.23: Case 17 Self-Correlations

Mode	SAP [Hz]	FDD [Hz]	SSI-CVA [Hz]	Damping [%]	MAC [%]
1	7.25	7.227	7.244	0.276	99.55
2	7.57	7.52	7.507	0.032	99.72
3	13.90	13.9	13.90	0.156	99.96
4	20.37	20.38	20.37	0.006	99.80
5	21.37	21.35	21.36	0.278	99.79

Table 5.24: Case 18 Self-Correlations

Mode	SAP [Hz]	FDD [Hz]	SSI-CVA [Hz]	Damping [%]	MAC [%]
1	7.21	7.227	7.202	0.348	89.64
2	7.60	7.617	7.584	0.426	99.86
3	13.82	13.80	13.81	0.112	100.00
4	20.06	20.05	20.02	0.492	96.40
5	21.70	21.71	21.67	0.263	97.02

Table 5.25: Case 19 Self-Correlations

Mode	SAP [Hz]	FDD [Hz]	SSI-CVA [Hz]	Damping [%]	MAC [%]
1	7.45	7.454	7.441	0.286	98.70
2	7.65	7.682	7.680	0.135	99.99
3	14.19	14.19	14.19	0.139	100.00
4	20.44	20.44	20.43	0.019	99.98
5	21.64	21.65	21.64	0.072	99.96

Table 5.26: Case 20 Self-Correlations

Mode	SAP [Hz]	FDD [Hz]	SSI-CVA [Hz]	Damping [%]	MAC [%]
1	7.38	7.406	7.404	0.247	94.39
2	7.75	7.764	7.765	0.120	98.64
3	14.21	14.21	14.21	0.128	99.75
4	19.48	19.48	19.49	0.072	98.63
5	21.85	21.83	21.86	0.096	93.09

Table 5.27: Case 21 Self-Correlations

Mode	SAP [Hz]	FDD [Hz]	SSI-CVA [Hz]	Damping [%]	MAC [%]
1	7.30	7.324	7.298	0.409	99.83
2	7.72	7.747	7.778	0.130	99.93
3	14.05	14.06	14.05	0.100	100.00
4	20.40	20.41	20.40	0.013	99.94
5	21.41	21.42	21.44	0.114	99.86

Table 5.28: Case 22 Self-Correlations

Mode	SAP [Hz]	FDD [Hz]	SSI-CVA [Hz]	Damping [%]	MAC [%]
1	7.42	7.422	7.423	0.290	95.75
2	7.80	7.764	7.771	1.404	91.28
3	14.00	14.00	14.00	0.126	99.98
4	19.97	19.97	19.97	0.008	98.40
5	21.60	21.60	21.61	0.060	99.52

Table 5.29: Case 23 Self-Correlations

Mode	SAP [Hz]	FDD [Hz]	SSI-CVA [Hz]	Damping [%]	MAC [%]
1	7.43	7.422	7.44	0.463	98.70
2	7.72	7.747	7.737	0.161	99.94
3	14.22	14.23	14.22	0.124	99.93
4	20.14	20.15	20.13	0.056	95.79
5	21.49	21.48	21.55	0.133	99.72

Table 5.30: Case 24 Self-Correlations

Mode	SAP [Hz]	FDD [Hz]	SSI-CVA [Hz]	Damping [%]	MAC [%]
1	7.40	7.402	7.404	0.358	96.08
2	7.66	7.65	7.645	0.769	97.59
3	14.12	14.13	14.13	0.104	100.00
4	20.05	20.05	20.05	0.022	99.88
5	21.71	21.71	21.73	0.083	99.97

Table 5.31: Case 25 Self-Correlations

Mode	SAP [Hz]	FDD [Hz]	SSI-CVA [Hz]	Damping [%]	MAC [%]
1	7.21	7.227	7.214	0.318	99.70
2	7.53	7.520	7.210	0.176	99.87
3	13.82	13.83	13.82	0.123	99.84
4	19.55	19.89	19.89	0.012	99.83
5	21.69	21.68	21.70	0.069	99.64

Chapter 6. Development of the Damage Detection Methodology

This chapter will discuss the initial development of the damage detection methodology (DDM) that is used in this project. As discussed in Chapter 4, the intention is to develop a framework for a DDM that will be implemented in the SHM system. Consequently the DDM described here is an example using a select number of algorithms as per the scope of this project. In a larger sense, the framework is expandable to include other damage detection algorithms (DDAs). In this thesis the type of damage detection methodology that will be used is one that requires ambient vibration signals as input, a pre-event database (for example a set of signals when the structure is undamaged), then finally a set of signals from the structure after a potentially damaging event.

Two important concepts for the development of the DDM are:

- The methodology is based on the idea that it must use at least two independent techniques (DDAs) with the purpose of:
    i. creating redundancy in the system, particularly if one technique fails to predict damage in a certain case
    ii. improving the overall damage prediction
- The methodology is evaluated by two parameters:
    i. the 'success rate' (SR) which is defined as the *total identified damaged members over the total damaged members in the case(s)*
    ii. the 'efficiency rate' (ER) which is defined as the *total identified undamaged members over the total undamaged members in the case(s)*

The second point is important since it helps to define the design goals for the methodology. The methodology must not only be successful at identifying the damaged members, but it also must be successful at identifying the undamaged members. A method with a satisfactory SR but very low ER is essentially ineffective. False predictions in this thesis are referred to as 'overpredictions'. Also introduced in this chapter is the development of a third parameter, which describes the distribution of the overpredicted members. This is essentially just as important as the ER, since a large distribution of the overpredictions can cause problems. The design targets for SR and ER will be described later.

In this chapter, the DDM is applied to a 2D truss example first, and then to a 3D frame. In fact, the 2D truss was used first to implement the individual DDAs; these were then applied to the 3D frame and then DDM was created accordingly. Then the modified DDM was applied back to the 2D truss to observe improvements. These initial steps are applied to simplified simulations of both structures. Lastly in this chapter, the DDM is applied to the calibrated simulations of the 3D frame (from Chapter 5) and to the real datasets that are available. More modifications are made as necessary, and then the final DDM from this chapter is applied to the real building cases presented in Chapter 7.

Section 6.1 discusses the original development for the DDM; this includes the original selection of damage detection techniques and their implementation. Section 6.2 will present the DDM as it was developed from the analysis on the first two examples. The next several sections will present the application of the DDM to examples, including discussion of the development where applicable. Section 6.3 presents its application to the 2D truss; Section 6.4 presents its application to a set of plain 3D frame simulations; Section 6.5 presents its application to the calibrated simulations of the 5 benchmark cases; Section 6.6 presents its application to the real data and Section 6.7 presents the results of a performance study on the DDM using 10 random damage cases. These 10 cases feature lower damage levels and distributed damage. Section 6.8 presents a generalization of the DDM; this is done to illustrate the DDM as a framework that can be built upon depending on the specific case.

6.1. Initial Development of the Damage Detection Methodology

The DDM is a critical part of the implementation method, as it is a framework for implementation of the DDA's into the SHM system. As mentioned in Chapter 4, the basis of implementing the DDA's for this thesis is to combine several together to create a combined prediction. For this thesis, originally two DDA's were chosen to explore this concept: the Stochastic Damage Locating Vector (SDLV) technique and a Sensitivity-Based Model Updating (SBMU) technique. Both of these were initially implemented and tested using a simple 2D frame example. It was found that while the SDLV technique provided satisfactory results, the SBMU technique did not. The problem was that when using model updating for damage detection, the set of parameters for updating includes all of the members, since the location of damage is unknown. This tends to be very large and the updating does not tend to converge on the damaged members.

It was found with further development that if the damage prediction from the SDLV technique was used as the updating parameter set, the SBMU technique could converge on the correct damaged members. This uses the SBMU as a secondary or dependent damage detection technique. To examine another independent technique, the Proportional Flexibility Matrix technique was added; through several iterations and modifications the DDM as presented in the next section was developed.

6.2. The damage detection methodology (DDM)

The DDM is shown in detail in Figure 6.1. It integrates several commercial software products, and various concepts of signal processing and damage detection. The DDM as it is shown here uses the DLV technique as its main damage detection algorithm. It was chosen to demonstrate the overall development of the DDM, and does not intend to endorse the technique as being better or worse than other algorithms. Also, in reference to Section 3.7 to Section 3.9, the DLV technique is stated to provide exact results when exact flexibility matrices are obtained. Here in the discussion of the DDM, it is stated that 'false' predictions must be dealt with. These false predictions do not come from the DLV technique itself; rather come from practical issues such as the approximations of the flexibility matrices obtained and other issues within the DDM.

The methodology can be summarized in seven steps (the steps as related to points in the figure are identified with a superscript):

Step 1: Process signals

The ambient vibrations signals[1a] obtained from the structure (or the simulation) are first processed[1b] in ARTeMIS Extractor using the various system identification techniques available. The modes and frequencies[1c] from the SSI-CVA technique are output to MATLAB[1d].

Step 2: Selection of sensor set

The next step in the process is the selection of which sensors to use for the analysis. As mentioned in Chapter 3, the DLV concept relies on finding the null space in the change in flexibility. Therefore it is necessary to ensure that the number of sensors used is not significantly greater than the number of modes identified in step *i)*, and should be limited to twice that number. In addition to the number chosen, the sensor distribution must also be

selected. To allow for a good distribution of sensors in the system, it is important to identify as many modes as possible in step *i)*.

Step 3: DLV Analyses

Next the DLV analyses are carried out. For the SDLV technique[3a], once the sensor set is chosen, the only variable that remains is the threshold for selection of singular values. In this methodology the threshold is set to 20% of the maximum singular value. In the paper by Bernal [2006], it is set to 10%. This introduces the concept of internal vs external optimization of the DLV predictions. Internal optimization attempts to filter out non-DLV's inside the damage detection technique. This is typically done by taking a lower threshold, resulting in less possible DLV's. External optimization takes as many possible DLV's from the method, and filters out the false predictions later. A higher threshold allows for more possible DLV's to be computed[3d].

For the PFM technique[3b], the DLV threshold is also set to 20%. Another variable, the normalization element must also be selected[3c]. For use in this methodology, the PFM analysis is repeated a total of n times, one for each DOF. This way each element of the real mass matrix is chosen as the normalization element, and n separate sets of DLV's are computed[3e].

Step 4: Static Analysis and Prediction Set Normalization

The DLV's are computed and then input to SAP2000 as static load vectors[4a]. The FEM of the structure is processed and the element forces are computed[4b]. The resulting force sets are input to MATLAB and normalized to a maximum of 1[4c]. This creates the 'prediction sets', and the number of sets is equal to the number of DLV's found[4d]. In any given prediction set, the elements with a normalized force less than 0.1 are considered to be possibly damaged. Of these prediction sets, some will not computed from real DLV's and are considered to be random.

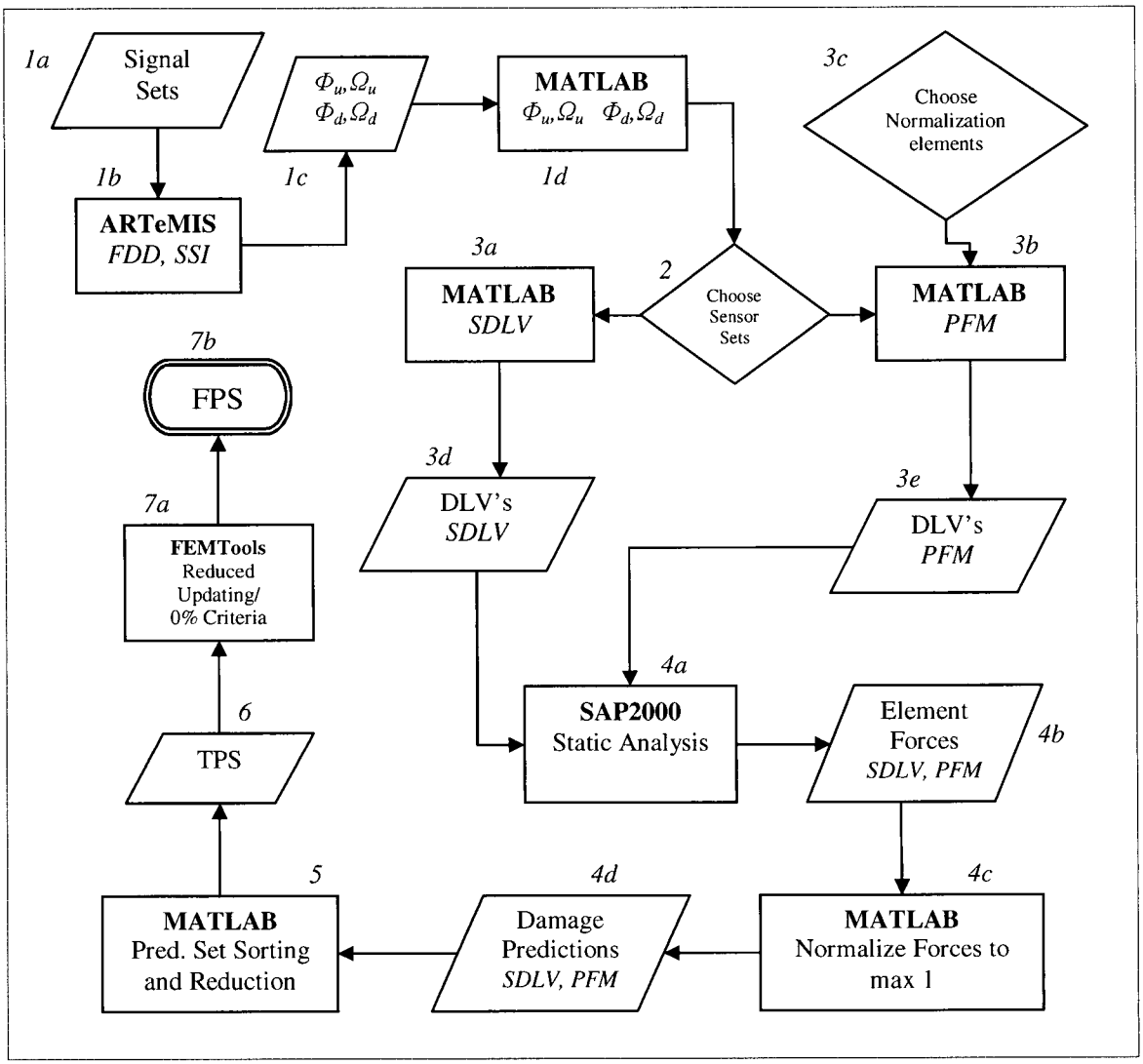

Figure 6.1: Damage Detection Methodology

Step 5: Prediction Set Reductions

The normalized prediction sets are then processed with MATLAB for a reduction. The idea is to obtain the best overall prediction, knowing that some of the prediction sets have been computed from load vectors that are not DLV's, and are instead random. The prediction sets are assembled in a matrix form, so that each of the elements has a 'sample set' of normalized predictions. An example from the truss that will be presented is shown in Figure 6.1. The example is taken from the PFM results, where a total of 18 DLV's formed the sample set (the idea of a sample set for element #4 is highlighted in Table 6.1). The simplest way to calculate the overall prediction would be to average all values for an element. However, it is easily shown that one outlier could raise the average above 0.1, thus resulting in a false prediction. To

address this, several ways of sorting the prediction set were explored. The results of the various methods are shown in Table 6.2.

Table 6.1: PFM Normalized Damage Predictions

0.08	0.09	0.05	0.01	0.02	0.04	0.04	0.31	0.05	0.01	0.12	0.06	0.04	0.01	0.03	0.03	0.02
0.07	0.70	0.28	0.04	0.13	0.06	0.06	0.37	0.00	0.06	0.13	0.65	0.57	0.63	0.32	0.00	0.09
0.07	0.07	0.05	0.00	0.01	0.04	0.03	0.25	0.03	0.01	0.10	0.05	0.03	0.01	0.02	0.02	0.02
0.05	0.05	0.03	0.01	0.01	0.02	0.02	0.18	0.03	0.00	0.07	0.03	0.03	0.00	0.02	0.02	0.01
0.24	0.61	1.00	0.80	0.02	0.76	0.09	0.81	0.30	0.20	0.23	1.00	0.27	1.00	0.09	0.14	0.42
0.08	0.33	0.33	0.44	0.15	0.40	0.01	0.12	0.18	0.18	0.27	0.04	0.41	0.03	0.38	0.09	0.35
0.19	0.49	0.79	0.66	0.03	0.64	0.08	0.65	0.25	0.16	0.18	0.79	0.20	0.80	0.08	0.11	0.35
0.09	0.32	0.58	0.48	0.00	0.45	0.07	0.31	0.21	0.12	0.07	0.58	0.13	0.60	0.07	0.07	0.25
0.06	0.74	0.33	1.00	0.58	0.83	0.68	0.42	1.00	0.07	0.10	0.89	0.93	0.08	0.54	0.52	0.14
0.04	0.12	0.51	0.16	0.19	0.09	0.43	0.38	0.43	0.22	0.22	0.51	0.14	0.07	0.05	0.39	0.26
0.10	0.34	0.84	0.78	0.25	0.26	1.00	0.23	0.79	0.58	0.00	0.95	0.35	0.23	0.31	0.95	0.10
0.09	0.96	0.33	0.15	0.52	0.36	0.00	0.65	0.42	0.24	0.05	0.95	1.00	0.68	0.34	0.03	0.01
0.06	0.31	0.72	0.05	0.29	0.50	0.55	0.15	0.03	0.66	0.10	0.28	0.51	0.20	0.15	0.68	0.26
0.09	0.19	0.74	0.20	0.16	0.06	0.70	0.17	0.51	0.46	0.26	0.46	0.16	0.38	0.23	0.66	0.44
0.10	0.24	0.08	0.04	0.11	0.06	0.00	0.29	0.13	0.05	0.06	0.23	0.25	0.15	0.09	0.00	0.00
0.04	0.27	0.67	0.32	0.67	0.76	0.79	0.48	0.23	1.00	0.17	0.26	0.60	0.23	0.31	1.00	0.19
0.17	1.00	0.04	0.13	0.19	0.29	0.26	0.10	0.38	0.03	0.49	0.60	0.73	0.97	0.86	0.08	0.67
0.05	0.13	0.11	0.18	1.00	1.00	0.28	0.75	0.79	0.78	0.47	0.13	0.59	0.10	0.62	0.59	0.68
0.13	0.43	0.35	0.07	0.27	0.36	0.34	0.37	0.14	0.44	0.00	0.07	0.54	0.28	0.18	0.41	0.17
0.80	0.60	0.37	0.26	0.52	0.48	0.21	0.79	0.23	0.08	0.13	0.14	0.45	0.51	0.82	0.05	0.82
0.42	0.54	0.26	0.07	0.19	0.05	0.08	0.50	0.23	0.08	0.60	0.49	0.40	0.60	0.25	0.03	0.07
1.00	0.74	0.47	0.34	0.63	0.57	0.28	1.00	0.26	0.08	0.17	0.17	0.55	0.62	1.00	0.07	1.00
0.16	0.34	0.28	0.17	0.33	0.24	0.16	0.10	0.34	0.04	0.29	0.01	0.19	0.34	0.55	0.06	0.58
0.58	0.71	0.33	0.10	0.27	0.08	0.10	0.67	0.28	0.11	0.80	0.65	0.52	0.77	0.32	0.05	0.07
0.71	0.90	0.42	0.12	0.31	0.10	0.13	0.85	0.36	0.13	1.00	0.82	0.66	0.98	0.42	0.06	0.10
0.44	0.10	0.00	0.03	0.05	0.10	0.00	0.69	0.18	0.01	0.39	0.12	0.14	0.04	0.06	0.02	0.04

In the table, damage predictions (less than 0.1) are highlighted. In the example shown, one of the two members is missed by simply taking the mean. Therefore another approach should be applied. The damaged members are highlighted.

The two initial criteria explored were the μ-σ and μ-σ^2 criteria. These two criteria tended to form the bounds of the reduction, with the standard deviation providing a higher success rate, while the variance has a higher efficiency rate, but tends to miss more damaged members. This is seen in the example, with the μ-σ method finding both damaged members, but overpredicting by 13 members (ER = 46%). It is seen that μ-σ can result in values that are negative. These are

considered to be less than 0.1. The μ-σ^2 method also finds both damaged members, but only overpredicts by 2 members (ER = 92%).

Table 6.2: Examples of the Prediction Set Reductions (Truss Case 4 – PFM Technique)

Element	μ	μ-σ	μ-σ^2	*S and R*
1	**0.057**	**-0.013**	**0.052**	**0.016**
2	0.232	**-0.014**	0.171	**0.039**
3	**0.046**	**-0.011**	**0.043**	**0.013**
4	**0.033**	**-0.008**	**0.031**	**0.010**
5	0.489	0.133	0.362	0.159
6	0.237	**0.081**	0.213	**0.087**
7	0.395	0.111	0.314	0.129
8	0.273	**0.064**	0.229	**0.079**
9	0.551	0.196	0.425	0.215
10	0.242	**0.083**	0.216	0.101
11	0.476	0.147	0.368	0.185
12	0.394	**0.060**	0.282	0.112
13	0.327	**0.099**	0.275	0.125
14	0.332	0.113	0.284	0.141
15	0.108	**0.018**	0.100	**0.036**
16	0.465	0.172	0.379	0.213
17	0.391	**0.056**	0.279	0.100
18	0.489	0.170	0.387	0.182
19	0.269	0.119	0.246	0.129
20	0.405	0.126	0.327	0.142
21	0.272	**0.061**	0.227	**0.076**
22	0.500	0.156	0.382	0.177
23	0.234	**0.069**	0.207	**0.092**
24	0.358	**0.081**	0.281	0.103
25	0.451	0.100	0.328	0.125
26	0.135	**-0.053**	**0.099**	**0.019**

Another criteria explored is to eliminate the outliers (above $\mu+\sigma$) criteria, and then compute the average of the remainder of the sample set. The difficulty with using these types of criteria is that with normalized values from 0 to 1, the deviations tend to be high and important information can be missed.

A better and more conservative approach is to simply sort the sample set and remove the highest values. Specifically, the sample set is sorted from lowest to highest, the highest values are eliminated and the mean is computed. In this way, random values that contribute to high predictions will not interfere if the general trend is of values below 0.1. Random values that are lower are included in the prediction, therefore causing it to be conservative. This concept is referred to as the '*sort and remove*' criteria.

The rationalization of the sort and remove criteria can be explained in the following way. It is reasonable to assume that half of the predictions are from real DLV's. Then in the half from the real DLV's (ie. true predictions), the number of values less than 0.1 and those between 0.1 and 1.0 are fixed, based on the state of the structure (ie. the number of damaged members). For the half that are not based on DLV's (ie. false predictions), the prediction values are random. If it can be said that the random values have a mean of 0.5 and some unknown standard deviation, then it is reasonable to assume that the amount of values less than 0.1 is typically small. In other words the majority of false prediction values would be above 0.1 (ie. identified as being not damaged). So then by sorting the values and eliminating the highest ones, it will not eliminate any true damage predictions, and with the above logic most of the random values are higher so they would be eliminated. (Numerically a true-undamaged and a false-undamaged prediction contribute the same to the analysis, so sorting and eliminating has the same effect even if some true-undamaged predictions are eliminated).

Step 6: Total Prediction Set

Next the Total Prediction Set (TPS) is formulated. It is defined as the set which contains all of the elements predicted by each of the two damage detection techniques. In addition to this, the Common Set (CS) can be defined, which only includes those members predicted by both techniques. The TPS has a higher SR with a lower ER. The CS is typically the best way to improve ER, but will miss any members not predicted independently by both techniques.

Step 7: Reduced Model Updating

Once the TPS has been formulated, it can be used as the parameter set for a reduced model updating[7a]. The software FEMTools is used to apply a sensitivity-based model updating. In the updating the damaged modes are input and correlated with the undamaged FEM modes. The undamaged model is then updated to match the damaged modes. Only the members in the TPS are allowed to change in the process. This is done in an attempt to improve the overall results of the DDM by eliminating false predictions. Elements that do not contribute to the updating (ie. those with 0% Parameter Change), are eliminated from the TPS. This will give the final prediction set (FPS)[7b]. Different criteria can be introduced, such as 10%, 30% etc. However, while these will have a higher ER by eliminating more false predictions, the SR tends to decrease. The combined method (Step 6 and 7) is referred to as the TPS-MU0% criteria.

6.3. 2D Truss Example

For the initial development of the DDM, a 7-bay truss was created in SAP2000, shown in Figure 6.2. In the example, a total of 15 damage cases were created, each by reducing the cross-sectional area of specific members. The first five damage cases (1-10) were created to find damage in a particular type of member or set, specifically a diagonal, vertical, and chord member; and also a situation where two members and then three members were damaged. The next ten cases (6-15) all contain two damaged members randomly distributed. The members that were damaged in the various cases are shown in Table 6.3 and Table 6.5. The frequencies for all the cases including the undamaged case are given in Table 6.4 and Table 6.6. In addition to the 15 damaged cases, 3 cases with no damage were created to test the DDM.

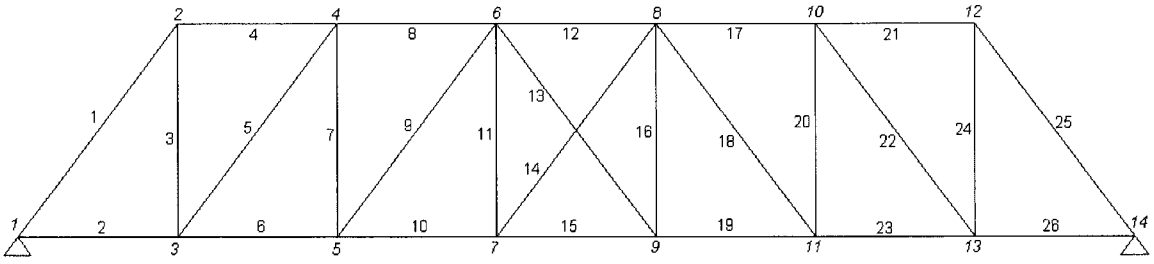

Figure 6.2: 2D Truss Example

Table 6.3: Damage Cases 1-5

Case	1	2	3	4	5
Damage	5	20	23	5,8	14,17,22

Table 6.4: Damage Cases 1-5 Frequencies

		Frequency [Hz]						
	Case	1	2	3	4	5		Undamaged Case
Mode Number	1	2.701	2.704	2.828	2.574	2.575		2.828
	2	6.647	6.667	6.496	6.476	6.285		6.669
	3	9.517	9.003	9.745	9.464	9.433		9.760
	4	11.882	12.012	13.655	11.823	11.507		13.790
	5	14.999	15.205	15.418	14.982	14.934		15.570
	6	17.588	17.650	17.641	17.572	16.184		17.140

Table 6.5: Damage Cases 6-15

Case	6	7	8	9	10	11	12	13	14	15
Damage	7,17	10,14	21,22	3,26	7,16	9,12	15,23	4,18	16,17	6,25

Table 6.6: Damage Cases 6-15 Frequencies and Undamaged Case

		Frequency [Hz]									
	Case	6	7	8	9	10	11	12	13	14	15
Mode Number	1	2.435	2.815	2.469	2.567	2.689	2.387	2.844	2.625	2.507	2.394
	2	6.352	6.416	6.366	6.100	6.601	5.833	6.331	5.767	6.239	5.485
	3	8.847	9.483	8.365	9.200	8.910	8.367	9.609	7.862	9.405	8.851
	4	11.93	13.04	10.08	13.61	11.51	13.73	13.53	13.57	13.41	13.12
	5	14.93	15.36	14.90	15.45	14.28	13.94	15.30	13.80	14.14	14.96
	6	17.63	16.46	17.55	17.44	15.77	16.83	17.55	16.80	15.68	17.51

For each of the above cases, the SAP truss model was subjected to white noise loading in the two orthogonal planar directions at the each support. The vertical excitation was set to 10% of the horizontal. The white noise loads were created in MATLAB, with a uniformly generated

random frequency from 0.1 to 50 Hz, and a uniformly distributed random amplitude from 0 to 1. Each of the four signals was random and independent, so that each support had different loadings in both directions (primarily to ensure out-of-phase excitation for part of the time-history). The mode superposition method of time-history analysis was applied, with damping values of 0.02, 0.01, 0.005, 0.005, 0.001 and 0.001 for each of the first six modes.

To demonstrate the performance of the DDM and the application of the DLV techniques, three detailed examples are presented here. All of the results for the 18 cases will be presented in a Table 6.10 with respect to their success and efficiency rates. For each case, the prediction set was sorted by the five methods described in Section 6.1: μ, μ-σ, μ-σ^2, remove outliers above $\mu+\sigma$ (denoted as *Rem*[$\mu+\sigma$]), and Sort and Remove (*S*+*R*). Each of the figures displays the average normalized prediction value (from 0 to 1) versus the element number. The damage threshold is 0.1, and is displayed as a dotted line on each figure. It is noted that in the calculation of the μ-σ criteria, it is possible to get negative values; those are still considered to be less than 0.1 and therefore belong in the damage set. Case 5, 9 and 10 are chosen for these examples and are shown in Figure 6.3 to Figure 6.5. Following each figure is a table showing the predictions from the SDLV and PFM *S*+*R* criteria. The actual damaged values are shown in bold. Then the results from the TPS-MU0% criteria are shown.

Case 5 – Damaged elements 14, 17, 22

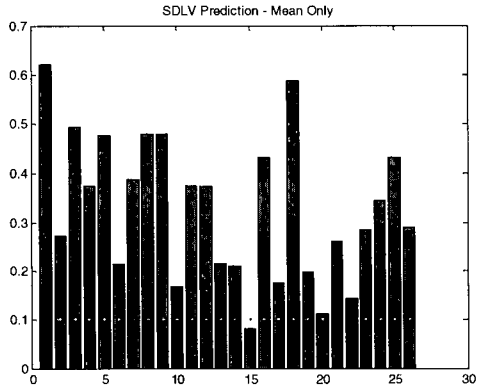

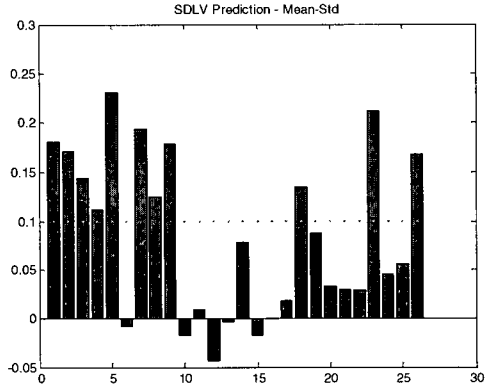

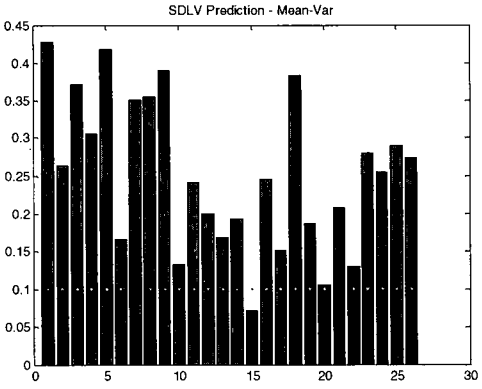

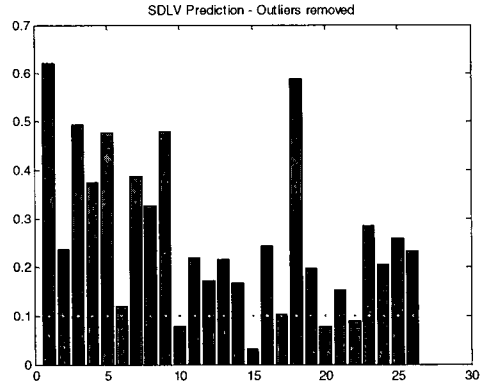

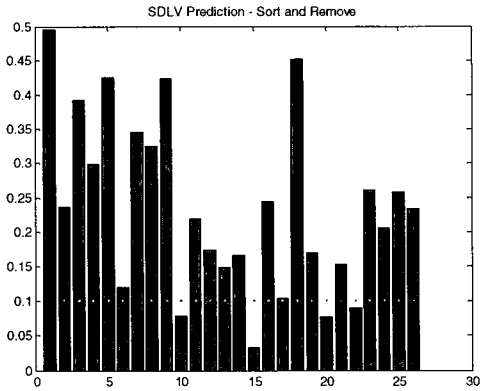

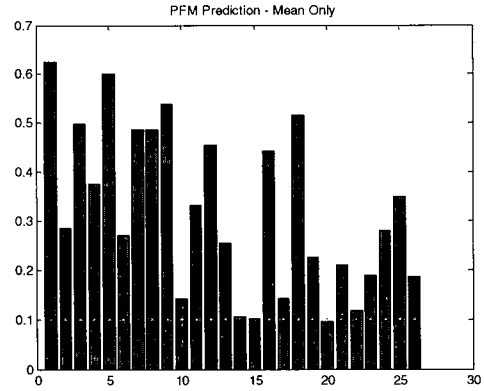

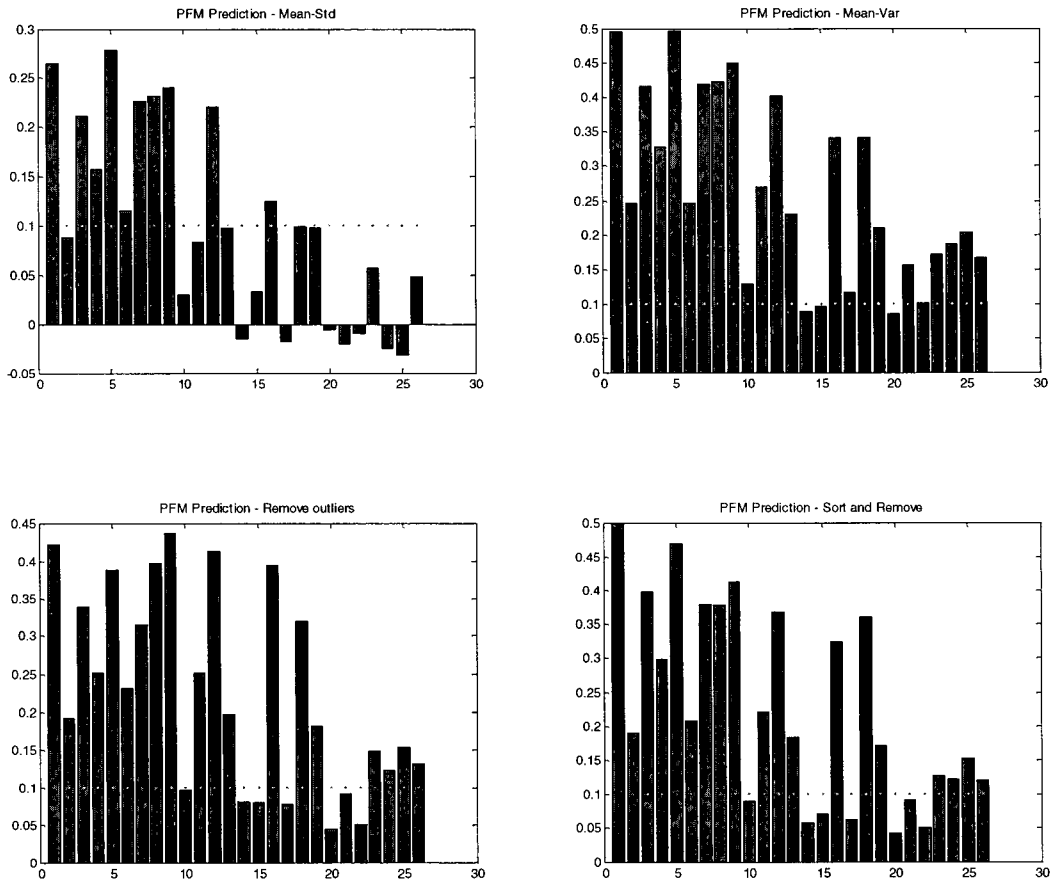

Figure 6.3: Case 5 Prediction Plots

Table 6.7: Case 5 Predictions

	SDLV	PFM
μ	15	15,20
μ-σ	6,10,11,12,13,**14**,15,16,**17**,19,20,21,**22**,24,25	2,10,11,13,**14**,15,**17**,18,19,20,21,**22**,23,24,25,26
μ-σ^2	15	**14**,15,20
Rem[μ+σ]	10,15,20,22	10,**14**,15,**17**,20,21,**22**
S+R	10,15,20,22	10,**14**,15,**17**,20,21,**22**
TPS-MU0%	10,**14**,15,**17**,20,21,**22**	

Case 9 – Damaged elements 3,26

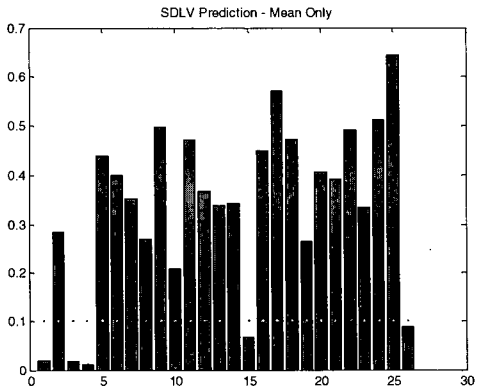

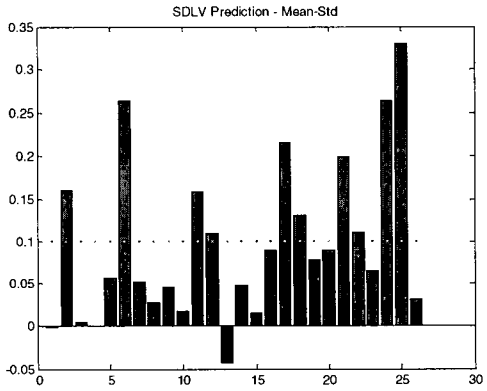

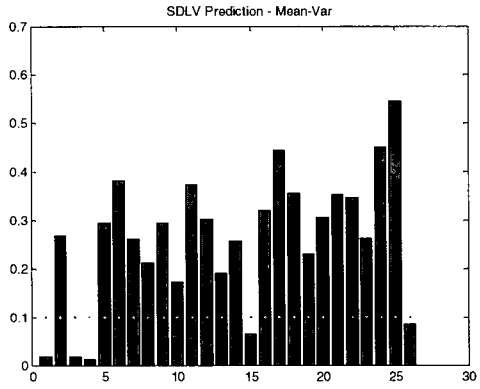

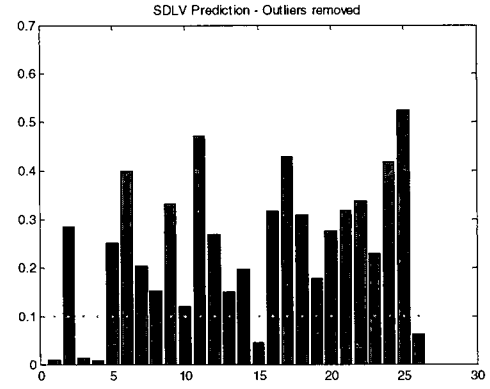

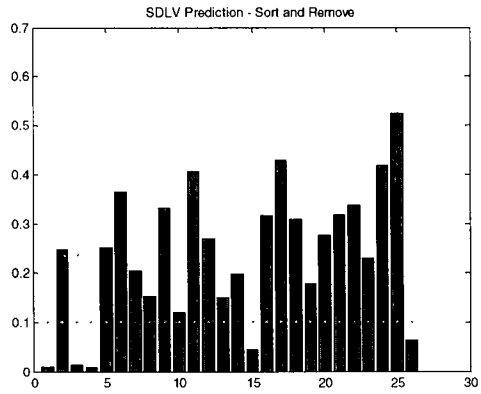

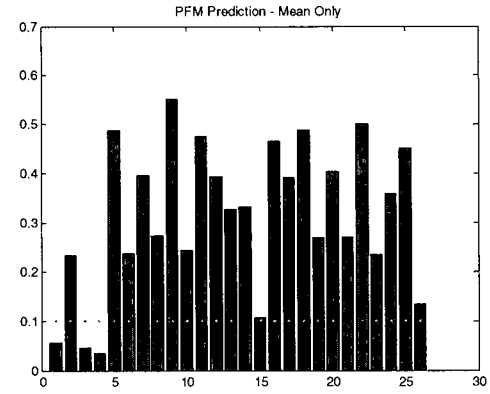

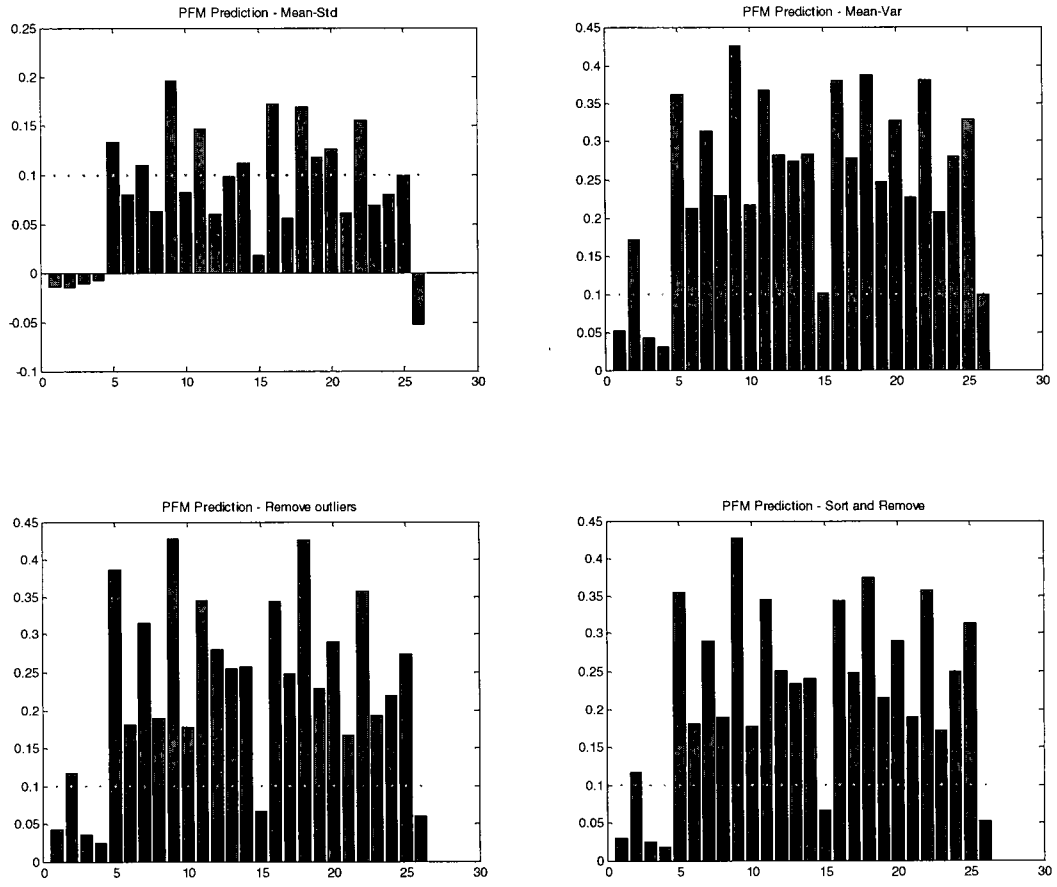

Figure 6.4: Case 9 Prediction Plots

Table 6.8: Case 9 Predictions

	SDLV	PFM
μ	1,**3**,4,15,**26**	1,**3**,4
μ-σ	1,**3**,4,5,7,8,9,10,13,14,15,16,19,20,23,**26**	1,2,**3**,4,6,8,10,12,15,17,21,23,24,**26**
μ-σ^2	1,**3**,4,15,**26**	1,**3**,4
Rem[μ+σ]	1,**3**,4,15,**26**	1,**3**,4,15,**26**
S+R	1,**3**,4,15,**26**	1,**3**,4,15,**26**
TPS-MU0%	1,**3**,4,15,**26**	

Case 10 – Damaged elements 7, 16

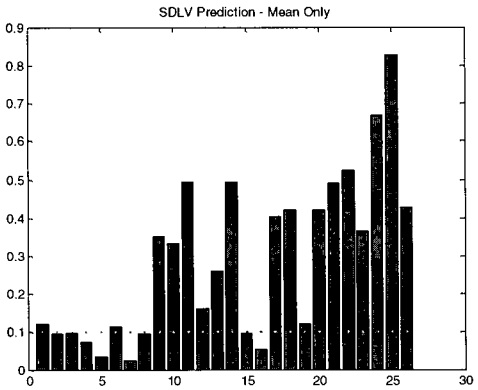

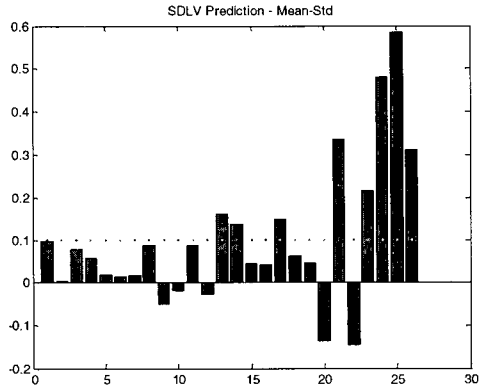

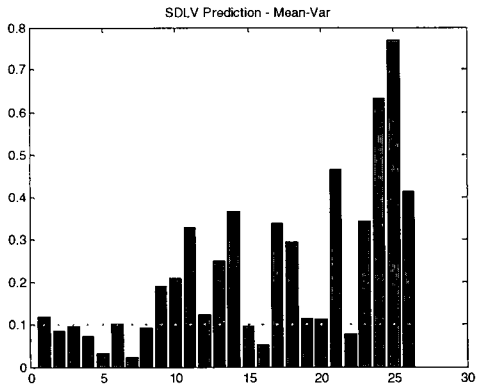

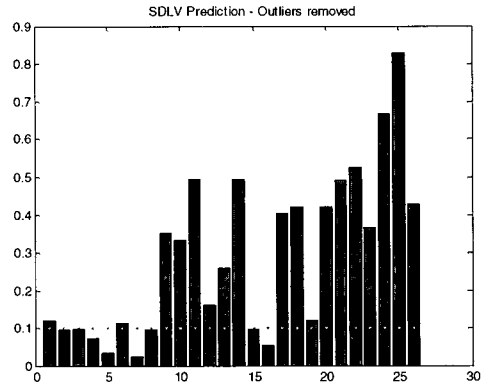

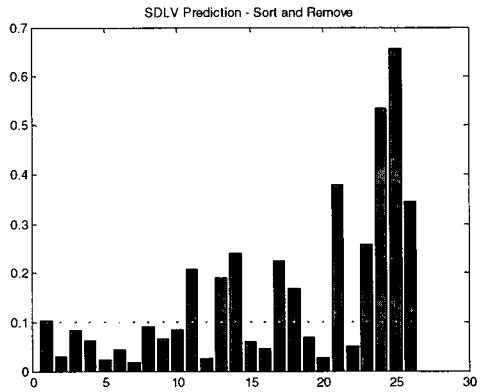

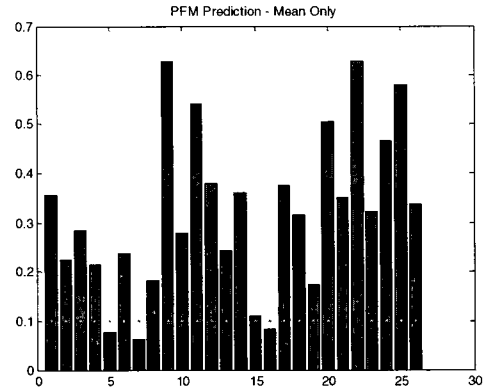

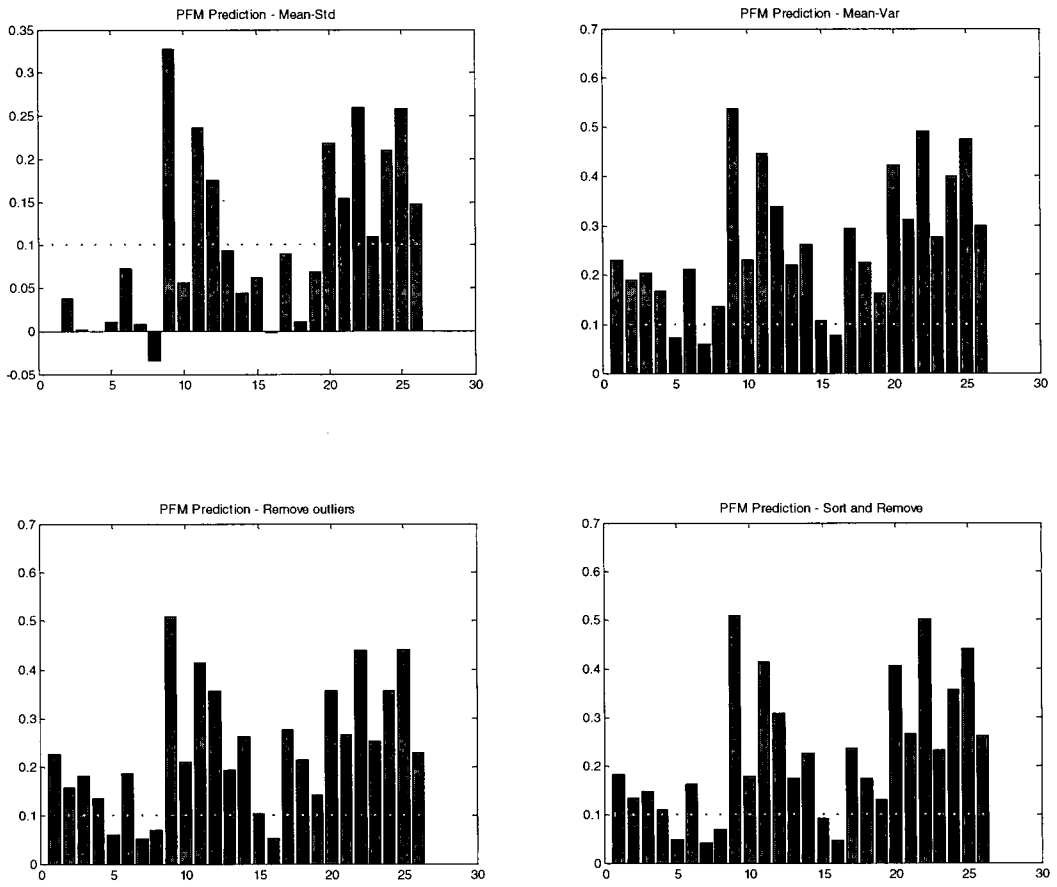

Figure 6.5: Case 10 Prediction Plots

Table 6.9: Case 10 Predictions

	SDLV	PFM
μ	2,3,4,5,**7**,8,15,**16**	5,**7**,**16**
μ-σ	1,2,3,4,5,6,**7**,8,9,10,11,12,15,**16**,18,19,20,22	1,2,3,4,5,6,**7**,8,10,13,14,15,**16**,17,18,19
μ-σ^2	2,3,4,5,**7**,8,15,**16**,22	5,**7**,**16**
Rem[μ+σ]	2,3,4,5,**7**,8,15,**16**	5,**7**,8,**16**
S+R	2,3,4,5,6,**7**,8,9,10,12,15,**16**,19,20,22	5,**7**,8,15,**16**
TPS-MU0%	~~2~~,3,4,5,~~6~~,**7**,~~8~~,9,10,12,15,**16**,19,20,22	

Table 6.10: Summary of 2D Truss Results

	Case	μ		μ-σ		μ-σ^2		*Rem*[μ+σ]		S+R			
		SR	ER	SR	ER	SR	ER	SR	ER	SR	ER		
SDLV	1	1/1	24/25	1/1	14/25	1/1	24/25	1/1	24/25	1/1	24/25		
	2	1/1	24/25	1/1	11/25	1/1	23/25	1/1	24/25	1/1	23/25		
	3	1/1	23/25	1/1	9/25	1/1	20/25	1/1	16/25	1/1	15/25		
	4	2/2	20/24	2/2	13/24	2/2	20/24	2/2	19/24	2/2	19/24		
	5	0/3	22/23	3/3	11/23	0/3	22/23	1/3	20/23	1/3	20/23		
	6	2/2	22/24	2/2	12/24	1/2	21/24	1/2	21/24	2/2	20/24		
	7	2/2	20/24	2/2	13/24	2/2	20/24	2/2	18/24	2/2	18/24		
	8	2/2	20/24	2/2	9/24	2/2	19/24	2/2	16/24	2/2	16/24		
	9	2/2	21/24	2/2	10/24	2/2	21/24	2/2	21/24	2/2	21/24		
	10	2/2	18/24	2/2	8/24	2/2	17/24	2/2	18/24	2/2	11/24		
	11	2/2	23/24	2/2	16/24	2/2	23/24	2/2	23/24	2/2	23/24		
	12	2/2	24/24	2/2	9/24	2/2	24/24	2/2	22/24	2/2	22/24		
	13	2/2	20/24	2/2	15/24	2/2	20/24	2/2	19/24	2/2	19/24		
	14	2/2	21/24	2/2	10/24	2/2	20/24	2/2	20/24	2/2	20/24		
	15	1/2	22/24	2/2	11/24	2/2	20/24	2/2	21/24	2/2	18/24		
	16	---	25/26	---	15/26	---	25/26	---	25/26	---	20/26		
	17	---	25/26	---	18/26	---	25/26	---	25/26	---	24/26		
	18	---	23/26	---	9/26	---	23/26	---	21/26	---	20/26		
	Totals	25 /29	397 /440	29 /29	213 /440	25 /29	387 /440	26 /29	373 /440	27 /29	353 /440	TPS-MU0%	
	%	86	90	100	48	86	88	90	85	93	80	SR	SR
PFM	1	1/1	23/25	1/1	10/25	1/1	23/25	1/1	23/25	1/1	23/25	1/1	23/25
	2	1/1	23/25	1/1	10/25	1/1	23/25	1/1	23/25	1/1	22/25	1/1	23/25
	3	1/1	24/25	1/1	16/25	1/1	23/25	1/1	23/25	1/1	23/25	1/1	19/25
	4	2/2	22/24	2/2	14/24	2/2	19/24	2/2	19/24	2/2	19/24	2/2	19/24
	5	0/3	21/23	3/3	10/23	1/3	21/23	3/3	19/23	3/3	19/23	3/3	19/23
	6	2/2	22/24	2/2	13/24	2/2	22/24	2/2	22/24	2/2	22/24	2/2	20/24
	7	2/2	23/24	2/2	13/24	2/2	23/24	2/2	23/24	2/2	23/24	2/2	20/24
	8	2/2	19/24	2/2	12/24	2/2	19/24	2/2	17/24	2/2	17/24	2/2	19/24
	9	1/2	22/24	2/2	12/24	1/2	22/24	2/2	21/24	2/2	21/24	2/2	21/24
	10	2/2	23/24	2/2	10/24	2/2	23/24	2/2	22/24	2/2	21/24	2/2	15/24
	11	2/2	23/24	2/2	5/24	2/2	23/24	2/2	23/24	2/2	23/24	2/2	24/24
	12	2/2	23/24	2/2	14/24	2/2	23/24	2/2	20/24	2/2	20/24	2/2	22/24
	13	2/2	22/24	2/2	13/24	2/2	21/24	2/2	21/24	2/2	21/24	2/2	21/24
	14	2/2	24/24	2/2	13/24	2/2	24/24	2/2	23/24	2/2	23/24	2/2	21/24
	15	2/2	22/24	2/2	10/24	2/2	22/24	2/2	22/24	2/2	22/24	2/2	18/24
	16	---	25/26	---	10/26	---	25/26	---	23/26	---	22/26	---	26/26
	17	---	25/26	---	10/26	---	25/26	---	25/26	---	25/26	---	26/26
	18	---	22/26	---	11/26	---	22/26	---	21/26	---	21/26	---	26/26
	Totals	25 /29	408 /440	29 /29	212 /440	26 /29	403 /440	29 /29	390 /440	29 /29	387 /440	29 /29	382 /440
	%	86	93	100	48	90	92	100	89	100	88	100	87

From the results for Case 5, it is seen that for the *Rem[μ+σ]* and *S+R* criteria the SDLV technique does not work particularly well while the PFM technique does. It can be seen in all of

the examples that the μ-σ criteria tends to have a perfect SR, but it overpredicts too much, hence having a very low ER which makes it essentially ineffective.

From the results for Case 9, it can be seen that the SDLV technique works well for all five criteria, while the PFM misses one element in the first two. This illustrates the usefulness of the *S+R* criteria, because the μ tends to exclude elements (ie. higher ER).

The results for Case 10 mainly show that while both techniques have a successful SR, in this case the SDLV technique tends to overpredict much more than the PFM. It can be seen in all of these results that the *S+R* criteria provides the best SR, and that by combining the two sets of *S+R* predictions into a single TPS, all of the damaged members can be found. Also, when using the MU0% criteria, the ER can be brought up to an acceptable level.

In general, from the above results and the summary table, several points can be made.

- There are cases where the SDLV misses a member but the PFM does not (5), and vice versa (10).
- In general the μ, μ-σ^2, and *Rem[*μ+σ*]* criteria had the highest efficiency rates while the μ-σ and *S+R* criteria had the highest success rates.
- The *Rem[*μ+σ*]* and *S+R* are similar in nature, however the *S+R* criteria tends to be more direct, eliminating a specific number of predictions rather than those above a certain value. This seems to make it more consistent.
- The *TPS-MU0%* technique is effective at providing acceptable results.
- A reasonable target for SR would be ~100% and for ER > 80%.

6.4. Development of the Overprediction Scatter Index

Having an ER > 80% is a reasonable target value, however this does not tell us anything about the distribution of the false predictions; the DDM may not be very useful if the overpredictions are scattered around the structure. Therefore it is useful to create some manner of index that describes that distribution. The simplest way to do this would to look at the relative position of the overpredictions to the damaged members. This can be done simply by counting the number of joints separating a member to its nearest damaged member. In the following table, several

statistical indicators are examined discussing the number of joints to the nearest damaged member. A representation of the OSI could be as follows:

$$OSI = Round\ ((\mu_i+\sigma_i)*(OP)/(TE)\ *10)$$

Where OP is the number of overpredictions, TE is the total number of elements and the subscript i refers to the number of joints separating the overprediction from its nearest damaged member.

Table 6.11 shows results from the development of the OSI. Also shown in the table is the ER calculated from the *S+R TPS-MU0%* results for illustration of the fact that although the ER values are identical, the actual scatter varies.

Table 6.11: Development of the Overprediction Scatter Index (OSI)

Case	μ	σ	$\mu+\sigma$	OSI	ER
1	1.0000	1.4142	2.4142	2	92
2	0.5000	0.7071	1.2071	1	92
3	2.2000	2.1679	4.3679	9	80
4	0.4000	0.5477	0.9477	2	79
5	0.0000	0.0000	0.0000	0	83
6	0.5000	0.5774	1.0774	2	83
7	1.5000	0.5774	2.0774	4	83
8	1.4000	2.1909	3.5909	7	79
9	0.6667	1.1547	1.8214	3	88
10	0.2500	0.4629	0.7129	3	67
11	0.0000	0.0000	0.0000	0	100
12	0.5000	0.7071	1.2071	1	92
13	0.6667	0.5774	1.2441	1	88
14	0.0000	0.0000	0.0000	0	88
15	0.8333	0.7528	1.5861	4	75

It is difficult to see large differences on a small structure such as this one, where in most cases any member would be within a small distance of the damaged members. However, some

differences are evident, and in particularly in cases 5, 6 and 7 the usefulness of such an index becomes apparent. Even though all three have the same ER value, Case 5 has a low scatter value while Case 7 tends to be more distributed. In a physical sense, this means that in Case 5, even thought there are 8 overpredictions, all of them are close to the two damaged members. However in Case 7, there are only two overpredictions, but one of those is at the top of the truss, while both damaged members are along the bottom chord.

6.5. 3D Frame Example

Initially the 2D truss example above was used simply to implement the DDAs in MATLAB and ensure that they worked correctly. Then the DDAs were applied to a simplified simulation from the IASC/ASCE Benchmark model; this led to the development of the DDM as it is presented in Section 6.1. The results of those cases are presented in this section. These first cases were from a slightly different variation of the finite element model than the one presented in Chapter 5; it did not feature any automated updating. Also, the simulation input was only white noise and no 'measurement noise' was added to the signal set. The only aspect of the real frame that was added to the simulation was the damping; this was done in order to improve the picking of modes in ARTeMIS. The damage cases are presented in Table 6.12. The first five are from the benchmark cases described in Chapter 5; the last four were created to examine the behaviour of the method with a more distributed damage set. Also while the benchmark cases always had the members completely removed, cases 13 and 14 featured only a reduction in cross-section.

Table 6.12: 3D Frame Damage Case Members

Case	2	3	4	5	6	11	12	13	14
Members	1,2,9,10 17,18,25,26	1,9,17,25	1,25	1	11,12	5,6,7,32	11,30	9,10,18	1,6,31

The results are presented in a similar way as the truss example. The challenge for analysis of the 3D Frame was that fewer modes were available (5 for each case) and more sensors were available (a total of 15). Therefore the number of sensors needed to be reduced, and the reduced set needed to be chosen. A set of 6 sensors was used, which included 3 sensors each on the 2nd and 4th floors. Similar to the results presented for the 2D truss, a few detailed cases are presented and then a summary table of all of the cases. One difference here is that only plots for

the *S+R* criteria are shown, since it has been established to provide the best results. For the TPS-MU0% criteria, the TPS values are shown, and then those eliminated with the MU0% are indicated with a strikethrough.

Case 3 – Damaged Members 1, 9, 17 and 25

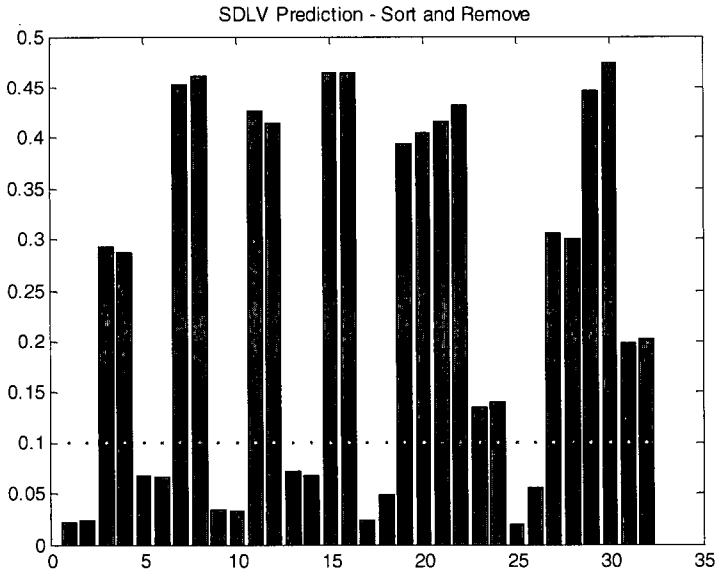

Figure 6.6: 3D Frame Case 3 SDLV Prediction Plot

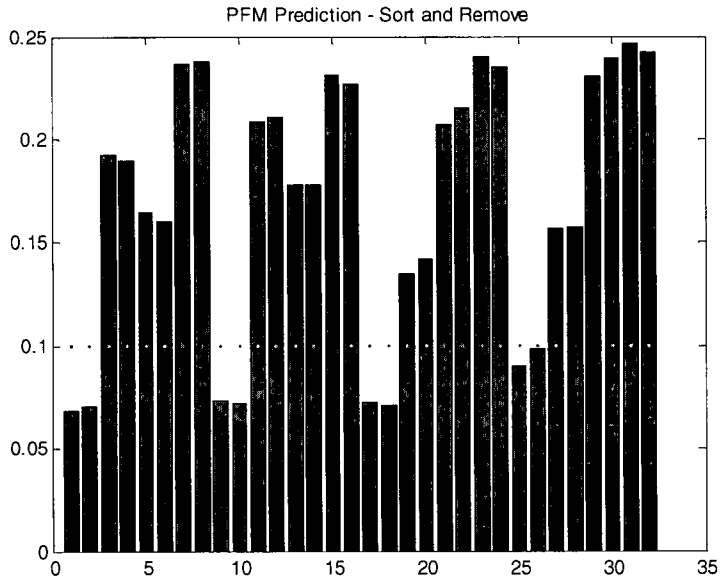

Figure 6.7: 3D Frame Case 3 PFM Prediction Plot

Table 6.13: 3D Frame Case 3 Predictions

	SDLV	PFM
S+R	**1**,2,5,6,**9**,10,13,14,**17**,18,**25**,26	**1**,2,**9**,10,**17**,18,**25**,26
TPS-MU0%	**1**,2,5,6,**9**,10,~~13,14~~,**17**,18,**25**,26	

Case 6 – Damaged Members 11, 12

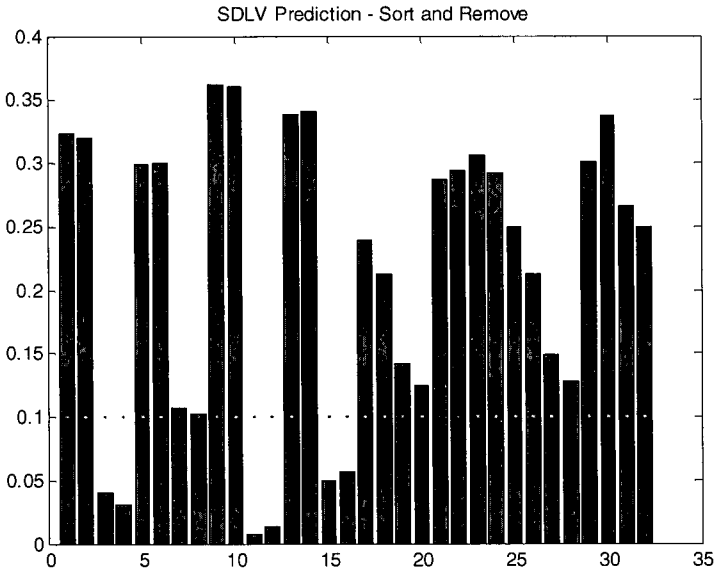

Figure 6.8: 3D Frame Case 6 SDLV Prediction Plot

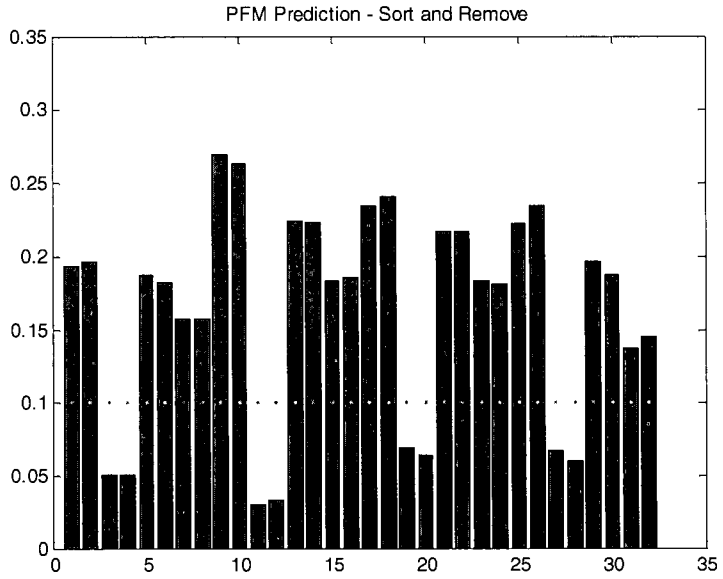

Figure 6.9: 3D Frame Case 6 PFM Prediction Plot

Table 6.14: 3D Frame Case 6 Predictions

	SDLV	PFM
S+R	3,4,**11**,**12**,15,16	3,4,**11**,**12**,19,20,27,28
MU0%	3,4,**11**,**12**,15,16,~~19,20,27,28~~	

Case 11 – Damaged Members 5, 6, 7 and 32

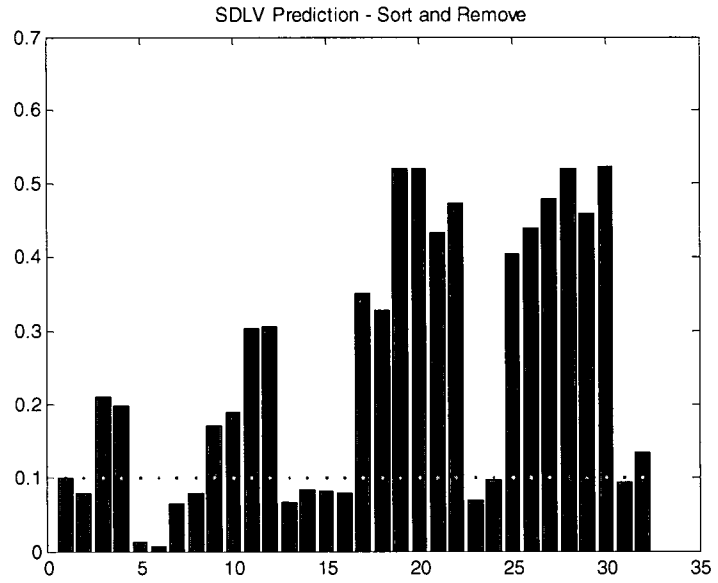

Figure 6.10: 3D Frame Case 11 SDLV Prediction Plot

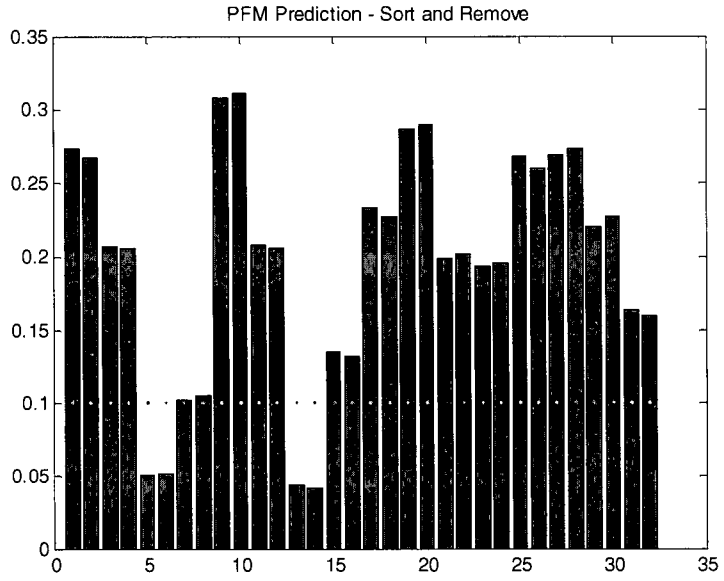

Figure 6.11: 3D Frame Case 11 PFM Prediction Plot

Table 6.15: 3D Frame Case 11 Predictions

	SDLV	PFM
S+R	2,**5**,**6**,**7**,8,13,14,15,16,23,24,31	**5**,**6**,13,14
MU0%	2,**5**,**6**,**7**,8,13,14,15,16,23,24,31	

Case 13 – Damaged Members 9, 10 and 18

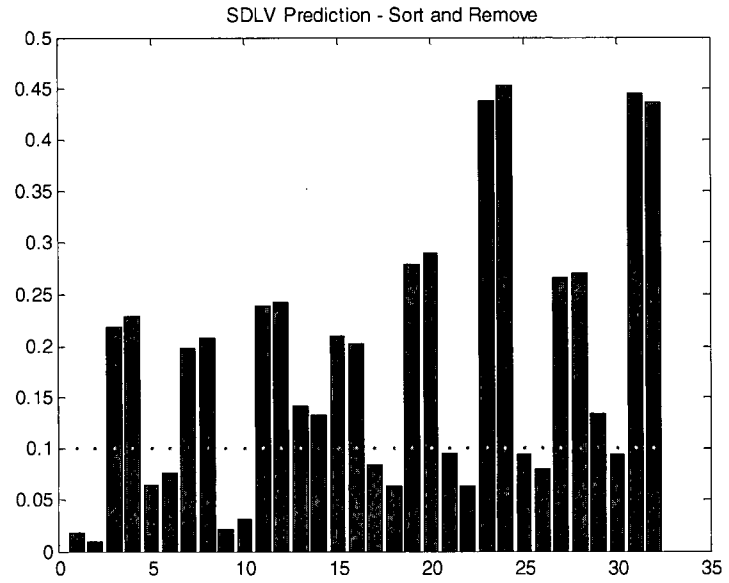

Figure 6.12: 3D Frame Case 13 SDLV Prediction Plot

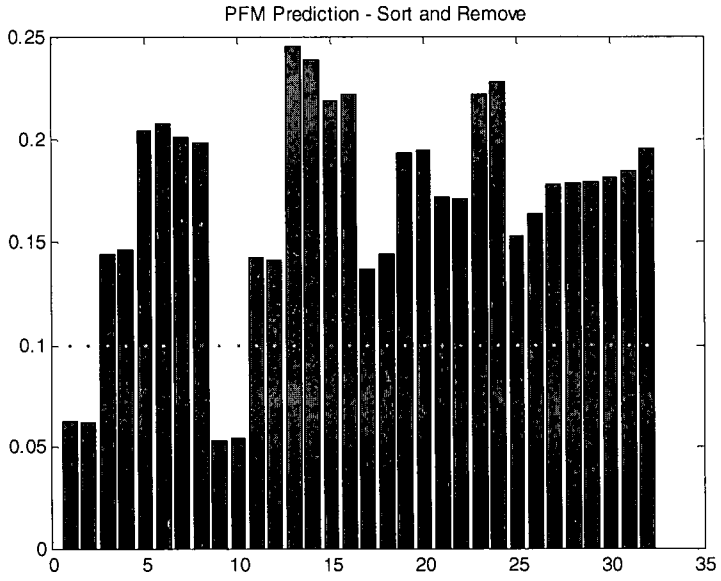

Figure 6.13: 3D Frame Case 13 PFM Prediction Plot

Table 6.16: 3D Frame Case 13 Predictions

	SDLV	PFM
S+R	1,2,5,6,**9**,**10**,17,18,21,22,25,26,30	1,2,**9**,**10**
MU0%	1,2,5,6,**9**,**10**,17,18,21,22,~~25,26,30~~	

Table 6.17: 3D Frame Plain Simulations Summary (Part 1)

	Case	μ		μ-σ		μ-σ²	
		SR	ER	SR	ER	SR	ER
SDLV	2	8/8	24/24	8/8	15/24	8/8	24/24
	3	4/4	24/28	4/4	14/28	4/4	24/28
	4	1/2	27/30	1/2	18/30	1/2	27/30
	5	1/1	28/31	1/1	8/31	1/1	25/31
	6	2/2	28/30	2/2	19/30	2/2	28/30
	11	2/4	26/28	4/4	18/28	2/4	26/28
	12	2/2	24/30	2/2	24/30	2/2	24/30
	13	2/3	27/29	3/3	6/29	2/3	27/29
	14	0/3	29/29	1/3	20/29	0/3	25/29
	U2	---	32/32	---	26/32	---	32/32
	Totals	22/29	269/291	26/29	168/291	22/29	262/291
	%	76	92	90	58	76	90
PFM	2	0/8	24/24	8/8	24/24	0/8	24/24
	3	0/4	28/28	4/4	21/28	0/4	28/28
	4	0/2	30/30	2/2	14/30	0/2	30/30
	5	0/1	31/31	1/1	23/31	0/1	31/31
	6	0/2	30/30	2/2	20/30	0/2	30/30
	11	0/4	28/28	4/4	22/28	0/4	28/28
	12	0/2	30/30	2/2	16/30	0/2	30/30
	13	0/3	29/29	2/3	21/29	0/3	29/29
	14	0/3	29/29	1/3	10/29	0/3	29/29
	U2	---	32/32	---	30/32	---	32/32
	Totals	0/29	291/291	28/29	201/291	0/29	291/291
	%	0	100	97	69	0	100

Table 6.18: 3D Frame Plain Simulations Summary (Part 2)

	Case	*Rem*[μ+σ]		S+R					
		SR	ER	SR	ER				
SDLV	2	8/8	24/24	8/8	22/24				
	3	4/4	20/28	4/4	20/28				
	4	1/2	27/30	1/2	23/30				
	5	1/1	18/31	1/1	19/30				
	6	2/2	20/30	2/2	26/30				
	11	2/4	26/28	3/4	20/28				
	12	2/2	24/30	2/2	24/30				
	13	3/3	19/29	3/3	19/29				
	14	0/3	29/29	1/3	20/29				
	U2	---	32/32	---	32/32				
	Totals	23/29	247/291	25/29	225/291	TPS-MU0%			OSI
	%	79	85	86	77	SR	ER	ER %	
PFM	2	1/8	24/24	8/8	24/24	8/8	22/24	92	2
	3	0/4	28/28	4/4	24/28	4/4	20/28	71	7
	4	0/2	28/30	2/2	20/30	2/2	20/30	67	11
	5	1/1	30/31	1/1	28/31	1/1	20/31	65	16
	6	2/2	28/30	2/2	24/30	2/2	26/30	87	3
	11	1/4	28/28	2/4	26/28	3/4	19/28	68	5
	12	0/2	30/30	1/2	27/30	2/2	24/30	80	3
	13	0/3	29/29	2/3	27/29	3/3	22/29	76	6
	14	0/3	29/29	2/3	22/29	2/3	16/29	55	8
	U2	---	32/32	---	32/32	---	32/32		
	Totals	5/29	286/291	24/29	254/291	27/29	221/291		
	%	17	98	83	87	93	76		

From the results shown for Cases 3, 6, 11 and 13, several important issues can be noted. First, with Case 3, it can be seen that with the SDLV prediction, the technique can identify damage

being in the E/W direction of the frame, but cannot distinguish whether it is the E or W side; the PFM technique is able to do this. Also, for both techniques, the damaged members cannot be separated from the member that shares the same bay; ie. even though only member 1 is damaged, member 2 is also predicted. A small improvement to the ER from using the MU0% criteria is observed.

For Case 6, the results from both techniques are much better. This seems to be due to several factors. For one, the damage occurs in the weak direction of the frame, therefore there is no modal order switching (ie. in the first several cases the damage occurs in the strong direction, consequently making it the 'new' weak direction. This changes the order of the modes). Secondly, since both members in the bay are damaged, there is no issue with separation of the two close members. The PFM method predicts the entire north face, which is the correct face, but overpredicts by 6 members. The MU0% criteria eliminates more overpredictions than the previous cases, and reduces the prediction to the correct two members but for floors 1, 2 and 3. This will lead to a good OSI value since the overpredictions are close to the damaged members.

For Cases 11 and 13, the results are not as good. The DDM beings to show signs that it does not work as well for distributed damage. The main issue with both cases is that damage in the upper floors is not predicted; this could be due to a lack of significant mode shape difference at that point, and/or not enough measured resolution due to the low number of sensors. In Case 11, although the fourth damaged member is missed, the member right next to it is 'overpredicted'. This creates a good OSI.

It is seen in Table 6.17 and Table 6.18 that the *S+R* results are significantly better than the other criteria, and also by using the TPS MU0% criteria, an improvement in the SR values can be achieved. This is the main purpose of the overall DDM, to get additional improvement in ER while maintaining the highest possible SR value. The performance of the OSI is also illustrated in the table, with differences from the 2D truss. First, only the lateral braces are used here; in the truss all members were used. This means that from floor to floor none of the braces are directly in contact (due to the chevron framing pattern); while in the truss OSI values of 0 and 1 were seen, for the 3D frame OSI values of 2 and 3 are the lowest. It can be stated that since the 3D frame members are already more distributed, the undamaged members would be as well.

From these results some generalizations of the OSI values can be made, and are shown in Table 6.19.

Table 6.19: Degree of Distribution for OSI Values

OSI Value	Category	Description
0-1	None	Either no overpredictions or immediate to damage
2-3	Minimal	All close to damage
4-6	Medium	Most close to damage; some scatter
7-9	High	Some close to damage; more scatter
10+	Severe	All scatter; random

6.6. Application of DDM to Calibrated Simulations: Cases 2 to 6

The calibrated simulation sets that were created in Section 5.6 were used to evaluate the DDM that has been developed to this point. The main idea behind the calibrated simulations is that they are more realistic than the plain simulations and are intended to reveal any issues with the DDM.

The first application of the DDM to the datasets was not successful. The best results achieved initially were based on cases 2, 4, 5 and 6 (there were problems with the Case 3 simulation so it was skipped). They had a SR of 92.3% and an ER of 60%. Several of the DDM settings were modified from the plain simulations, such as the threshold level (between 20% and 40%), and arrangement of the sensors used (1st and 3rd floor, 2nd and 4th floor). These results are shown in Table 6.20, splitting into the two sensor sets, and the TPS-MU0% results.

Table 6.20: Initial Calibrated Simulation Predictions

1st and 3rd Floor Set	Case	SDLV Prediction	PFM Prediction
	2	2,9,10,16,16,17,18,21,22	1,2,9,10,17,18
	4	1,2,3,4,5,6,7,8,15,16,21,22,23,24	---
	5	1,2,5,6,9,10,13,14,17,18,21-24	---
	6	3,4,11,12,19,20	11,12,19,20
2nd and 4th Floor Set	**Case**	**SDLV Prediction**	**PFM Prediction**
	2	1,2,9,10,11,12,17,18,21-32	1,2,9,10,17,18,25,26
	4	1,2,5-10,13,14,19,20,28	----
	5	1,2,5,6,9-14,20,28	1,2,9,10
	6	3-6,11-16,19,20,27,28	3,4,11,12,19,20,27,28

Case	TPS-MU0%	SR	ER (Pre-MU0%)	ER
2	1,2,9,10,11,12,~~15~~,~~16~~,17,18,21,22,~~23~~,~~24~~,25,26 27,28,29,30,~~31~~,~~32~~	8/8	10/24	16/24
4	1,2,3,4,5,6,7,8,9,10,13,14,15,16,19,20,21,22,23 24,28	1/2	10/30	10/30
5	1,2,5,6,9,10,11,12,13,14,17,18,~~20~~,21,22,23,24,~~28~~	1/1	15/31	17/31
6	3,4,5,6,11,12,~~19,20,27,28~~	2/2	22/30	26/30
		92.3	49.6	60.0

Ultimately, it was found that errors in the identified modes were the cause of the poor results. Of the 6 cases simulated, 5 modes were used for each for a total of 30 modes. Of those 30 that were identified in ARTeMIS it was found that 8 were incorrectly identified, at least one for each of the damage cases. This can occur due to the nature of the peak picking in the FDD method.

To deal with this issue, first the SAP model was examined and the exact modes were tabulated, and the identification was performed again taking care to correctly identify each mode. Then the analysis was performed, and the best results came from increasing the threshold in both the PFM and SDLV techniques to 30% and using the obtained modes from Table 5.15 toTable 5.20. The results are summarized in Table 6.21. From the table it is seen that the DDM fulfils both the SR criteria (=100%) and the ER criteria (>80%).

Table 6.21: Calibrated Simulation Predictions

Case	SDLV Prediction	PFM Prediction
2	**1,2,9,10,17,18,25,26**	**1,2,9,10,17,18,25,26**
3	**1**,2,**9**,10,**17**,18,**25**,26	**1**,2,**9**,10,**17**,18,**25**,26
4	**1**,2,9,10,11,17,18,19,20,**25**,26,28,31,32	17,18,**25**,26
5	**1**,2,7,8,15,16,19,20,27,28	No Damage
6	3,4,**11**,**12**,19,20,28	3,4,7,8,**11**,**12**,15,16

Case	TPS-MU0%	SR	ER (Pre-MU0%)	ER
2	**1,2,9,10,17,18,25,26**	8/8	24/24	24/24
3	**1**,2,**9**,10,**17**,18,**25**,26	4/4	24/28	24/28
4	**1**,2,9,10,~~11~~,17,18,19,~~20~~,**25**,26,~~28~~,~~31~~,~~32~~	2/2	18/30	23/30
5	**1**,2,~~7~~,~~8~~,15,16,~~19~~,~~20~~,~~27~~,~~28~~	1/1	22/31	28/31
6	3,4,7,8,**11**,**12**,15,16,~~19~~,~~20~~,~~28~~	2/2	21/30	24/30
		100%	76%	86%

This illustrates two points: the DDM is sensitive to the identified modes; the calibrated simulation can shed light on peaks that are not modes in the real data and can create problems with the analysis (the plain simulation can not).

6.7. Application of Methodology to Real Damage Cases

The DDM was then applied to the real datasets using the developed settings. It was found that the DDM performed very well using a threshold of 30%. The results are shown in Table 6.22 and it is seen that the design targets of SR and ER are met.

Table 6.22: Real Data Predictions

Case	SDLV Prediction	PFM Prediction
2	**1**,**2**,3,4,**9**,**10**,11,12,13,14,**17**,**18**,**25**,**26**	**1**,**2**,**9**,**10**,**17**,**18**,**25**,**26**
3	**1**,2,3,4,**9**,10,**11**,12,13,14,**17**,18,**25**,26	**1**,2,5,6,**9**,10,**17**,18,**25**,26
4	**1**,2,9,10,17,18,**25**,26	**1**,2,9,10
5	**1**,2,9,10	**1**,2,9,10
6	3,4,5,6,**11**,**12**,15,16,20,27,28	3,4,**11**,**12**

Case	TPS-MU0%	SR	ER (Pre MU0%)	ER
2	**1**,**2**,3,4,**9**,**10**,~~11~~,~~12~~,13,14,**17**,**18**,**25**,**26**	8/8	20/24	22/24
3	**1**,~~2~~,~~3~~,4,~~5~~,6,**9**,10,~~11~~,~~12~~,13,14,**17**,18,**25**,26	4/4	14/28	19/28
4	**1**,2,9,10,17,18,**25**,26	2/2	24/30	24/30
5	**1**,2,9,10	1/1	28/31	28/31
6	3,4,~~5~~,~~6~~,**11**,**12**,15,16,~~20~~,27,~~28~~	2/2	20/30	24/30
		100%	74%	82%

It is seen from the results in the last two sections that they are similar in general to those from the plain simulations. However, some modifications were necessary, including increasing the singular value threshold level from 10% to 20, 30 and in another case 40%. One of the main issues that must be taken from these results, is that although this demonstrates that the DDM will now work not only for the simulations, but for the real benchmark data cases, these cases are not necessarily very realistic. In each case, from 2 to 6, the braces are completely removed, and the damage is localized. The next section explores issues due to lower levels and distribution of damage.

6.8. Performance Study: Lower Damage Levels and Distribution of Damage

Next the DDM was applied to the 10 random cases from Section 5.6. The damaged members in each case are listed in Table 6.23. Details of the frequencies are given in Chapter 5. The purpose of these cases is to examine the performance of the DDM for a more realistic damage scenario where the braces aren't removed completely but only reduced in cross-section; and also to examine its performance when the damage is distributed. A summary of the initial

results is presented in Table 6.24. The TPS-MU0% criteria was not applied due to the poor results.

Table 6.23: 3D Frame Calibrated Simulations: Random Damage Cases

Case	16	17	18	19	20	21	22	23	24	25
Members	6	1,12,22	14,16,23	22	27,28	16,29	10,18,27	25,31	6,28	8,9

Table 6.24: Initial 10 Random Case Results

Case	SDLV		PFM	
	SR	ER	SR	ER
16	0/1	28/31	1/1	20/31
17	1/3	24/28	1/3	23/29
18	2/3	25/29	1/3	24/29
19	1/1	30/31	1/1	30/31
20	0/2	30/30	2/2	30/30
21	0/2	27/30	1/2	27/30
22	0/3	27/29	1/3	27/29
23	0/2	28/30	1/2	27/30
24	1/2	25/30	2/2	26/30
25	1/4	23/28	2/4	13/28
	26%	90%	57%	83%

From the results in the table it is seen that the DDM did not perform well for these 10 cases. To isolate the possible problems with the DDM in these cases, the two issues, level and distribution of damage can be addressed separately. First the effect of the lower level of damage can be evaluated by taking one of the cases from the table with the poorest results (ie. Case 22) and re-simulate it using the braces completely removed as damage. A summary of this is presented in Table 6.25.

Table 6.25: Case 22 Repeated with Braces completely removed (100% Loss of Section)

New Frequencies	7.133	7.380	13.677	19.273	21.325
PFM	1,2,3,4,7,8,11,12,15,16,20,23				
SDLV	3,4,7,8,9,**10**,11,12,15,16,19,24,**27**,28,31,32				
TPS-MU0%	1,2,3,4,7,8,9,**10**,~~11~~,~~12~~,15,16,19,20,23,24,**27**,28,31,32				
Damage	10,18,27	SR	67%	ER	45%

It is seen from the table that the SR has increased, although still not to 100%, and has done so at the expense of the ER, which has dropped dramatically. It can be said then that the damage level is not the main reason for the failure of the DDM in these cases. It was seen previously in cases 13 and 14 (see Table 6.5), in which the damage was simulated as a 40% loss of section, that the DDM found 5 of 6 damaged members. So instead it is likely that the problem is with the distribution of damage, and a result of the small number of sensors being used in the analysis. Comparatively in Cases 2 to 6 the DDM worked well, but as mentioned the damage was localized. It can also be seen in Table 6.24 that for the cases with localized damage (Cases 16, 19, 20) the method works better (PFM has SR of 4/4).

The logical way to deal with problems relating to distribution of damage is to increase the number of sensors used in the analysis. In the DDM to this point, a total of 6 sensors have been used; 3 on the 2nd floor and 3 on the 4th floor. It appears that this may be too low to accurately find damage that is well distributed in the structure. One solution is to take 12 sensors, ie. 3 from each floor. However, in using the DLV technique this creates new problems when the number of modes (in these cases only 5) is much less than the number of sensors used in the analysis. The way to deal with this is to increase the number of modes used in the analysis. This is straight forward for a simulation; more modes can be computed. Since the excitation was a white noise with a bandwidth of 0.1 to 50 Hz, and the real ground motion was hardware filtered at 50 Hz, this creates an upper limit of 50 Hz (of excitable modes) and therefore modes above this frequency are not computed. To examine the results from extension to 10 modes, Case 22 is used again and to confirm the results Case 17 is included.

Table 6.26 to Table 6.28 presents the updated modal results; this includes the exact SAP frequencies, the FDD and SSI-CVA values from ARTeMIS. Also shown are the damping values

from the SSI-CVA method and the MAC value correlating the two ARTeMIS methods. The undamaged case (1) is also updated for 10 modes since it is required in the DDM.

Table 6.26: Case 1 Extended to 10 Modes

Mode	Description	SAP [Hz]	FDD [Hz]	SSI-CVA [Hz]	Damping [%]	MAC [%]
1	1 E/W	7.450	7.471	7.511	0.212	97.28
2	1 N/S	7.750	7.764	7.754	0.827	98.84
3	1 Tor	14.269	14.26	14.27	0.138	100.00
4	2 E/W	20.467	20.46	20.47	0.171	99.99
5	2 N/S	21.867	21.88	21.86	0.045	99.99
6	3 E/W	29.869	29.83	29.73	0.369	99.65
7	3 N/S	33.212	33.35	33.22	0.688	97.68
8	4 E/W	35.137	35.06	35.26	0.280	97.88
9	2 Tor	38.730	38.77	38.76	0.522	99.97
10	4 N/S	40.617	40.63	40.73	0.663	85.52

Table 6.27: Case 17 Extended to 10 Modes

Mode	Description	SAP [Hz]	FDD [Hz]	SSI-CVA [Hz]	Damping [%]	MAC [%]
1	1 E/W	7.248	7.246	7.24	0.589	99.68
2	1 N/S	7.571	7.559	7.558	0.463	97.96
3	1 Tor	13.899	13.92	19.90	0.145	100.00
4	2 E/W	20.375	20.36	20.38	0.031	100.00
5	2 N/S	21.372	21.39	21.37	0.610	100.00
6	3 E/W	29.472	29.54	29.52	0.315	99.82
7	3 N/S	32.906	32.91	32.87	0.828	97.65
8	4 E/W	34.965	35.06	35.02	0.549	95.88
9	2 Tor	38.212	38.23	38.19	0.508	99.94
10	4 N/S	40.112	40.19	39.99	0.082	77.80

Table 6.28: Case 22 Extended to 10 Modes

Mode	Description	SAP [Hz]	FDD [Hz]	SSI-CVA [Hz]	Damping [%]	MAC [%]
1	1 E/W	7.417	7.407	7.396	0.147	98.61
2	1 N/S	7.500	7.480	7.474	0.221	98.91
3	1 Tor	14.000	14.01	14.01	0.107	100.00
4	2 E/W	19.967	19.97	19.96	0.120	99.99
5	2 N/S	21.605	21.63	21.61	0.062	100.00
6	3 E/W	29.198	29.20	29.24	0.398	99.92
7	3 N/S	32.859	32.81	32.83	0.520	99.53
8	4 E/W	34.957	35.06	35.00	0.518	99.34
9	2 Tor	37.959	37.99	37.95	0.529	99.97
10	4 N/S	40.214	40.23	40.20	0.587	84.65

Using the same model (with 12 sensors), setting the DLV threshold to 10%, and using the sort and remove criterion, results were obtained for the two cases. They are shown in the following tables.

Table 6.29: Case 17 Results for 12 Sensors, 10 Modes

PFM	No Damage				
SDLV	1,2,3,4,11,12,19,20,21,22				
TPS-MU0%	1,2,~~3,4,11,12,19,20~~,21,22				
Damage	1,12,22	SR	67%	ER	93%

Table 6.30: Case 22 Results for 12 Sensors, 10 Modes

PFM	3,4,7,8,11,12,15,16				
SDLV	1,2,7,8,9,10,11,12,17,18,27,28,29,30				
TPS-MU0%	1,2,3,4,7,8,9,10,11,~~12~~,15,~~16~~,17,18,27,28,~~29~~,30				
Damage	10,18,27	SR	100%	ER	56%

The results show two things: the SDLV method functions well using a denser set of sensors, and that the PFM method is not contributing to the results at all in either case. Also it is seen in Case 17 that the application of the MU0% criteria eliminates one of the damaged members from the set. It was expected that the SDLV method would perform better with more sensors. Since the PFM technique worked better for the 6 sensor case, those results can be combined to the 12 sensor SDLV prediction to create the TPS. For the MU-0% criteria, the 5 mode cases are used. There can be are other possibilities that are not explored here such as using an intermediate number of sensors, such as 9, in the PFM analysis.

Table 6.31: Case 17 Results for 12 Sensors SDLV, 6 Sensors PFM

PFM	1,2,18,23,24				
SDLV	1,2,3,4,11,12,19,20,21,22				
TPS	1,2,3,4,11,12,18,19,20,21,22,23,24				
Damage	1,12,22	SR	100%	ER	66%

Table 6.32: Case 22 Results for 12 Sensors SDLV, 6 Sensors PFM

PFM	5,6				
SDLV	1,2,7,8,9,10,11,12,17,18,27,28,29,30				
TPS	1,2,5,6,7,8,9,10,11,12, 17,18,27,28,29,30				
Damage	10,18,27	SR	100%	ER	56%

It is important to note that while using more modes is possible for the simulations, this is not possible in most real cases. With the results of the 3D frame that were presented in Chapter 5, identifying up to 8 modes may be possible; however, obtaining 10 or 12 modes for this structure is not possible using current ambient vibration techniques.

6.9. Generalization of the Damage Detection Methodology

The DDM that is shown in Figure 6.1 can be generalized as shown in Figure 6.14. The idea is that for many of the steps shown in the figure, different methods can be either added or replaced to improve the DDM, or to adjust it for a specific case.

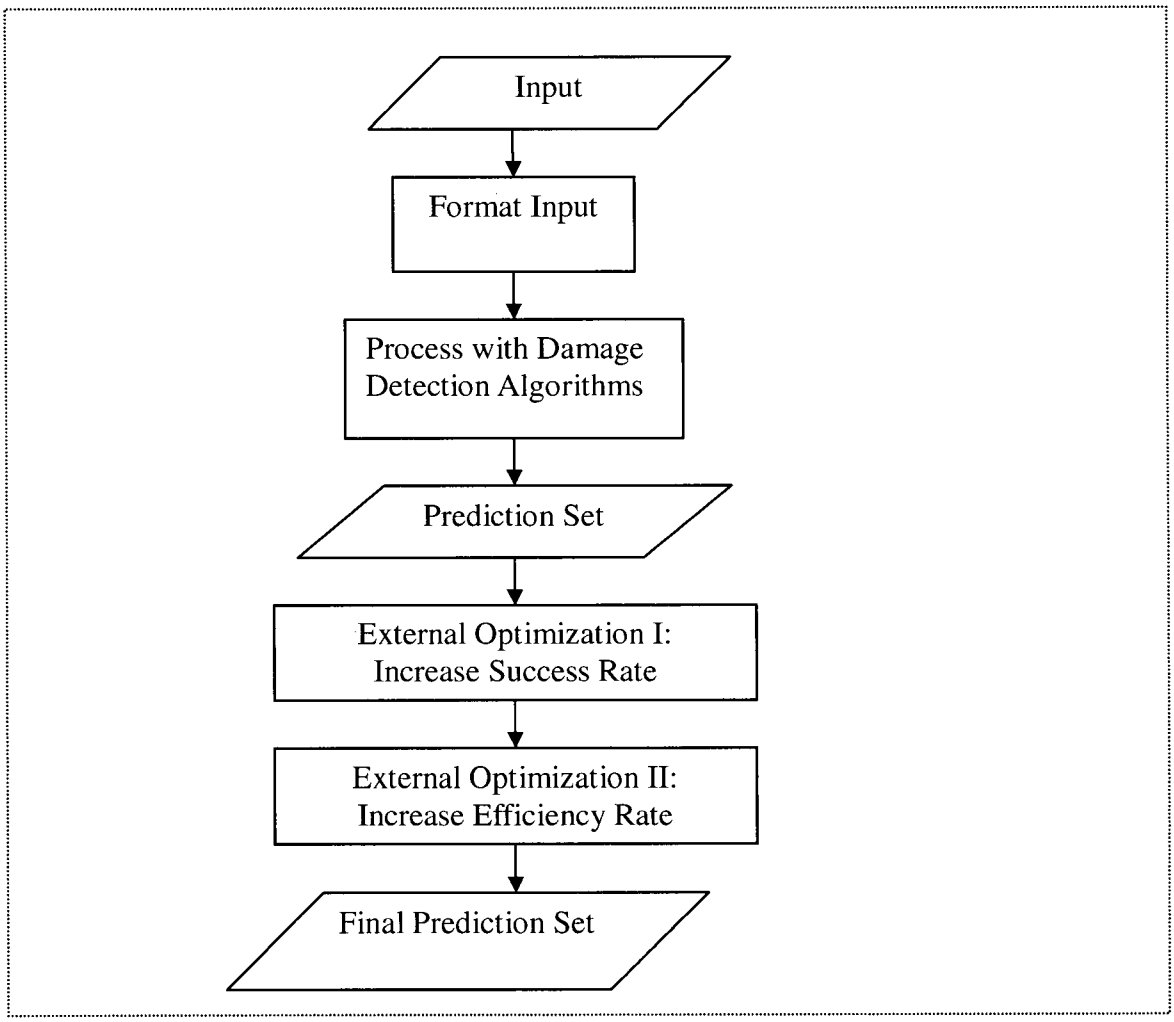

Figure 6.14: Generalization of Damage Detection Methodology

In the figure, the steps are described as follows. The input refers to any measured input, such as strains or accelerations. Formatting the input can be any process, from as simple as formatting a datafile for input to the damage detection algorithm, to performing a system identification to obtain the natural frequencies and mode shapes, as was required for the DDM in this chapter. Next the formatted input is processed with the damage detection algorithms, and the prediction

set is created. The prediction set is then optimized externally, first to increase the success rate, ensuring that no damage is missed. Then the prediction is optimized again, this time to eliminate false predictions and increase the efficiency rate. Last the final prediction set is presented.

Chapter 7. Application of Implementation Method to Real Buildings

The purpose of this chapter is to illustrate the application of the implementation method to real buildings. As shown in Chapter 4, the goals of the method are to determine the DDM and the optimal layout of the sensors. The initial development of the DDM was made in Chapter 6 using simpler examples; it must then be determined if and how it can be applied to the real buildings. While Chapters 5 and 6 were presented in detail to illustrate the development of the implementation method, this chapter presents the application of the method; therefore this chapter is presented as a summary and detailed discussions of each section are presented in the appendix. Throughout this chapter, references will be made to figures and tables from the appendix.

In the application of the implementation method to the cases studies, it was found that there were difficulties at several stages, including the damage detection. Initially a single building was chosen for the example, but in an attempt to understand the issues with the DDM, a second, simpler case study was also examined. Section 7.1 introduces the first building, and summarizes the analysis results and describes a modification to the DDM to improve the results. Section 7.2 describes that modification, the 'Equivalent Frame Model for Damage Detection approach' in more detail. Section 7.3 introduces the second case study, and summarizes the application of this approach. A second method to improve the performance of the DDM is introduced. Section 7.4 presents a summary of a set of additional analyses, with the intention of making conclusions on some of the issues found with the DDM on the two cases studies. Section 7.5 presents a discussion of the results, and Section 7.6 presents the conclusions of the application.

7.1. Application to the Melville Building

The first case study is based on the *Melville*, a 44-storey concrete building located in downtown Vancouver, Canada. The building is of typical construction for high-rise towers in Vancouver, with a central core designed to form the lateral resisting system, and the remaining columns and walls only taking gravity loads. At the time of testing, the building was under construction external cladding was only in place up to the 34th floor. A photo of the building is shown in Figure 7.1. For the simulations and the initial damage detection a finite element model in

ETABS [CSI, 2006] was used. The model (referred to as the full 3D model) is shown in Figure 7.2.

Figure 7.1: Photo of the Melville Building

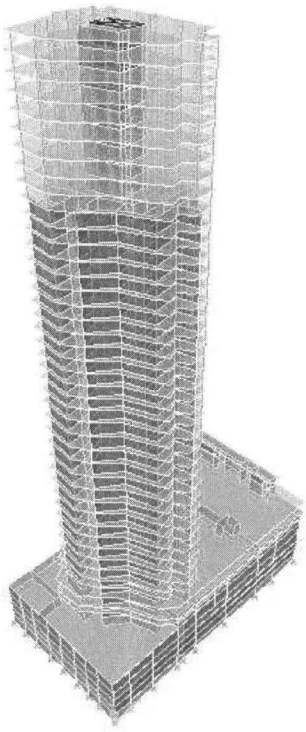

Figure 7.2: Melville ETABS Model

The first step in the implementation method is to create the Calibrated Damage Simulations. The first step of the CDS is to perform an ambient vibration test. A test of the building was performed in June 2006, and was able to obtain 9 modes (Table A.1). The second step of the CDS is to design and update a finite element model. The ETABS model, as shown in the figure, was created and manually updated to match as closely as possible the measured modes (Table A.2). For the model updating step, it was found that the finite element model of the Melville was difficult to recreate in FEMTools, and would require an unknown amount of time; it was decided then to move on to the next step of the simulation, and return to the automated updating if possible. For the simulations, only the measured ground input and the obtained damping values were used. It was found that the addition of noise did not contribute to the realism of the simulations; therefore no noise was added (Figs A.9 to A.11). Several initial damage cases were chosen; these involved simply removing elements from the model. A series of cases were examined, with an emphasis on the change in frequencies of the model (Table

A.4). It was found that damage to the core was necessary to observe significant frequency changes.

The first issue with the damage detection analysis of the Melville is with respect to the choice of sensors used in the analysis. In the 3D frame, a set of 3 sensors on 2 separate floors were used. For the Melville, 45 sensor locations were available; there are many different possible sets for analysis that can be chosen. A discussion of this is shown in Section A.1.6; three possible sets are illustrated in Figs A.12 to A.14. However, it was found that the best results came from choosing a 2D distribution of horizontal measurements along the height of the building; this formed a single column of sensors facing the same direction. There are then 3 sets of sensors available, the analysis is repeated 3 times.

For the application of the DDM, the simulated datasets were processed, and the resulting DLV's were applied to the ETABS model. The initial results were inconclusive; it was not possible to determine the location of the damage in a meaningful way (Figs A.15 and A.16). It was observed that when applying the DLV's to a more complex finite element model (as opposed to the 3D frame example) it was difficult to interpret the location of the zero stress elements. A proposed solution was to create a simpler 'equivalent' model for the damage detection phase. This idea is presented in the next section. Several more damage cases were created, and although some better results were obtained, in general the predictions were still inconsistent (Figs A.38 to A.53). In the results shown in the figures, to simplify the presentation the average stresses of all of the elements on a floor were taken. It was found that there are elements below the damage threshold (0.1) scattered throughout the building; therefore in order to determine if the DDM was at least generally localizing the damage the average was taken. By doing this however, the requirement of having a damage threshold of 0.1 must be reconsidered, since taking the average generally raises that value.

7.2. The Equivalent Frame Model for Damage Detection Approach

From the analysis of the Melville it was found that the results using the ETABS model for the damage detection were difficult to interpret. For the ETABS model, there are several element types, and in particular it was found that for area elements it was difficult to resolve the damage locations. In contrast, the interpretation of the results from the 3D frame example from Chapter 6 was straight forward; only the axial stresses were examined, and damage was indicated by

those members with zero (or negligible) axial stresses. Several simpler models based on the Melville were explored (Fig A.17), and it was then found that an equivalent model could be used in lieu of the fully detailed model (Fig A.32). The equivalent model was chosen to be a frame, based on the simplicity of the 3D frame example.

The concept of the equivalent frame model for damage detection (EFMDD) can best be described in two parts. The idea of a 'damage detection model' means that an equivalent simplified model is created for damage detection. The idea of an 'equivalent frame model' is that instead of using area or shell elements, a simplified frame model is used. So the concept of the EFMDD approach is to use an equivalent frame model for the damage detection. In the implementation method, the original FEM is still used for the simulations.

Requirements for the EFMDD approach to hold are as follows:

1. The location of the sensors must be present in the geometry of the frame model;
2. The geometry of the frame should be similar to the overall geometry of the building (in order to identify regions of damage in a meaningful way);
3. The mode shapes and frequencies of the frame model should correlate well with the measured ones.

7.3. Application to the Heritage Court Tower Building

The EFMDD approach as described above was applied to the Melville. The results from the first case were seemingly better; several more cases were created (Table A.7). The results from these additional cases were inconsistent; some of the cases showed promising results but in general they were inconclusive. In order to better identify issues within the DDM that caused the results of the Melville to be inconclusive, a second, simpler case study was introduced. The second case study was based on the Heritage Court Tower (HCT), which is a simpler building both in size and geometry.

The HCT building is a 15-storey concrete building also located in downtown Vancouver, Canada. It is similar in construction to the Melville with a central core to resist the lateral loads. The ambient vibration test of the HCT was performed in 1998; it was the focus of a benchmark

study examining the performance of various system identification methods [Ventura and Horyna, 2000]. The first six identified modes were used for this analysis (Table A.8).

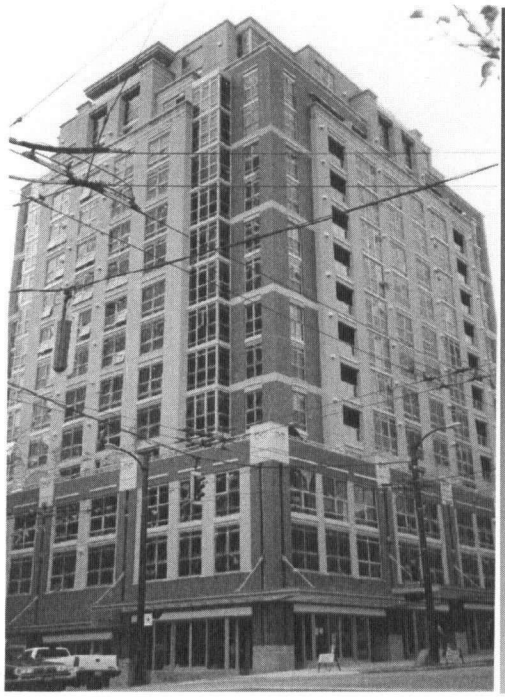

Figure 7.3: Photo of Heritage Court Tower Building

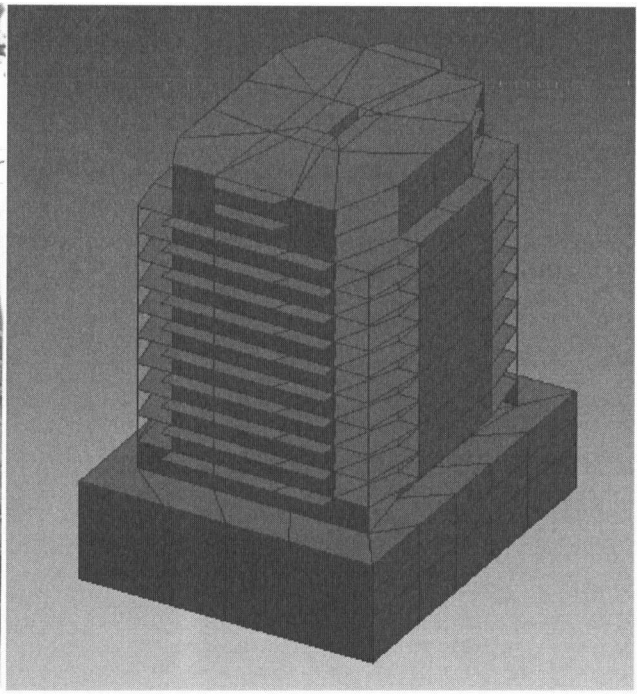

Figure 7.4: HCT Building FEMTools Model

For the model updating, a previous work on the automated updating of the building had been performed [Ventura et al., 2005]; the results showed a reasonable correlation (Table A.9). Similar to the Melville, only the measured ground input and the obtained damping values were used for the simulations. Again the addition of noise did not contribute to the realism of the simulations; therefore no noise was added (Fig A.58).

In the application of the DDM, the EFMDD approach was used. The first sensor set for the analysis was a 3D set, using 9 sensors and 6 modes. This provides 3 measurements per floor over 3 floors. The results again were inconclusive; it was possible that the number of sensors was insufficient for the analysis (Figs A.60 to A.67). Also in each of the cases, there was a bias in the results, with floors 6, 7 and 8 always having the lowest normalized force values. It was then discovered that due to an observation in MATLAB it would be possible to use more sensors than simply twice the number of modes used. The number of sensors was then

increased to 18; the results did not improve, but the bias moved to floors 8, 9 and 10 (Figs A.68 and A.69). The number of sensors was then increased to 48 (8 per floor); the bias was still there, and was becoming more distinct (Figs A.70 to A.73). This indicates that the bias is simply an effect of statics; depending on where the sensors were located certain elements were loaded more than others. One possible solution was to apply a weighting factor to the resulting forces in the frame; however, if certain members are not loaded than even with a weighting factor they still can not provide information on their condition. An attempt to apply weights to the HCT results was made; the weights were determined by applying unit loads to the sensor locations and obtaining the normalized element forces. The results were still inconclusive; it was not apparent how to apply the weights in an effective manner (Figs A.74 to A.80). The normalized forces when the frame was subjected to unit loads were found (Fig A.81). It was very clear that there was a bias on floors 8, 9 and 10. In addition, the effect of the loads being applied to a cantilever was apparent, with the highest loads being at the base.

7.4. Additional Analyses

From the results from the Melville and the HCT, the results were generally inconclusive. This indicates that the DDM is not as effective when applied to the larger buildings and their corresponding FEMs. Two ideas were explored to improve the results as described above: using a simplified model for damage detection and using more sensors in the analysis. Both of these showed promise at improving the results, but were not conclusive. Therefore several more analyses were created as an attempt to make conclusions on the performance of the DDM.

7.4.1. 3D Frame 32 Sensor Analysis

The first additional analysis applied more sensors for the 3D frame for the last 10 damage cases (Section 6.7). In the initial analysis of the 3D frame, 3 sensors were used per floor. This was increased to 8 per floor; two orthogonal horizontal sensors in each corner for a total of 32. The results from the analysis with 32 sensors on the 10 cases were significantly better, with a SR of 100% and ER of 67% (Table A.16). This is compared to SR values of 26% for the SDLV and 57% for the PFM analyses with the previous sensor set. The ER value of 67% is not satisfactory according to the target value of 80%. However, it was seen from the normalized force plots that the damage was typically very clearly indicated with a sharp difference between the damaged members and those that were undamaged (see Fig A.82; the first four members are below 0.1 but are much higher than the damaged members 6 and 28). The problem arises when

using a fixed damage threshold of 0.1; for example the damaged member may have a value of 0.001 and several others that are undamaged may have values that are slightly less than 0.1; these still become included in the damage set. Therefore a new idea was explored, that if the damage threshold was no longer fixed (ie. at 0.1), a better value of ER could be obtained. It was shown that for the ER values were increased to 94% for the SDLV and 84% for the PFM when the damage threshold was adjusted to a value that was slightly higher than that of the maximum normalized force value for a damaged member. If the idea of a variable threshold was to be used however, a relationship between the damage threshold and some measured quantity must be developed. Some possible relationships were examined, but no consistent results were found.

7.4.2. 3D Frame 32 12-Storey modified analysis

It was shown in the analysis of the 10 cases from the 3D frame, that when using more sensors the results were much better. In order to determine if this was a phenomenon of the 3D frame only due to the small size of the example, a new larger model was created. The new model was similar to the 3D frame; the original model was simply stacked on itself three times, to create a total of 12 stories (Fig A.83). The same number of sensors was used (32), located on every third floor. The results of the analyses showed that for localized damage, the damage could be identified. However, when the damage was distributed, only some of the damage was identified (Table A.18).

7.4.3. HCT analysis – Severe Damage

To examine the possibility that the level of damage in the cases was too small, an additional case was explored that featured more severe damage to the model. For the case, the modulus of elasticity was reduced by 90% for half of the elements in the lower 5 stories. The results were still inconclusive (Figs A.88 to A.89). The necessity for the weighting factor was apparent again, in the same three upper floors.

7.5. Discussion

It is apparent from the results of the application on the Melville and the HCT that the DDM in its current form was not successful. This implies that the DLV technique may not be suitable for large buildings. However, two ideas were explored that showed some improvement in the results: simplifying the damage detection model and increasing the number of sensors used in

the analysis. Both of these ideas can be explained using statics, and then limits of the DLV technique can be established.

The first issue is that based on the location of the DLV load points, certain elements may not be loaded. This 'unbalanced' loading effect can occur regardless of the size of the structure; however, as the structure increases in size, the effect becomes pronounced, particularly if the number of load points does not change. One way to balance the loads as described above is to apply weights. In order to determine how to weight the loads in the structure, it is described in the appendix (A.2.4) that the simplest way to define the undamaged state of loading was to apply unit loads at the sensor locations. One problem with using weights however is that zero force members are always zero; and the additional of a weighting factor will not provide any new information on the condition of that member based on the theory of the DLV technique. Figure 7.5 shows a truss example with the absolute values of the normalized forces resulting from an unbalanced loading condition. The loads shown are from sensor locations that would be typical for a bridge, with several vertical measurements along the deck and a single longitudinal measurement in the plane of the deck. The measurement locations are shown as arrows; the normalized loads result from unit loads applied.

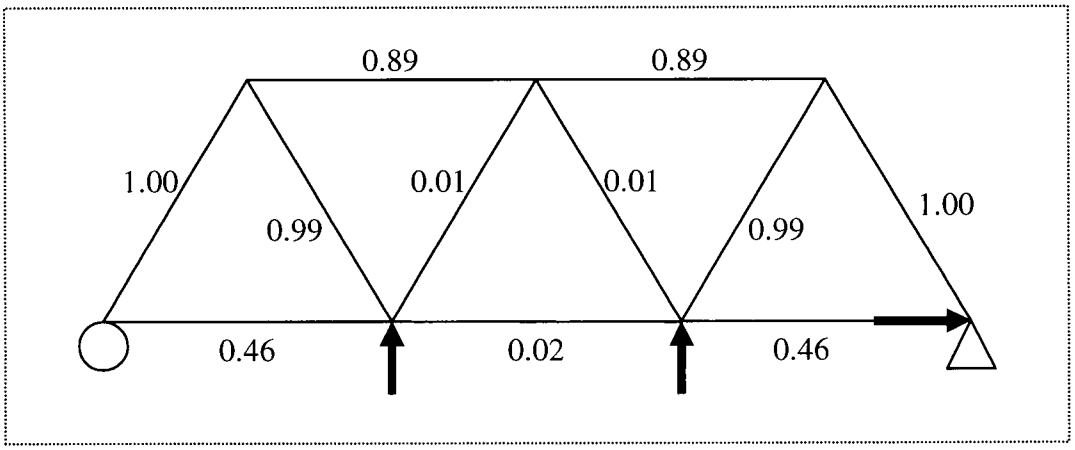

Figure 7.5: Example of Unbalanced Loading

An alternative to the idea of weights is to introduce a scheme to balance the loads in the structure by optimally locating the sensors. For example, in the truss shown in the figure, instead of simply adding more sensors, they can be added in a way as to balance the resulting forces. This improves the efficiency of the system by only adding sensors that will improve the

results. Figure 7.6 illustrates this idea; although the normalized forces in the example are not all equal, they all have values above the damage threshold of 0.1.

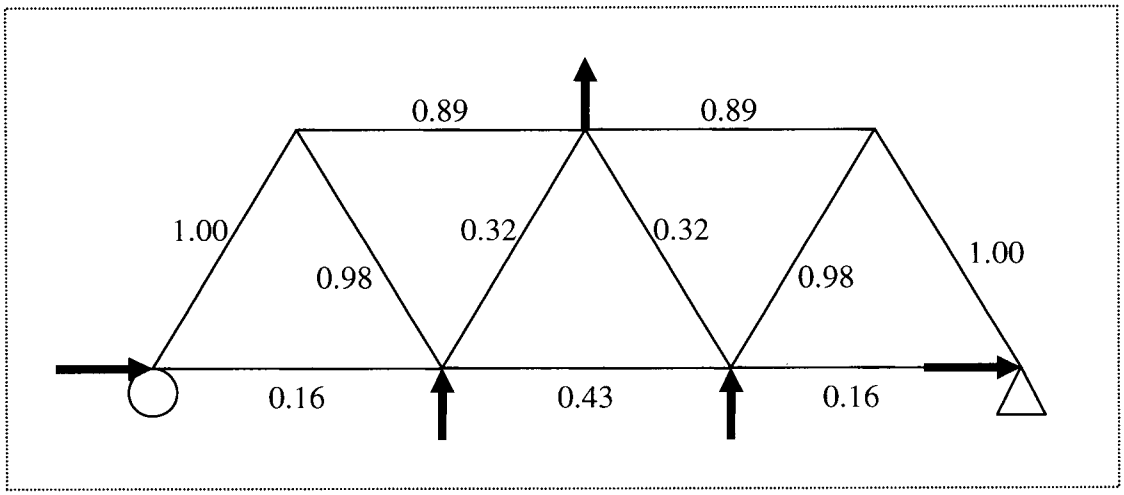

Figure 7.6: Example of Balanced Loading

An optimization scheme can then be developed with the following two requirements:

1. The minimal sensor layout can be found such that when unit loads are applied at the sensor locations, a better balance of forces in each element result (ie. balanced loading); the balance should result in normalized forces being greater than the damage threshold.
2. Those forces must not be zero (ie. there must be at least one sensor).

In addition to the layout of the sensors, there is a limit to the amount of damage that can be found with the number of available sensors. This can also be explained using statics; for each 'mode' of deformation of an element that is damaged, one additional sensor is needed to find that damage. For example, in a truss element that has one deformation mode (axial), if only one sensor was used, the only condition that results in a zero stress is a zero force. Therefore two sensors are needed to resolve a zero stress in that element if the loads are not zero. For a beam element with three deformation modes (axial and two bending), four sensors are needed. For a shell element with six deformation modes, seven sensors are needed. Likewise if two shell elements are damaged, 14 sensors are needed to locate the damage. This confirms the idea that the use of an equivalent frame model is useful, since more damage can be localized using fewer sensors. This can also be described in terms of the flexibility matrices: if the amount of change

in flexibility affects a single member with n dof's, then $n+1$ dof's are required for the measured flexibility matrix in order to detect this change.

For both of the above mentioned limits, it is important to consider that the measured flexibility is a representative portion of the actual flexibility matrix; it may represent 'regions' of the total flexibility. Therefore, for the portions that have been obtained, the amount of damage that can be detected is limited to:

1. The size (and/or number) of the measured portions (determined by the number of sensors);
2. The size of the 'detectable' regions of the total flexibility matrix; this means that if a change occurs in that region, it is detectable in the smaller measured region.

An additional important issue with flexibility-based methods using output-only data is the approximate formation of the flexibility matrix. Since they are formed using unscaled modes, the approximations may be very poor. The DLV localization provides exact results from the flexibilities provided, but the accuracy of the prediction depends on the quality of those flexibilities. This is difficult to quantify; quality of those flexibility matrices would have to be controlled at the system identification stage.

7.6. Application Conclusions

In the application of the CDS, it was apparent from these two buildings that the addition of measurement noise was not necessary. This is likely due to the fact that for larger buildings the signal to noise ratio was sufficiently high to eliminate any significant effects of the noise (when using the FDD method). For the model updating phase, the correlation of the various models (particularly the damage detection model) is important. This is due to the nature of the DLV technique, where it has been seen that the technique is sensitive to the accuracy of the identified modes.

It can be concluded from the application of the DDM to these case studies that in general flexibility-based methods are not the best choice for ambient-vibration based damage detection. This is primarily due to the fact that the results are sensitive to the approximations of the flexibility matrices obtained, and that the quality of the approximation is difficult to define.

However, if the approximation of flexibility is acceptable, the technique can be used within its other limitations. In particular, a sufficient number of sensors must be available in order to obtain successful results. A method for optimization of the sensors was proposed; by using this idea the minimum number of sensors can be found. It is possible that the DLV technique would be useful for finding the optimal sensor locations for the SHM system.

The goals of the implementation method are to provide an evaluation of the DDM and the optimal sensor layout. From these results it is concluded that the DDM in the form presented in Chapter 6 can only be used under certain conditions:

1. A sufficient number of sensors is used ;
2. A simpler equivalent model is used for the damage detection phase (EFMDD approach is suggested);
3. The mode identification is satisfactory.

The sensor layout when using the DLV technique can then be found using the optimization scheme.

It is noted that the minimum number of sensors required was not determined; the maximum numbers of sensors used in these analyses was 48. The addition of more sensors requires considerable more time for not only analysis but preparation for analysis. However, the more important consideration is a practical one; using 48 sensors would already make this a heavily instrumented building at only 15-stories. The cost of the system would be generally prohibitive, and it likely would be necessary to explore other damage detection techniques.

Chapter 8. Conclusions and Recommendations

8.1. Summary

The goal of this thesis was to develop an implementation method for damage detection algorithms in SHM systems. The implementation method has two main requirements:

1. The damage detection methodology for the system must be developed;
2. The developed DDM must be properly evaluated.

The damage detection methodology that is developed for implementation in this thesis is one that is composed of damage detection algorithms found in the literature. The main concept of the DDM is that is must contain at least two independent damage predictions. For the evaluation of the DDM, the best way to do so is by a physical damage study on the building of interest. However, since this is not feasible for real structures, a simulation of damage is then required. A method for creating a set of calibrated damage simulations was developed using the results of an ambient vibration test of the structure.

The process of the implementation method involves creating a DDM, a set of calibrated damage simulations, and then applying the DDM to those datasets. The DDM can then be modified to obtain the desired results, and also the layout of the sensors on the structure can be effectively chosen. One of the main reasons for the method is to identify potential flaws of the system in a simulated environment that is as close to the real situation as possible.

In Chapter 1 four problems with the use of damage detection algorithms were defined. These were:

5) Low sensitivity of modal parameters to damage
6) Incomplete nature of measured vibration characteristics
7) Complexity of DDA's
8) Effects other than damage

From the implementation method proposed, the first three issues can be addressed. Point 1 can be addressed in the simulations by determining the damage cases that can be identified by the algorithm; Point 2 can be addressed by finding the optimal array of measurements for the best

performance of the algorithms; Point 3 can be addressed by studying simple examples and working towards the structure of interest. Point 4 considers many important issues that strongly affect the performance of the damage detection algorithms. This is not considered in the implementation method, primarily because these issues will most likely be dealt with in the process of monitoring the structure using several sets of data, which falls beyond the scope of this research. An overview of these issues and some potential solutions that are found in the literature was presented in Section 2.6 of this thesis.

8.2. Conclusions I: Calibrated Damage Simulations

The first main part of the implementation method is the Calibrated Damage Simulations. The intention of the CDS is to create a series of simulations that best represent the actual measured ambient data from the structure. This is done by performing an ambient vibration test of the structure and using various results from that test to calibrate the simulations.

The benefits of using this method to improve the quality of a vibration simulation were demonstrated in Chapter 5. A comparison of a simulation with the measured data from the IASC/ASCE Benchmark frame was performed. From the ambient vibration test, the modes, frequencies, damping values, and signal amplitudes can be obtained. The first step after the ambient vibration test is to create and update a FEM of the structure; this is done in a typical way by correlating the dynamic characteristics of the model with the measured ones. Then the simulations are carried out, being adjusted for input, damping and noise using the AVT results. The simulated datasets are then used for evaluation and design of the DDM.

One of the important results from the CDS method is from the model updating of the 3D frame. A process of design/update was shown that resulted in a FEM that had very good correlation with the real structure. As a result of doing this, the error was minimized in the undamaged state, and comparisons of future damage simulations also showed a low error. These comparisons were possible because in the benchmark study real datasets were available. This is an important consideration for real structures, when the damage cases are not available. Therefore a similar process of design/update should be performed to maximize correlation.

8.3. Conclusions II: Damage Detection Methodology

The second main part of the implementation method is the Damage Detection Methodology. The DDM is intended to provide a framework for within the damage detection algorithms can be applied into the SHM system. The main philosophy behind the DDM is that it should contain multiple damage detection algorithms. This is done due to the fact that none of the algorithms that are available have shown consistent success in all damage scenarios; therefore by combining them together the advantages of each technique can be exploited.

An example DDM was developed and presented in Chapter 6. The methodology utilizes the Damage Locating Vector technique for the primary damage predictions. The DLV technique requires the flexibility matrices from the measurements; for ambient vibration data only approximations of the flexibilities can be obtained. Therefore the SDLV and PFM techniques were used as means to deal with the output-only data and obtain those equivalent flexibilities. This provides two independent predictions to illustrate the point of combining the algorithms. A model updating method was later used to further improve the final predictions.

It was shown through the application to a 2D truss example and a 3D frame example that the DDM provided better results than either of the two damage detection algorithms individually. The method should improve with the addition of other damage detection techniques that offer independent predictions.

8.4. Conclusions III: Implementation Method

The implementation method as developed in Chapter 4, 5 and 6 was applied to two building case studies in Chapter 7. It was shown that through the application of the method it was possible to determine that the proposed DDM (from Chapter 6) was not necessarily suitable for use on these buildings. It did however identify limitations of the DLV technique; and from there two possible solutions were developed. The first solution proposed used an alternative model for the damage detection phase. The alternative model was an equivalent frame that shared the measured points, natural frequencies and mode shapes. The second solution was to use a denser distribution of sensors throughout the structure. These ideas were illustrated on the two cases and on the 3D frame example from Chapter 6. Using these solutions it may be possible to use

the DDM for larger structures. Also it was found that based on the DLV theory an optimization scheme for determining the sensor locations could be developed.

Although the particular DDM that was chosen in this study was not completely successful when applied to the case studies, it was shown that by using the implementation method the DDM can be evaluated for real structures and its limitations identified. It is evident from this application that the method can be used for successful implementation of the technology.

8.5. Recommendations

Based on what was learned from this project, several recommendations regarding the application of the implementation method and for further study can be made. They are described here in terms of the CDS, the DDM, the implementation method, and general issues regarding implementation of SHM systems.

8.5.1. Calibrated Damage Simulations

- Further applications of the CDS method should be applied, to existing datasets or for new structures; this is done to both validate the CDS as described in this thesis and to allow for further refinements.
- The focus of development and application of the CDS method should be on:
  - The model updating phase and reduction of initial errors;
  - The measurement of the ground motion as a means to improve the input; in particular using more sensors on the ground than would normally be used.
- A more comprehensive comparison between the simulations and the real data should be performed.
- Explore the use of more complex analysis to define the noise and errors.
- The simulation of damage needs to be further developed; interaction between the analyst and the design engineers is required to define the realistic damage scenarios that need to be identified in the final SHM system.

8.5.2. Damage Detection Methodology

- Additional damage detection algorithms need to be added to expand the DDM and improved the accuracy and robustness as demonstrated in this thesis.

- Explore additional statistical combination methods for the prediction set.
- Explore the relationship between the measurements and damage threshold (specific to the DLV technique).
- Automation of the DDM, particularly with the FEM analysis; this should allow for more variations to be tested with respect to the current algorithms and new ones that may be added.
- Introduce a method to determine if the structure is damaged; this also requires setting a threshold with respect to changes in the modal properties (ie. identification vs. localization).
- The DDM should be expanded to incorporate other effects on the measured data, such as temperature, which can cause changes in the modal parameters that are unrelated to damage. One possible way to deal with this is by creating a database of undamaged state data, at various temperatures and environmental conditions. Then when the analysis is performed on a new future dataset, a dataset with similar conditions can be utilized.
- A probabilistic/reliability analysis or component should be added to the DDM. This would be done to provide a value of probability with the final predictions.
- Additional refinement of the EFMDD approach can be made; instead of a frame model a truss model could be used to allow for better determination of the damage location.
- The method should address boundary condition variations; in particular, the case where a strong-ground-motion event could change the soil stiffness, potentially changing the observed system. From an experimental perspective, this may be dealt with using microtremor measurements to establish an idea of the soil properties.

8.5.3. Implementation Method

- The optimization scheme for the location of sensors should be developed.
- Criteria for the performance of the DDM should be established, depending on the DDA's that are used and the requirements for the SHM system. This is important since the purpose of the implementation method is to aid in designing the DDM.

8.5.4. General

- The implementation method described in this thesis deals with implementation of the damage detection algorithms; it is required to expand this method to include other issues that will results in a final SHM system.
- The implementation method for a final SHM system needs to include the interaction with the owner/final user. This includes both issues regarding the input (ie. what measurements are available for a practical standpoint) and the required output (ie. what does the owner/final user need).
- Practical issues with respect to the input vary depending on the system; typically the main limitation is with the number of sensors available. This is changing however with the advent of more inexpensive sensors
- Practical issues with respect to the output are difficult to define; there is a divide between what the owner needs, and with what the SHM system can offer in the most effective way.

References

Aenlle, M.L., Brincker, R., Canteli, A.F., "Load Estimation from Natural Input Modal Analysis", Proc. of the 23rd International Modal Analysis Conference, Orlando, Fla, February 2005, Paper 155

Aktan, A.E., Helmicki, A.J, Hunt, V.J., (1998) "Issues In Health-Monitoring For Intelligent Infrastructure," Journal of Smart Materials and Structures, Oct., 1998

Aktan, A.E., Catbas, F.N., Grimmelsman, K.A., Pervizpour, M., "Development of a Model Health Monitoring Guide for Major Bridges", Drexel Intelligent Infrastructure and Transportation Safety Institute Report, July 2003

Aktan, A.E., Catbas, F.N., Ciloglu, S.K., Grimmelsman, K.A., Pan, Q., "Opportunities and challenges in health monitoring of constructed systems by modal analysis", International Conference on Experimental Vibration Analysis for Civil Engineering Structures, Bordeaux, France, Oct 2005

Ansari, F., "Sensing Issues in Civil Structural Health Monitoring", Springer Publishing, 2005, 528 pp.

Balageas, D., Fritzen, C-P., Gűemes, A., "Structural Health Monitoring", iSTE Publishing, 2006, 496pp.

Balmès, E., Basseville, M., Mevel, L., Nasser, H., "Handling the temperature effect in vibration-based monitoring of civil structures: a combined subspace-based and nuisance rejection approach", Proceedings of the 6th Symposium on Fault Detection, Supervision and Safety of Technical Processes (SAFEPROCESS), Pages 655-660, Beijing, China, August 2006

Basseville, M., Mevel, L., Goursat, M., (2004) "Statistical model-based damage detection and localization : subspace-based residuals and damage-to-noise sensitivity ratios", Journal of Sound and Vibration, 275(3):769-794, August 2004

Bernal, D. (2002). "Load vectors for damage localization", Journal of Engineering Mechanics, ASCE, Vol.128, No.1, pp.7-14.

Bernal, D., Gunes, B., (2004) "Flexibility Based Approach for Damage Characterization: Benchmark Application", ASCE Journal of Engineering Mechanics, January 2004, pp61-70

Bernal, D., Henandez, E., "Identification of Damage Induced by Earthquakes", Proc. of 23rd International Modal Analysis Conference, Orlando, Fla, 2005, Paper 435

Bernal, D., (2006) "Flexibility-Based Damage Localization from Stochastic Realization Results", ASCE Journal of Engineering Mechanics, Vol. 132, Issue 6, pp. 651-658

Bogdanovic, A., "Esplanade Riel Pedestrian Bridge – Canada", ISHMII Case Study, 2005 (REF: www.ishmii.org/literature/casestudiesmain.html)

Brincker, R., Zhang, L., Andersen, P., "Modal Identification from Ambient Responses using Frequency Domain Decomposition", 18th International Modal Analysis Conference, San Antonio, Texas, pp 625-630, 2000

Brincker, R., Andersen, P., "Understanding Stochastic Subspace Identification", Proc. of IMAC XXIV, St. Louis, MO, Paper 48, Jan 30 – Feb 2, 2006

Brinkman, B.A., Macioce, D.J., "Understanding Modal Parameter Terminology and Mode Shape Scaling", Proc. of IMAC I, Orlando, FLA, November 8-10, 1982 pp.840-844

Buyukozturk, O., and T.-Y. Yu, "Structural Health Monitoring and Seismic Impact Assessment", The Fifth National Conference on Earthquake Engineering, 26-30 May 2003, Istanbul, Turkey.

Caicedo, J.M., Dyke, S.J., Johnson, E.A., (2004) "Natural Excitation Technique and Eigensystem Realization Algorithm for Phase I of the IASC-ASCE Benchmark Problem: Simulated Data", ASCE Journal of Engineering Mechanics, January 2004, pp49-60

Catbas, F.N., Aktan, A.E., (2002) "Condition and Damage Assessment: Issues and Some Promising Indices" (2002), ASCE Journal of Structural Engineering, August 2002, pp. 1026-1036

Catbas, F.N., Brown., D.L., Aktan, A.E., (2004) "Parameter Estimation for Multiple-Input Multiple-Output Modal Analysis of Large Structures", ASCE Journal of Engineering Mechanics, August 2004, pp. 921-930

Catbas, F.N., Brown, D.L., Aktan, A.E., (2006) "Use of Modal Flexibility for Damage Detection and Condition Assessment: Case Studies and Demonstrations on Large Structures", ASCE Journal of Structural Engineering, November 2006, pp. 1699-1712

Celebi, M., Purvis, R., Hartnagel, B.A., Gupta, S., Clogston, P., Yen, P., O'Connor, J., Franke, M., "Seismic Instrumentation of the Bill Emerson Memorial Mississippi River Bridge at Cape Girardeau (MO): A Cooperative Effort", 4th National Seismic Conference and Workshop on Bridges and Highways, Memphis, TN, February 2004

Celebi, M., Sanli, A., Sinclair, M., Gallant, S., Radulescu, D., (2004) "Real-Time Seismic Monitoring Needs of a Building Owner and the Solution", Earthquake Spectra, Vol. 20, Issue 2, pp333-346, May 2004

C. M. Chang, Chin-Hsuing Loh, Kung-Chun Lu, Ping-Yin Lin, Jerome P. Lynch (2006), "Experimental Verification of Wireless Structural Sensing and Centralized/ Decentralized Control of Building Using MR-Dampers," Journal of Intelligent Material Systems and Structures, Sage Publications, submitted.

Chopra, A.K., "Dynamics of Structures: Theory and Application to Earthquake Engineering", 2nd Edition, Pentice Hall, 2000, 844 Pages

Chung, H-C., Enomoto, T., Shinozuka, M., Chou, P., Park, C., Yokoi, I., Morishita, S., "Real Time Visualization of Structural Response with Wireless MEMS Sensors", Proc. of the 13th World Conference on Earthquake Engineering, Vancouver, Canada, August 2005, Paper 121

Cunha, A., Caetano, E., "From Input-Output to Output-Only Modal Identification of Civil Engineering Structures", 1st International Operational Modal Analysis Conference, Copenhagen, Denmark, Keynote Lecture, 2005

Dascotte, E., Strobbe, J., Hua, H., "Sensitivity-Based Model Updating using Multiple Types of Simultaneous State Variables", Proc. of the 13th International Modal Analysis Conference, Nashville, TN, February 1995, pp1035-1040

Duan, Z., Yan, G., Ou, J., Spencer, B.F., (2005) "Damage localization in ambient vibration by constructing proportional flexibility matrix", Journal of Sound and Vibration, 284 p 455-466

Dyke, S.J., Bernal, D., Beck, J., Ventura, C., "Experimental Phase II of the Structural Health Monitoring Benchmark Problem", Proc. of the 16th ASCE Engineering Mechanics Conference, Seattle, WA, July 2003, Paper 496

Dynamic Design Solutions, "FEMTools Theoretical Manual –Version 3.1", Copyright 1994-2006, DDS

Farrar, C.R., Doebling, S.W., "An Overview of Modal-Based Damage Identification Methods", DAMAS Conference, Sheffield, UK, June 1997

Farrar, C., Sohn, H., Doebling, S., "Structural Health Monitoring at Los Alamos National Laboratory", Proc. of the 13th International Congress and Exhibition on Condition Monitoring and Diagnostic Engineering Management, Houston, TX, 2000

Farrar, C.R., Sohn, H., "Condition/Damage Monitoring Methodologies", Consortium of Organizations for Strong-Motion Observation Systems – Workshop on Structural Instrumentation, Emeryville, CA., November 2001

Farrar, C.R., Lieven, N.A.J., (2007) "Damage prognosis: the future of structural health monitoring", Philosophical Transactions of the Royal Society A, 365, 623-632

Gajic, Z, "Linear Dynamic Systems and Signals", Prentice Hall, 2002, 700p.

Giraldo, D., "A Structural Health Monitoring Framework for Civil Structures", PhD Thesis, Washington University at St. Louis, Department of Civil Engineering, May 2006

Giraldo, D.F., Dyke, S.J., Caicedo, J.M., (2006) "Damage Detection Accomodating Varying Environmental Conditions", Structural Health Monitoring (Sage), Vol. 5(2): 0155-18

Gsell, D., Motavalli, M., "Indoor Cable Stayed GFRP-Bridge at Empa, Switzerland", 4th International Conference on Advanced Composite Materials in Bridges and Structures, Calgary AB, July 20-23, 2004, pp.

Handbook for Dynamic Data Acquistion and Analysis, IES-RP-DTE012.1, Institute of Environmental Sciences, Illinois, USA, 1995.

Hera, A., Hou, Z., (2004) "Application of Wavelet Approach for ASCE Structural Health Monitoring Benchmark Studies", ASCE Journal of Engineering Mechanics, January 2004, pp96-104

Hjelm, H.P., Brincker, R., Graugaard-Jensen, J., Munch, K., "Determination of Stress Histories in Structures by Natural Input Modal Analysis", Proc. of 23rd International Modal Analysis Conference, Orlando, Fla, 2005, Paper 165

Housner, G. W., Bergman, L.A., Caughey, T.K., Chassiakos, A.G., Claus, R.O., Masri, S.F., Skelton, R.E., Soong, T.T., Spencer, B.F., Yao, J.T.P., (1997) "Structural Control: Past, Present, and Future", ASCE Journal of Engineering Mechanics, September 1997, pp 897-971

Hsieh, K.H., Halling, M.W., (2006) "Overview of Vibrational Health Monitoring with Representative Case Studies", ASCE Journal of Bridge Engineering, Nov/Dec 2006, pp.707-715

Humar, J., Bagchi, A., Xu., H., (2006) "Performance of Vibration-Based techniques for the Identification of Structural Damage", Structural Health Monitoring (Sage), Vol. 5(3) 0215-27

Huth, O., Feltrin, G., Ulfkjaer, J.P., Kilic, N., "Model update and damage identification on a prestressed concrete bridge using modal parameters and projective input residuals ", IMAC XXI, 21st International modal analysis conference, Kissimmee, FL, USA, February 3–6, 2003, CD, 8 p.

Huth, O., Feltrin, G., Maeck, J., Kilic, N., Motavalli, M., (2005) "Damage Identification Using Modal Data: Experiences on a Prestressed Concrete Bridge", ASCE Journal of Structural Engineering, December 2005, pp. 1898-1910

ISHMII (Unknown Author), "Confederation Bridge – Canada", ISHMII Case Study, CHCanada04, 2004 (REF: www.ishmii.org/literature/casestudiesmain.html)

ISHMII (Unknown Author), "Putlitz Bridge – Germany", ISHMII Case Study, CHCanada01, 2003 (REF: www.ishmii.org/literature/casestudiesmain.html)

ISHMII (Unknown Author), "Ting Kau Bridge – Hong Kong, China", ISHMII Case Study, CHChina01, 2004 (REF: www.ishmii.org/literature/casestudiesmain.html)

Ivanovic, S.S., Trifunac, M.D., Todorovska, M.I., "Ambient Vibration Tests of Structures – A Review", Bullentin of Indian Society of Earthquake Technology, Special Issue on Experimental Methods, pp 1-49, Dec. 2000

Kharrazi, M.H.K., Ventura, C.E., Brincker, R., Dascotte, E., "A Study on Damage Detection Using Output-Only Modal Data", Proc. of the 20th International Modal Analysis Conference, Los Angeles, CA, 2002, paper

Ko, J.M., Sun, Z.G. and Ni, Y.Q. (2002), "Multi-stage identification scheme for detecting damage in cable-stayed Kap Shui Mun Bridge", Engineering Structures, Vol. 24, No. 7, 857-868.

Kouchmeshky, B., Aquino, W., Lipson, H., Bongard, J.C., (2006). "Coevolutionary Strategy for Structural Damage Identification using Minimal Physical Testing", International Journal for Numerical Methods in Engineering, in Press

Lam, H.F., Katafygiotis, L.S., Mickleborough, N.C., (2004) "Application of a Statistical Model Updating Approach on Phase I of the IASC-ASCE Structural Health Monitoring Benchmark Study", ASCE Journal of Engineering Mechanics, January 2004, pp34-48

Lu, K.C., Yang, Y.S., Loh, C.H., Lynch, J.P., Law, K.H., "Structural Health Monitoring and Damage Diagnosis: Based on Embedded Algorithm and Visualized User Interface," Proc. of the US-Taiwan Workshop on Smart Structural Technology for Seismic Hazard Mitigation, Taipei, Taiwan, October 12-14, 2006.

Luş, H., Betti, R., Yu, J., De Angelis, M., (2004) "Investigation of a System Identification Methodology in the Context of the ASCE Benchmark Problem", ASCE Journal of Engineering Mechanics, January 2004, pp71-84

Lynch, J.P., "Overview of Wireless Sensors for Real-Time Health Monitoring of Civil Structures", Proc. of the 4th International Workshop on Structural Control and Monitoring, New York, NY, June 2004

Lynch, J.P., Wang, Y., Swartz, A., Lu, K-C., Loh, C-H., (2006), "Implementation of a Closed-Loop Structural Control System using Wireless Sensor Networks," Journal of Structural Control and Health Monitoring, Wiley, submitted.

Maeck, J., De Roeck, G., (2003) "Description of Z24 Benchmark", Mechanical Systems and Signal Processing, Vol. 17, No. 1, pp. 127-131

Mevel, L., Basseville, M., Goursat, G., (2003) "Stochastic subspace-based structural identification and damage detection - Application to the steel-quake benchmark", Mechanical Systems and Signal Processing, Special issue on COST F3 Benchmarks, 17(1):91-101, January 2003

Mirza, K., "Seismic Structural Health Monitoring of Bridges", PhD Thesis, Department of Civil Engineering, The University of British Columbia, June 2006

Moon, F.L., Aktan, A.E., (2006) "Impacts of Epistemic (Bias) Uncertainty on Structural Identification of Constructed (Civil) Systems", The Shock and Vibration Digest, September 2006, pp. 399-420

Mufti, A., "Guidelines for Structural Health Monitoring", ISIS Canada Design Manual No. 2, 2001

Naeim, F., Hagie, S., Alimoradi, A., "Automated Post-Earthquake Damage Assessment and Safety Evaluation of Instrumented Buildings", SMIP-05 Seminar on Utilization of Strong-Motion Data, Los Angeles, CA, May 2005

Nasser, H., Mevel, L., Chapelle, D., "Damage detection under the environmental constraints", Proc. Of the 23rd IMAC, Orlando, FLA, January 2005

Owen, J.S., Pearson, S.R., "The use of Dynamic Data for the Structural Health Monitoring of Bridges", Proc. Of the 1st FIG International Symposium on Engineering Surveys for Construction Works and Structural Engineering, Nottingham, UK, 28 June – 1 July 2004

Paek, J., Gnawali, O., Jang, K-Y., Nishimura, D., Govindan, R., Caffrey, J., Wahbeh, M., Masri, S., "A Programmable Wireless Sensing System for Structural Health Monitoring", 4th World Conference on Structural Control and Monitoring, July 11-13 2006, San Diego, CA, Paper 317

Park, S., Stubbs, N., Bolton, R.W., "Damage Detection on a Steel Frame Using Simulated Modal Data", Proc. of the 16th International Modal Analysis Conference, Santa Barbara, CA, February 1998, pp. 612-622

Peeters, B., Maeck, J., De Roeck, G., (2001) "Vibration-based damage detection in civil engineering: excitation sources and temperature effects", Smart Mater. Struct. 10 518-527

Phares, B.M., Wipf, T.J., Greimann, L.F., Lee, Y-S., "Health Monitoring of Bridge Structures and Components Using Smart Structrual Technology: Volume 2", Wisconsin Highway Research Program Report, WHRP 05-03, January 2005

Pridham, B.A., Wilson, J.C., *"An application example illustrating the practical issues of subspace identification"*, Proc. of IMAC XXI, Kissimmee, FLA, Feb 3-6, 2003, Paper 220

Pridham, B.A., "State Space Modeling and Identification of Stochastic Linear Structural Systems", PhD Thesis, McMaster University, August 2004

Ritdumrongkul, S., "Quantitative Health Monitoring Using Piezoceramic Actuator Sensors", PhD Thesis, University of Tokyo, 2005

Rodgers, J.E., Celebi, M., (2006) "Seismic Response and Damage Detection Analyses of an Instrumented Steel Moment-Framed Building", ASCE Journal of Structural Engineering, October 2006, pp. 1543-1552

Rohrmann, R.G., Said, S., Schmid, W., "Load and condition monitoring of the Putlitz Bridge in Berlin-Moabit", Proc. Symposium Topics from civil and bridge engineering, BAM, Berlin 2003

Rytter, A., "Vibration-based inspection of Civil Engineering structures", PhD Thesis, Dept. of Building Technology, Aalborg University, 1993

Saadat, S., Noor, M.N., Buckner, G.D., "Health monitoring and damage detection in base-excited structures using the Intelligent Parameter Varying (IPV) technique", International Conference for the Application of Statistics and Probability in Civil Engineering, San Francisco, CA, 2003, pp 467-472

Siddique, A.B., Wegner, L.D., Sparling, B.F., "Application of vibration-based damage detection to an integral abutment bridge", Proc. Of Non-Destructive and Health Moniroting of Aerospace Materials, Composites, and Civil Infrastructure IV, (SPIE 2005), Bellingham, WA, Vol. 5767

Straser, E., Sohn, H., Kiremidjian, A., Law, K.H., "A Framework for Health Monitoring of Structures", Proc. of ASCE Structures Congress, 2000

Sohn, H., Farrar, C.R., Hunter, N.F., Worden, K. (2001) "Structural Health Monitoring Using Statistical Pattern Recognition Techniques", Journal of Dynamic Systems, Measurement and Control, Volume 123, Issue 4., pp. 706-711 December 2001

Sohn, H., (2007) "Effects of environmental and operating variability on structural health monitoring", Phil. Trans. R. Soc. A, 365, pp. 539-560

Turek, M., Ventura, C., "Finite Element Model Updating of a Scale-Model Steel Frame Building", Proc. of the 1st International Operational Modal Analysis Conference, Copenhagen, Denmark, April 2005, paper 68

Turek, M., Ventura, C., "Damage Detection Studies of IASC-ASCE Benchmark Test Frame Using Vibration Data", 3rd International Conference on Construction Materials, Vancouver, Canada, August 2005

Turek, M., Thibert, K., Ventura, C., Kuan, S., "Ambient Vibration Testing of Three Unreinforced Masonry Brick Buildings in Vancouver, Canada", Proc. Of IMAC 24, St. Louis, MO., 2006, Paper 77

Wu, J.R., Li, Q.S., (2006) "Structural parameter identification and damage detection for a steel structure using a two-stage finite element model updating method", Journal of Construction and Steel Research, 62, 231-239

Van Overshcee, P., De Moor, B.L., (1996), "Subspace identification for linear systems: theory, implementation, applications", Kluwer Academic Publications, Boston

Ventura, C.E., Prion, H.G.L., Black, C., Rezai K., M., Latendresse, V., "Modal Properties of a Steel Frame used for Seismic Evaluation Studies", Proc. of the XV IMAC, Orlando, Fla, 1997

Ventura, C., Horyna, T., "Measured and Calculated Characteristics of HCT Building", Proc. of the 18th International Modal Analysis Conference, San Antonio, Texas, 2000, pp 1070-1074

Ventura, C.E., Kharrazi, M.H.K., Turek, M., Horyna, T., "Dynamic Analysis of a Pedestrian Walkway, University of British Columbia, Canada", Proc. Of the 20th International Modal Analysis Conference, Los Angeles, CA, 2002

Ventura, C.E., Lord, J.F., Turek, M., "Experimental Studies and Remote Monitoring of IASCASCE Benchmark Test Frame", Proc. of the 21st International Modal Analysis Conference, Orlando, Florida, February 2003, paper no. 330

Ventura, C., Turek M., "Fifteen Years of Ambient Vibration Testing in Western Canada", 1st International Operational Modal Analysis Conference, Copenhagen, Denmark, paper 105, 2005

Ventura, C.E., Jord, J-F., Turek, M., Brincker, R., Andersen, P., Dascotte, E., "FEM Updating of Tall Buildings Using Ambient Vibration Data", EURODYN September 2005, Paris, France

Yang, J.N., Lei, Y., Lin, S., Huang, N., (2004) "Hilbert-Huang Based Approach for Structural Damage Detection", ASCE Journal of Engineering Mechanics, January 2004, pp85-95

Yuen, K-V., Au, S.K., Beck, J.L., (2004) "Two-Stage Structural Health Monitoring Approach for Phase I Benchmark Studies", ASCE Journal of Engineering Mechanics, January 2004, pp16-33

Zhang, L., Brincker, R., Andersen, P., "An Overview of Operational Modal Analysis: Major Development and Issues", 1st International Operational Modal Analysis Conference, Copenhagen, Denmark, paper 93, 2005

Zhao, J., DeWolf, J.T., (1999) "Sensitivity study for vibrational parameters in damage detection", ASCE Journal of Structural Engineering, April 1999, pp. 410-416

Zonta, D., Bernal, D., "Strain-Based Approaches to Damage Localization in Civil Structures", Proc. of IMAC XXIV, St. Louis, MO., Paper 197, Jan 30 – Feb 2, 2006

Zukewich, J., "Tsing Ma Bridge – Hong Kong (PRC)", SAMCO Final Report, F04 Case Studies, 2006 (REF: www.ishmii.org/literature/casestudiesmain.html)

Zukewich, J., "I40-Bridge, New Mexico, USA", SAMCO Final Report, F04 Case Studies, 2006b (REF: www.ishmii.org/literature/casestudiesmain.html)

Software References:

ARTeMIS Extractor Pro, Release 3.5, (Copyright 1998-2005) Structural Vibration Solution A/S

ETABS Version 9.09, (Copyright 1984-2006), Computers and Structures Inc.

FEMTools Version 3.1.2, (Copyright 1994-2006), Dynamic Design Solutions N.V.

MATLAB Version 7.0.0.19920 (R14) (Copyright 1984-2004), The Mathworks, Inc.

SAP2000 Advanced Version 10.0.9 (Copyright 1976-2006), Computers and Structures Inc.

Appendix A. Details of Application of Method to Real Buildings

This appendix provides the details of the application of the implementation method to the two case study buildings. Chapter 7 presented a summary of the application based on the key results and the conclusions; the details include all of the steps of the method and show the progression of the analysis towards those conclusions.

A.1. Melville Building

The Melville is a mixed development in downtown Vancouver, Canada, composed of a high rise 46-storey residential tower at the west end of the development and a 10-storey hotel at the east end. Both share a common podium structure which includes three levels above ground and 5 underground parking levels. The total height of the residential tower is 146 m from the slab on grade at parking level 5 to the roof of the tower. The total height underground is 15 m. The podium structure height is 21m. A photo of the tower at the time of testing is shown in Figure A. 1. The typical tower floor plan and sensor layout is shown in Figure A. 2.

The gravity system carries only vertical loads due to self-weight and occupancy, consisting of flat concrete slabs at the tower levels. The ground floor is a transfer slab, and in this case a slab/slab-band system was used. All the slabs are simply supported by columns distributed along the surface of the building. The foundations for the columns are simple spread footings.

Along the perimeter of the building at the underground parking levels, continuous basement walls have the double function of carrying vertical loads as well as working as retaining walls for the soil surrounding the construction. A central core placed approximately at the centre of the tower defines the lateral system. The core foundation is a massive raft footing bearing directly on the natural soil. In addition a slab on grade was poured at the lower parking level directly bearing on the existing soil.

Figure A. 1: Melville Building

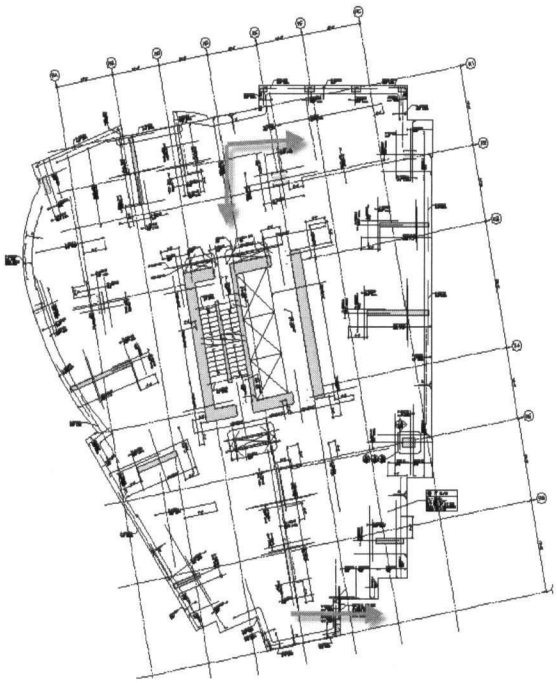

Figure A. 2: Typical Sensor Layout

A.1.1. Melville Ambient Vibration Test

The AVT was performed in June of 2006. For the test, reference sensors were placed with the data acquisition system on the 39th floor. Three teams of 2 people were deployed to move the roving sensors, two from the top of the building down, and one from the bottom of the parking garage up. Typically every second or third floor was measured. For each floor, a sensor layout as shown in Figure A. 2 was applied. This is a typical layout for a building that allows the translation in both directions and the torsional movements to be measured. The only measurement that varied from Figure A. 2 was for level P5, where only a single point was measured in both horizontal directions.

For each setup 30 minutes of data was recorded at 500 samples per second. The long length of the tests was required due to the low frequencies of the building. A high sampling rate was chosen for two reasons. First, it has been found that in building tests previously [Turek et al., 2006] that more samples can provide a better definition of the mode shapes. Also, that for a difficult building to test such as this one, it is better to acquire more data than possibly necessary and decimate at a later time.

The data analysis was performed using the ARTeMIS Extractor software using the five methods available. Those methods are the Frequency Domain Decomposition (FDD) Method, Enhanced FDD (EFDD), and three variations of the Stochastic Subspace Identification (SSI) method. Figure A. 3 shows the plot of the singular value lines from the FDD analysis on the Melville data. The modes are numbered on the plot.

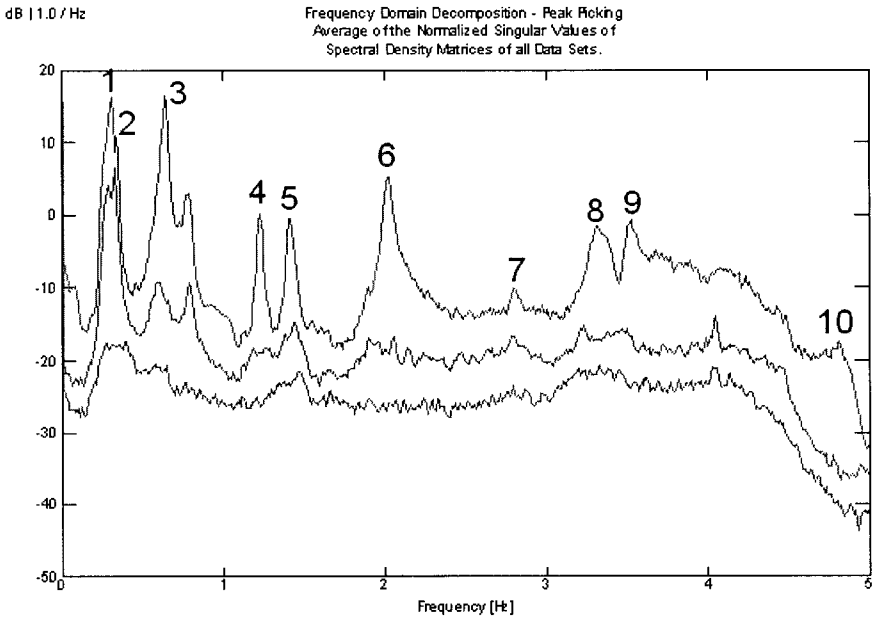

Figure A. 3: SVD Plot of Complete Building Test (With Mode Numbers)

From the results of the analysis, 9 modes were identified under 5 Hz using the SSI-CVA method. Before the analysis, the data was decimated in MATLAB to 100 sps for better management of the data. Then during the actual analysis, it was decimated down to 10 sps, which allows for better results using the SSI technique. A total of 512 frequency lines were used. Table A.1 presents the natural frequency, and damping ratio found using the SSI method. Examples of the mode shapes are shown in Figure A. 4 and Figure A. 5. In each figure, the mode is shown from four views, including a 3D view of each of the 2D orthogonal views.

Table A. 1: Melville Building Ambient Vibration Results

Method		Freq	Damping
Mode	Descrip.	[Hz]	[%]
1	1 E/W	0.303	1.441
2	1 N/S	0.329	2.148
3	1 Tor	0.649	2.076
4	2 E/W	1.226	1.326
5	2 N/S	1.417	0.614
6	2 Tor	2.023	1.094
7	2 E/W	2.810	1.495
8	2 N/S	3.318	1.320
9	3 Tor	3.510	1.127

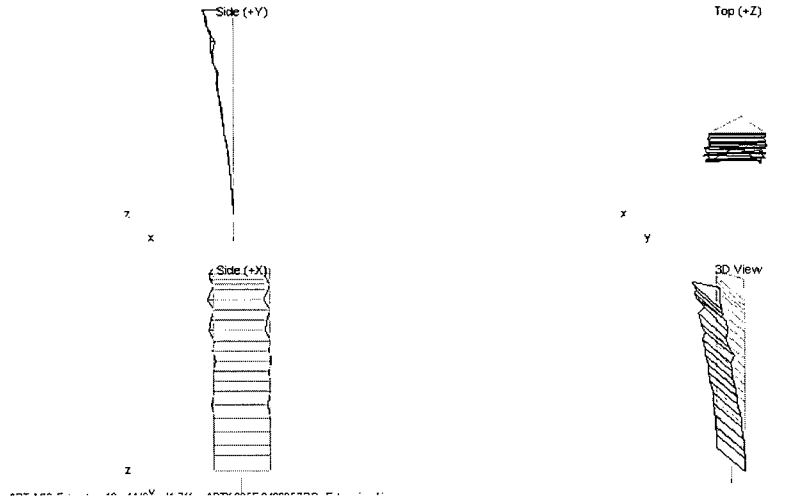

Figure A. 4: Mode 1 – *1st E/W (0.312 Hz)*

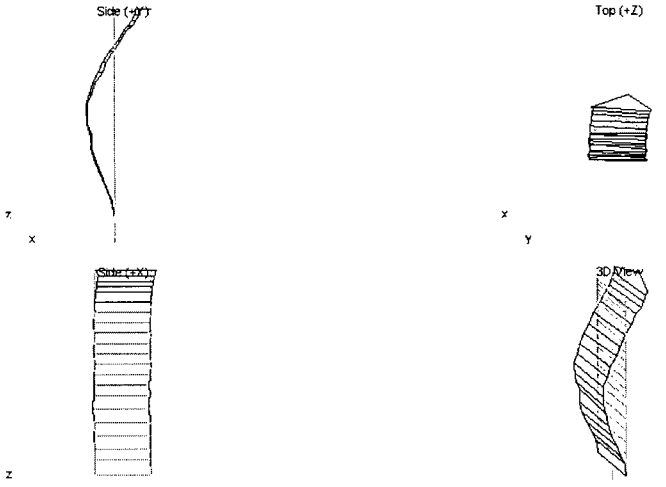

Figure A. 5: Mode 4 – *2nd E/W (1.221 Hz)*

A.1.2. Melville Finite Element Model

One of the objectives of the ambient vibration test was to generate several computer models of the building and perform a sensitivity analysis until the natural frequencies and modes shapes were close to the ones obtained from the ambient vibration test. Four different models were developed using two different commercial software systems widely known in structural engineering, ETABS version 8.0 [CSI, 2006] for 3D analysis and SAP version 9.0 for 2D. The first two were 2D models, and only the core in each direction (E/W and N/S) was modeled for the tower levels, and the core walls plus the basement walls for the basement levels. The first 3D model contained all of the structural elements present in the building including gravity system, columns, walls and the Lateral Resisting System (LRS) elements.

A second 3D model was generated (Figure A. 6), including the exterior cladding and the partition walls, up to level 35 since this was the state of the construction at the time of testing. The results obtained with the 2D models were very similar to the ones obtained with the 3D model containing only the structural elements. This comparison was used as a verification of the 3D model before going to the more complex full 3D model, and also confirming that it is a valid assumption to just model the LRS elements since the gravity elements in this type of building do not have a large influence on the dynamic response of the building. The results obtained with the complete 3D model including the non-structural elements confirmed their influence at least in the initial response of the building; however, when the building is excited by major shaking such as by an earthquake it is expected that the non-structural components will not have any significant influence in the response of the building. Table A. 2 gives the initial design comparison for the full 3D model. Test modes shown are from EFDD. Figure A. 7 shows an example of two of the FEM modes.

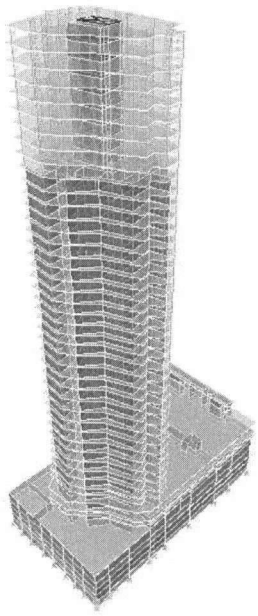

Figure A. 6: ETABS Full 3D Model

Table A. 2: Initial FEM Design Correlations

Mode	ETABS	Test	Direction
1	0.270	0.309	1 E/W
2	0.301	0.346	1 N/S
3	0.763	0.648	1 Tor
4	1.316	1.228	2 E/W
5	1.471	1.413	2 N/S
6	2.381	2.022	2 Tor
7	3.030	2.801	2 E/W
8	3.571	3.320	2 N/S
9	4.000	3.518	3 Tor
10	5.000	4.773	4 Tor

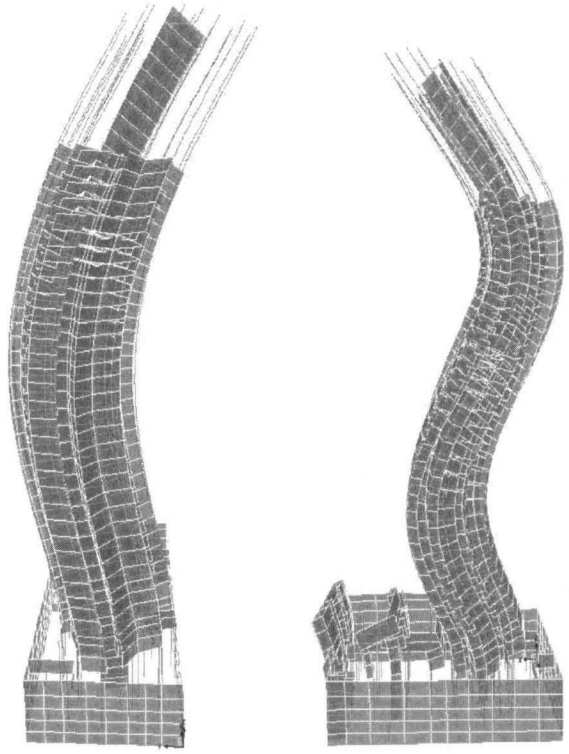

Figure A. 7: Melville FEM Mode 5 – *2nd N/S*; Mode 7 – *3rd E/W*

A.1.3. Melville Model Updating

As presented in Chapter 5, an automated updating of the FEM using a tool such as FEMTools is ideal. This allows for the updating of several parameters simultaneously, and also allows for a better overall match in general. Due to the complexity of the model in ETABS, it was not a straight forward task to recreate the model in FEMTools. Some FEA software have interfaces with FEMTools directly, but such an interface is not available for ETABS. As a result of this, an attempt was made at creating an equivalent model in FEMTools to the one in ETABS was created for the purpose of updating the material parameters. It was found that the primary difficultly with the equivalent model, and is also seen in the ETABS model, is that the ratio of translational modes and the torsional mode is different. This was also seen with the 3D frame model; in that case it was dealt with by adjusting the torsional mass distribution. The best update that was performed on the equivalent model used the cladding modulus of elasticity and changed the values locally (ie. for each individual member). The results are shown in Table A.3.

Table A. 3: Local Updating Results: Cladding Modulus of Elasticity

Mode	FEM [Hz]	EMA [Hz]	Diff. [%]	MAC [%]
1	0.29	0.31	-7.65	97.3
2	0.33	0.34	-3.74	96.1
3	0.74	0.64	14.53	92.9
4	1.16	1.22	-5.38	89.4

From the above results, it is likely that the best matching would come from a change in the arrangement of the cladding. Instead of having a global change in cladding properties for the ETABS model, a variation of properties across each floor will be necessary. Since the results from the equivalent model updating were not significantly better than the initial matching of the FEM, it was decided to move on the simulations using the original ETABS model.

A.1.4. Melville Calibrated Simulations

Once the FEM has been correlated reasonably with the test results, it is used for the simulations. The first notable challenge in the analysis of the Melville is that there was a change in FEM software. For the two previous examples, SAP2000 was used for the simulations and damage detection. For the Melville, the model was created using ETABS [CSI, etc]. ETABS is essentially a specialized version of SAP, designed for modeling of buildings. It has many features that make it convenient for building designers, such as specialized floor elements and walls/columns, and interface possibilities for detailing and analysis software for buildings. However, ETABS, like SAP, is not easily compatible with the analysis in this project. In particular, with SAP, the model and loading can be input/output using Excel. This is convenient for doing analysis that needs to be done externally outside of the main FEM software. ETABS does not offer this convenient input/output interface. This makes it difficult for analysis with large amounts of input data such as with the DLV analysis.

For the calibrated simulations however, the setup with ETABS is more or less the same as with SAP so it was run in the same way. The first step was to extract the recorded base signals from the dataset. These were combined using MATLAB and an example of the input spectrum is shown in Figure A. 8. In this example, as opposed to the 3D Frame, there is less influence from the measured ground motion at the lower frequencies.

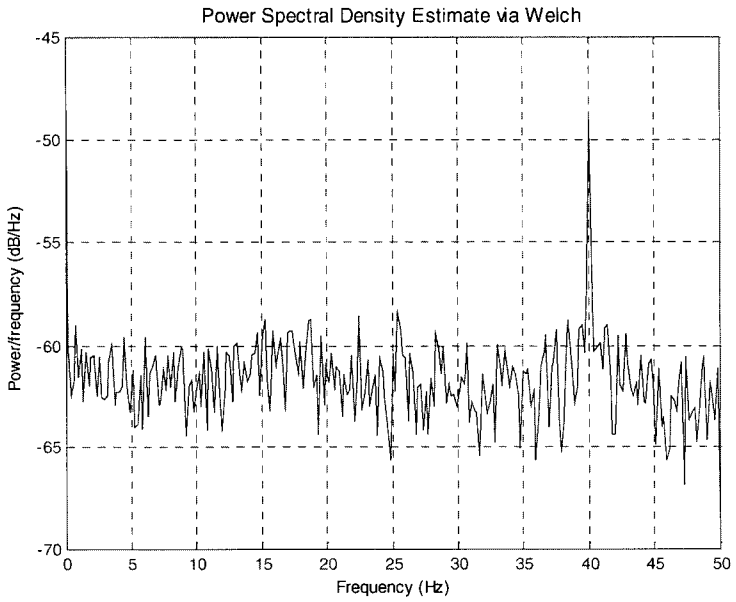

Figure A. 8: PSD of Melville Input

For the simulation input, 18 separate combined inputs were created, in a similar way as with the 3D frame. The combined inputs were applied to the base of the building in 9 sections, with 2 orthogonal inputs at each excitation point; this was done so that different sections had independent white noise components in order to excite all of the modes. The damping values using for the analysis were taken from the SSI-CVA values shown in Table A.1. The results from the noise-free simulation are shown in Figure A. 9 and Figure A. 10.

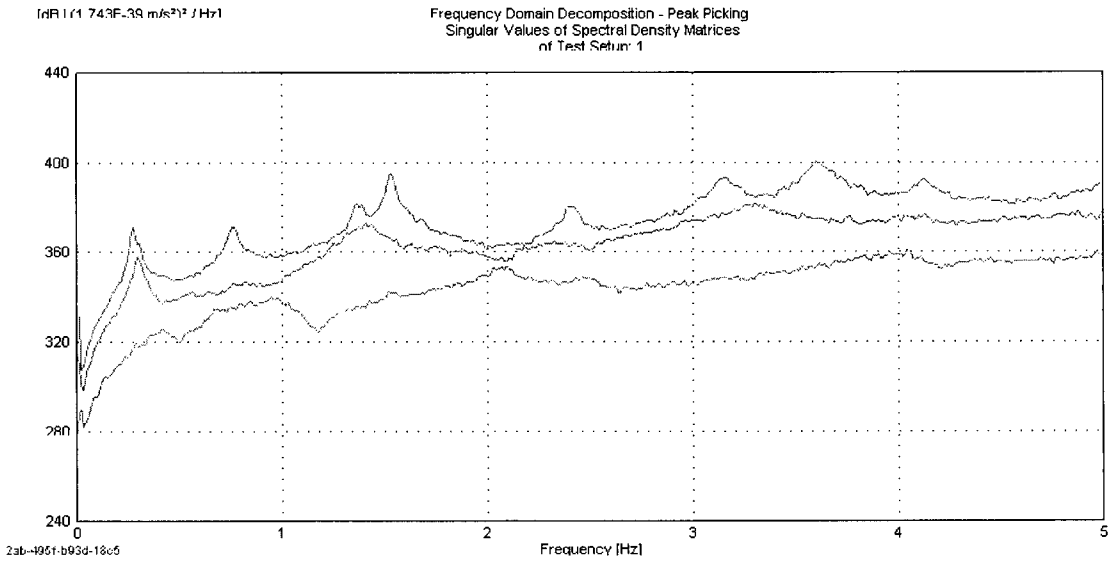

Figure A. 9: Melville Undamaged Configuration – No Noise (0 to 5Hz)

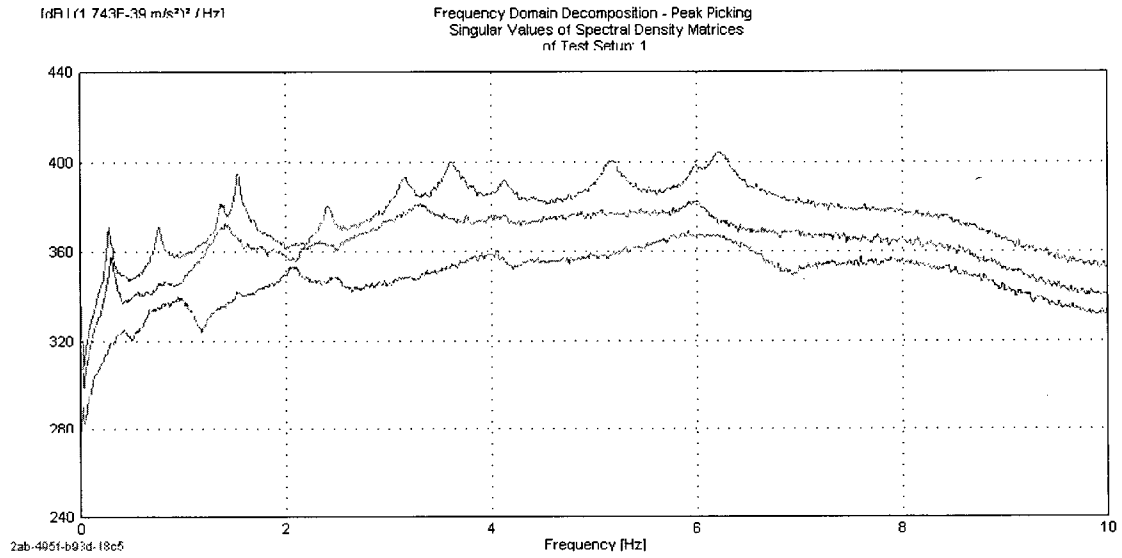

Figure A. 10: Melville Undamaged Configuration – No Noise (0 to 10Hz)

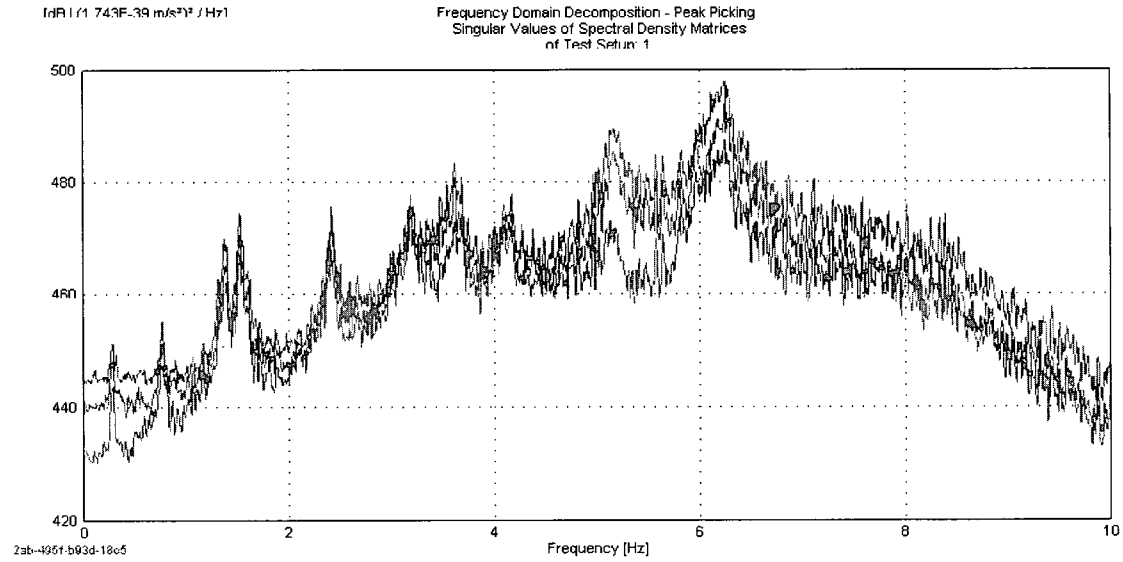

Figure A. 11: 5% RMS Noise added to Melville

It is seen from Figure A. 9 to Figure A. 11 that for this test, the cases with no noise added best resemble the results from the ambient vibration test (Figure A. 3). This is likely due to the fact that this is such a tall building with a high signal to noise ratio. Therefore it was deemed not necessary to add noise to the simulations for this case.

A.1.5. Choice of Damage Cases

The most challenging part of developing the simulations for a building such as the Melville is in the selection of the damage cases. From the 3D Frame study, the damage was chosen simply

as either removing the braces or loosening the end connections. For the simulations, the options were extended to reducing the area of the braces. For the model of the real building however, the choices become greater and more complex. For instance, the failure behaviour of concrete is not as simple as removing elements. However, for the first run of the damage detection study, elements were removed as a simple way to quickly create several damage cases. The first case examined had two columns removed from floor 25. Case 2 removed the same columns from floors 24 and 26 also; then case 3 examined damaging the shear core, by removing one wall. The frequencies for the undamaged case and the four damage cases are shown in Table A. 4. This would be considered mild damage and consequently is a challenge for the DDM to identify.

Table A. 4: Initial Damage Cases Frequency Comparison

Mode	Description	Undamaged	Case 1	Case 2	Case 3
1	1 E/W	0.272	0.272	0.272	0.272
2	1 N/S	0.302	0.302	0.302	0.302
3	1 Tor	0.758	0.758	0.758	0.757
4	2 E/W	1.371	1.370	1.370	1.349
5	2 N/S	1.528	1.528	1.528	1.525
6	2 Tor	2.410	2.410	2.410	2.406
7	3 E/W	3.158	3.156	3.156	3.138
8	3 N/S	3.610	3.610	3.610	3.604
9	3 Tor	4.119	4.120	4.120	4.113
10	4 E/W	5.168	5.167	5.167	5.150
11	4 Tor	5.977	5.978	5.978	5.970
12	4 N/S	6.223	6.224	6.224	6.205

In the table it is seen that for the first two damage cases, there is very little change in frequency from the undamaged case. Even when one of the core walls is removed (case 3) there are still only small changes in the frequencies; although the change becomes more observable. It is also evident that the lowest modes do not change, and that the most significant changes are observed in the highest modes (Mode 4, 7, 10). Also, these are all E/W modes. This small change is potentially problematic; to what degree the damage detection algorithms can detect damage is uncertain. Also, there is much controversy in the research community with respect to natural changes in the modes, ie. due to temperature and other environmental effects.

A.1.6. Melville Damage Detection

The next step in the implementation method is to apply the DDM as it was developed in Chapter 6. The main issue that involves the DDM is with the number of sensors used in the

analysis. Since with the DLV technique the number of sensors used must not be much greater than twice the number of modes obtained, this has a strong influence on the DDM performance. With the 3D Frame analysis, the number of sensors (not including the base) was 12; the number of modes was 5. For most of the analyses, the sensor set was chosen to be 6. For the Melville, the number of modes is 12, but the sensor set is 45. This creates a difficult situation, since using a total number of sensors equal to twice the number of modes creates a sensor set that is less than half the number available (considering that the number available still only measures every third floor). Therefore a sensor set with a significantly reduced number of sensors must be chosen; there are three obvious choices for this, and in each case the analysis would be repeated depending on the number of sensors used versus the number available. They are as follows:

1. A line of sensors along the height of the building, using one of the three horizontal sensors for each line (Figure A. 12).
2. A 3D group of sensors and analyze part of the building at a time (Figure A. 13).
3. A 3D distributed set of sensors (Figure A. 14).

These will be referred to as the 2D distributed set, the 3D moving set and the 3D distributed set respectively. The figures show a representation of the building, which is a simple frame. For each sensor set, three possible analysis cases are shown.

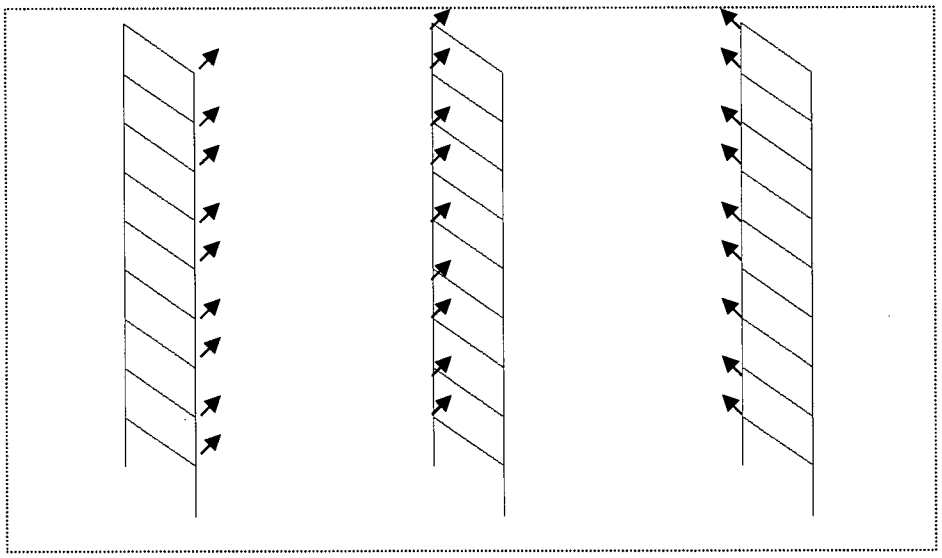

Figure A. 12: 2D Distributed Sensor Set

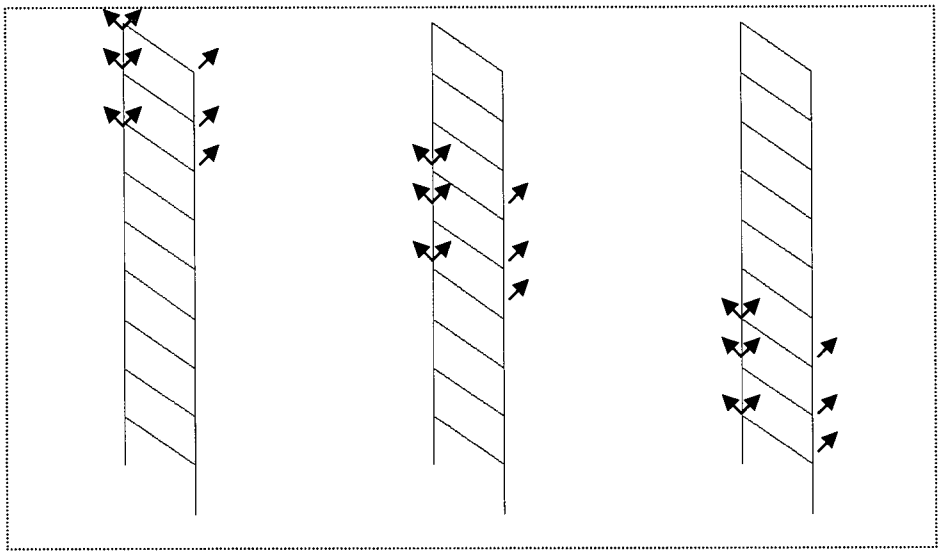

Figure A. 13: 3D Moving Sensor Set

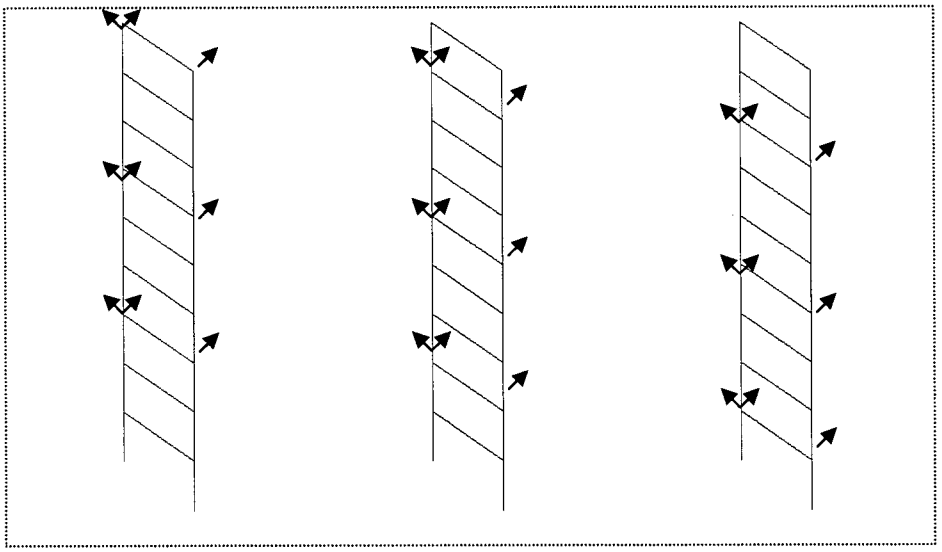

Figure A. 14: 3D Distributed Sensor Set

A.1.7. Primary Application of DDM to Melville Full 3D Model Simulations

The first attempt at applying the DDM to the simulations from the full 3D model was made using the 3D moving sensor set. A total of 5 analyses (one for each of the 5 sets) were performed using the SDLV and PFM techniques. For the initial analyses, the MU0% part of the DDM was not used; this was due to the fact that the FEMTools model was not available.

The analysis on the Melville featured many difficulties that were not seen with the 3D frame; this was mostly due to the complexity of the model (there were also issues with respect to using

ETABS). First, the number of elements and element types was much larger than in the previous cases. This was simplified by looking only at the core elements; all of the other element types were removed from the post-processing. Next, each area element had four values (one for each corner) for each of its various forces and stresses. Therefore the interpretation of the various stress definitions added the next difficulty, since it was apparent that depending on which stress was examined (ie. axial, shearing, bending etc.) the results of the damage prediction were different. It was decided ultimately to examine the average of the maximum stresses, and also to average the four values for each element.

The first way to post-process the results was simply to add each of the 4 results sets together (ie. for all of the elements of the building). It is seen in Figure A. 15 that the interpretation is difficult (ie. finding the elements less than 0.1 normalized stress). The implication of the figure is that the lower stories are damaged; this is not correct.

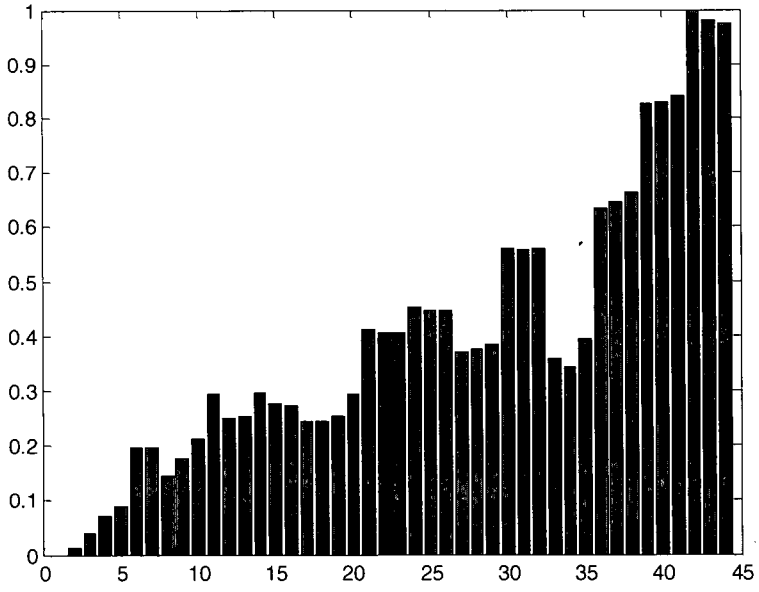

Figure A. 15: Sum of the four cases (floor averaging)

The next way to interpret the stresses is to separate into the four sensor set analyses. These are shown combined in Figure A. 16. For each analysis, the results are computed for the entire building; however, in the post-processing only those elements on the floors which were loaded by the DLV's are shown (ie. the 3D moving set). From the plot with the element stresses averaged to a floor, there is no clear indication of damage.

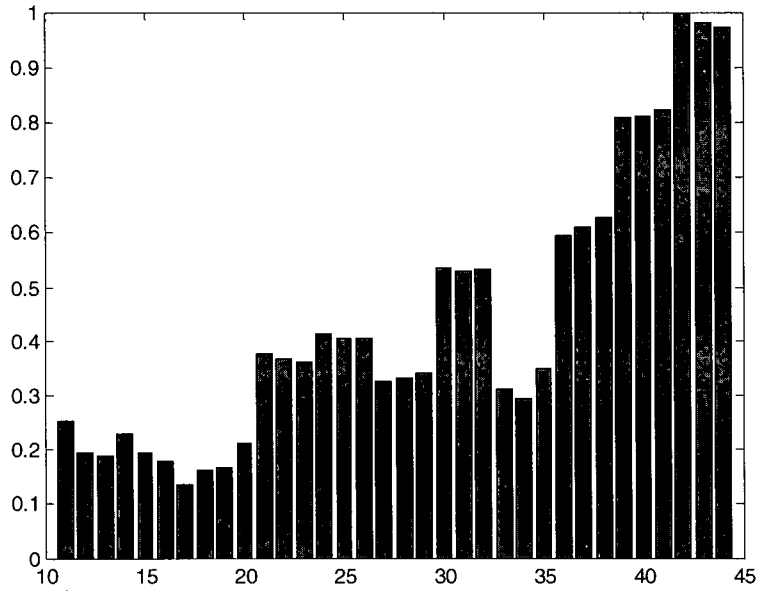

Figure A. 16: Separate Analysis of each set (combined figure)

From the above results it was not entirely clear if and where there was damage, although there appeared to be some lower stresses on floors 16 to 19. In each floor for the first 3 sensor sets, there are elements that have stresses lower than 0.1. This does not necessarily indicate damage however, since depending on the loads some members may be minimally stressed to begin with. To explore the issues with the application of the DDM to this problem, it was decided to create some simpler models to avoid dealing with the complexity of the full 3D model.

A.1.8. Alternative Models

Two alternative models were created to examine issues when applying the DDM to more complicated structures, particularly when they are created using area elements. In these cases the models were used for both the simulation and the damage detection analysis. The first alternative model featured a simplified core, floor slabs and columns placed along the perimeter of each floor. The model was created roughly using the dimensions of the Melville, but was intended to simplify the number and arrangement of the elements to aid in the examination of the results. The first alternative model, identified as AM1, was 44 stories. The second alternative model, AM2, was only 16 stories; it was simplified to only feature the core. These two models are shown in Figure A. 17. It is noted that both models were created with rectangular plans in order to avoid repeated modes (ie. due to axial symmetry).

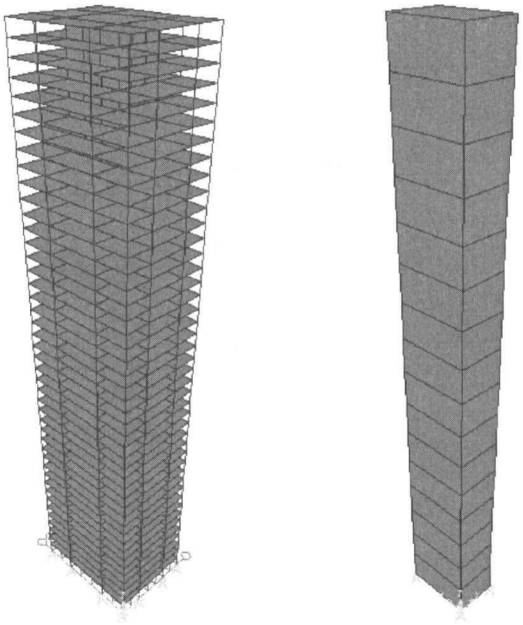

Figure A. 17: Alternative Models: AM1 and AM2

For the analysis in AM1, damage was simulated by disconnecting elements at the floor slabs to simulate cracks, rather than removing entire elements as before. This is desirable for creating more realistic damage scenarios. The damage was created at floors 15, 17 and 19. It was necessary to skip floors so that the disconnected elements were still connected at least at one end.

Similar to the analysis of the full 3D model, the damage detection focused only on the core elements. For the full 3D model analysis, only the 3D moving sensor set was used. For AM1, all three sensor set analysis types were applied to explore any advantages one of them may have. The results are shown in Figure A. 18 to Figure A. 21. Only two of the sets for each SDLV and PFM are shown for brevity. Also these figures show the element average values, not the floor average values as above. The damaged elements are indicated by a red arrow on the figure.

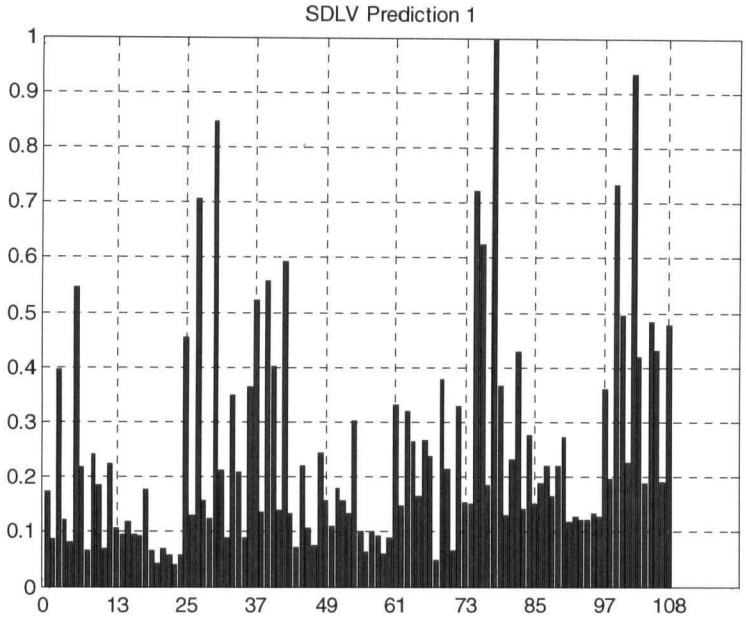

Figure A. 18: AM1, SDLV - 3D moving set #1 (Element averaging)

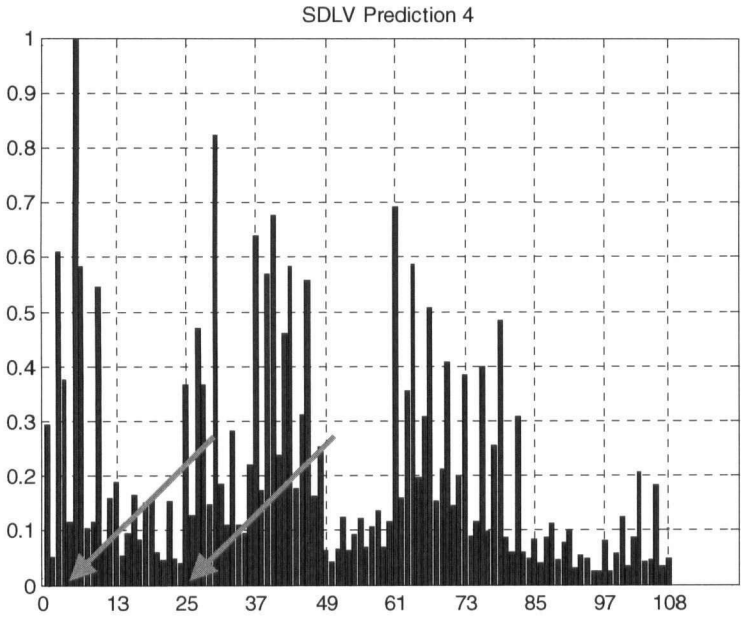

Figure A. 19: AM1. SDLV – 3D moving set #4 (Element averaging)

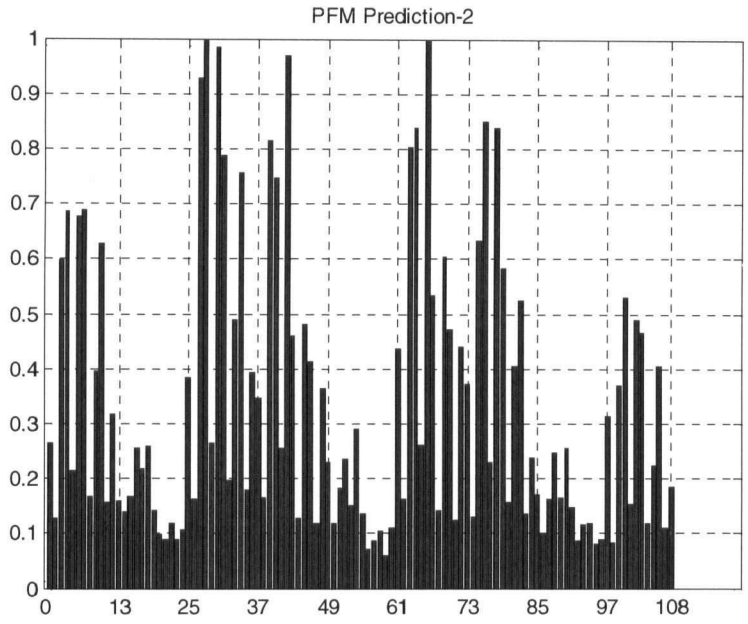

Figure A. 20: AM1, PFM – 3D moving set #2 (Element averaging)

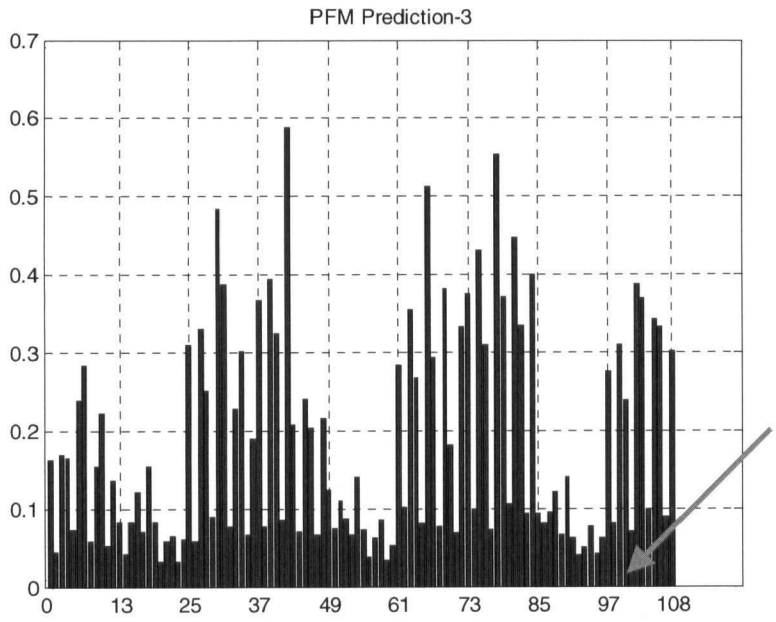

Figure A. 21: AM1, PFM – 3D moving set #3 (Element averaging)

It is seen from these figures that there is no clear indication of damage; instead a pattern appears with alterations of low/high stresses near the loading points.

Next the 3D distributed sensor set was used for the analysis. The results are shown in Figure A. 22 to Figure A. 25. For this analysis, only 4 sets of sensors were needed to cover the entire

building. Also note that for cases 2 and 3, there are no loads applied at the upper floors, and as a result there are no stresses there.

These results are the average stresses per floor. It is seen that again there is no clear indication of damage in any of the figures. Again only a selection of the results is shown for brevity.

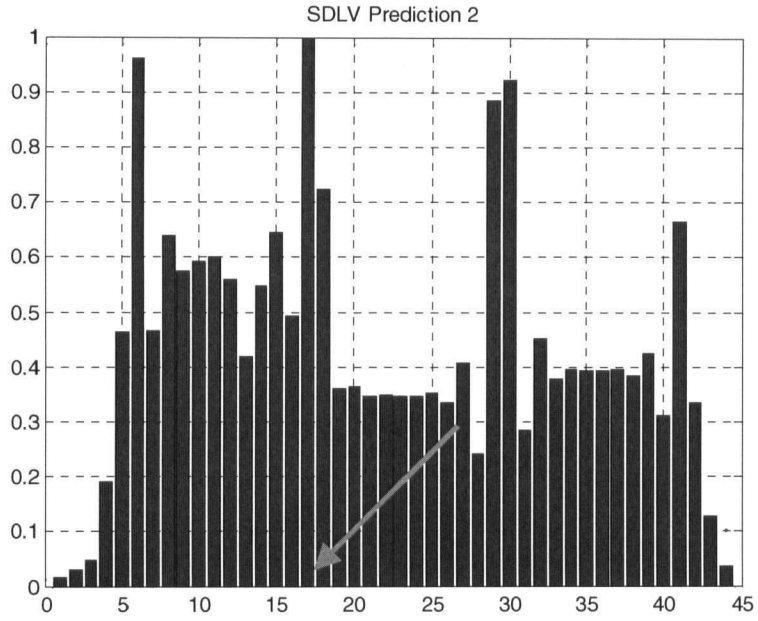

Figure A. 22: AM1, SDLV – 3D distributed set #2 (Floor averaging)

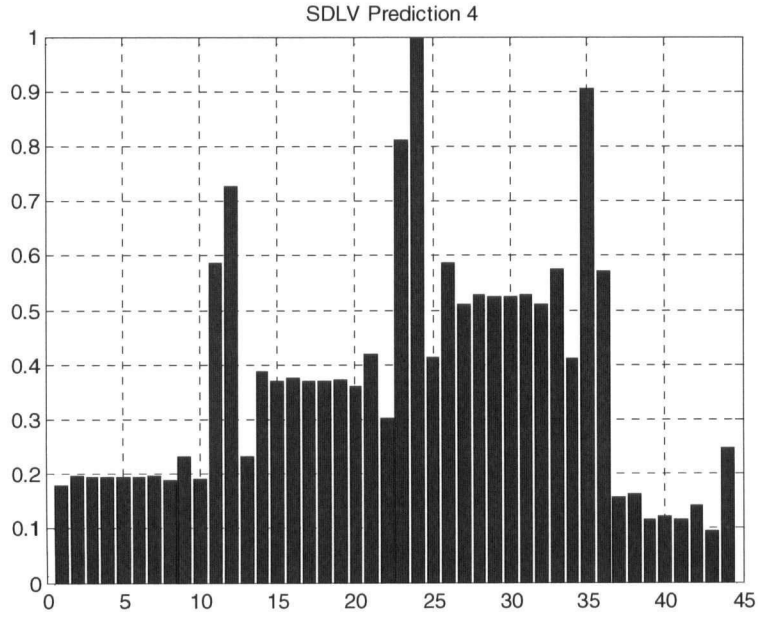

Figure A. 23: AM1, SDLV – 3D distributed set #4 (floor averaging)

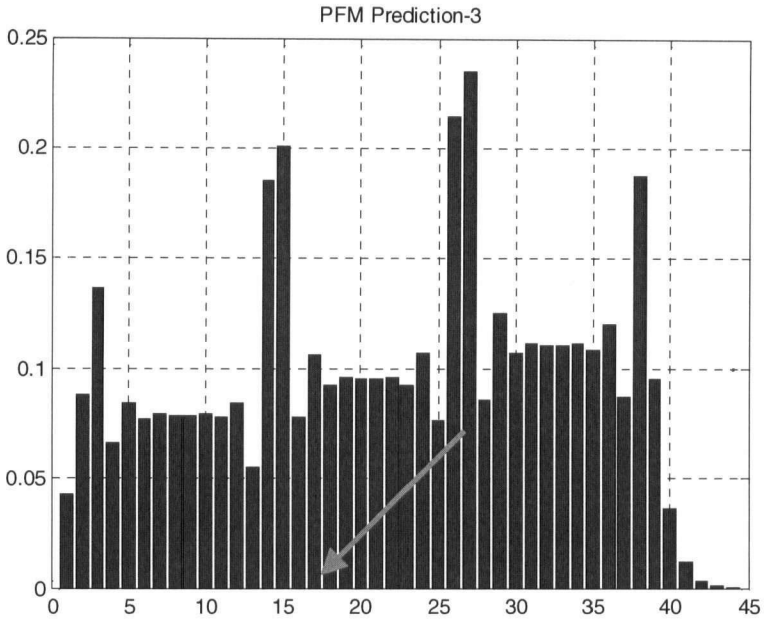

Figure A. 24: AM1, PFM – 3D distributed set #3 (floor averaging)

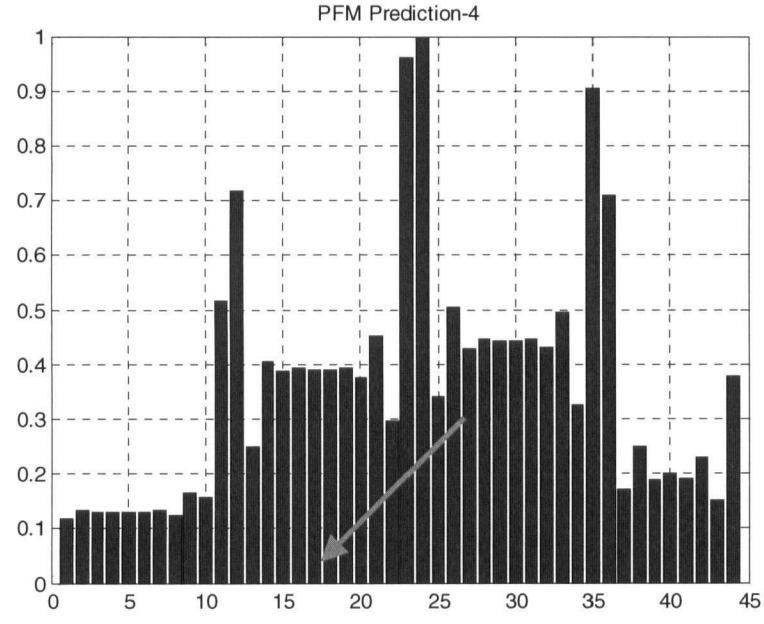

Figure A. 25: AM1, PFM – 3D distributed set #4 (floor averaging)

These results again showed no clear indication of the location of damage. Since the problem with the analysis could be due to the lack of detail based on not using the entire mode shape, the last analysis was done using the 2D distributed sensor set. Although the 3D nature of the modes is lost, a better comparison of the entire mode shape along the height of the building is available. For the analysis done here, 12 sensors are used in a vertical line, and repeated three

times as in Figure A. 12. The results of the three analyses are shown in Figure A. 26 to Figure A. 29.

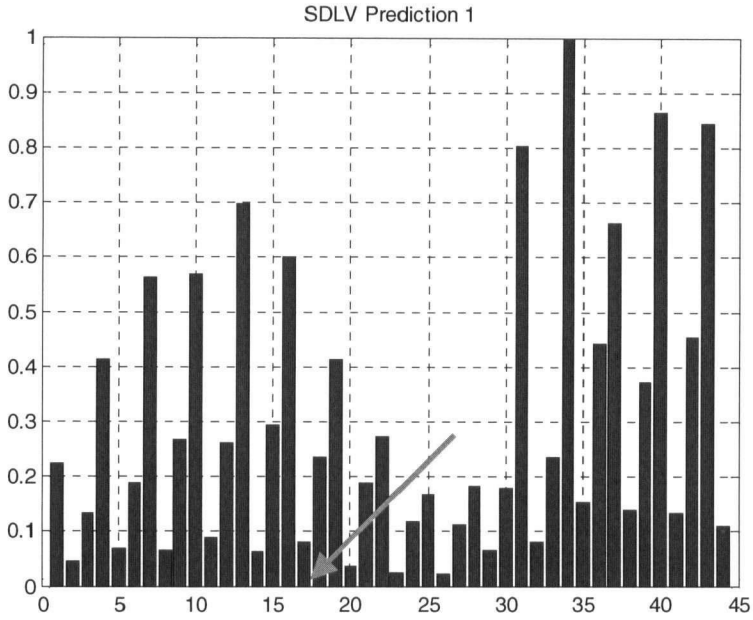

Figure A. 26: AM1, SDLV – 2D distributed set #1 (floor averaging)

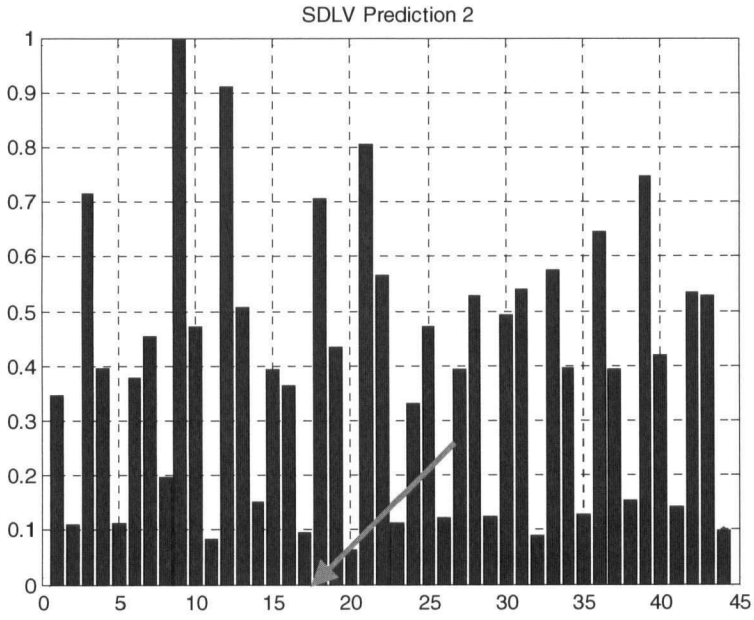

Figure A. 27: AM1, SLDV – 2D distributed set #2 (floor averaging)

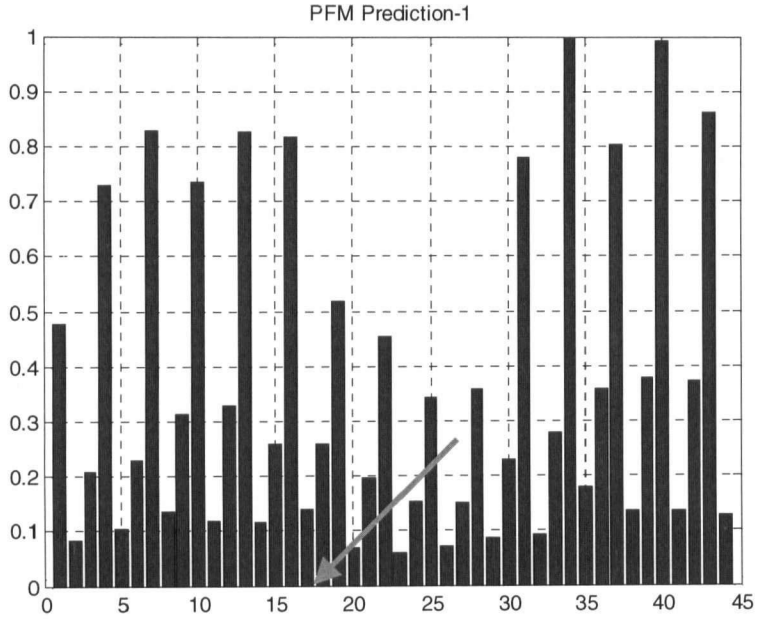

Figure A. 28: TB 2, PFM 2D distributed set #1 (floor averaging)

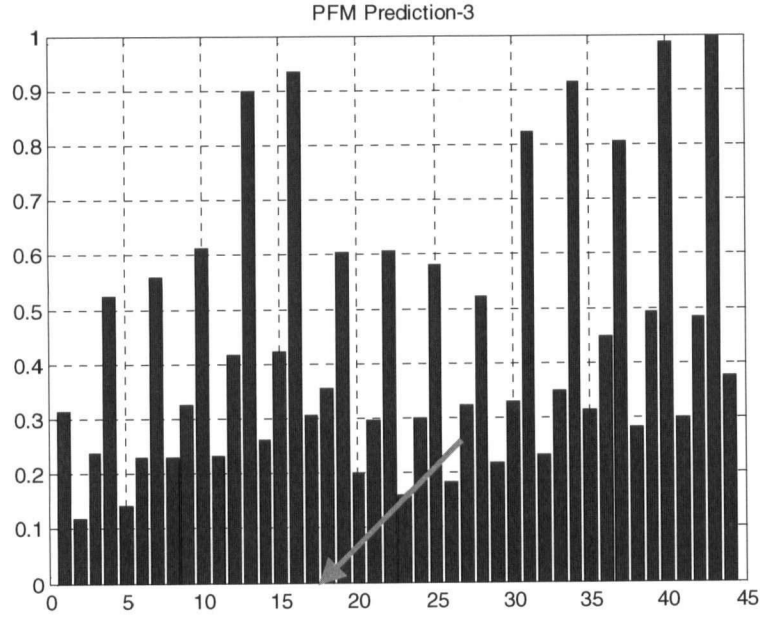

Figure A. 29: AM1, PFM – 2D distributed set #3 (floor averaging)

As with the previous analyses, there is still no clear indication of damage. There is also a distinct pattern appearing, with spikes in stress at the floors where the loads are applied. A study was then performed examining all of the possible stress orientations for each element, and a wide scatter of results was found. It was then decided that a simpler model would be useful to examine the effect of using different stress orientations on the results, and to set up the

method the best way when using area elements. The model AM2 was created, using only a single element on each face, and a single floor element. The model was limited to 16 stories. Damage was simulated by removing the negative-x element from the 7^{th} and 8^{th} floors. The results were similar (and not shown here), and no clear indication of damage was identified. A few representative stress diagrams are shown (Figure A. 30) in an attempt to examine the propagation of stress in the core.

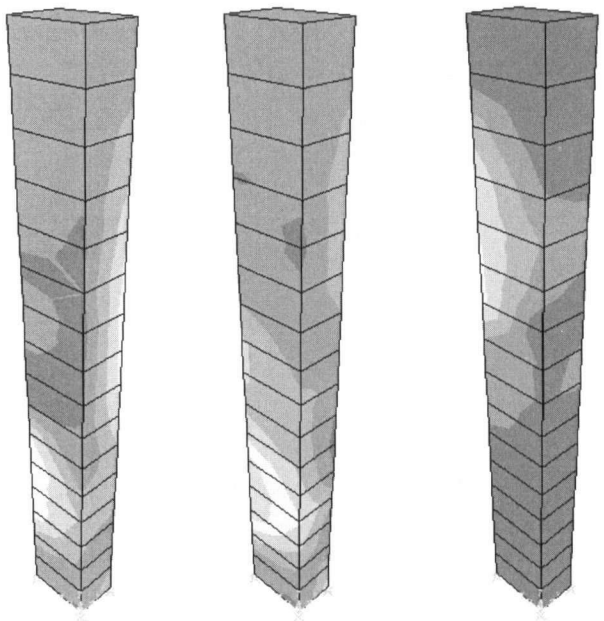

Figure A. 30: Stress diagrams (stress max average) for DLV cases 4, 14, 63

Three different area element outputs were examined for interpretation of the damage analysis:

1. element stresses
2. element forces
3. joint forces

For each of these three output types, there are many variations, such as shear, bending, axial stress; axial force and moments; and minimum/maximum forces. After examining all of the possibilities, no consistent results could be found. In comparison, the results from both the 2D Truss and the 3D Frame used simple beam elements, and the results were taken from the axial force only. This is easier to deal with from the point of view of stress/force normalization to find damage. One possible reason explored for the inconsistencies in the results, was in the propagation of stresses through the area elements. Figure A. 32 shows a stress diagram from a

floor in the AM1 model. It can be seen that the loads are applied at the outside of the perimeter (at the sensor locations) and then the stresses propagate towards the core. Since the analysis was interested in the core stresses only, this means that the loads are not applied directly at the location of interest, as they were with the 3D frame previously. Also, the stresses can propagate in three dimensions, meaning that there could be significant distortion of the DLV's before they reach the core (Figure A. 31).

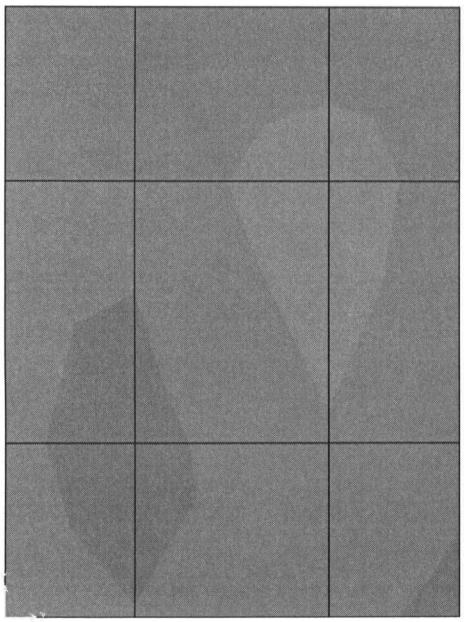

Figure A. 31: Example of floor stresses from AM1 analysis

To look at it another way, the DLV's are essentially computed from the modes and frequencies only; a mathematical representation of the structure based only on the measured dof's is created. If the model used for damage detection is significantly more complex than that simple representation, the results may be meaningless. For example, the DLV's are computed for points at the perimeter and by the time the loads propagate to the points of interest they have lost their meaning, which is to show where the locations of zero stress exist. To explore this idea, a new approach using an equivalent frame model rather than one using area elements is used. It is described in the next section.

A.1.9. Equivalent Frame Model for Damage Detection (EFMDD) Approach

The concept of the equivalent frame model for damage detection can best be described in two parts. First the idea of a 'damage detection model', which means that an equivalent simplified model (different than either the real structure or the model used for simulations) is created for

damage detection. This model will have a level of detail that is sufficient for the degree of damage desired, ie. the full model could find element level damage, whereas a model with a limited number of elements may only find damage in a floor. The second idea of an 'equivalent frame model' is that instead of using area or shell elements, create a simplified frame model, which is better suited for the DLV analysis. So the combined concept of the EFMDD approach is to use an equivalent frame model for the damage detection. In the example of AM2, the original model is still used for the simulations, while the frame model (Figure A. 32) is used for the DD only.

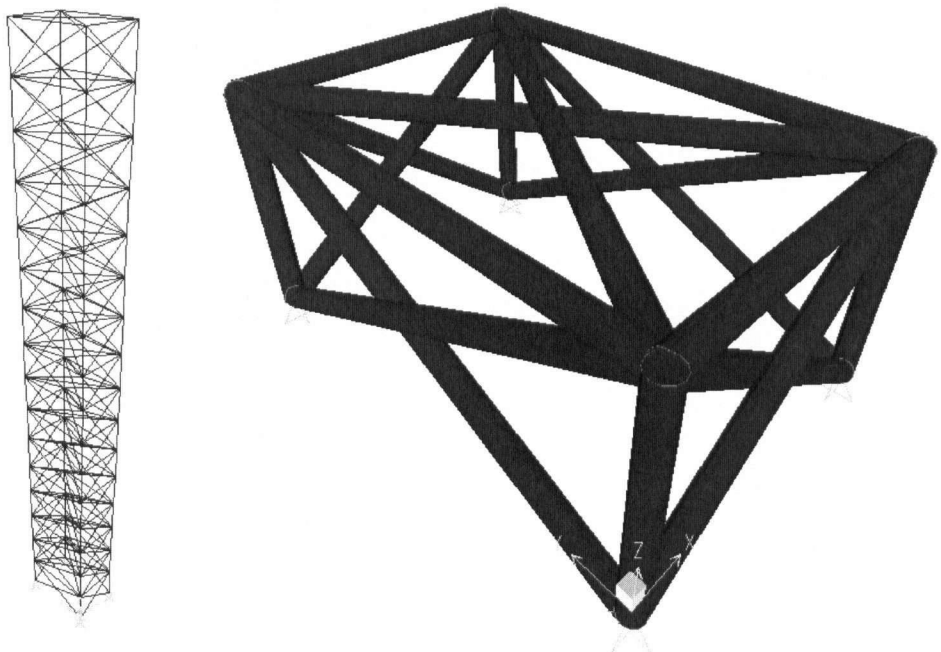

Figure A. 32: AM2 Frame Model and Single Floor Close-up

The frame model was created in FEMTools, by essentially framing each area element with a box and two diagonals. A closeup of a floor is also shown in the figure. An arbitrary circular cross-sectional area was chosen, and the model was updated using the modulus of elasticity as the parameter to change. As opposed to the updating procedure that has been described in this thesis where it is desired to maintain a realistic structural model throughout the updating, a black-box approach is used here (ie. the parameters are allowed to change freely). The updated modulus was 279000MPa, and the mode correlations are shown in Table A.5. These correlations are very good, with high MAC values and frequency differences less than 10%.

Table A. 5: Correlations with AM2 Frame Model

Mode	Frame Model [Hz]	Original Model [Hz]	Freq. Diff. [%]	MAC [%]
1	1.02	1.10	-6.94	100.0
2	1.56	1.46	6.16	100.0
3	5.93	6.20	-4.33	93.7
4	8.23	7.96	3.46	99.9
5	15.06	15.11	-0.35	99.6
6	19.35	19.09	1.34	99.3
7	26.35	25.71	2.49	99.1
8	31.71	31.91	-0.63	99.4

The model was then rebuilt in SAP2000 with the new E value, and the damage detection analysis was run. As before, only the lateral resisting elements are used in the final damage assessment. The results are shown in Figure A. 33 to Figure A. 36.

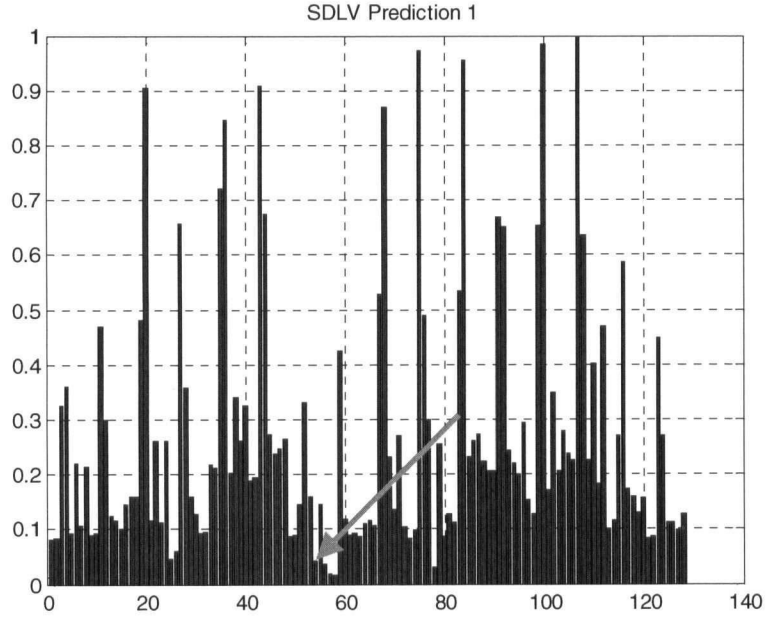

Figure A. 33: AM2 Frame Model, SDLV – 2D Distributed Set #1

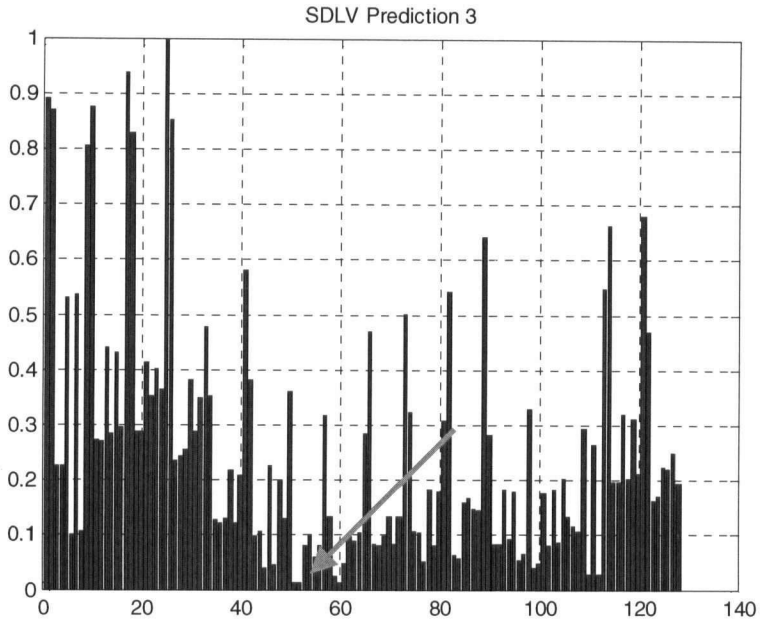

Figure A. 34: AM2 Frame Model, SDLV – 2D Distributed Set #3

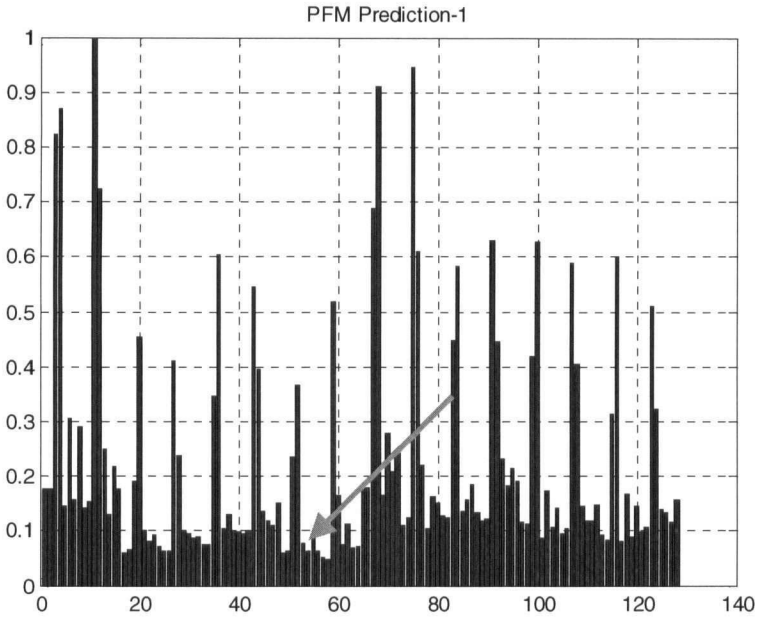

Figure A. 35: AM2 Frame Model, PFM – 2D distributed set #1

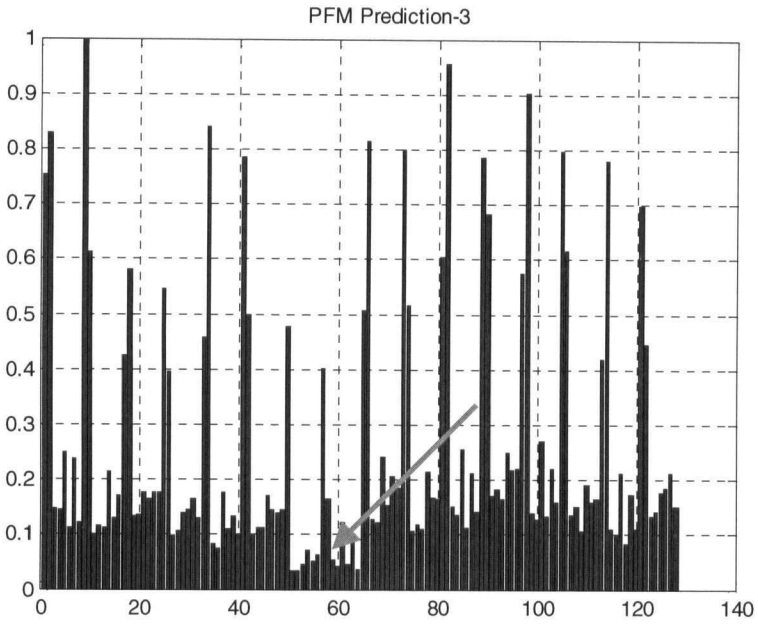

Figure A. 36: AM2 Frame Model, PFM – 2D distributed set #3

Although there are spikes of stress at each floor, these figures are beginning to indicate the correct location of damage. In both cases, the 2nd analysis (Y sensor set) does not indicate the damage and is not shown here, while the 1st and 3rd analyses, particularly the 3rd PFM, clearly indicate the 7th and 8th floors as being damaged. The Y sensor set likely does not indicate damage because the Y modes have not changed. These were positive results that showed that the EFMDD approach could provide better results than by using the original model with area elements. It is next applied to the Melville damage case described above.

A.1.10. Full 3D Model Second Analysis

The EFMDD approach was applied to the first damage case from the full 3D model of the Melville. The frame model as constructed is shown in Figure A. 37. For the FEMTools update, the frame elements were split into 22 groups, 1 for each direction, in sets of 4 floors. The correlations are shown in Table A. 6.

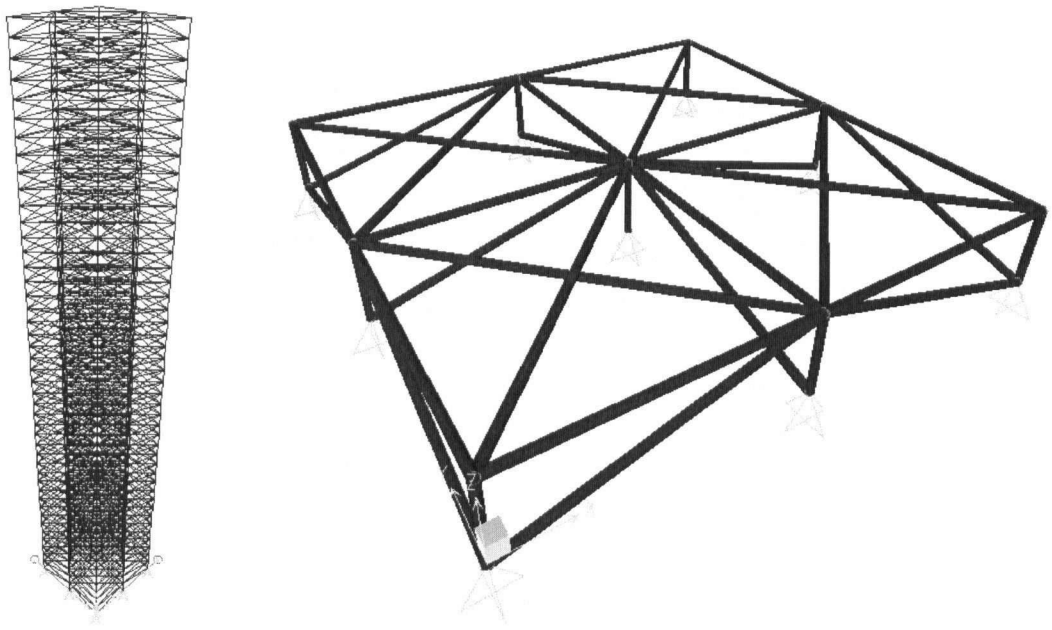

Figure A. 37: Melville Frame Model and Close-up of one floor

Table A. 6: Correlations of Melville Frame Model to Melville full 3D model

Mode	Frame Model [Hz]	Full 3D Model [Hz]	Freq. Diff. [%]	MAC [%]
1	0.27	0.27	0.17	99.0
2	0.28	0.30	-8.34	92.6
3	0.82	0.75	9.08	92.0
4	1.30	1.36	-4.49	93.9
5	1.37	1.52	-10.36	92.9
6	2.42	2.39	1.17	90.3
7	2.86	3.16	-9.53	81.1
8	3.05	3.60	-15.28	87.4
9	4.02	4.12	-2.36	77.4
10	4.48	5.18	-13.48	64.9
11	4.82	6.20	-22.24	61.3

The correlations for the full model were not as good as with the simple model (AM2), however in the case of AM2 both the full model and the frame model shared the exact same geometry. For the Melville case, the geometries varied significantly and this is a better illustration of how the EFMDD approach is supposed to work. The results of the damage detection analysis are shown in Figure A. 38 to Figure A. 43. For this analysis, the axial forces are averaged per floor.

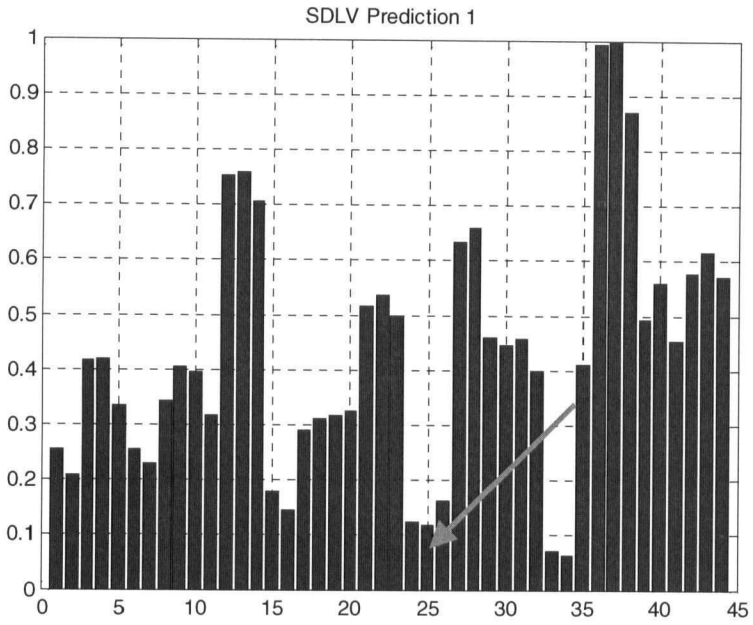

Figure A. 38: Melville Frame Model, SDLV – 2D distributed set #1

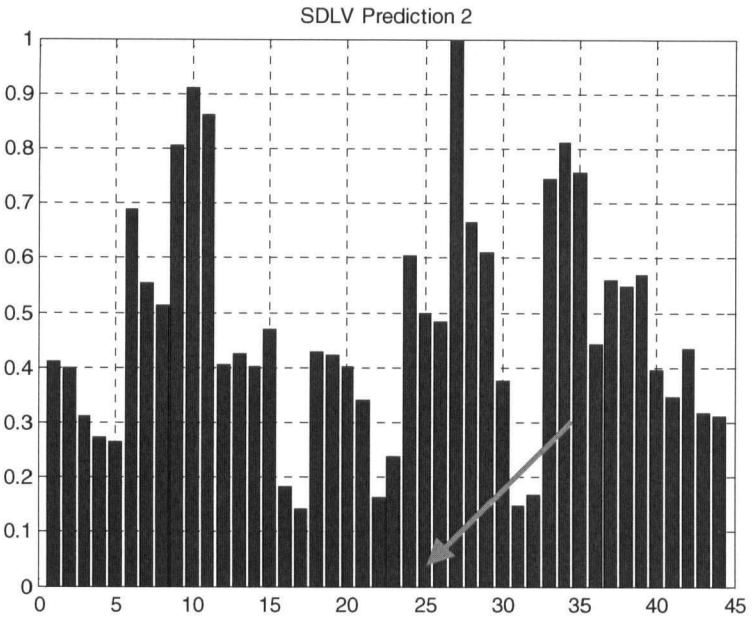

Figure A. 39: Melville Frame Model, SDLV – 2D distributed set #2

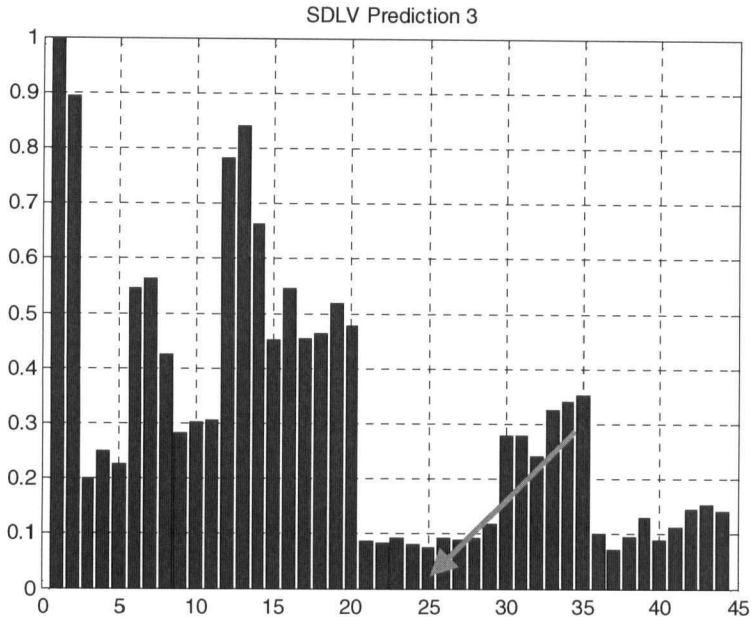

Figure A. 40: Melville Frame Model, SDLV – 2D distributed set #3

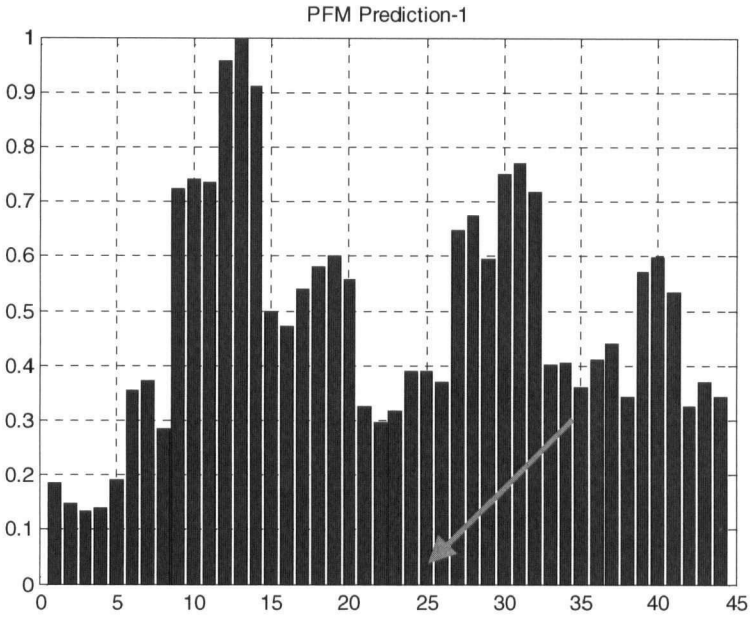

Figure A. 41: Melville Frame Model, PFM – 2D distributed set #1

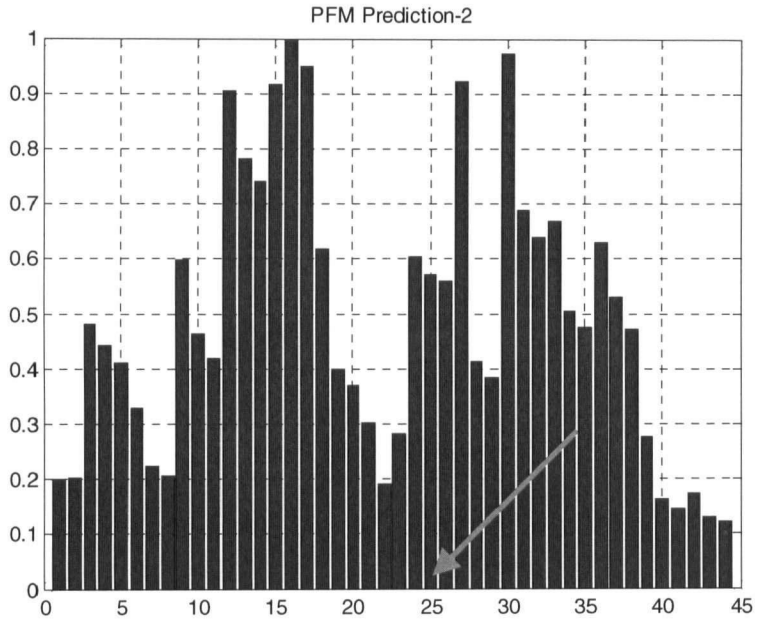

Figure A. 42: Melville Frame Model, PFM – 2D distributed set #2

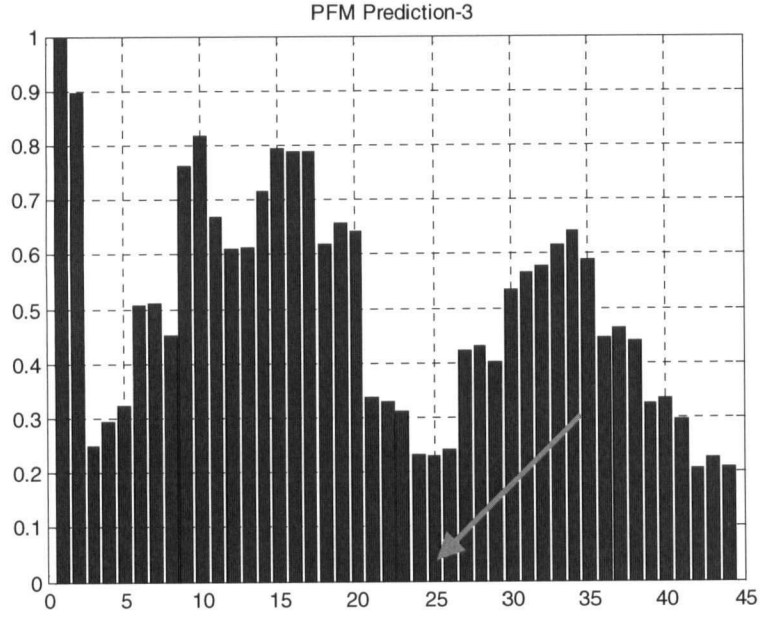

Figure A. 43: Melville Frame Model, PFM – 2D distributed set #3

From these results, the damage is being indicated as around the 25th floor. In particular the results from the 1st and 2nd SDLV analysis show the damage clearly. The DDM is unable to find damage closer than 1 or 2 stories, however in a relative sense this case has a small amount of damage. One possible reason is that the damage location is sensitive to the correlation between the frame model and the simulated data; the less correlated they are the less the DDM can find

damage. Also it is noted that for these results the damage threshold of 0.1 does not really apply due to the averaging of the elements on a single floor.

A.1.11. Melville Additional Damage Cases

It is seen from the results above that there is indication of success however in general they are inconclusive. To further examine the performance of the DDM using the EFMDD approach, additional damage cases were created; these are shown in Table A.7. For these results, all of the plots in Figure A. 48 to Figure A. 53 show floor averaging. Only a few representative results are shown, considering some with reasonable results, and some with poor or incorrect results.

Table A. 7: Melville Additional Damage Cases

Case	Damaged Members
M2	F11-W305; F31 W309
M3	F10-W302, 310; F17-W303; F40-W303
M4	F6-W304; F7-W302
M5	F5-W305,C55,C82,C119; F6-W309,W345,W383,W401,C55,C60
M6	F39-W304,C69,C82,C119; F41-W309,W345,W383,W401,C60,C116
M7	No damage
M8	No damage
M9	No damage

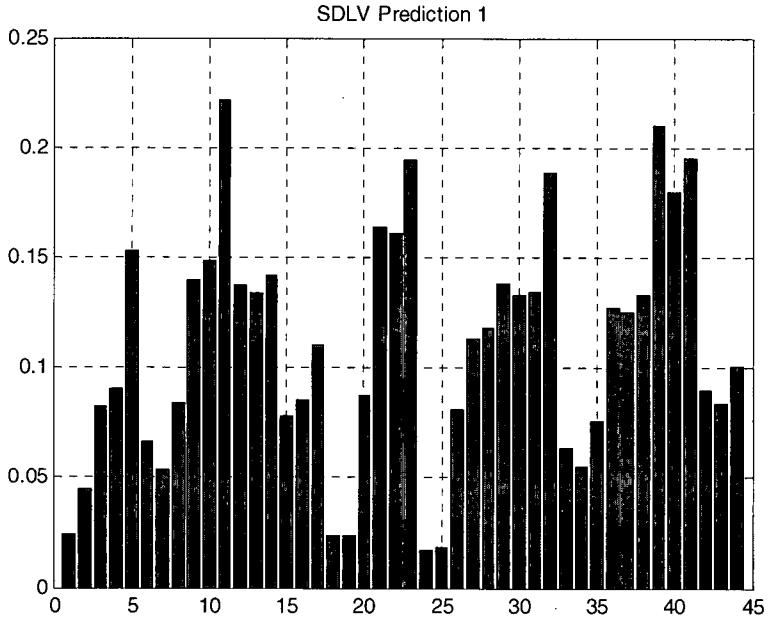

Figure A. 44: Damage case M2, SDLV Prediction 2D Distr. Set 1

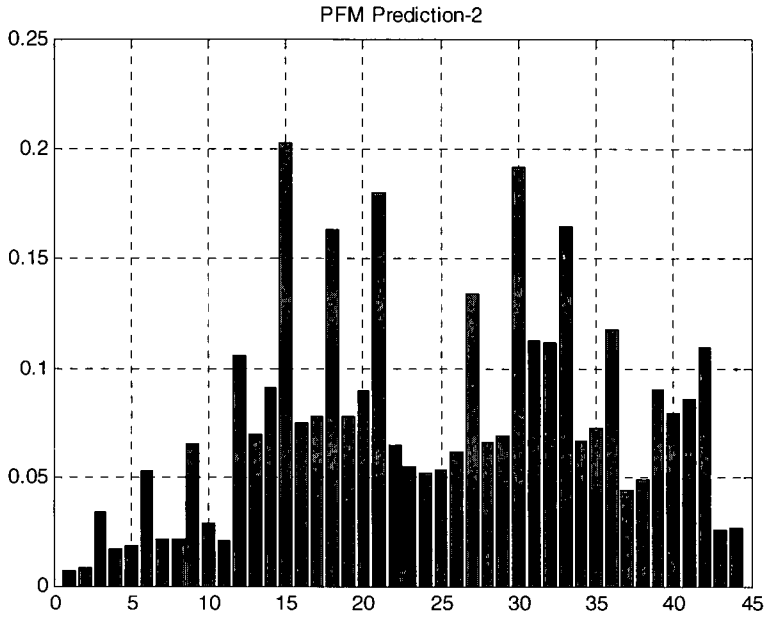

Figure A. 45: Damage Case M2, PFM Prediction 2D Distr.Set 2

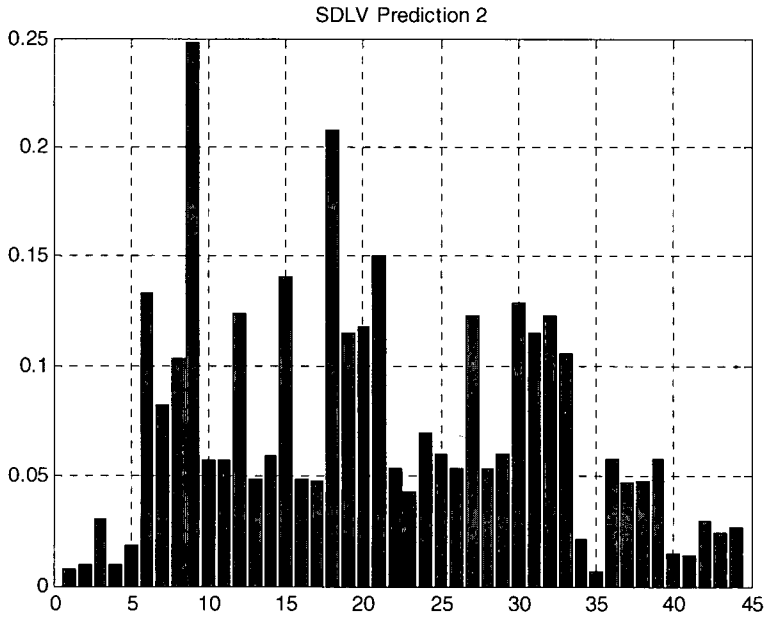

Figure A. 46: Damage Case M3, SDLV Prediction 2D Distr. Set 2

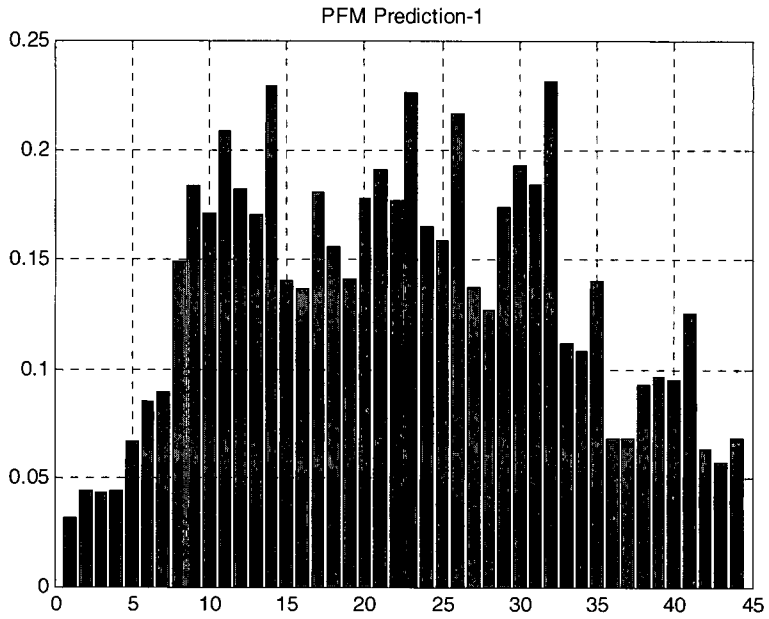

Figure A. 47: Damage Case M3, PFM Prediction 2D Distr. Set 1

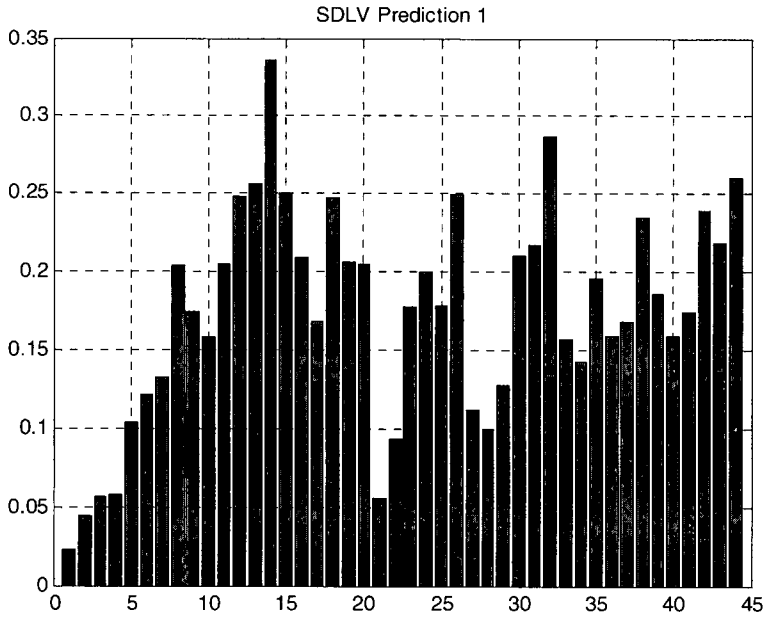

Figure A. 48: Damage Case M4, SDLV Prediction 2D Distr. Set 1

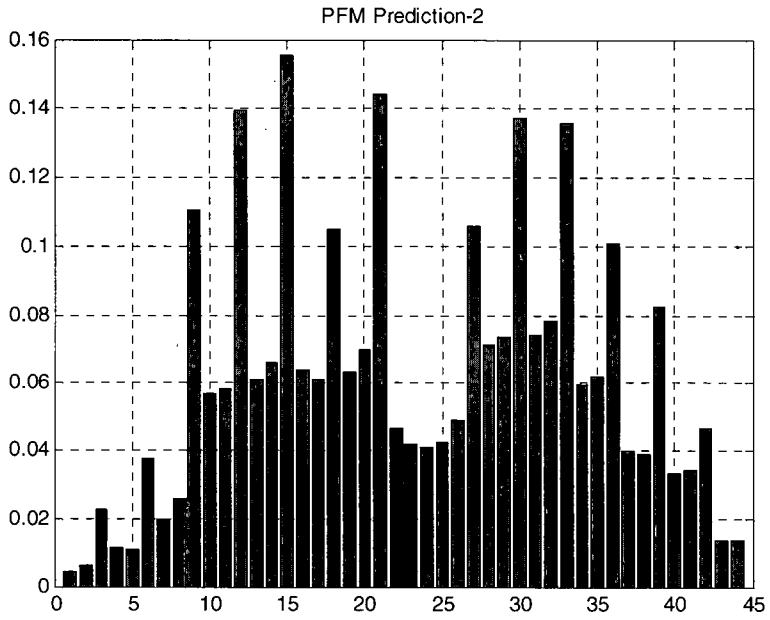

Figure A. 49: Damage Case M4, PFM Prediction 2D Distr. Set 2

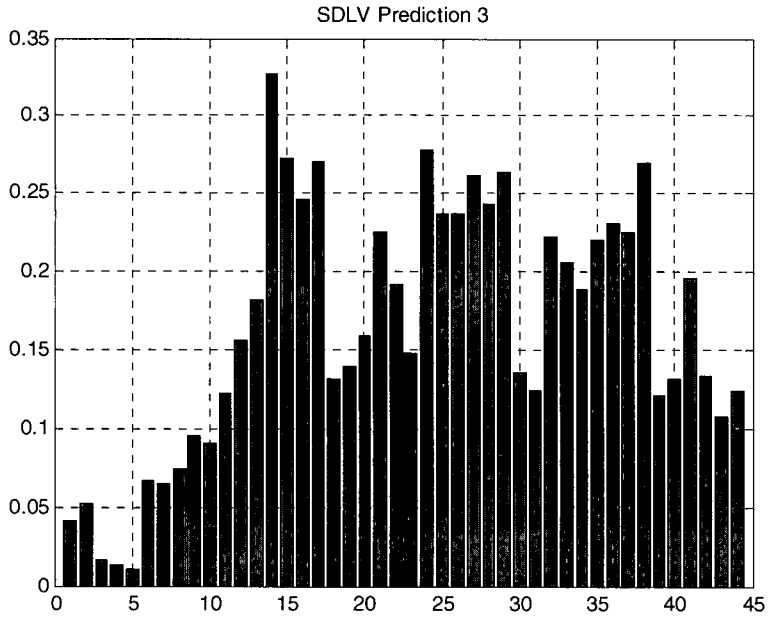

Figure A. 50: Damage Case M5, SDLV Prediction 2D Distr. Set 3

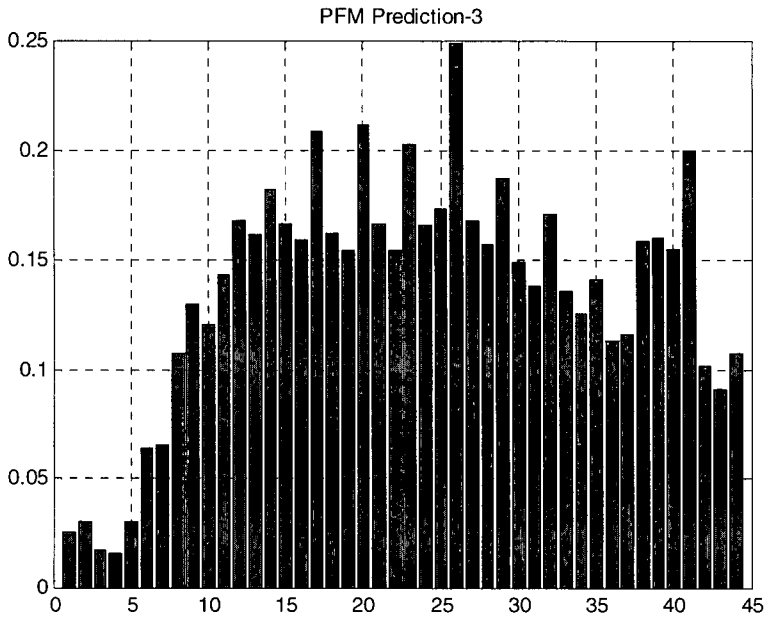

Figure A. 51: Damage Case M5, PFM Prediction 2D Distr. Set 3

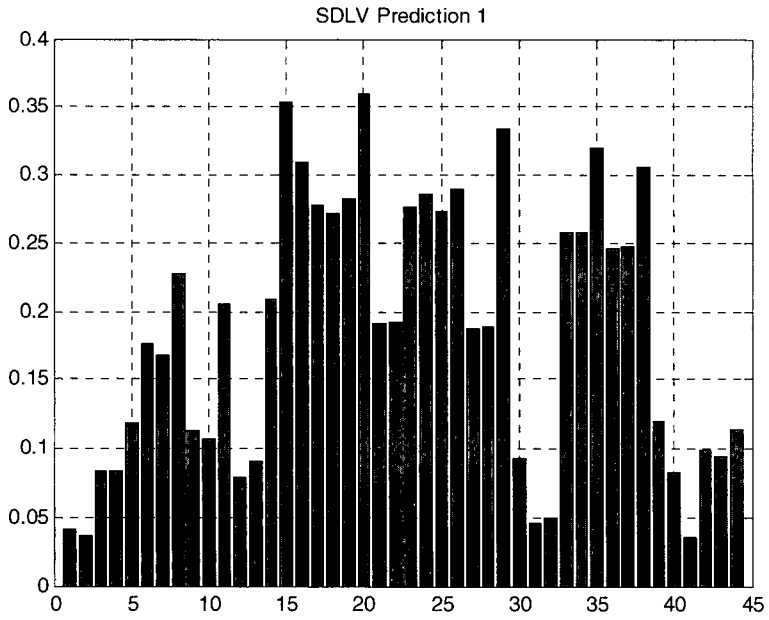

Figure A. 52: Damage Case M9, SDLV Prediction 2D Distr. Set 1

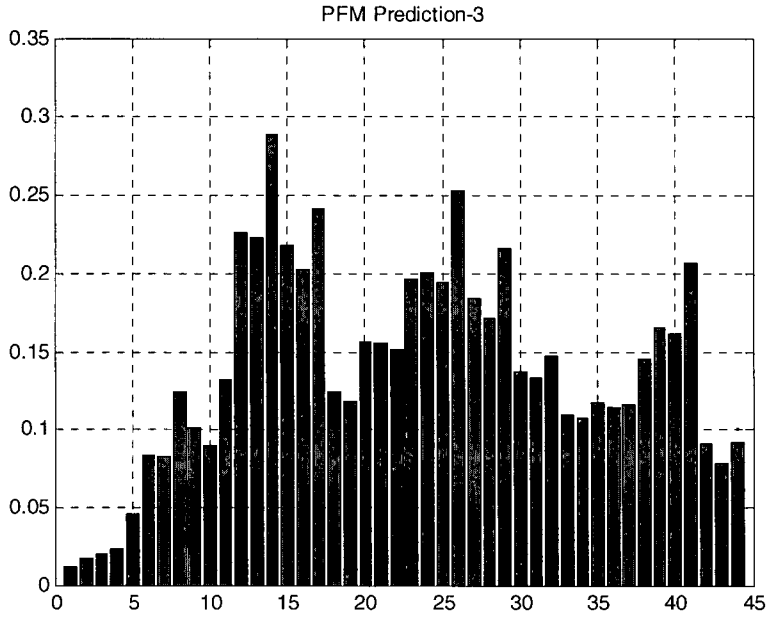

Figure A. 53: Damage Case M9, PFM Prediction 2D Distr. Set 3

From the results presented above, several points can be made:

1. The results are generally very inconsistent
2. Certain floors, such as the lower ones, tend to have a lower force in all cases
3. The threshold level of 0.1 may not be generally applicable; these plots vary because they contain average of normalized values. Renormalization does not always work in the favor of the correct results.

From a subjective examination of these plots, only a few cases can be suggested to be predicting the damage. From those cases it can be taken that the DLV technique should work, however the interpretation of the results is critical. The two main things that need to be explored further are the sensor layout, and a potential weighting of the elements. Due to the complexity of the Melville structure and its models, it is not reasonable to explore these issues using these models. Therefore it will be better to move on to a simpler example to continue the development of the DDM.

A.2. Heritage Court Tower

The second case study chosen for continued development of the DDM is the Heritage Court Tower. The two main reasons for choosing this structure are that it:

1. Is smaller than the Melville (15 Stories)
2. Has a rectangular plan (vs. the oblong shape of the Melville).

These two features should make it easier to detect issues with the DDM; in addition the total analysis time will be reduced. As for the building itself, it is a reinforced-concrete shear core building, similar to the Melville in construction.

The Heritage Court Tower (HCT) is located in downtown Vancouver, Canada. It is a relatively regular 15-story reinforced concrete shear core building. In plan, the building is essentially rectangular in shape with only small projections and setbacks. Typical floor dimensions of the upper floors are about 25 m by 31 m, while the dimensions of the lower three levels are about 36 m by 30 m. The footprint of the building below ground level is about 42 m by 36 m. Typical story heights are 2.70 m, while the first story height is 4.70 m. The elevator and stairs are concentrated at the center core of the building and form the main lateral resisting elements against potential wind and seismic lateral and torsional forces.

The tower structure sits on top of four levels of reinforced concrete underground parking. The parking structure extends approximately 14 meters beyond the tower in the south direction forming an L-shaped podium. The parking structure and first floors of the tower are basically flush on the remaining three sides. The parking structure extends approximately 14 m beyond the tower in the south direction but is essentially flush with the first floor walls on the remaining three sides. The building tower is stocky in elevation having a height to width aspect ratio of approximately 1.7 in the east-west direction and 1.3 in the north-south direction. A photo of the building is shown in Figure A. 54.

Figure A. 54: View of HCT building

A.2.1. HCT Ambient Vibration Testing

A series of ambient vibration tests was conducted in 1998 by researchers from the University of British Columbia to obtain modal characteristics of this building. It was of practical interest to test this building because of its shear core, which concentrates most of lateral and torsional resisting elements at the center core of the building. The dynamic characteristics of interest for this study were the first few lateral and torsional natural frequencies and the corresponding mode shapes. The degree of torsional coupling between the modes was also investigated. The modal identification for the HCT building was performed using computer program ARTeMIS Extractor. The results are shown in Table A. 8. Figure A. 55 and Figure A. 56 show the mode shapes. More than six modes were actually identified, but these are the ones that are used for the updating.

Table A. 8: HCT Ambient Vibration Results

Mode	Description	Freq [Hz]	Damping [%]
1	1st N/S	1.23	2.12
2	1st Torsion	1.27	1.77
3	1st E/W	1.44	1.20
4	2nd Torsion	3.87	1.16
5	2nd N/S	4.25	1.52
6	2nd E/W	5.35	1.69

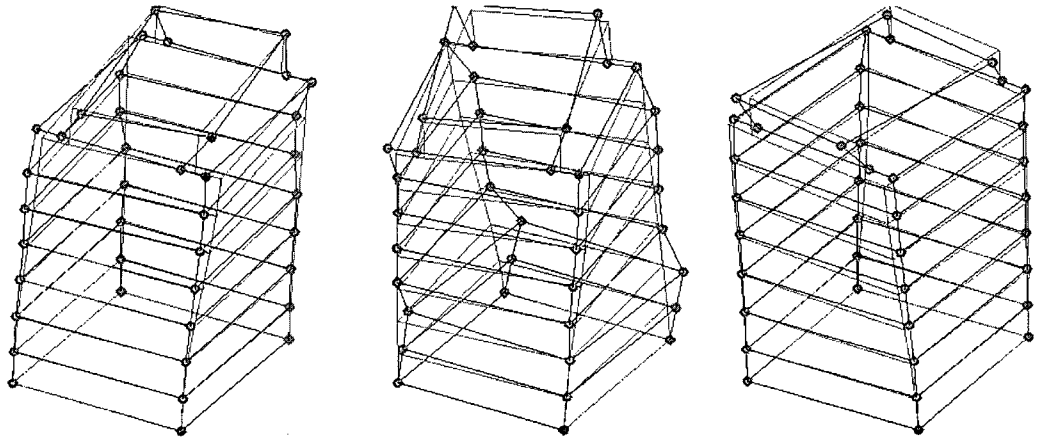

Figure A. 55: HCT Experimental Modes 1 to 3

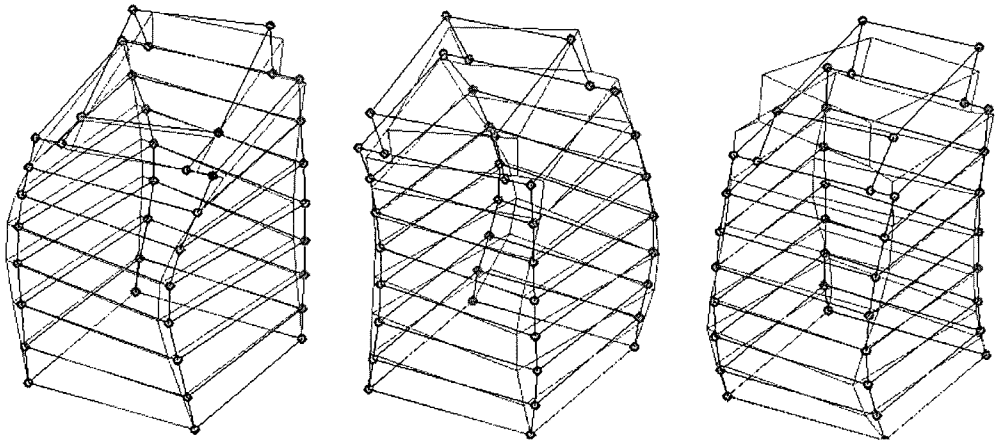

Figure A. 56: HCT Experimental Modes 4 to 6

A.2.2. HCT FEM and Model Updating

A finite element of the HCT was created using the FEMTools software. This model was used for the automated updating. The model used area elements for the floor, shear core and cladding. Frame elements were used for the columns. It is shown in Figure A. 57.

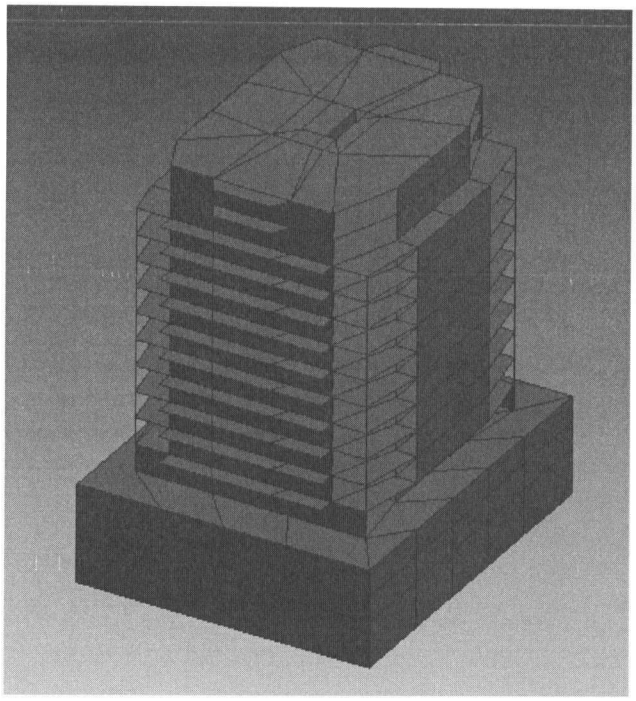

Figure A. 57: HCT Finite Element Model (FEMTools)

For the model updating, the parameters that were chosen were the modulus of elasticity of all elements, the mass density of all elements, the moment of inertias of the frame elements and the thickness of the area elements. For each case, sets of elements were established based on whether it represented walls, cladding, columns, beams, etc. A total of 15 sets were created. The results of the updating are shown in Table A. 9, and the parameter changes are shown in Table A. 10. This was more of a black-box updating than that of the 3D frame; hence there are some drastic changes in properties. This type of an updating is typically justified as having elements and parameters that are representative; ie. modulus of elasticity can be considered a 'stiffness' parameter that accounts for more than just the material property that it signifies. Therefore some of the results are unrealistic for real properties, however the global dynamic behaviour of the structure is more realistic.

Table A. 9: HCT FEM Updated Correlations

#	FEA	Hz	EMA	Hz	Diff. [%]	MAC [%]
1	1	1.24	1	1.23	0.52	80.3
2	2	1.34	2	1.29	3.73	85.7
3	3	1.58	3	1.45	8.94	85.1
4	4	3.99	4	3.86	3.38	89.6
5	5	4.39	5	4.26	3.05	85.0
6	6	5.38	6	5.36	0.41	86.4

Table A. 10: Parameter Changes

#	Level	Type	Old	Actual	Difference
1	Global	E	2.5000E+010	1.4115E+010	-4.3541E+001
2	Global	E	2.5000E+010	4.9606E+010	9.8422E+001
3	Global	E	3.0000E+011	3.2061E+011	6.8694E+000
4	Global	E	2.5000E+010	1.5317E+010	-3.8730E+001
5	Global	E	3.0000E+010	3.0983E+009	-8.9672E+001
6	Global	RHO	2.4000E+003	7.2000E+003	2.0000E+002
7	Global	RHO	2.4000E+003	7.0421E+003	1.9342E+002
8	Global	RHO	3.0000E+003	2.0462E+003	-3.1794E+001
9	Global	RHO	2.4000E+003	1.9200E+003	-2.0000E+001
10	Global	RHO	3.0000E+003	4.6890E+003	5.6300E+001
11	Global	IY	7.3660E-004	4.4196E-003	5.0000E+002
12	Global	IY	7.3170E-003	4.4073E-003	-3.9767E+001
13	Global	IZ	7.3660E-004	3.6830E-004	-5.0000E+001
14	Global	IZ	5.8330E-003	3.4786E-002	4.9637E+002
15	Global	H	2.0000E-002	2.0251E-003	-8.9874E+001

A.2.3. HCT Simulations

The updated model was then recreated in SAP2000 using the properties from the FEMTools model. As per the previous cases, simulations were performed with the CDS method. Similar to the Melville results, the addition of noise in the suggested manner was not needed. A spectrum from the undamaged case is shown in Figure A. 58. This plot includes the measured ground motion input combined with white noise only.

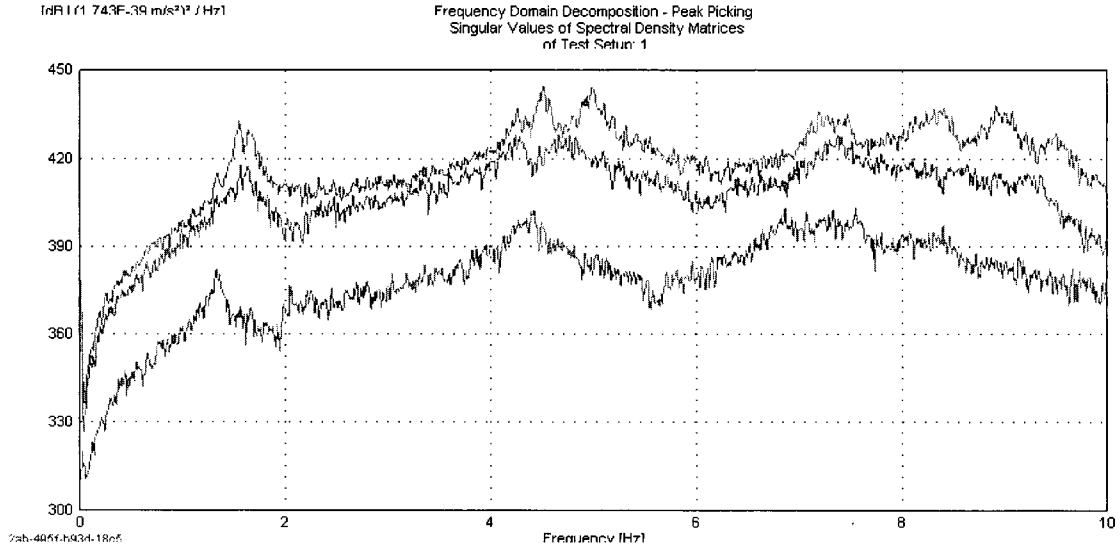

Figure A. 58: Spectrum from the HCT Simulation, Undamaged Case

Several damage cases were simulated using the model. Initially, 9 sensors were used with 6 modes. This was taken as 3 sensors per floor over 3 floors in the building. As the analysis progressed, more sensors were used, first 18, then 48 (this will be explained later). These are shown in parentheses in Table A. 11. The table denotes the damage location, as well as the frequencies in each case.

Table A. 11: HCT Damage Cases

Case	Members	Freq 1 [Hz]	Freq 2 [Hz]	Freq 3 [Hz]	Freq 4 [Hz]	Freq 5 [Hz]	Freq 6 [Hz]
1 (9)	Cladding South Face Floor 5,6	1.3047	1.4294	1.6131	4.1519	4.4583	5.1567
2 (9)	Core South face Floor 6,7,8	1.2574	1.3614	1.6009	4.0078	4.1328	5.0744
3 (9)	Core West Side Fl. 12,13,14	1.3043	1.4288	1.6177	4.0122	4.3582	5.1363
4 (18)	Core North face Floor 1,2	1.2654	1.4163	1.5733	4.0784	4.4022	4.9869
5 (48)	Core North face Floor 2,3,4	1.2650	1.4016	1.5636	4.0840	4.4383	5.0033
6 (48)	Core North face Fl. 10,11,12	1.3068	1.4233	1.6074	4.0159	4.3808	5.1065

A.2.4. HCT Damage Detection

The EFMDD approach was applied to the HCT datasets. This first requires creation of the equivalent frame model; it is shown in Figure A. 59. The first model updating of the frame used 43 parameter sets, updating the values of E in each. A total of 58 iterations were performed, with a CC criteria limit of 0.001 for each iteration. A second updating was performed with the same parameter sets, this time using the Ax and rho values for each. Only 9 iterations were used.

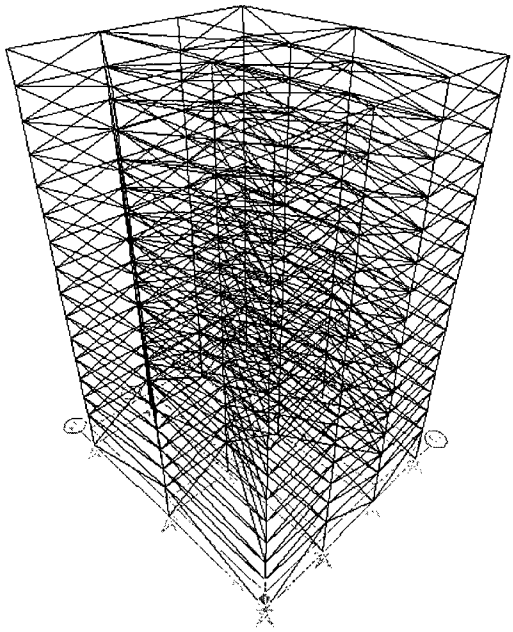

Figure A. 59: HCT Frame Model

For the updating of the frame model for the HCT, it was necessary to create more parameter zones than in the Melville, which essentially only divided the building up into x and y directions. This was done in order to properly update the modal order, which has the torsional mode second, and shows torsional coupling in both translational modes. This would not be possible to model if all of the elements in one direction of the frame were forced to have the same properties.

Table A. 12 to Table A. 14 show the updating process in three steps, from the initial correlations to the final values. The final correlations have a good frequency match, but lower MAC correlations (mainly in the first few modes).

Table A. 12: HCT Pre-Updating Correlations

#	FEA	Hz	EMA	Hz	Diff.	MAC
1	1	2.63	1	1.32	99.33	85.7
2	2	2.86	3	1.61	77.75	91.5
3	3	4.23	2	1.44	194.62	71.0
4	5	8.03	6	5.21	54.01	96.6
5	6	8.37	5	4.49	86.40	93.8
6	7	12.71	4	4.18	204.00	67.3

Table A. 13: HCT First Update (E only)

#	FEA	Hz	EMA	Hz	Diff.	MAC
1	1	1.33	1	1.32	0.71	86.5
2	2	1.54	3	1.61	-4.70	88.2
3	3	1.65	2	1.44	15.15	69.5
4	5	4.24	5	4.49	-5.58	94.6
5	6	4.49	6	5.21	-13.83	94.9
6	7	4.95	4	4.18	18.49	69.6

Table A. 14: HCT Second Updating (Ax and rho)

#	FEA	Hz	EMA	Hz	Diff.	MAC
1	1	1.34	1	1.32	1.85	68.3
2	2	1.42	2	1.44	-1.13	54.3
3	3	1.61	3	1.61	0.08	98.2
4	4	4.22	4	4.18	0.92	86.7
5	5	4.46	5	4.49	-0.61	78.2
6	6	5.17	6	5.21	-0.95	96.6

Figure A. 60 to Figure A. 73 shows the results of the damage detection analyses on the HCT datasets. In these analyses, a single 3D distributed set is used, starting with 9 sensors. The intention of the analysis is to find out why the results of the DDM when applied to the 3D frame are successful, but not when expanded to a larger structure. The first important discovery that was made during this analysis was that a larger sensor set could be used. Therefore the results were then expanded to sensor sets of 18 and 48. The reason for this expansion is explained at the beginning of the next section. For each case, the results of the PFM and SDLV prediction are presented.

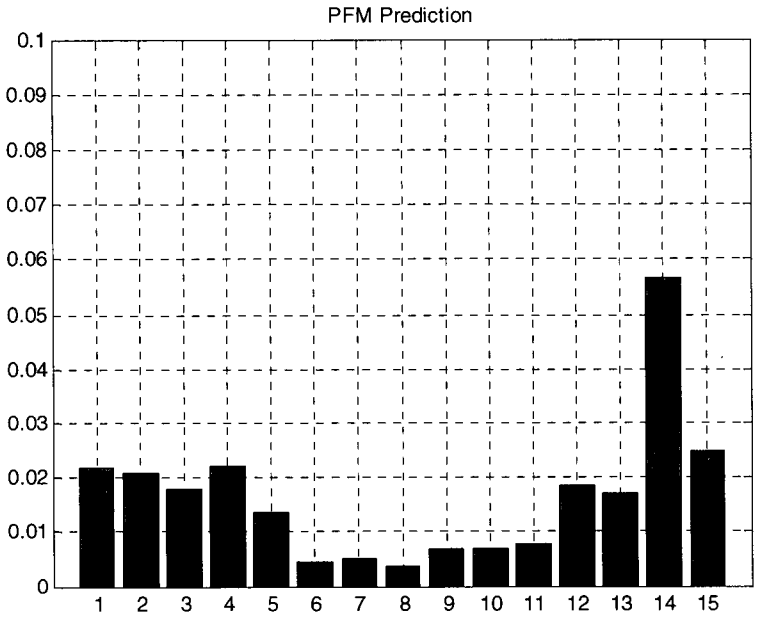

Figure A. 60: HCT Damage Case 1, PFM Prediction, 9 Sensors

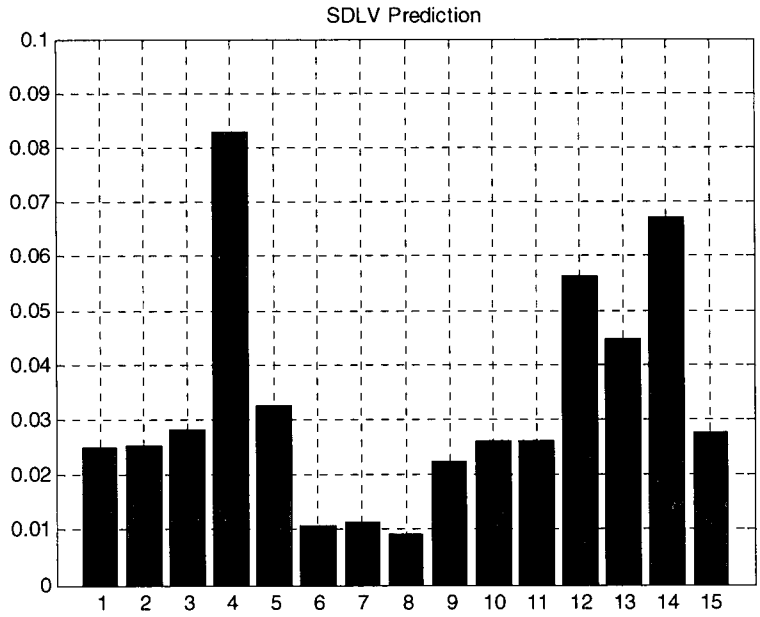

Figure A. 61: HCT Damage Case 1, SLDV Prediction, 9 Sensors

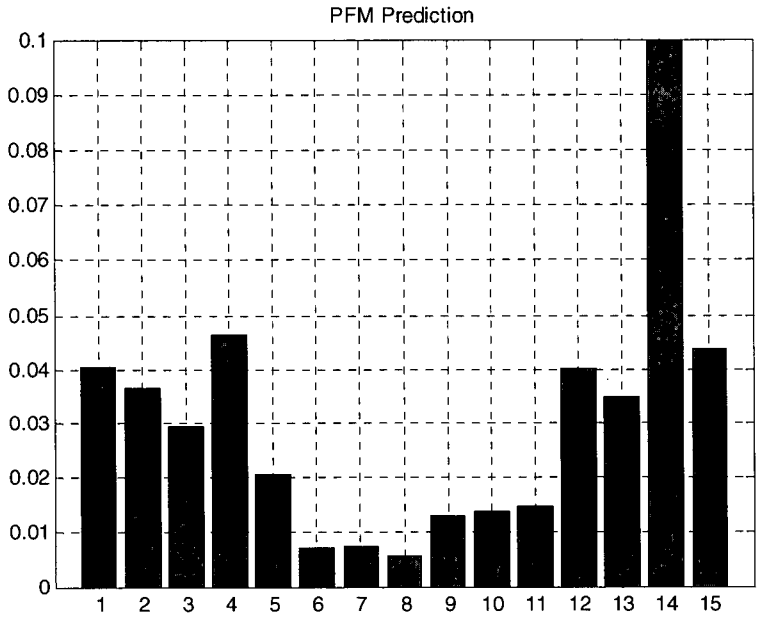

Figure A. 62: HCT Damage Case 2, PFM Prediction, 9 Sensors

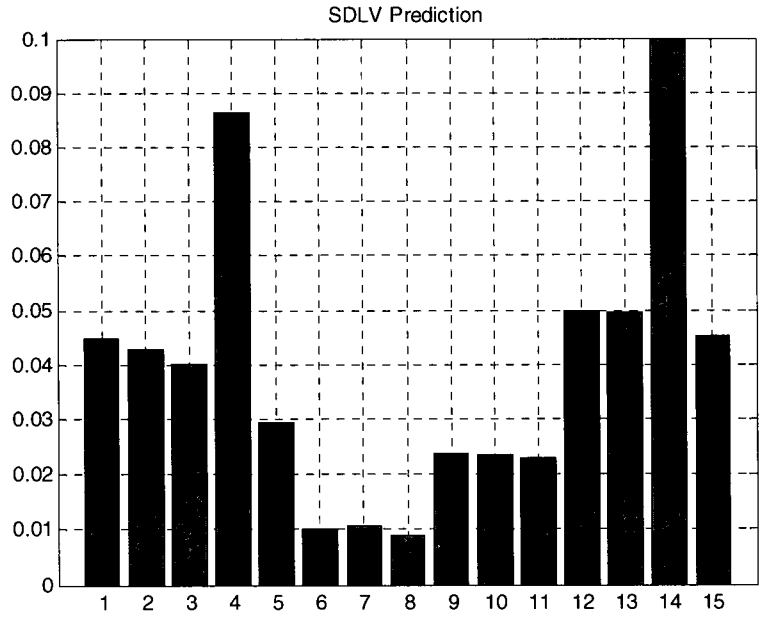

Figure A. 63: HCT Damage Case 2, SDLV Prediction, 9 Sensors

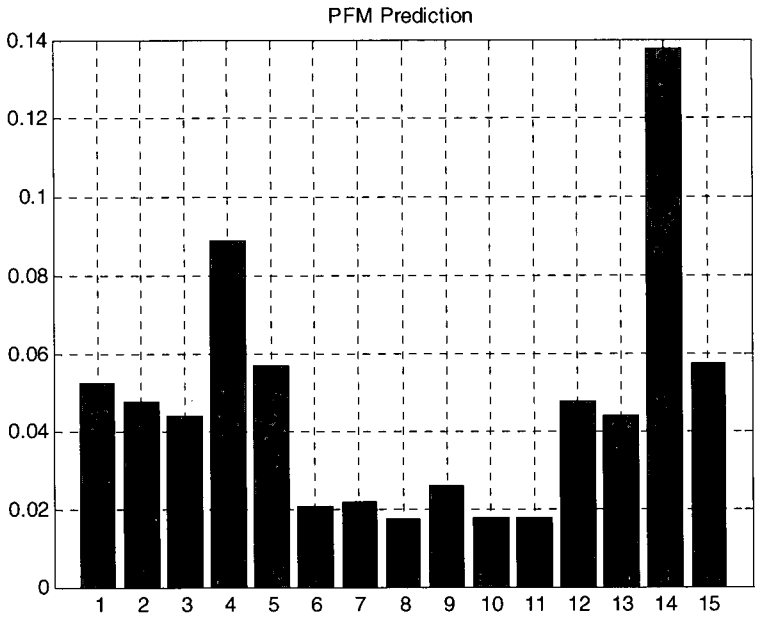

Figure A. 64: HCT Damage Case 3, PFM Prediction, 9 Sensors

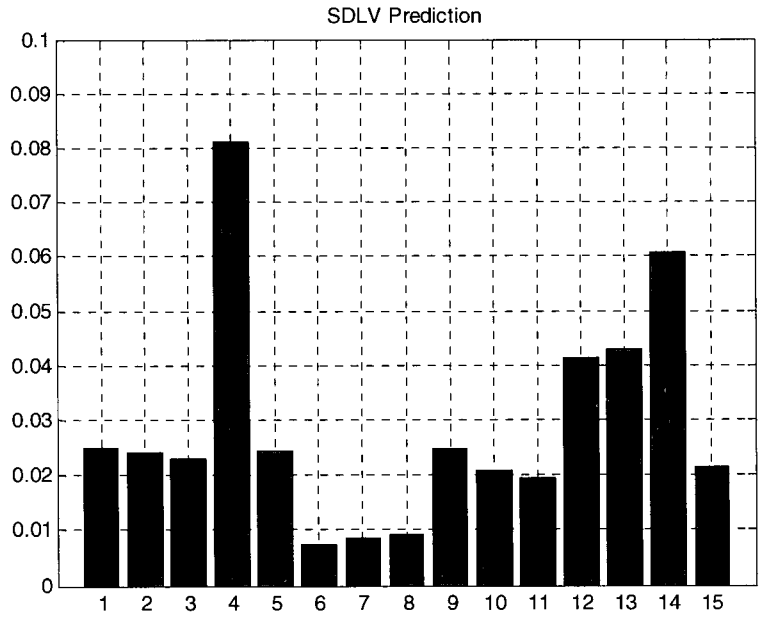

Figure A. 65: HCT Damage Case 3, SDLV Prediction, 9 Sensors

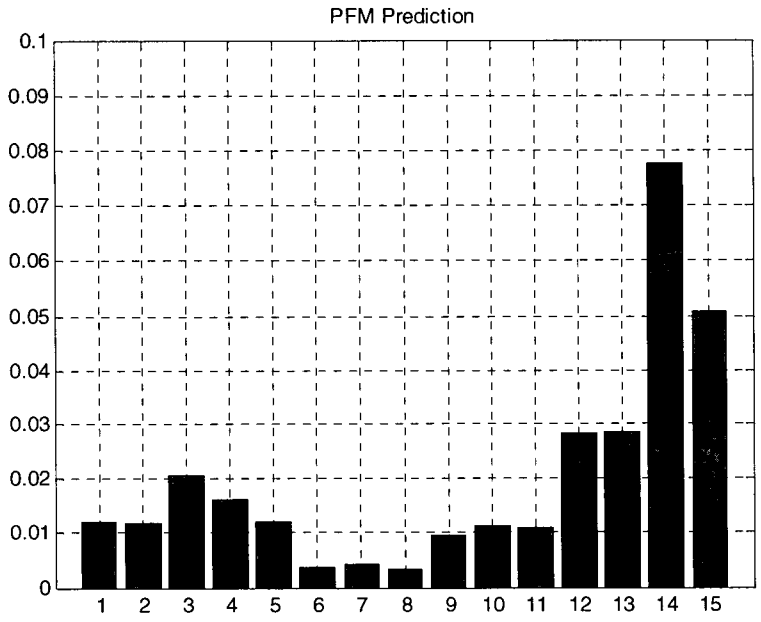

Figure A. 66: HCT Damage Case 4, PFM Prediction, 9 Sensors

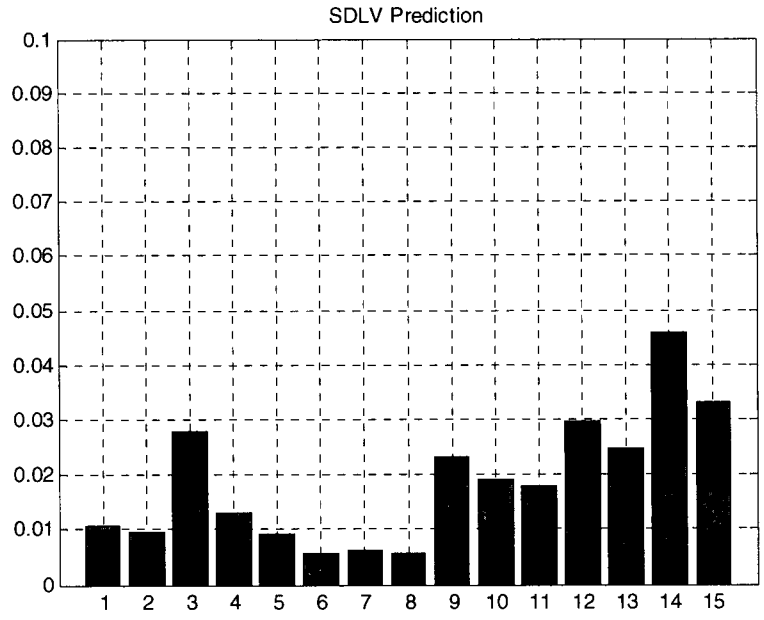

Figure A. 67: HCT Damage Case 4, SDLV Prediction, 9 Sensors

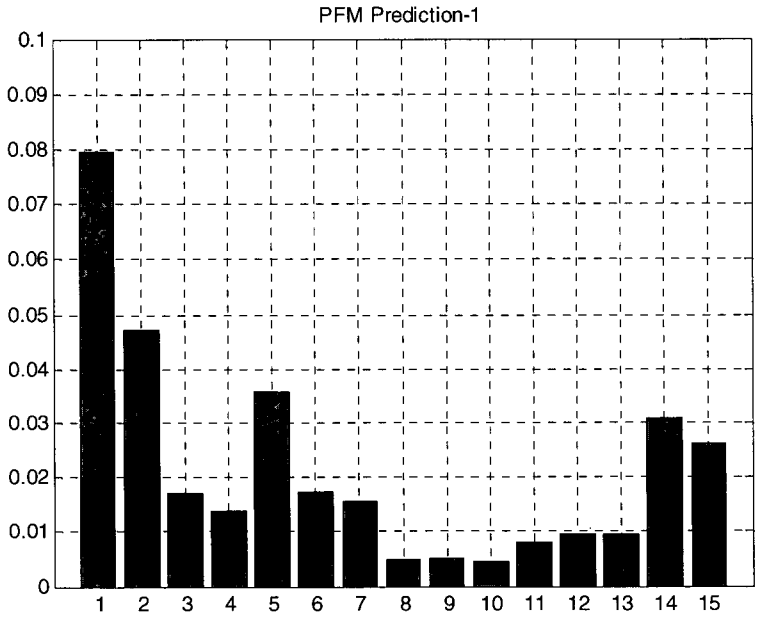

Figure A. 68: HCT Damage Case 4, PFM Prediction, 18 Sensors

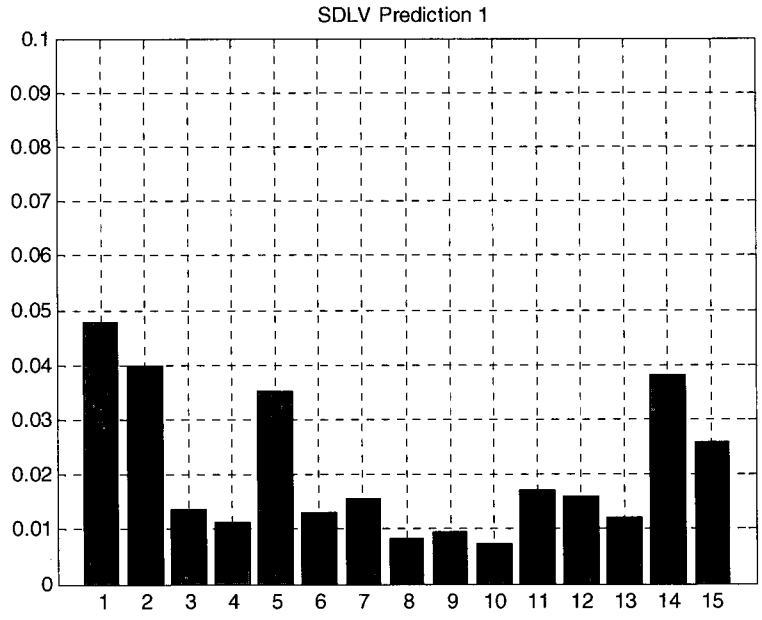

Figure A. 69: HCT Damage Case 4, SDLV Prediction, 18 Sensors

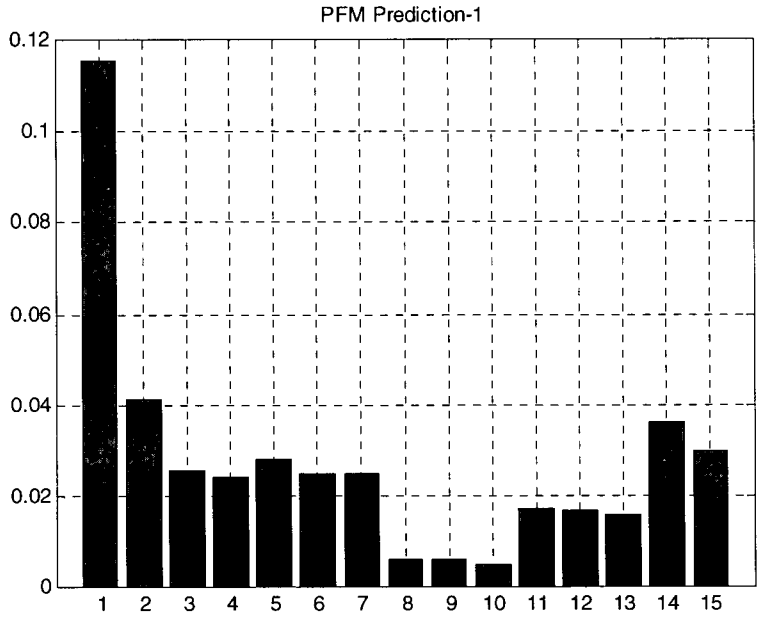

Figure A. 70: HCT Damage Case 5, PFM Prediction, 48 Sensors

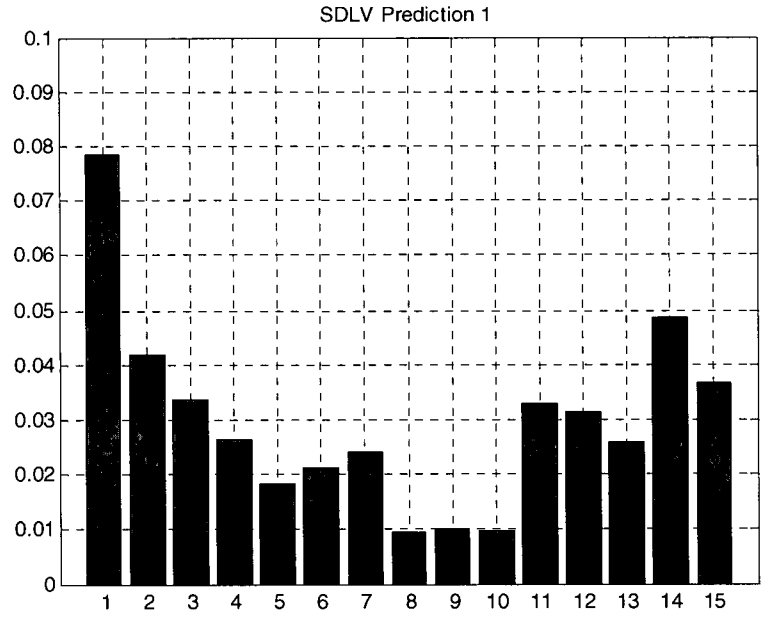

Figure A. 71: HCT Damage Case 5, SDLV Prediction, 48 Sensors

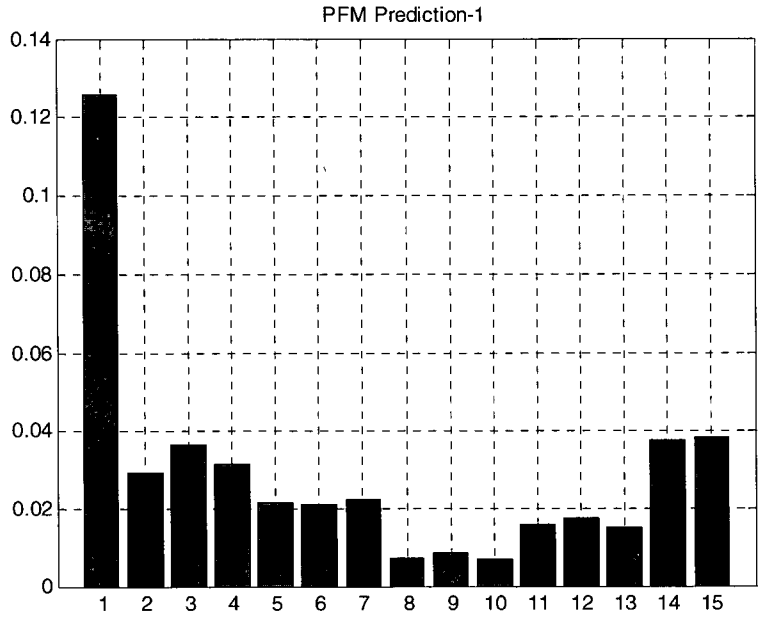

Figure A. 72: HCT Damage Case 6, PFM Prediction, 48 Sensors

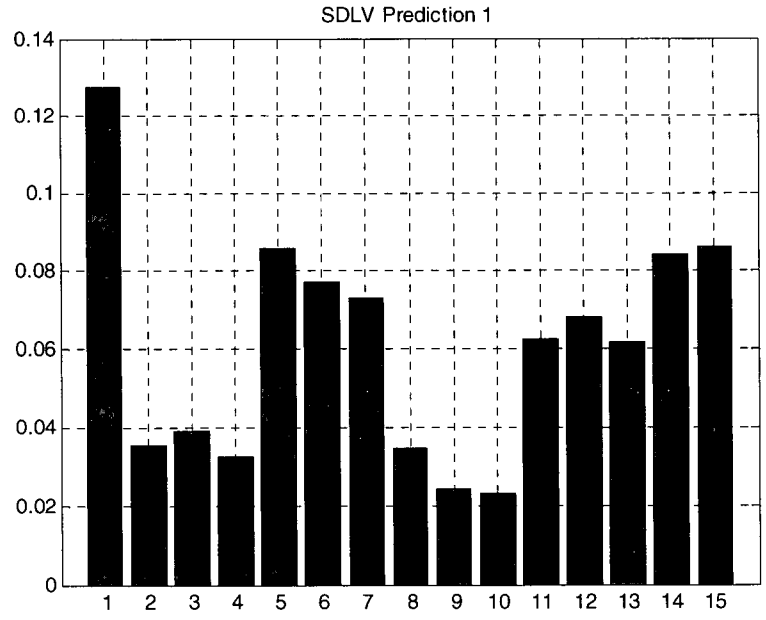

Figure A. 73: HCT Damage Case 6, SDLV Prediction, 48 Sensors

In all of the results above, is it obvious that there is a bias in the damage predictions towards the centre of the structure regardless of the actual damage location. In the derivation of the DLV method, it is stated that the normalized stresses can be multiplied by a set of weighting factors. In the simple examples, the weights are set to 1. It is apparent with these results that the bias has a more pronounced effect on the results, and the weights need to be considered. To

explore this, a set of weights is computed and applied to the normalized force results. The uncertainty is in the choice of weights to use. For the perfect case of no change in the structure, or the 'default' loading, the change in flexibility matrix would be zero. At first glance this means nothing; but if a singular value decomposition of a zero matrix is taken, the resulting singular vectors produce a diagonal matrix of ones. This suggests that a series of DLV's with unit loads applied would be the default loading. How they would be combined into one loading set is not obvious, so the simplest solution is to apply them at the same time; ie unit loads at each measurement location and then find the resulting force values. To create a weighting factor from this, the simplest thing to do is normalize those forces to a maximum of one, and then subtract the set of normalized values from 1. This set can then be added to a new normalized set: the idea is that if the DLV loads were 1, ie. the undamaged case, the normalizations would make all elements equal to 1. The results for cases 5 and 6 are shown next.

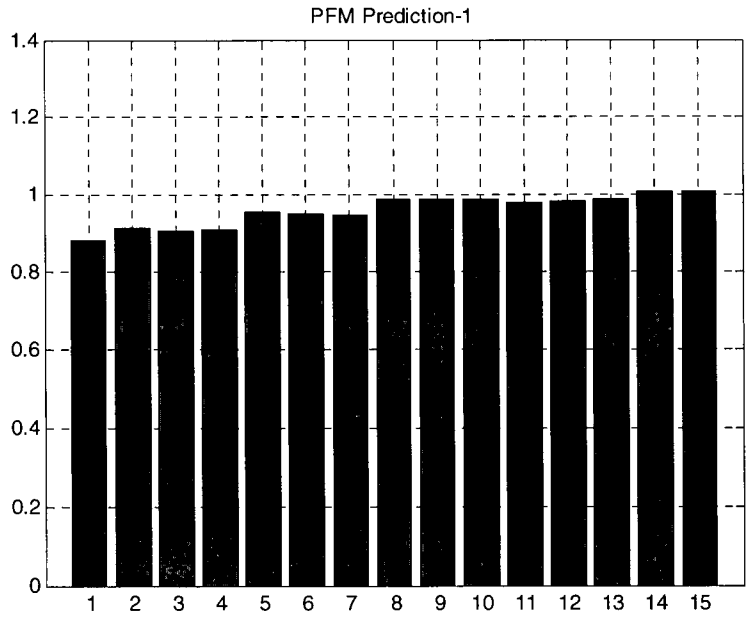

Figure A. 74: HCT Damage Case 5, PFM Prediction, 48 Sensors, Weighted

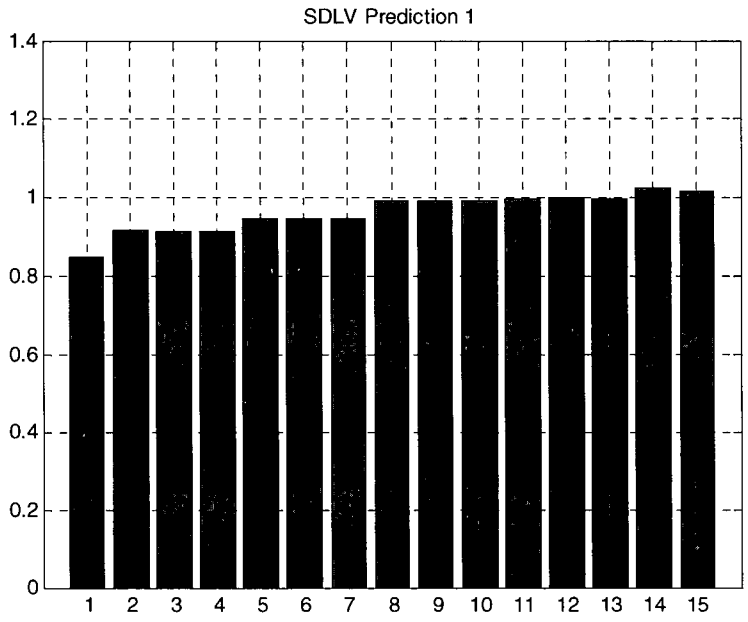

Figure A. 75: HCT Damage Case 5, SDLV Prediction, 48 Sensors, Weighted

It is seen from these figures that if there is damage apparent in the structure, the weighting values tend to average out each floor to be about the same. It is therefore useful to examine the weighted element by element plots. The results are shown in Figure A. 76 to Figure A. 79

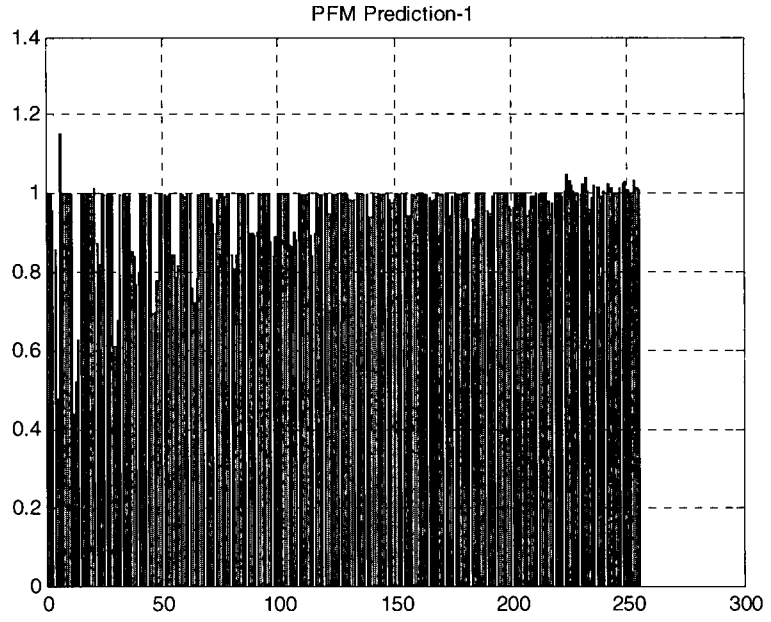

Figure A. 76: HCT Damage Case 5, PFM Prediction, 48 Sensors, Weighted, Element Values

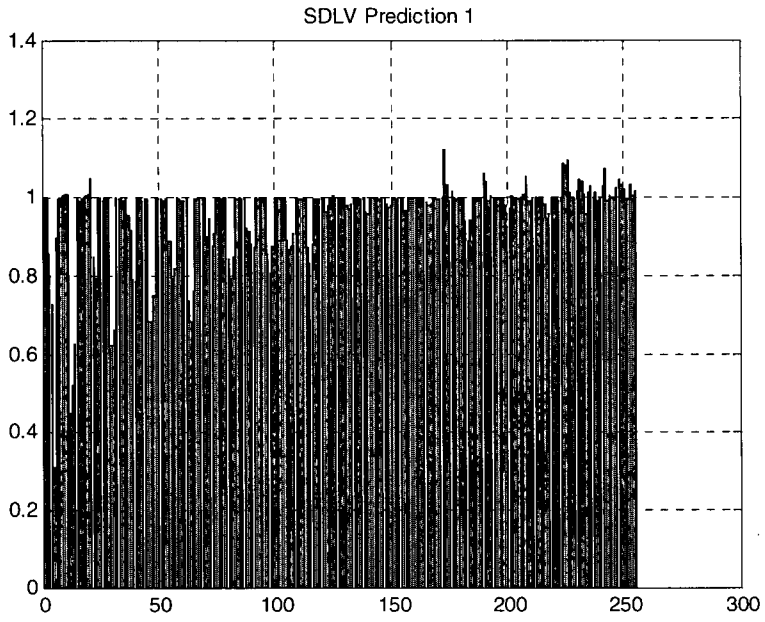

Figure A. 77: HCT Damage Case 5, SDLV Prediction, 48 Sensors, Weighted, Element Values

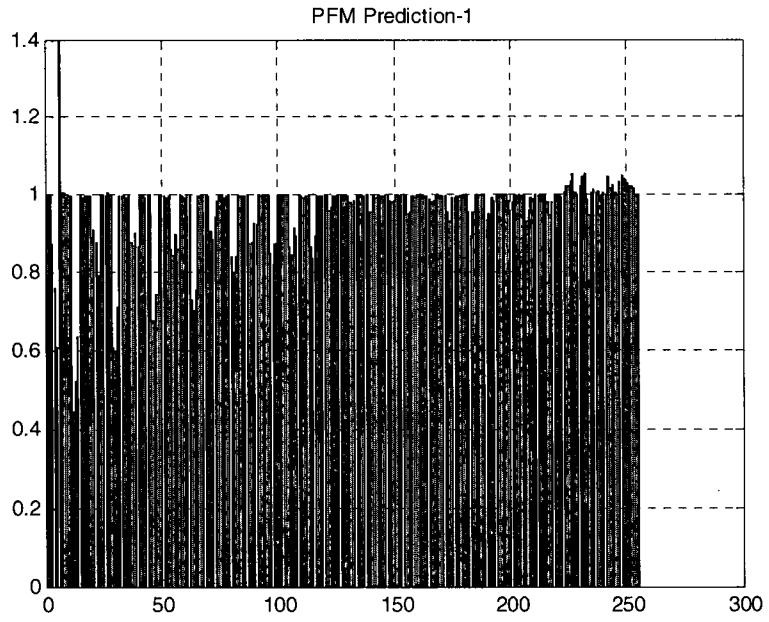

Figure A. 78: HCT Damage Case 6, PFM Prediction, 48 Sensors, Weighted, Element Values

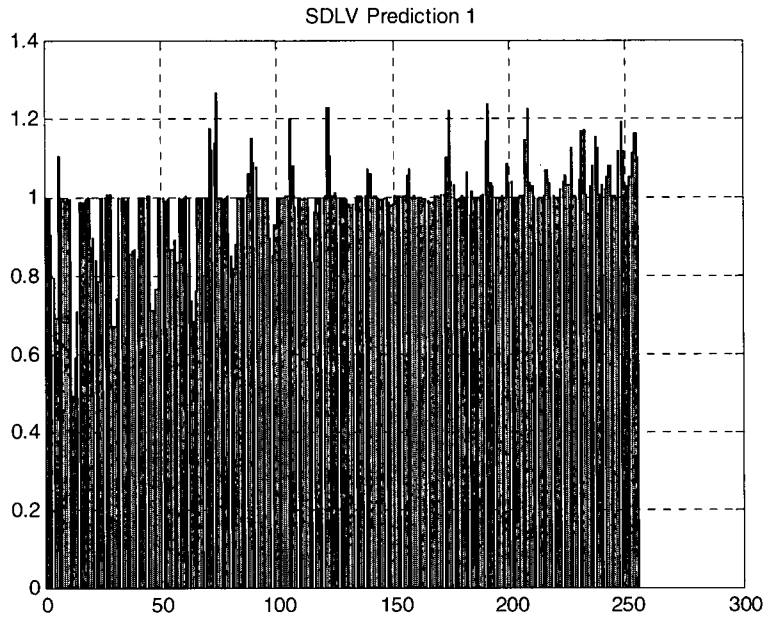

Figure A. 79: HCT Damage Case 6, SDLV Prediction, 48 Sensors, Weighted, Element Values

These results are similar, suggesting that there is still bias and that the weights are not having their intended effect. The next modification is to adjust the level of weights added; this requires introducing a linear combination of the case results and the weight. An example from case 5 is shown in Figure A. 80. Since the results were still not clear, it was useful to examine the results of the weights separately. A plot of the results from the unit loads is shown in Figure A. 81. The bias can be seen, both by excessive loading at the base of the building, and the lack of loading in the mid-levels.

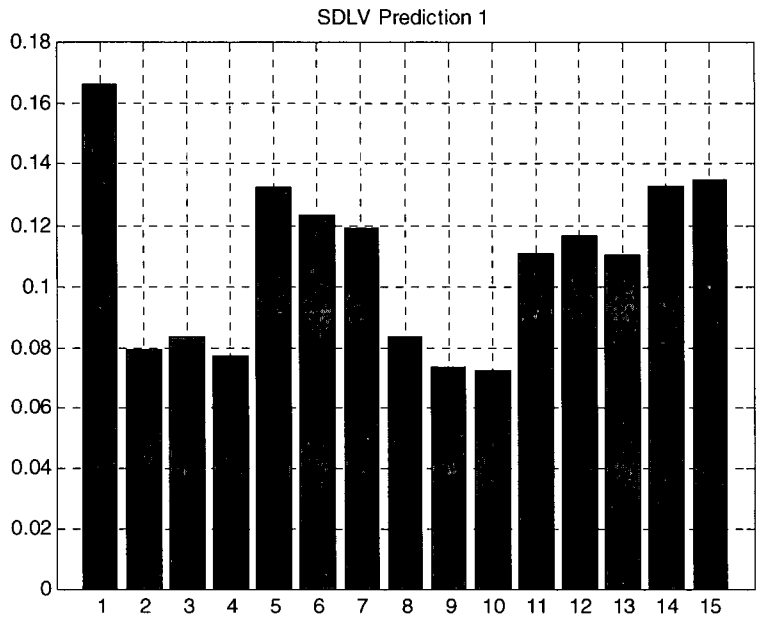

Figure A. 80: HCT Damage Case 5, SDLV Prediction, 48 Sensors, Less Weighted

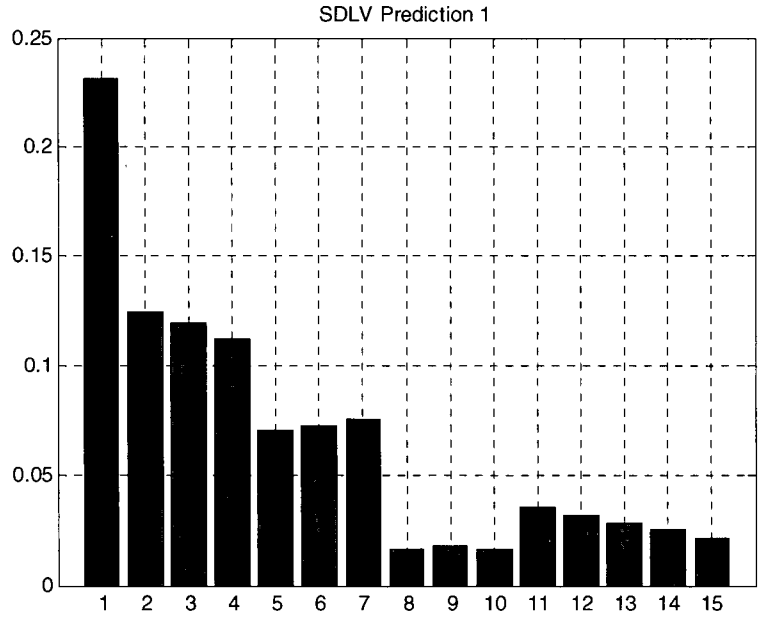

Figure A. 81: Unit load forces (weights)

A.3. Additional Analyses

The results of the analyses from the Melville and the HCT raised many questions about the performance of the DDM when applied to larger structures. Some conclusions can already be made; however, in order to be more conclusive above some specific issues several additional analyses can be performed. These analyses include:

- Application of a larger sensor set to the 3D frame (to the calibrated simulations from Section 6.6)
- Modification of the 3D frame to a 12 storey structure to check the DDM when applied to more distributed damage and a structure with more elements
- A case of the HCT with very severe damage to test the DDM

A.3.1. 3D Frame: 32 Sensor Set Analysis

Above it was mentioned that it was possible to use a larger sensor set then what was used in Chapter 5 and with the Melville example. This is based on the idea that with the DLV method, care must be taken to use a number of sensors (ie. number of dof's), that is not much larger than twice the number of modes used. As described in Chapter 3, this is due to the fact that the method examines the change in flexibility matrix to find zero or near-zero singular values. Those values are associated with singular vectors that are taken to be the DLV's. However, if the flexibility matrix is assembled from a lesser number of modes, or independent vectors, it will have a set of zero singular values equal to the rank deficiency (ie. number of dof's minus the number of modes). This will then cause the method to find singular vectors which are not DLV's. Based on this notion, the maximum number of sensors is twice the number of modes, provided that all of the modes are independent (ie. the change due to damage affects all modes).

The exception as mentioned in the HCT analysis is this: since the modes being used are approximations to the real modes, and the resulting flexibilities are also approximations, the zero singular values are not exactly zero. When using a software such as MATLAB however, the singular values that are computed due to rank deficiency of a matrix are exactly zero. For example, if 18 sensors are used, with only 6 modes, the rank deficiency is $18 - 2 \times 6 = 6$. In the computation of the singular values, 6 exact zeros appear. The singular values due to the change in flexibility show up in the results are values being *close* to zero. Therefore the exact zero values and the corresponding singular vectors can be removed from the DLV set. From the

results in the HCT above, this was the case for all SDLV predictions and all PFM predictions. This phenomenon is important for two reasons:

1. A better resolution of mode shape can be used in the analysis;
2. The applied DLV loads will have a better resolution.

The second point is more relevant, as shown with the alternative models of the Melville, where the propagation of the loads is important. If there are more DLV load points throughout the structure, this can be addressed.

In order to validate this idea, it was applied to the 3D frame 10 random cases (Section 6.7). This is useful since the results from that analysis were not as successful as desired. Here a complete sensor array is used, with 2 measurements at each corner of the frame for a total of 8 per floor, 32 sensors in alll. The initial analysis results are shown in Table A. 15.

Table A. 15: 3D Frame 32 Sensor Analysis Results

Case	SDLV		PFM		TPS-MU0%	
	SR	ER	SR	ER	SR	ER
16	1/1	24/31	1/1	20/31	1/1	22/31
17	3/3	26/29	3/3	25/29	3/3	25/29
18	3/3	18/29	3/3	18/29	3/3	16/29
19	1/1	28/31	1/1	20/31	1/1	22/31
20	2/2	25/30	2/2	20/30	2/2	25/30
21	2/2	25/30	2/2	17/30	2/2	15/30
22	3/3	22/29	3/3	18/29	3/3	16/29
23	2/2	21/30	2/2	21/30	2/2	22/30
24	2/2	21/30	2/2	20/30	2/2	18/30
25	4/4	20/28	2/4	23/28	4/4	18/28
Totals	21/21	230/297	19/21	202/297	21/21	199/297
%	100	77	90	68	100	67

It is seen from these results that the SDLV method works very well with the addition of more sensors. The PFM method works better than in the previous chapter, however misses a few damaged members and has a poor ER value. By combining the two into the TPS-MU0% method the ER consequently becomes poor, but the SR is 100%.

One important observation was that the results tend to be affected negatively by using a constant threshold for the damage (ie. 0.1). By examination of the plots, an example of which is

shown in Figure A. 82, it can be seen that if a variable threshold (ie. just above the highest value of a damaged members) is taken, the ER values can be improved dramatically. This obviously only has an improvement when the new threshold is below the old one (0.1). The results are shown in Table A. 16; the SR values are all 100% so they are not included.

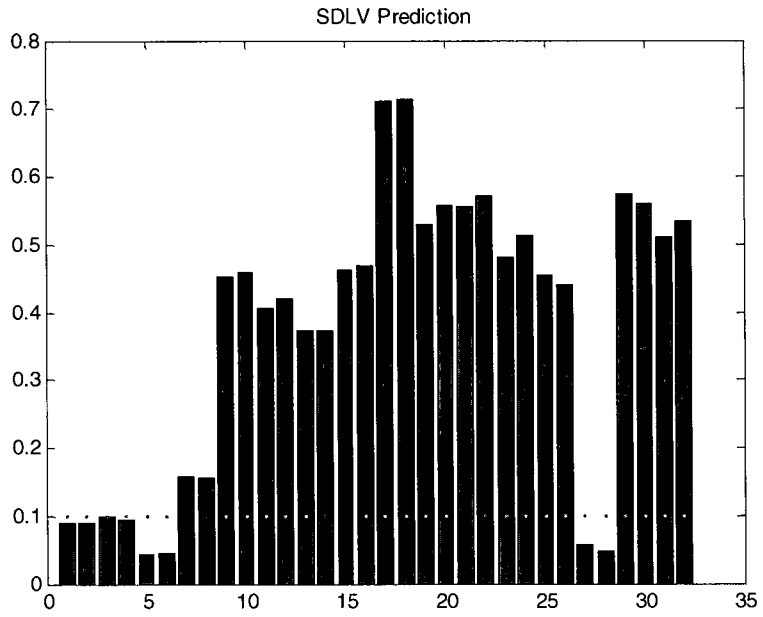

Figure A. 82: Example of the effect of variable damage threshold

Table A. 16: 3D Frame Variable Damage Threshold Analysis

Case	SDLV		PFM	
	Threshold	ER	Threshold	ER
16	0.03	30/31	0.14	30/31
17	0.08	26/29	0.34	25/29
18	0.14	26/29	0.37	13/29
19	0.03	31/31	0.12	30/31
20	0.04	30/30	0.17	30/30
21	0.11	28/30	0.18	28/30
22	0.15	27/29	0.32	25/29
23	0.08	28/30	0.35	24/30
24	0.06	28/30	0.25	28/30
25	0.16	25/28	0.40	17/28
Totals		279/297		250/297
%		94		84

The results shown in the table are very good; it is then useful to attempt to develop a relationship between something that is known from the analysis to the new threshold level. The simplest method is to renormalize; for the SDLV method it works most of the time but some members are missed. For the PFM, no damage is predicted when the values are renormalized. If only the SDLV is considered, a threshold of 0.26 would provide the following results as in Table A. 17. Additional relationships were explored but no conclusive results were found.

Table A. 17: 3D Frame SDLV ER Values, Damage Threshold 0.26

Case	SDLV
	ER
16	26/31
17	26/29
18	22/29
19	28/31
20	30/30
21	28/30
22	26/29
23	24/30
24	22/30
25	25/28
Totals	257/297
%	87

A.3.2. 3D Frame: Modified 12-Storey Analysis

For the next analysis, it was useful to expand the original 3D frame model to 12 stories, as a means of investigating whether the DDM would still identify the damage using 32 sensors, but with a sparser distribution. Therefore 8 were used on every third floor. The model is shown in Figure A. 83. The model is slightly different than that from Chapter 6; the links and point masses were removed. This was acceptable for this analysis because it is not intended to compare these results to the real test. Two damage cases were created. The damage cases were as follows: Case 1: braces 9, 10, 17, 18 (East face, Floors 2 and 3) and Case 2: braces 35, 37 (South face, Floor 5); 65, 66 (East face, Floor 9). In both cases the braces were completely removed. The results are presented in Table A. 18.

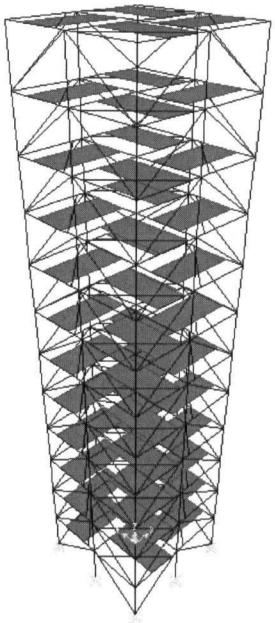

Figure A. 83: 3D Frame 12-Storey Model

Table A. 18: 3D Frame 12-Storey Model Results

Case	SDLV Prediction	PFM Prediction
1	1,2,7,9,10,15,17,18,23,24,25	1,2,3,4,6,9,10,15,17,18,23,24
2	9,27,29,35,43,45,49	3,4,5,6,11,12,13,14,19,20,21,22,27,28,29,30,35

Case	SDLV	PFM		
1	SR	ER	SR	ER
1	100	92	100	91
2	25	93	25	82

These results show that for the cases of localized damage, the sparser sensor set still works well. For cases with distributed damage however, much of the damage is missed. It is worth pointing out that the value of SR=25% is slightly biased because one of the damaged members identified (35) is right next to another damaged member (37). The plots of these results are shown in Figure A. 84 to Figure A. 87.

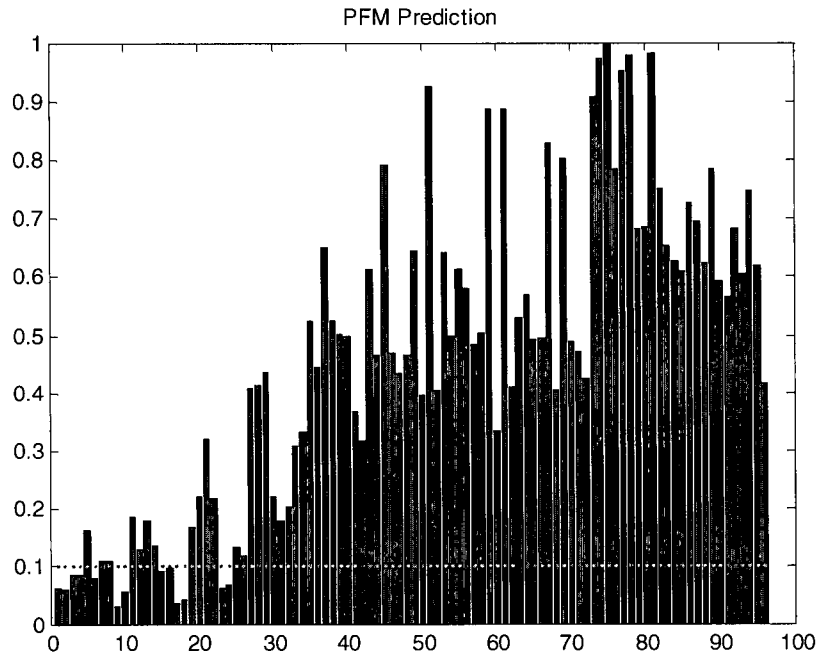

Figure A. 84: 3D Frame 12-Storey Model Damage Case 1, PFM Prediction

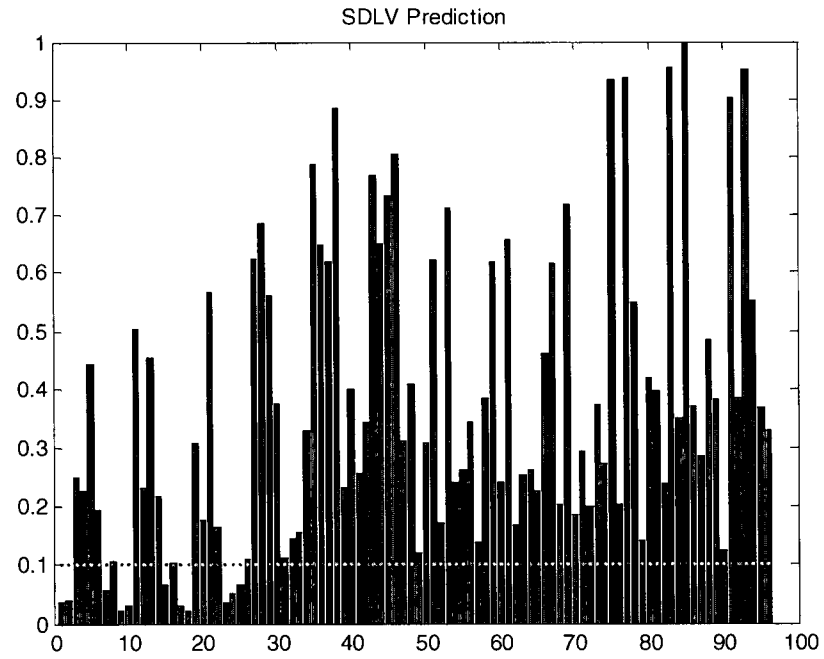

Figure A. 85: 3D Frame 12-Storey Model, Case 1, SDLV Prediction

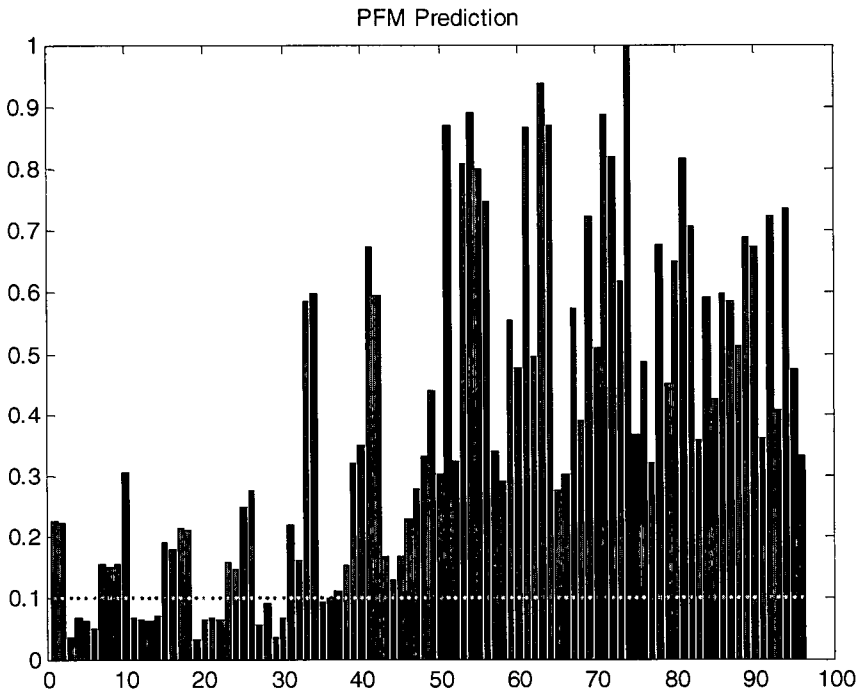

Figure A. 86: 3D Frame 12-Storey Model, Case 2, PFM Prediction

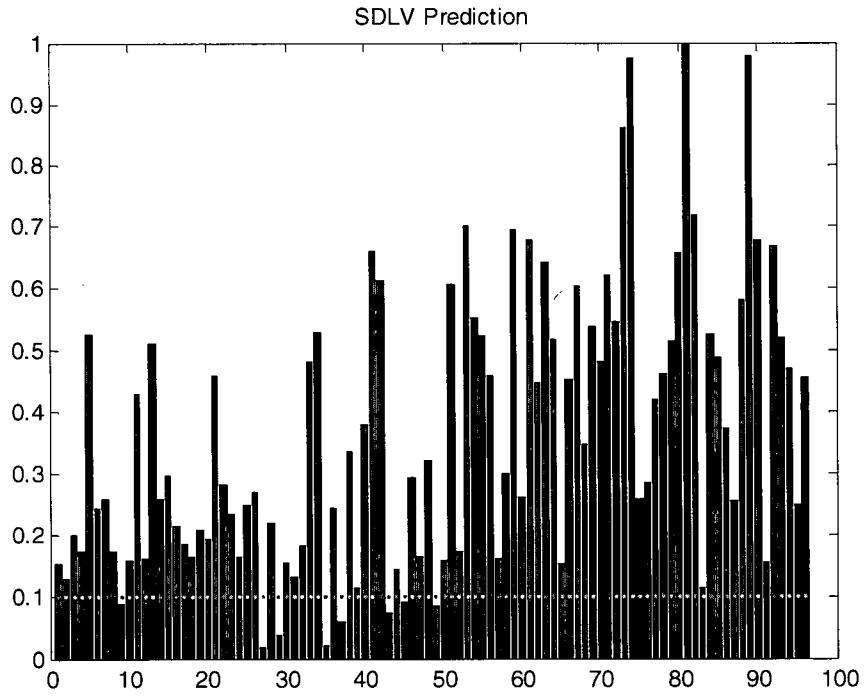

Figure A. 87: 3D Frame 12-Storey Model, Case 2, SDLV Prediction

A.3.3. HCT Full Model Analysis – Severe Damage

In order to examine if the low levels of damage simulated was having an effect on the results, an additional case was run with a much more severe level of damage. This damage case features a drastic reduction in properties for members in the first five floors on the north side of the building. The frequencies from the additional case are shown in

Table A. 19. The unweighted floor averaged results are shown in Figure A. 88 and Figure A. 89. It can be seen from these results that they are still affected strongly by the bias on the 8, 9, and 10^{th} floors, and that there is no improvement in localizing the damage by having a larger damage level.

Table A. 19: HCT Damage Case 7 Frequencies

Mode	Description	Frequency [Hz]
1	1 N/S	1.165223
2	1 Tor	1.277910
3	1 E/W	1.477762
4	2 Tor	3.751451
5	2 N/S	4.197272
6	2 E/W	4.657228

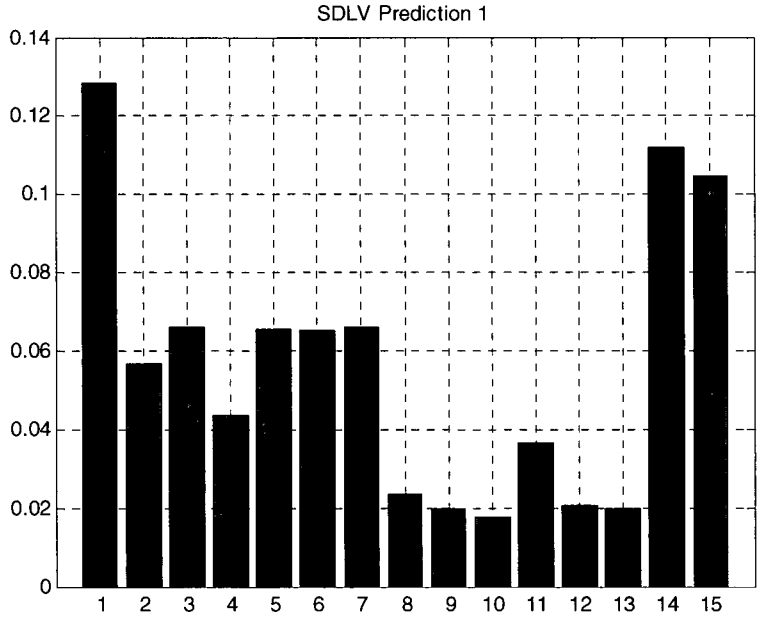

Figure A. 88: HCT Damage Case 7 Unweighted SDLV Prediction

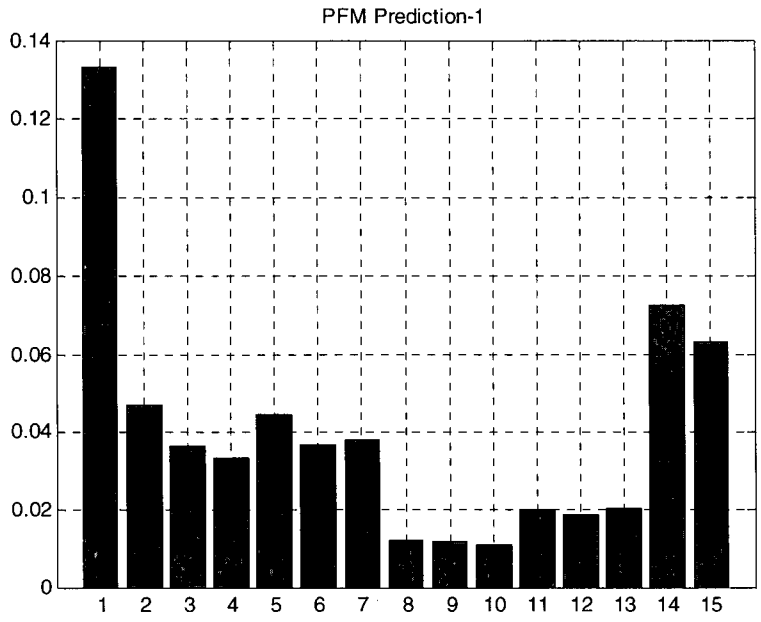

Figure A. 89: HCT Damage Case 7 Unweighted PFM Prediction

A.3.4. Summary of Additional Analysis Results

1. 3D Frame 32 Sensor Analysis
   - showed that the full sensor set will provide much better results under distributed damage cases
   - showed that if a variable damage threshold was used, near perfect results could be used
   - a relationship between the damage threshold and several parameters obtained during the analysis was explored, but for the quantities examined the results were scattered
2. 3D Frame 32 12-Storey modified analysis
   - showed that when the same DDM is applied with the same number of sensors (32) to a 'stretched' version of the model, the DDM worked well with localized damage, but not distributed damage
   - this confirms the suggestion that the DDM requires a denser set of measurements to correctly identify damage locations
3. HCT full building analysis – severe damage
   - a case of severe damage was simulated using the HCT to further explore the performance of the DDM

- the results still were not clear; however some indication of the damage was present
- the results suggest that the weighting factor should have a significant effect on the analysis and needs to be explored further